On cooperativity in cellular habitats, with quantitative experiments and modelling

Daneshpour Aryadi, H.

DOI
10.4233/uuid:e5a05014-d3b7-4566-8d1b-9faf67fa0260

Publication date
2021

Document Version
Final published version

Citation (APA)
Daneshpour Aryadi, H. (2021). *On cooperativity in cellular habitats, with quantitative experiments and modelling*. [Dissertation (TU Delft), Delft University of Technology]. https://doi.org/10.4233/uuid:e5a05014-d3b7-4566-8d1b-9faf67fa0260

ON

COOPERATIVITY

IN

CELLULAR HABITATS,

WITH

QUANTITATIVE EXPERIMENTS

AND

MODELLING

Dissertation

for the purpose of obtaining the degree of doctor

at Delft University of Technology,

by the authority of the Rector Magnificus prof.dr.ir. T.H.J.J. van der Hagen,

Chair of the Board for Doctorates,

to be defended publicly on Friday 29 October 2021 at 12:30 PM

by

Hirad DANESHPOUR ARYADI

Master of Science in Applied Physics,
Delft University of Technology, the Netherlands,

born in Vlaardingen, the Netherlands.

This dissertation has been approved by the promotors.

Composition of the doctoral committee:

Rector Magnificus,	chairperson
Prof.dr. Y.M. Blanter,	Delft University of Technology, promotor
Prof.dr. H.O. Youk,	University of Massachusetts, promotor
Prof.dr. G.E. Bokinsky,	Delft University of Technology, copromotor
Independent members:	
Prof.dr. S.M. Depken,	Delft University of Technology
Prof.dr.ir. T.F.A. de Greef,	Eindhoven University of Technology
Prof.dr. A.E. Sgro,	Boston University
Prof.dr. A. Mitchell,	University of Massachusetts
Prof.dr. N.H. Dekker,	Delft University of Technology, reserve member

Keywords: embryonic stem cells, differentiation, cell-cell communication, cooperative behaviours, systems biology, mathematical modelling

Printed by: Gildeprint B.V.

Cover design: James Jardine | www.jamesjardine.nl

Casimir PhD Series, Delft-Leiden 2021-22

ISBN 978-90-8593-488-2

An electronic version of this dissertation is available at
http://repository.tudelft.nl/.

To achieve great things, two things are needed.
A plan, and not quite enough time.

Leonard Bernstein

Contents

Summary

Tales of a *Fountain of Youth* and the invention of medicine illustrate our age-long obsession with two themes: life and death.

What it takes to stay alive, and not to be dead, is a basic question in science that is easy to state, and yet difficult to address at a profound level. One striking feature of many living organisms is the ability of individuals to behave in unison by communicating with each other, like an orchestra playing in sync but without a conductor. Collective behaviours ranging from traffic patterns in cities to schooling of fish increase chances of survival, or else the individual makes lethal decisions, falls prey to predators or fails at finding resources when acting on its own. One may ask about such collective behaviours that involve individuals communicating with each other: (1) *who is communicating with whom*, (2) *what are the signals*, and (3) *how do the signals work over space and time?*

Living cells – the microscopic building blocks of life – also communicate with each other, for example by secreting and sensing chemical signals in their habitat, to activate their internal signalling pathways and in turn the expression of important genes, and ultimately enabling themselves to coordinate their behaviours. Specifically, collective behaviours may require nearby or distant cells (locally or nonlocally) communicating with each other through multiple signals over time, complicating a quantitative understanding of the lines of communication and how they may yield a "community effect" – a term originally coined by Nobel laureate, John Gurdon, in describing his discovery of cooperative differentiation in frog embryos.

We sought to systematically explore how living cells communicate with each other and navigate themselves in their habitat by using quantitative experiments and modelling. Specifically, we studied how both known and unknown signals that are secreted by mouse Embryonic Stem (ES) cells – isolated from the inner cell mass of a 4-day-old preimplantation embryo and adapted for *ex vivo* culturing – collectively and spatiotemporally regulate ES cells' behaviour during their differentiation into the first two lineages (Neural Ectoderm (NE) or Mesendoderm (ME)). Taking ES-cell differentiation as our case study, we sought to find to what extent ES cells form a collective entity in which they cooperate to survive and differentiate.

This dissertation tells one coherent story through five chapters (Chapters 2-6). To begin with, **Chapter 1** introduces the reader to related background information,

including mechanisms of cellular communication, modelling of community effects, and embryonic stem cells as a model system.

We began by hypothesizing that suboptimal growths of ES cells at lower densities (widely known from practical experience) may be masking a community effect involving nonlocal communication among ES cells. Setting and varying the initial density of ES cells (i.e., the number of sparsely scattered ES cells on the surface of a 10-cm diameter dish) over a wide range, and then studying the resulting growth of differentiating ES cells, may reveal such community effect. This starting point led us to discover that survival and differentiation are collective phenomena for differentiating ES cells (**Chapter** 2). We discovered that neither a single ES cell nor a few ES cells can survive the differentiation process. Instead, we found that ES cells require to start their differentiation into all lineages above a critical density threshold on a dish (~1700 cells / cm^2) for the population to expand (up to ~10 fold) and differentiate efficiently (up to ~80% becoming progenitors of NE lineage), or else the entire population of differentiating ES cells becomes extinct over six days. Moreover, populations that start their differentiation near the density threshold stochastically either survive or become extinct after not appreciably expanding nor shrinking in size during six days. We found that pluripotent (non-differentiating) ES cells do not exhibit this sharp, switch-like response to the initial population density. We observed that ES cells nonlocally communicate by secreting and sensing soluble factors, which diffusive over several millimetres, to determine their survival-vs-extinction fate in the first three days of differentiation (**Chapter 3**). These diffusible factors accumulate over time as the population of secreting cells expands, but we show that only populations starting at above-threshold densities express anti-apoptotic genes (such as *Bcl2*) by sufficiently activating the transcriptional co-activator, YAP1 (**Chapter 4**). Moreover, we found that cooperatively amassing the secreted signalling factor, FGF4, is sufficient and FGF signalling is necessary for preventing extinction of the ES-cell population during differentiation (**Chapter 5**). We built relatively simple mathematical models – often using key experimental findings as their basic ingredients – to recapitulate the main phenomena and to guide ourselves in making quantitative predictions of new behaviours. In doing so, we discovered that both global cooperativity (set by the initial density of ES cells) and habitat (volume of liquid medium) dictate the ES cells' survival-vs-extinction fate during differentiation (**Chapter 6**). The materials and methods we used for our quantitative experiments are summarized in **Chapter 7**.

Our findings tell us that it takes differentiating ES cells to cooperatively and nonlocally interact with each other by secreting and sensing long-range signals (including FGF4) in their habitat in order to stay alive. We can cast this "global community effect" as an extension of Gurdon's community effect originally describing local

communication among cells (**Chapter 8**). Additionally, we discuss design principles of death and differentiation, other features of critical transitions in systems of interacting cells, and preliminary results on the effects of incubation temperature on ES cells' proliferation, exit of pluripotency and differentiation.

Understanding the full spatiotemporal range of the lines of cellular communication, and the cooperative behaviours they enable, will likely open new doors for synthetic biology and regenerative medicine. Moreover, by revealing a large-scale cooperation during differentiation, our work provides a basis for and shows that it would be possible to harness and control long-range communication for building systems – one without a necessary *in vivo* analogue – consisting of spatially disconnected microscopic cells that span many centimeters (the scale of the tissue-culture dish), and yet coherently function as one entity. Such basis helps in quantitatively studying how microscopic cells use cell-cell communication to bridge vast length-scales to perform a coherent, biological function as well as help in elucidating physical principles that underlie multicellular systems.

Samenvatting

Verhalen over een *Fontein der Jeugd* en het ontstaan van de geneeskunde illustreren onze eeuwenlange obsessie voor twee thema's: leven en dood.

Wat het vereist om in leven te blijven, en niet dood te zijn, is een basisvraag in de wetenschap die gemakkelijk te stellen maar moeilijk te beantwoorden is op een diep niveau. Een opvallende eigenschap van vele levende organismen is het vermogen van individuen om harmonieus samen te werken door te communiceren met anderen, net als het spelen van een toporkest maar zonder dirigent. Collectief gedrag variërend van verkeerspatronen in steden tot het zwemmen van vissen in scholen verhoogt de kansen op overleven, of anders maakt een individu fatale keuzes, valt ten prooi aan roofdieren of faalt in het vinden van middelen (zoals voedsel) als het voor zichzelf zou handelen. Men kan zich afvragen over dit soort collectief gedrag waarbij individuen met elkaar communiceren: (1) *wie communiceert er met wie*, (2) *wat zijn de signalen*, en (3) *hoe werkt de communicatie in de ruimte and tijd?*

Levende cellen - de microscopische bouwstenen van het leven - communiceren ook met elkaar, bijvoorbeeld door het uitscheiden en detecteren van chemische signalen in hun habitat om intracellulaire signaalsystemen en daarmee belangrijke genen te activeren, en uiteindelijk het mogelijk te maken om hun gedrag met andere cellen te coördineren. In het bijzonder, collectief gedrag vereist cellen die in de buurt of ververwijderd van elkaar zijn (lokaal of non-lokaal) te communiceren met elkaar door middel van meerdere signalen in de tijd, wat een kwantitatief begrip van de communicatiellijnen compliceert, en hoe deze lijnen zouden leiden tot een "gemeenschapseffect" - een term die bedacht is door de Nobel-laureaat, John Gurdon, om zijn ontdekking van coöperatieve differentiatie in embryonale cellen van kikkers te beschrijven.

Op een systematische manier hebben wij onderzocht hoe levende cellen met elkaar communiceren, en zichzelf navigeren in hun habitat, door middel van kwantitatieve experimenten en modellen. We bestudeerden hoe zowel bekende als onbekende signalen die uitgescheiden worden door muis Embryonale Stamcellen (ES cellen) - op hun beurt geïsoleerd uit de binnenste celmassa van een 4-dagen-oud pre-implantatie embryo en geschikt voor *ex vivo* celkweek - collectief en tijdruimtelijk het gedrag van ES cellen reguleren tijdens het differentiëren in de eerste twee kiemlagen (Neurale Ectoderm (NE) en Mesendoderm (ME)). Door ES-

celdifferentiatie als casus te gebruiken hebben we onderzocht in hoeverre ES cellen een (collectieve) eenheid vormen waarbinnen ze samenwerken om te overleven en te differentiëren.

Dit proefschrift vertelt één samenhangend verhaal in vijf hoofdstukken (Hoofdstukken 2-6). Om te beginnen legt **Hoofdstuk 1** de lezer de benodigde achtergrondinformatie voor, zoals mechanismen van cellulaire communicatie, modelleren van gemeenschapseffecten, en embryonale stamcellen als een modelsysteem.

We begonnen met de hypothese dat alombekende, suboptimale groei van ES cellen bij lagere populatiedichtheden wel eens op een onderliggend "gemeenschapseffect" kan duiden door middel van non-lokale communicatie van ES cellen. Het kiezen en ruim variëren van de initiële populatiedichtheid van ES cellen (dat wil zeggen, het aantal individuele ES cellen verdeeld over het oppervlak van een 10-cm diameter cultuurplaat), en vervolgens bestuderen van de resulterende groei van differentiërende ES cellen, zou een dergelijk effect kunnen onthullen. Dit startpunt leidde ons naar de ontdekking dat het overleven en differentiëren een collectief fenomeen zijn voor differentiërende ES cellen (**Hoodstuk** 2). We ontdekten dat niet een enkele ES cel noch een paar ES cellen het differentiatieproces overleeft. In plaats daarvan vonden we dat ES cellen het volledige differentiatieproces boven een kritieke grensdichtheid (~1700 cellen / cm^2) moeten starten zodat de populatie expandeert (tot wel ~10 maal) en differentieert (tot wel ~80% differentieert in cellen van de NE laag), of anders zal de gehele populatie van differentiërende ES cellen uitsterven over een periode van 6 dagen. Celpopulaties die het differentiatieproces starten in de buurt van de kritieke grensdichtheid overleven of sterven uit op een stochastische manier nadat er nagenoeg geen verandering in de grootte van de populatie opgetreden heeft gedurende 6 dagen. We vonden dat populaties van pluripotente (ongedifferentieerde) ES cellen niet een dergelijk, kritiek gedrag vertonen ten opzichte van hun initiële dichtheid. Daarnaast zagen we dat ES cellen non-lokaal communiceren door het uitscheiden en detecteren van factoren (moleculen), die over afstanden van enkele millimeters diffunderen, om hun lot (overleven of uitsterven) binnen de eerste 3 dagen van het differentiatieproces te bepalen (**Hoofdstuk 3**). Deze diffunderende factoren accumuleren over tijd terwijl de populatie van ES cellen expandeert, maar wij laten zien dat alleen populaties die het differentiatieproces starten boven de kritieke grensdichtheid niet-apoptotische genen (zoals *Bcl2*) activeren middels het tijdig activeren van een transcriptionele co-activator, YAP1 (**Hoofdstuk** 4). Bovendien vonden we dat het gezamenlijk accumuleren van een signaalfactor, FGF4, voldoende is en dat FGF-signaalsystemen vereist zijn om het uitsterven van een populatie te voorkomen tijdens het differentiatieproces (**Hoofdstuk 5**). We maakten relatief simpele wiskundige modellen - vaak gebruikmakend van de belangrijkste experimentele resultaten - om fenomenen samen te vatten en om onze weg te vinden bij het maken van kwantitatieve

voorspellingen van nieuwe fenomenen. Zodoende hebben we vastgesteld dat zowel globale samenwerking (bepaald door initiële dichtheid van ES cellen) als de habitat (volume van de kweekvloeistof) het lot van ES cellen (overleven of uitsterven) bepalen tijdens het differentiatieproces (**Hoodstuk 6**). In **Hoofdstuk 7** beschrijven wij de materiaal en methoden van onze kwantitatieve experimenten.

Onze bevindingen vertellen ons dat - om in leven te blijven - vereist het differentiërende ES cellen om samen te werken en non-lokaal te interacteren door het uitscheiden en detecteren van langeafstandssignalen (waaronder FGF4) in hun habitat, en dat we dit "globaal gemeenschapseffectäls een extensie van Gurdon's gemeenschapseffect kunnen zien dat oorspronkelijk lokale communicatie tussen cellen beschreef (**Hoofdstuk 8**). Daarnaast bespreken we ook de connectie tussen celdood en differentiatie, andere kenmerken van kritieke fasetransities in systemen met interacterende cellen, en preliminaire resultaten van de effecten van incubatietemperatuur op de groei, pluripotentie en het differentiatieproces van ES cellen.

Het volledig begrijpen van het tijdruimtelijk aspect van de cellulaire communicatielijnen, en het resulterend collectief gedrag, zal mogelijk nieuwe deuren openen voor de synthetische biologie en regeneratieve geneeskunde. Het aan het licht brengen van een grootschalige samenwerking van ES cellen tijdens het differentiatieproces laat zien dat het mogelijk is om de langeafstandscommunicatie van cellen te benutten en te controleren om multicellulaire systemen te bouwen zonder een noodzakelijke *in vivo* analogie. Een dergelijke basis zal helpen bij kwantitatieve studies naar hoe microscopische cellen communiceren om lange afstanden te overbruggen en daardoor een coherent, biologische functie te vervullen. Ook zal deze basis licht werpen op fundamentele principes die onderliggend zijn aan (het ontwerpen van) multicellulaire systemen.

Preface

The COVID-19 pandemic revealed how connected we are in today's world.
And what happens when it's all suddenly down. Job losses, recessions, riots, break-ups, mental problems, physical illness and death. Life as we know it seems to halt.

This dissertation revolves around cellular life, death, and a kind of connection that separates the two. It tells a story about living cells that keep their connection by communicating with each other when confronted with a choice. But when the lines of communication weaken, all of a sudden, the whole community collapses, and what follows is death.

Over the past few years I experienced an adventure of a lifetime.

Freshly armed with Newton's laws as a physics graduate, I stepped into a new world centered on stem cells from mouse embryos and taking place in cave-like tissue culture rooms. To get settled I needed to adopt the courage of a lion, the mindset of a detective, the patience of a saint, and the vision of a systems thinker. The style of doing the science I embraced - called *systems biology* - aims to understand the sum and its parts, and how those parts interact with each other to give rise to emergent phenomena ranging from the flocking of birds to a rapid immune response. The slow-burning journey taught me a precious and universal skill: finding answers to simple questions about complicated matter through small steps in reasoning. And how to engagingly share those answers with others. I was driven by making a positive impact on people. But it was those around me who made settling and success possible.

Although a dissertation's front cover reads a single name, the content is never the output of one person alone. And this dissertation is by far no exception. The work rests heavily on the shoulders of my peers and betters. Mentors and collaborators, but also other books, studies, journal articles; all are acknowledged only at the end of this book.

H.D.A.
Delft, September 2021

1

Introduction: Life, death, and how cells tell the difference

Parts of this chapter are also reported in Daneshpour et al. [1] and [2]

1

1.1. What it takes to stay alive, and not to be dead

What is *life*? This timeless question boggles the minds of many people, ranging from philosophers, artists, scientists to an unemployed, single parent struggling to make ends meet. Whether it is referring to life's metaphysical or scientific meaning, or whether it is accompanied by a sense of joy or perhaps frustration why it is you life isn't treating well lately, the question appears deceptively simple to state and yet notoriously difficult to answer at a profound level.

We think we know how life looks like, to tell what is clearly alive: a rock is not, but a mouse certainly is. We often have a strong desire toward life, so much that we wish to seek and sustain it: here on Earth or elsewhere like on Mars. In the face of threats such as diseases, we look for smart ways to avert or get rid of them. Siddhartha Mukherjee[1] argues that cancer – which we are struggling with for at least 4500 years[2] – has always been smarter, more successfully oriented towards survival, than we are. We think we are trying to deal with death in fighting cancer, but in fact we are fighting life.

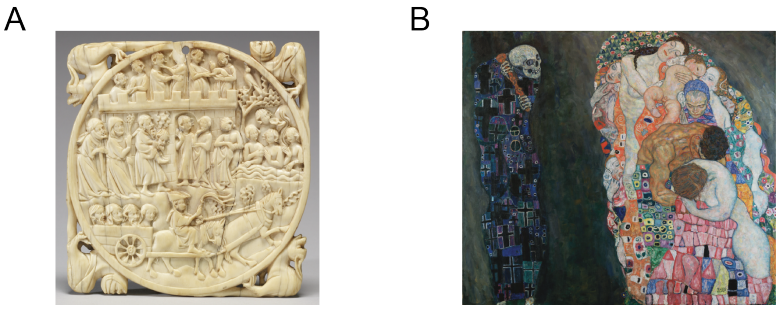

Figure 1.1: Human imagination and artist's impression of what it takes to stay alive. (A) *Fountain of Youth*, an early 14th Century, French ivory plague depicting a mythical tale that dates back to the Ancient Greek. It shows how old and diseased men and women (carried in from the left) restore their youth upon drinking or bathing in the fountain's mythical waters. From Wikimedia Commons. **(B)** *Death and Life*, Gustav Klimt (1910/15). Klimt puts a social life (a union of bodies) opposite a solitary figure of death (a disunion), at a time of his own awareness of aging. From Wikimedia Commons.

This dissertation aims not to answer the all-encompassing question, but one that appears at least as simple to state: what does it take to stay alive, and not to be dead? For thousands of years tales have been narrated that drinking or bathing in the mythical waters of a *Fountain of Youth* renews life by restoring the youth of those who are old and diseased (Fig. 1.1A). Since a few decades ago, stem cells from adult tissue or preimplantation embryos were found to hold the potential for what the imagination already allowed us to think possible. I will elaborate

[1] Physician, oncologist and author of bestsellers such as *The Emperor of All Maladies: A Biography of Cancer* which has been described as among the 100 best non-fiction books

[2] Skeletal remains of an adult man in Siberia that date back 4500 years to the Early Bronze Age show signs of metastatic carcinoma (from head to hip), possibly originating from the lung or prostate [3]

on embryonic stem cells in the next sections as they have been the main subject of study in addressing the question of what it takes to stay alive. The answer we found relates to Klimt's depiction of a social life represented by a "union" of bodies, contrary to a solitary figure as a symbol of closeness to death (Fig. 1.1B).

Living cells – the building blocks of life – possess remarkable properties to preserve their order and therefore existence in specific habitats. They control their internal state through homeostasis and metabolism and respond to their external environment to ultimately adapt by means of reproduction, organization and evolution. At the level of molecules and atoms – the building blocks of living and non-living matter – the appearance of life-like properties seems anything but obvious. How physics and chemistry explain the events that take place in space and time, within a living cell, is the same question the visionary Erwin Schroedinger raised in his 1944 classic[3] *"What is Life?"*. Living matter likely involves "other laws of physics" that describe how disorder at the smallest scale (the random motion of particles) can still result in order at a large scale (a piece of rock); Schroedinger's answer allegedly gave birth to new fields and ground-breaking discoveries.

One striking feature of "staying alive" oftentimes involves living organisms to interact by communicating with each other to coordinate their behaviours in reaching a desired goal. In the next section I present examples of such collective behaviours.

1.2. Collective behaviours across species, space and time

Emergent phenomena, ranging from fractal-like water crystals forming on the windows during winter times to cathedral-like mounds produced by termite colonies, illustrate the captivating properties a relatively large-scale entity has, which its many small-scale parts (water molecules or termites) do not have in the first place. That the *"whole is greater than the sum of its parts"* (in the words of Aristotle) is traceable to the connection between the parts due to the parts interacting with each other. From a physical point of view, connections are generally mediated by fundamental interactions such as the electromagnetic force (hydrogen bonds that keep water molecules in place in crystals) and gravitational force (keeping planets in orbit around the Sun). Living organisms interact by communicating with each other which involves sending and receiving signals.

Communicating is crucial for organisms to coordinate their individual behaviours. The resulting, collective behaviours allow the interacting individuals to achieve a desired goal they would otherwise not be able to achieve if they acted on their own (Fig. 1.2). Collective behaviours are often fuelled by the interactions of the (genetically or physically nearly identical) individuals themselves, rather than through

[3] The book had a remarkably huge and lasting impact for its size, allegedly leading to the birth of the field of molecular biology and the discovery of DNA

the presence of an authoritative leader or the manipulation by an external agent.

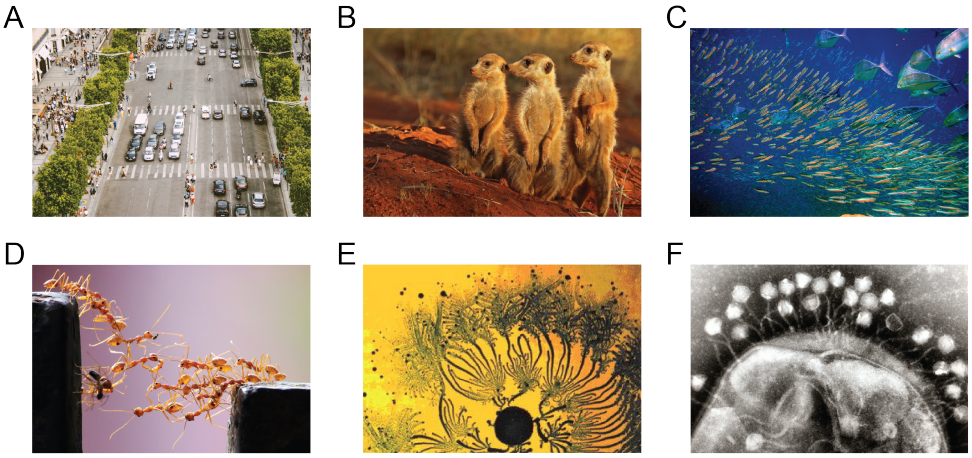

Figure 1.2: Collective behaviours across species, space and time. **(A)** Traffic patterns emerge from human interaction based on rules, signs and conventions [4]. Image courtesy of Viviana Ceballos. **(B)** Meerkats (*S. suricatta*) take turns in groups to keep guard while others rest or feed pups [5]. Image courtesy of Charles J. Sharp. **(C)** Schooling of predator bluefin trevally (*C. melampygus*) and prey anchovies increases chances of survival when catching preys and escaping from predators, respectively [6]. Image courtesy of Bruno de Giusti. **(D)** Forming armies helps ants (*S. geminata*) to hunt targets, migrate their nest or build living bridges [7]. Image courtesy of Vaishakh Manohar. **(E)** Bacteria, such as *B. subtilis*, communicate to form complex communities and perform collective tasks (such as vortex-like migrations) as a survival strategy in a wide variety of challenging environments [8–11]. Image courtesy of Eshel Ben-Jacob. **(F)** Viruses, such as the coliphage T1 that infects and replicates within bacteria, cooperate to suppress the host's immunity [12, 13]. Image courtesy of Graham Beards.

A main feature of collective behaviours is that one individual's action is determined by the interaction with and thus influence of the others, which – at the level of a group of interacting individuals – results in the individuals concurrently self-organizing their behaviour to a common pattern. Importantly, collective behaviours exist across many species, at the macroscopic scale of humans down to the microscopic scale of viruses (often considered to be on the edge of life), across length scales (interaction with direct neighbours to neighbours that are multiple individual-dimensions away) and across time scales.

Humans, when interacting in groups, can self-organize to produce "spontaneous order" which is evidenced by the structure of cities that architects often design based on worn pathways, the development and changes of language that produce structure and regularity in grammar, the existence of political systems and financial markets, and the emergence of traffic patterns based on signs, regulations and conventions (Fig. 1.2A) [4]. Ultimately, participating in collective behaviours benefits individuals and species to increase their fitness and the chances of survival by increasing their awareness of predator presence while resting or feeding ("collec-

tive vigilance" – Fig. 1.2B) [5], decreasing one's visibility to predators ("dilution effect" – Fig. 1.2C) [6], and overcoming (physical) hurdles when searching for food resources ("foraging" – Fig. 1.2D) [7].

Communicating by means of chemical signals is also crucial for living cells such as the bacterium, *B. subtilis*, to form complex multicellular structures by cooperating with each other, enabling successful aggregation (biofilms) and collective, vortex-like migration in a favourable niche ahead of other rivals (species) (Fig. 1.2E) [8–11]. Even viruses – often described as being on the edge of life as they depend on other living hosts for reproduction – cooperatively attack a host cell in waves to enable subsequent groups of viruses of a next wave to benefit from an already weakened immunity due to an earlier, collective attack (Fig. 1.2F) [12, 13].

A technical and conceptual challenge is to quantitatively describe collective behaviours (i.e., cooperativity) that involve multiple interacting individuals, length-scales and time-scales. In the next section I lay out our approach to studying the spatiotemporal aspects of a community of communicating cells (i.e., who is communicating with whom, over what distances, what the community size is), and ultimately to quantitatively establishing a cell's degree of autonomy when participating in a collective behaviour.

1.3. Mechanisms of cellular communication

Living cells often communicate with each other to coordinate their behaviours. Measuring the length-scales and time-scales of communication among multiple interacting individuals, identifying the communication signals and, generally, quantitatively describing collective behaviours can be a technical and conceptual challenge. In the 1970s there was a huge breakthrough in statistical physics when a new quantitative description (theory) showed that the main features of collective (phase) transitions of systems consisting of many interacting units are insensitive to the details of the interactions between the units [14]. Despite the wide number of cell types and communication signals in nature, one can group quantitative models that describe cell-cell communication into a few classes, thereby raising the hope that synthesizing a generalized modelling framework that is applicable to any living organism is a feasible goal. Throughout this and the next section, we present and discuss examples of cell-cell communication in various cell types – particularly immune cells, given their diversity of communication signals and distinct cell types [15, 16] – that can result in emergent behaviours such as a community effect. There are broadly three types of cell-cell communications: autocrine, paracrine, and juxtacrine signalling (Fig. 1.3A-C).

Communication between cells involves sending and receiving signals. One important mechanism of communication is the production and then secretion of soluble

signalling molecules (cytokines or chemokines) by one cell into its liquid environment that upon sensing of the signalling molecules by the cognate receptor of another cell can result in a cellular response, such as the upregulation or downregulation of one or more target genes depending on the intracellular (biochemical) pathway [17, 18]. The propagation of soluble signals by cells is determined by the secretion rates and the physicochemical aspects (e.g., diffusion constants and degradation rates) of the signalling molecules, and by secreting and sensing of signalling molecules a cell can either communicate with itself or a neighbouring cell [19, 20]. In autocrine signalling [21, 22], cells of the same type communicate with each other as they have the cognate receptors to sense their secreted signalling molecules (Fig. 1.3A). An immune cell, for example, secretes a cytokine, such as Interleuking-2 (IL-2) [23, 24] and Interferon-γ (IFN-γ) [25], and also has the cognate receptor, thereby allowing the cell to communicate with itself and other cells of the same type [19, 20]. Another example of autocrine signalling is the regulation of growth through secreted Epidermal Growth Factors (EGFs) by epithelial cells, which requires the tuning of the secretion rates of EGFs [26]. High secretion rates can lead to uncontrollable growth and the formation of tumours.

Paracrine signalling involves at least two types of cells (Fig. 1.3B); in the case of immune cells, one cell type without the cognate receptor, secretes a cytokine such as the Colony-Stimulating Factor-1 (CSF-1) [27] and Platelet-Derived Growth Factor (PDGF) [28], whereas another cell type has the cognate receptor but does not secrete the cytokine. Secreted signals allow for communication across distances that can be orders of magnitudes larger than the size of the cells. Variations of autocrine and paracrine signalling are synaptic signalling which allow neurons in the nervous system to communicate with one another along their axons by secreted neurotransmitters [29], endocrine signalling where cells secrete hormones that are in turn transported through the circulatory system (bloodstream) to reach distant target cells [18], and electrochemical signalling in bacterial biofilms [9, 10].

Another important mechanism of communication between cells involves non-secreted signals that one cell propagates to another cell through close (physical) contact (Fig. 1.3C). For immune cells, juxtacrine signalling (or contact-dependent signalling) involves two cells in which one cells has a membrane-bound ligand (e.g., peptide-bound Major Histocompatibility Complex (pMHC)) and another cell has a cognate receptor (e.g., T-Cell Receptor (TCR) for pMHC) [30]. Another well-studied example involves two membrane-bound proteins – Notch on one cell and Delta on an adjacent cell – to bind each other to transmit signals that influence morphogenesis and organ formation [31, 32]. Recent work unveiled the importance of juxtacrine signalling for tumour cells to escape immune surveillance (by upregulating PD-L1), and thus its tuning as a means to improve immunotherapies [33]. Direct contact between cells also allows for communication by passing

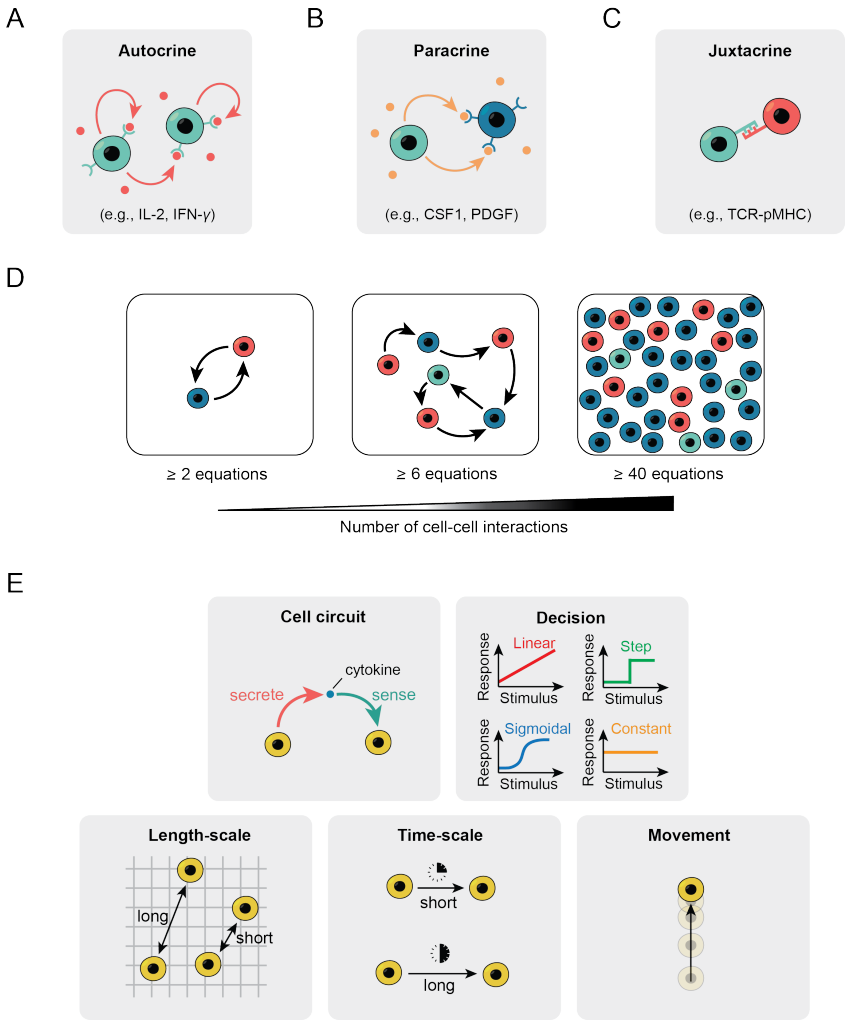

Figure 1.3: Ingredients for modelling cell-cell communication. **(A)** Autocrine signaling involves one cell-type and cytokines such as IL-2 and IFN-γ. **(B)** Paracrine signaling involves at least two cell-types, one that secretes a cytokine (e.g., CSF-1 and PDGF) without a cognate receptor and another cell-type has the cognate receptor but does not secrete the cytokine. **(C)** Juxtacrine signaling involves at least two cell-types communicating by a physical contact through a membrane-bound ligand (such as pMHC) and a receptor (such as TCR). **(D)** Models that describe communications among cells typically have as many equations as the number of cells involved. **(E)** Elements that enter a model for cell-cell communication. (Top left) Cell-circuit that describes which cell secretes and which cell senses a cytokine; (Top right) Distinct responses to cytokines; (Bottom left) Distinct length-scales involved in cytokine-mediated communication; (Bottom middle) Distinct time-scales involved in cytokine-mediated communication; (Bottom right) cell motility.

on mechanical stress and generating forces through actin and myosin filaments of the cytoskeleton for cell motility [34]. Cells can also communicate with physical

"bridges" (tunnelling nanotubes) that are membrane extensions connecting two cells, allowing exchange of cargo such as organelles (e.g., mitochondria) [32], and which may also initiate tumour formation [35].

Engineering communications, not only between cells themselves but also between cells and their habitat, allows for the understanding and improvement of collective pattern formations as a result of collective decisions by (synthetic or living) cells (e.g., optimizing the reaction-diffusion and positional information for chemical signalling) [36, 37]. In this way, synthetic cells can be designed to interact with their environment with applications in biotechnology and biomedicine (e.g., hydrogel-based *E. coli* secreting lysotaphin to inhibit the growth of *S. aureus*, which causes common human infections) [38]. Moreover, cell-habitat interactions allow cells to adapt to environmental variations (such as changing osmotic conditions [39]) or imposed conditions (such as lower chemotherapy impact in a host as a result of a drug-resistant microbiome [40]). Generally, effective coordination of secreted and non-secreted signals to control proliferation, apoptosis and motility is crucial for biological processes such as tissue repair [41, 42].

Modelling a biological process, such as those found in immune systems, can be challenging because the process may involve any of the three types of communications (autocrine, paracrine, juxtacrine), contain multiple cell types, and involve multiple cytokines (Fig. 1.3D). Another complication is that cell-cell communication often spans vast length-scales, depending on the diffusion length-scale of each cytokine (in the case of chemical signalling) and cell motility (Fig. 1.3E). Moreover, the time-scale at which cells respond to cytokines can vary and there can be a variety of responses to each cytokine (Fig. 1.3E). Despite these complications and similar to physical systems, there may exist universal principles of collective behaviours in biology [41, 43, 44].

1.4. Modelling community effects in biology at the smallest scale

Collective behaviours that occur in a group, or community, of cooperatively communicating cells result in "community effects". In 1988 John Gurdon coined this term to describe his discovery of a cooperative differentiation in frog embryos (*X. leavis*) [45] whereby a few embryonic cells cannot differentiate into the mesodermal lineage – they die instead – and the cells can differentiate only if they are aggregated together in sufficiently high numbers [45, 46] because only then the cells can accumulate sufficiently high concentrations of molecules that the cells must secrete and sense to survive differentiation. Since Gurdon's discovery, researchers observed such cooperative behaviours in a variety of cell types and organisms (e.g., mouse T-cells locally interacting with each other in a microwell by

secreting and sensing the cytokines, IL-2 and IL-6, that induce differentiation into memory T-cells [47]).

At a spatially large scale (orders of magnitudes larger than the size of the cells), cooperative communication involving everyone in a large cell population can result in the production of bioluminescence in quorum-sensing, bacterial communities [48–50] or the extension of the limits of habitable temperatures for antioxidant-secreting yeasts [51]. At a spatially small scale (a few microns), cells only cooperate with direct neighbours such as *E. coli* bacteria in coordinating metabolic processes [52, 53]. Often, however, cooperative communications involve various length-scales and time-scales, such as those observed in the formation of tumours only if enough healthy cells accumulate oncogenic mutations to collectively overcome the anti-tumour signals from surrounding, healthy tissue [54].

Several recent studies of immune cells serve as insightful case studies for revealing design principles of biological processes involving cooperative communications, such as immune responses, by coupling mathematical models of cell-cell communication with quantitative experiments.

Generally, an immune system's primary task is to distinguish the antigens that belong to the body from those of foreign cells, to eliminate the invading pathogens. Eliminating pathogens typically involves several types of immune cells that coordinate their actions by communicating across wide spatial and temporal scales with myriad cytokines [55, 56]. As an example, consider a skin inflammation that occurs because of the skin being injured or invaded by pathogens (Fig. 1.4A) [57]. Here, keratinocytes that reside in the epidermis sense the invasion and then respond by secreting cytokines such as IL-1α. Upon sensing IL-1α, macrophages, which are strategically positioned close to the blood vessels underneath the skin, recruit other cells such as the dendritic cells, CD8β T-cells, and neutrophils to the infected site. In this way, a short-range communication initially clusters nearby immune cells to halt the spread of pathogens, and a long-range communication results in initially distant immune cells being recruited to the site of injury to eliminate the trapped pathogens. A mathematical model that integrates all these processes, which does not yet exist, would likely enable one to determine whether there is any advantage to why certain parameters such as the secretion rate of IL-1α is set the way they are and how tuning such parameters may optimize the immune systems' response to skin infections.

Researchers showed that an autocrine-signalling cytokine, IL-2, controls the population density of CD4+ T-cells by simultaneously promoting proliferation and death of the T-cells (Fig. 1.4B) [58]. A minimal mathematical model – treating IL-2 as uniformly mixed (i.e., well-mixed) throughout the culture medium – revealed why this dual yet paradoxical action by IL-2 is beneficial. A nonlinearly

increasing proliferation rate (i.e., a sigmoidal function) and a linearly increasing death rate as a function of IL-2 concentration causes that populations above a certain threshold density avoid extinction and its density is stably maintained at a level that is below the carrying capacity [58, 59]. Having IL-2 control both proliferation and death is less error-prone for controlling a population density than having two separate cytokines [58]. Another recent study combined a similar mathematical model with experiments to show how two cell types – fibroblasts and macrophages – that exchange two paracrine growth factors, CSF-1 (sensed by macrophages) and PDGF (sensed by fibroblasts), stably and robustly maintain a fixed ratio of their cell densities (Fig. 1.4C) [60]. The model revealed three possible ratios of macrophage-population density to fibroblast-population density that can remain stable over time: both cell types are abundant, only fibroblasts are abundant whereas macrophages are nearly extinct, and both cell types are nearly extinct [61].

Such community effects due to secreted cytokines can propagate across vast distances, in part because of the body's endocrine system [62–65]. T-cells rely on signals from both their immediate surroundings (e.g., contact-dependent TCR) and more distant surroundings (e.g., diffusing IL-2) to distinguish multiple antigens [66]. Thus, discriminating body's own antigens from foreign ones often involves multiple cells.

At times, an immune cell needs to sense multiple cytokines from cells far away (e.g., via the body's endocrine system) as in the case of cytokines controlling the proliferation of T-effector cells [69] or the survival of resting T-cells [70]. At other times, immune cells locally interact, by creating a local niche of diffusing IL-2 around themselves, as in the case of CD4+ memory T-cells controlling their proliferation and differentiation by interacting with their neighbours [47]. Such local cytokine niches have a size that depends on the diffusivity of cytokines and the cytokine consumption rate of surrounding cells – together enabling sizes of 30-150 microns that surround a cytokine-secreting cell [64, 65, 71].

An example of a model involving multiple length-scales and time-scales comes from a recent study that revealed how hair follicles on the mouse skin regenerate plucked hairs by using a complex form of quorum-sensing that involves cytokines and chemo-taxing cells on a scale of 1 mm [67] (Fig. 1.4D). Here, the researchers discovered that a hair follicle regenerates its plucked hair if and only if enough damaged hair follicles (a "community") have created enough concentration of secreted the chemo-attractant, CCL-2, which in turn recruits TNFα-secreting M1 macrophages for regeneration. Such threshold response enables worthwhile hair regenerations to occur (i.e., only in major hair losses) while ignoring one or a few lost hairs.

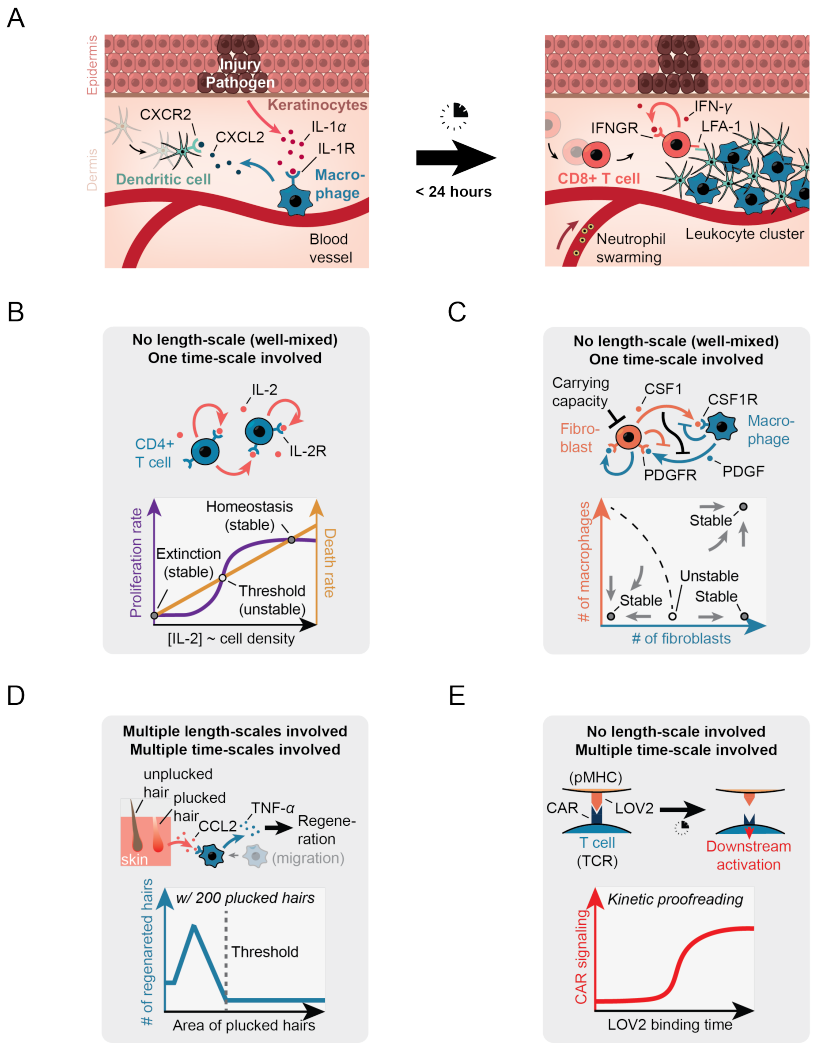

Figure 1.4: Case studies of cell–cell communication in immunological processes. **(A)** Schematic showing skin injury by invading pathogens. Left panel shows the immunological processes that occur soon after the skin injury, and the right panel shows how the skin injury is repaired [57]. **(B)** Population density of murine CD4+ T-cells controlled by their secreted IL-2 that they sense with the receptor (IL-2R). IL-2 simultaneously controls the proliferation rate (purple curve) and the death rate (orange curve) as shown in the graph. The graph shows two population densities that can be stably maintained (nearly zero and a value below a carrying capacity) and one that can be unstably maintained ("threshold" value) [58, 59]. **(C)** Stable and robust maintenance of a ratio between two population densities (densities of fibroblasts and of macrophages). Fibroblasts secrete the autocrine and paracrine growth factor CSF1 and express the receptor, PDGFR, to sense the PDGF and the receptor, CSF1R, to sense the CSF1. Macrophages secrete the paracrine growth factor, PDGF, and express the receptor, CSF1R, to sense the CSF1. The graph shows three ratios of population densities that can be stably maintained and one that is an unstable, steady-state ratio [60, 61]. (*Caption continued on next page.*)

Figure 1.4 ***(previous page)*****: (D)** Regeneration of hair follicles on mouse skin by quorum-sensing. Plucked, distressed hair follicles secrete CCL2 which is sensed by M1 macrophages that are in turn recruited to the distressed follicles. Then, macrophages secrete TNF-α which then activates regeneration of the distressed hair follicles. Graph shows the number of regenerated hairs (blue curve) as a function of the skin area from which 200 hairs are plucked—only high density (small area) leads to appreciable regenerations [67]. **(E)** Kinetic proofreading as a mechanism to explain how a T-cell can distinguish between self and foreign peptides. Top cartoon shows a schematic of a recent experiment in which the binding time of the CAR (TCR) to LOV2 (pMHC) was optogenetically controlled. Graph shows the downstream activation in T-cell (CAR signaling) occurring only when the pMHC-TCR complex lives longer than a certain threshold duration [68]

Ignoring the spatial distribution of cells does not necessarily mean that the model is simple. A model for a single cell can be highly complex if it includes multiple signals as variables. For example, T-cells perform computations to combine multiple signals into a coordinated response [71–75], as recently modelled for CD8+ T-cells controlling their proliferation by linearly summing TCR-mediated juxtacrine signals and ligands bound to other receptors (e.g., CD27, CD28) [76]. Different types of cells may also compete for multiple signals in their shared environment as in the case of T-helper and T-regulatory cells that compete for the extracellular IL-2 and other cytokines [71, 77].

A model of signal transduction within a single cell that involves multiple timescales can highlight the challenges in treating multiple scales [64, 65]. An example is the modelling of kinetic proofreading – a mechanism originally proposed by John Hopfield and Jacques Ninio [78, 79] and by which T-cells are thought to distinguish a small difference in the amount of time that peptides (pMHC) on the body's own cells spend being bound to T-cell's receptor (TCR) from the amount of time that pMHC on foreign cells spend being bound to TCR [80, 81] (Fig. 1.4E). Recent experiments that optogenetically controlled the binding-times (half-lives) of the LOV2-CAR complex partly support the idea that kinetic proofreading occurs in T-cells [68, 82]. These and other experimental results together with the model for kinetic proofreading can explain why a T-cell that encounters the myriad pMHCs that belong to the body remains inactive, whereas encountering a few rare foreign pMHCs would become active [83].

Models with simplifying assumptions such as treating cytokines as well-mixed, which allows one to ignore spatial arrangements of cells, can yield valuable insights. An important future endeavour is modelling collective behaviours based on cooperative communications in which cells move and interact across vast distances and involve multiple time-scales. Such phenomena include quorum-sensing bacteria invading a host [84, 89], swarming neutrophils fighting the invading pathogens [90, 91], and the series of cellular interactions that follow after bacteria (e.g., *S. aureus*) infecting the skin (Fig. 1.5A) [85]. In the case of *S. aureus* infecting the skin, various forms of cellular communication – including short-range and long-range

A

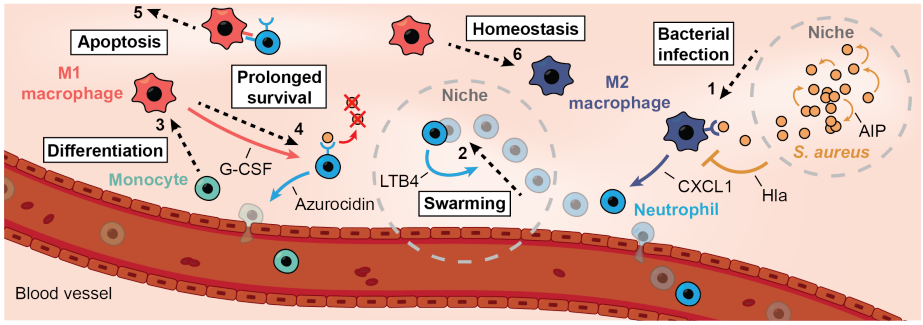

B

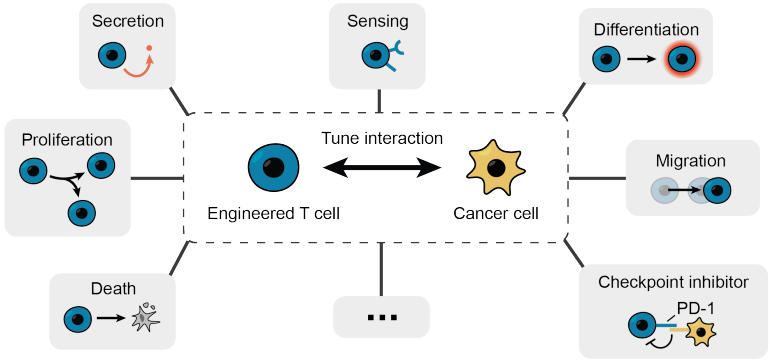

Figure 1.5: Prospects for studying cell–cell communication in immune systems. (A) Schematic showing an example of a multistep process — niche-to-niche communication — of the type for which no suitable models exist yet because multiple length-scales, time-scales and niches (or distinct communities of cooperating cells) are involved. Picture shows a step-by-step process (following the numbers in order) that occurs after *Staphylococcus aureus* infects the skin [84, 85]. **(B)** Various ingredients, shown in each box, that go into engineering T-cells (e.g., CAR-T) for cancer immunotherapy. Quantitative models will likely provide blueprints for better engineering CAR-T cells [86–88].

signalling (autocrine, paracrine, endocrine) – occur as well as multiple events that are spatially separate (indicated by dashed arrows in Fig. 1.5A) [89]. A single model that incorporates all these processes and signalling events is currently lacking and thus, unlike in the examples mentioned in Fig. 1.4, a design principle for this multistep phenomenon remains elusive.

A practical use of quantitative models for immune systems which can yield design principles that tell us why certain topologies of signalling circuits are more beneficial than others, would be as a blueprint for engineering T-cells for cancer immunotherapy [86–88]. An important question now is how one can tune features

such as secreting and sensing of cytokines, cell proliferation, apoptosis, differentiation, cell movements, and checkpoint inhibitors (Fig. 1.5B). Finding optimal ways to coordinate these processes would benefit from a model that incorporates all these processes under one roof and may lead to more effective means to target cancer cells in CAR-T therapies.

1.5. Embryonic stem cells: A model system

Stem cells are at the heart of some of the most intriguing questions in biology and medicine. Their discovery dates back to the early 1960s when researchers were looking to understand the formation of normal blood cells and leukaemia [92–94]. Ever since, stem cells were identified in various other tissue such as the intestine (carrying a Lgr5 marker [95]) or central nervous system (neural stem cells [96]). Two properties distinguish stem cells from any other cell: self-renewal (proliferating nearly indefinitely) and differentiation (giving rise to specialized cells). Adult or somatic stem cells reside undifferentiated near the specialized tissue they replenish and regenerate upon death or damage of the surrounding tissue. Over time their numbers are observed to decrease, as in the case of neural stem cells in the hippocampus leading to cognitive impairment through aging [97].

In 1954, Stevens and Little accidentally discovered[4] a new type of stem cell as they were examining the composition of a large testicular tumour (teratocarcinoma) on a mouse [98]. The tumour comprised different kinds of tissue, including bone, teeth, hair, muscle, skin and groups of undifferentiated cells – which Stevens later called "pluripotent embryonic stem cells" – that could give rise to various tissue types. Later, in 1981, Martin and Evans & Kaufman (independently) isolated and cultured mouse Embryonic Stem (ES) cells from embryos before their implantation in the uterus (i.e., blastocysts) [99, 100]. Blastocysts appear around 4 days after the fertilization of the egg cell (ovum) by the sperm when forming the zygote, which passes the morula stage of a few rounds of divisions before becoming a compact sphere containing two different layers of cells (Fig. 1.6) [101]. The outermost layer of the blastocyst (trophectoderm (TE) or trophoblast) eventually becomes the placenta whereas the cells within the blastocyst (inner cell mass (ICM)) become the adult mouse and thus give rise to all three germ layers being ectoderm (skin, neurons), endoderm (liver, lung, pancreas) and mesoderm (skeletal muscle, heart, blood) [101–103]. The cells of the ICM (*in vivo*) are the main source for ES cells (*ex vivo*) and are called "pluripotent" as they have the capacity to become all cell types in the adult mouse. Zygotes are "totipotent" as they can give rise to cells of both the ICM and TE. The developmental processes from zygote to adult mouse take about 20 days. The preimplantation phase of mouse and human embryonic

[4] The work was financed by a major tobacco company that wanted to prove it was the paper in cigarettes, not tobacco itself, causing diseases

development share many features [104], but the culturing of human embryonic stem cells – although identified and isolated [105, 106] – remains subject to both ethical and technical issues.

In the early stages, mouse ES cells were cultured together with mouse embryonic fibroblast (MEF) feeder cells (Martin originally used teratocarcinoma cells [99]) in medium supplemented with fetal calf or bovine serum[5]. The feeder cells secreted then-unknown signalling factors which stimulate the maintenance of self-renewal and counteract spontaneous differentiation. The responsible signalling factor was named, Differentiation Inhibitory Activity (DIA), which was found to be chemically identical to another cytokine, Leukemia Inhibitory Factor (LIF), that also inhibits the growth of myeloid leukemic cells by inducing their terminal differentiation [107]. LIF-supplemented medium is widely used, with or without serum, to culture mouse ES cells in the absence of feeder cells, although its pluripotency-stimulating effect is limited to certain types of genetic background, such as the E14Tg2A cell line derived from the 129/Ola mouse strain (originally used by Stevens [98]). As a member of the interleukin-6 (IL-6) cytokine family, LIF is a diffusible factor that upon binding to two of its cognate receptors, LIFR and GP130, activates Janus Kinases (JAKs) by auto-phosphorylation of their inhibitory domain. In the blastocyst, LIF likely has a paracrine role as it was found to be expressed in the cells of the TE whereas LIFR and GP130 (LIF's cognate receptors) were found to be expressed in the cells of the ICM [108]. A LIF signal induces downstream cascades, mainly the simultaneous activation of three major intracellular signalling pathways [107]: JAK-STAT3, PI3K-AKT and MAPK-ERK. These activated pathways transcriptionally control a major network of interacting pluripotency factors [109] – transcription factors such as Oct4, Sox2, Nanog, c-Myc, Klf4 and Rex1. Activated MAPK-ERK pathway induces differentiation, and survival through wave-like activity pulses traveling through a cell population [110], but the simultaneous activity of the JAK-STAT3 and PI3K-AKT pathways overwrite its differentiation-stimulating effect. Additionally, researchers showed the critical role of activated PI3K-AKT pathway to supress apoptosis both in mouse ES cells and mouse preimplantation embryos [111–113].

Often considered the "master" regulators of pluripotency, the three transcription factors Oct4 (also known as POU5F1), Sox2 and Nanog show binding affinity for a wide variety of promoter regions of genes, including those of each other, responsible for maintaining both *in vivo* and *in vitro* pluripotency [109, 114–116]. Moreover, researchers observed that cells expressing lower levels of Nanog[6] are prone to differentiate [118], and that both Oct4 and Sox2 additionally guide cells in ex-

[5] Fetal bovine serum (FBS) is processed blood (e.g., without red and white blood cells) from a bovine fetus, often collected at slaughterhouses, and still widely used for the *ex vivo* culture of eukaryotic cells because of its low level of antibodies and high level of growth factors

[6] Nanog's name is derived from the Irish phrase, Tír na nÓg, meaning "*Land of the Youth*" [117]

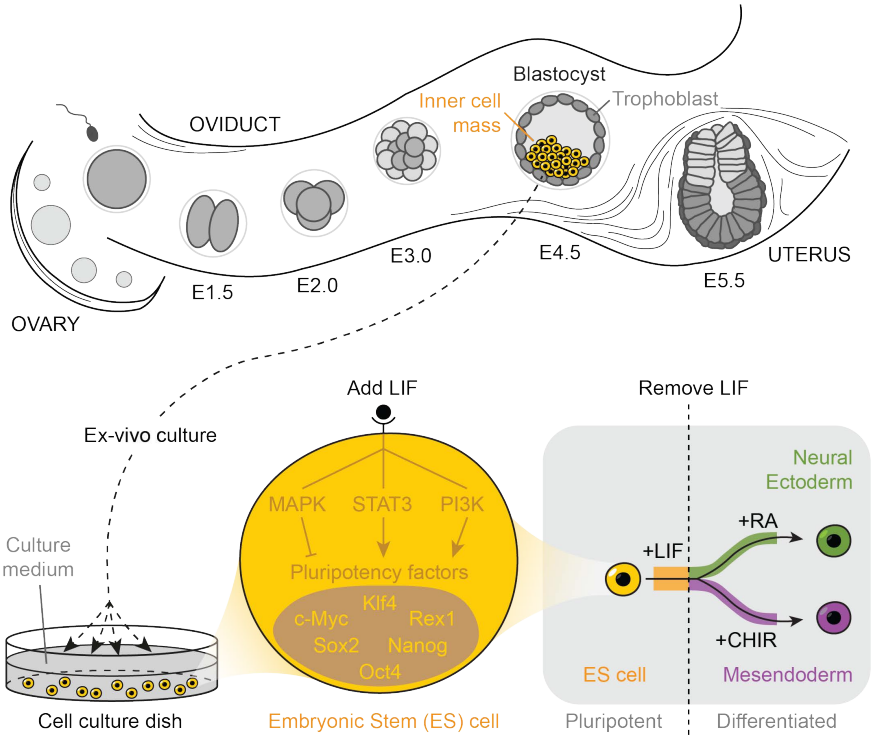

Figure 1.6: Mouse Embryonic Stem (ES) cells are an *ex vivo* model system for studying major topics in biology and medicine, such as cell signalling, cell-fate determination and cell therapy. (Top) Embryonic development of the mouse (*M. musculus*) starts with the fertilization of the egg cell (produced in the ovary) by the sperm to form the totipotent zygote, which then passes a few rounds of divisions when travelling through the oviduct during the first 3 days (indicated as "E"; e.g., "E2.0" means 2 days after fertilization) to become the blastocyst (E4.5). The blastocyst consists of two types of cell, trophoblast (which becomes the placenta) and inner cell mass (which becomes the adult mouse in about 20 days), before it implants itself in the uterus. The image is adapted from Ivan Bedzhov. (Bottom) Cells of the inner cells mass (shown in yellow) can be isolated and adapted for *ex vivo* culturing which are then known as "Embryonic Stem cells" (ES cells). Added signalling factors, most notably Leukemia Inhibitory Factor (LIF), maintain the pluripotency (ability to differentiate into all specialized cells in the adult mouse) of ES cells by upregulating pluripotency factors (such as Oct4, Sox2, Nanog, c-Myc, Klf4 and Rex1) through major signalling pathways (MAPK, STAT3, PI3K). Removing LIF causes ES cells to differentiate and to enter into either the Neural Ectoderm lineage (by adding Retinoic Acid (RA)) or Mesendoderm lineage (by adding CHIR99021 (CHIR)).

iting pluripotency and differentiating into all germ layers [119]. The pluripotency transcription factor Klf4 was found to contribute to the maintenance of telomerase activity, and thus the capacity of stem cells to proliferate indefinitely without shortening the ends of their chromosomes (telomeres), which usually underlies the aging process in most somatic cells [120]. Researchers observed that c-Myc, another transcription factor, not only is indispensable to maintaining pluripotency [121], its depletion causes both blastocysts and mouse ES cells to enter a reversible,

pluripotent dormant state (similar to embryonic diapause where a blastocyst autonomously delays its implantation in the uterus under unfavourable conditions) [122] and its variable expression allows embryos to maintain the purity of their pool of pluripotent cells before differentiation [123]. Yamanaka and others showed that an ectopic expression of only four factors – Oct4, Sox2, c-Myc and Klf4 – induces the reprogramming of any somatic cell, derived from a mouse [124] or a human [125], into a pluripotent cell. In 2012, Yamanaka and Gurdon, the latter of whom also discovered "community effects" in cells, were awarded the Nobel Prize for Physiology or Medicine for their ground-breaking discovery.

Upon the withdrawal of pluripotency-stimulating factors, most notably LIF, from the cell culture medium, mouse ES cells begin to exit the pluripotency state by breaking down the expressions of pluripotency factors [109, 114–116], and then choosing to differentiate into progenitor cells of the Neural Ectoderm (NE) lineage or Mesendoderm (ME) lineage [114, 119, 126–130]. Cells base their decision to enter one of the two lineages on signalling factors in their environment [131]. Entry into the NE lineage depends on endogenous factors such as Fibroblast Growth Factors (FGFs), notably FGF4 [132] (although FGF4 was found to be a major differentiation stimulus for both NE and ME lineage [133]), known to have an indispensable role in the regulation of proliferation and differentiation of mouse ES cells and preimplantation embryos [134–136], and depends on recombinant factors such as Retinoic Acid (RA) [129]. Entry into the ME lineage depends on other endogenous factors such as autocrine Wnt signals [137, 138], most notably Wnt3a [139] which was also shown to cause asymmetric division of stem cells (i.e., one daughter cell differentiates and the other daughter cell remains pluripotent) [140], and depends on recombinant factors such as the synthetic Wnt agonist, CHIR99021 (CHIR) [119]. Other factors – such as TGF-β [137], SCF (a major therapeutic target; also known as c-KIT) [141–144], Sonic Hedgehog (required for neurogenesis) [145], BMP (maintains pluripotency together with LIF in serum-free medium) [146], and the synthetic factor PD0325901 (inhibits MAPK and together with CHIR makes up the two inhibitors ("2*i*") in 2*i*+LIF medium as a serum-free, pluripotency medium) [119] – have essential roles in the maintenance of pluripotency or triggering of (terminal) differentiation. Moreover, mouse ES cells uniquely control their cell cycle (unusually short G1 phase, absence of cyclin D proteins, lacking G1-S transition) [131, 147], survival [148–150], apoptosis [151], quiescence [152, 153], and homeostasis of number of cells [154]. Major transcriptional regulators, such as Sox1 and Brachyury, serve as differentiation markers for the entry of cells into the NE or ME lineage, respectively [119, 126].

In summary, mouse ES cells serve as ideal testbeds for studying diverse processes and applications such as self-organization [155], autocrine and paracrine signalling e.g. with microfluidics [156, 157], molecular circuitry for reprogramming [109],

robustness of mammalian development based on growth factors [158], influence of cell aggregation on differentiation [159], stem cell secretome in regenerative engineering [160, 161], immunotherapy [70], and metastasis of cancer in the presence of cancer stem cells expressing pluripotency factors [162].

2

Embryonic stem cells collectively survive during differentiation

Parts of this chapter are also reported in Daneshpour et al. [2]

2.1. Introduction

Who is talking to whom? A basic question that is easy to state and yet notoriously difficult to address for cells in a population. Embryonic Stem (ES) cells, which are important for synthetic biology as *ex vivo* cell cultures, secrete and sense myriad diffusive factors that control their own proliferation, death, or exit from pluripotency on cell-culture plates [163]. By secreting and sensing the same molecule - that is, through an "autocrine signaling" [26] - an ES cell can communicate with itself (self-communicate) by capturing the molecule that it had just secreted or communicate with other ES cells (neighbor-communicate) due to its molecule diffusing to and being captured by those other cells [19, 20, 22, 164]. Although many autocrine-signaling molecules for ES cells are known - such as the Fibroblast Growth Factors (FGFs) that promote cell proliferation [158, 165–168] - it is unclear to what extent each of these autocrine-signaling molecules are used for self- versus neighbor-communication and how each type of communication controls one cell's differentiation. Determining which cell is communicating with which cell is challenging because a molecule does not leave a visible trace of its diffusive path, from a cell that secretes it to a cell that captures it (which may be the same cell).

Complicating the matter is that having two cells next to each other does not necessarily mean that they are communicating with each other. This is because a receptor may have a high binding-affinity for the autocrine-signaling molecule (e.g., EGF receptor), meaning that most copies of the molecule can be captured by the cell that secreted them and, therefore, very few remaining copies of the molecule are left for communicating with other cells [19, 158]. Conventional approaches for proving the existence of secreted factors and/or manipulating them – such as transferring medium from one cell-culture plate to another (i.e., transferring a "conditioned medium") or washing/flowing media over cells with microfluidics – cannot determine the degree of self- versus neighbor-communication for an autocrine factor and the spatial range of a neighbor communication. This is because the conventional approaches - despite providing valuable insights and showing that secreted factors exist - involve either pooling together all molecules from everywhere on a cell-culture plate, uniformly mixing them, and then giving this mixture to cells on a new plate (e.g., in the case of transferring a conditioned medium) or accumulating all molecules with a gradient along one direction (e.g., in the case of microfluidics). Hence, these widely used methods destroy crucial, spatial information such as how far each autocrine factor travels when undisturbed, which cells secreted the factor, and which cell senses the factor.

Moreover, while several effects that depend on ES-cell density are known – such as cell growth enhanced by accumulation of secreted growth factors at high cell-densities – it is unclear, due to the ambiguities mentioned above, whether these

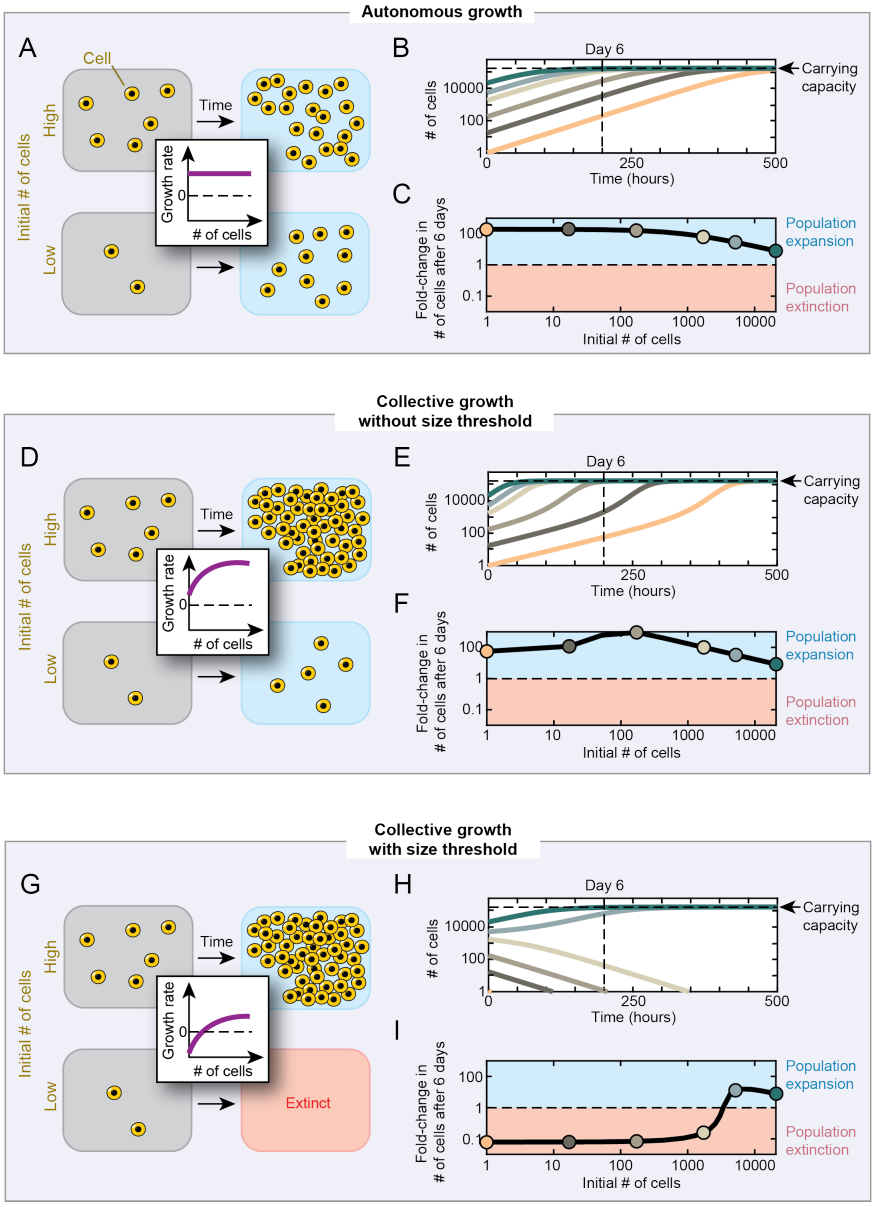

Figure 2.1: Modelling autonomous and collective growths of cells. To understand how the growths of cells, either independently (i.e., autonomous growth) or mediated by a communication signal (i.e., collective growth), differ from each other, we built a simple model to compare each of the possible scenarios.

(*Caption continued on next page.*)

Figure 2.1 ***(previous page)*****:** For the model, we assumed that cell populations grow according to the logistic equation (Verhulst model): $\frac{dN}{dt} = (1 - \frac{N}{K})rN$, where N represents the number of cells in time, K the carrying capacity of the cells' habitat (determined by the availability of food, space, etc), and r the net growth rate of the cells. The net growth rate r can be either a constant (a positive number) or depend on a communication signal (e.g., a molecule secreted by the cells and hence depending on the number of secreting cells) that controls the net growth rate according to the Michaelis-Menten equation: $r(N(t)) = \frac{\mu_{max}N(t)}{K_M+N(t)} + r_0$, where μ_{max} is the maximum net growth rate, K_M the Michaelis constant the number of cells at which the net growth rate equals half of the maximum net growth rate, and r_0 a constant (a positive or negative number). Here, we assumed that the net growth rate depends on the concentration of the communication signal which in turn is instantaneously set by the number of cells in time. We used a custom MATLAB script to solve the differential equation for the following initial number of cells $N(0)$: 1; 17; 172; 1724; 5172; 20690. We computed the number of cells in time between 0 and 500 hours and the fold-change in the number of cells at an intermediate time-point (called "day 6"). The carrying capacity K is indicated with a horizontal dashed line, and a "population expansion" (blue shade) and "population extinction" (red shade) refer to a fold-change that is above and below a fold-change = 1, respectively. Growth curves are shown in panels B, E and H. Fold-change in the number of cells after 6 days is shown in panels C, F and I. **(A)** Autonomous growth. The values of the model parameters: K = 172414 and r = 0.0264. Cells at any initial number (even 1 cell) always expand toward the carrying capacity. **(B)** Cells at any initial number of 1 (lowest) to 20690 (highest) always grow until they reach the carrying capacity (horizontal dashed line). **(C)** All initial number of cells result in population expansion. **(D)** Collective growth without a size threshold. The values of the model parameters: K = 172414, r = 0.0264, μ_{max} = 0.0519, K_M = 3500 and r_0 = 0.02. Cells at any initial number (even 1 cell) always expand toward the carrying capacity. **(E)** Similar to autonomous growth, cells at any initial number of 1 (lowest) at 20690 (highest) always grow until they reach the carrying capacity (horizontal dashed line). **(F)** All initial number of cells result in population expansion. **(G)** Collective growth with a size threshold. The values of the model parameters: K = 172414, r = 0.0264, μ_{max} = 0.0519, K_M = 3500 and r_0 = -0.0256. Unlike autonomous growth and collective growth without a size threshold, only cells above a threshold number of cells expand toward carrying capacity otherwise cells become extinct. **(H)** Only cells that start below ~3400 initially expand toward the carrying capacity, otherwise they become extinct. **(I)** Only above-threshold (~3400) initial number of cells result in population expansion.

density-dependent effects are due to a local communication between cells that are packed close to each other or due to cells that are millimeters-to-centimeters apart potentially stimulating one another through long-distance communication. In other words, does a cell survive because there are sufficiently many cells nearby that are all helping each other by secreting growth factors (as can be the case in a high density cell-culture in which cells tend to be near each other and only local communication exists) or does a cell survive because distant cells that are centimeters away help one another grow and survive (as can be the case in a high density cell-culture in which distant cells can communicate but local communication is weak or absent)? Ambiguity arises here because both scenarios can result in the same abundance of growth factors in the pooled medium.

Complicating the issue even further is that some ES-cell secreted factors remain unidentified and many well-known ones, such as FGF4, have new roles that are still being elucidated [158]. Given all these reasons, we generally do not know which pairs of cells - whether they are ES cells or not - are communicating through

diffusive molecules and exactly how far apart they can be before communicating becomes impossible. These questions are simple to state and are fundamental to understanding cell-cell communication. But they remain difficult to answer. Consequently, in the context of ES-cell cultures, we currently lack *a coherent, quantitative picture of how all the secreted factors - both known and unknown - collectively and spatiotemporally regulate ES cells' proliferation, death, and exit from pluripotency*. Such a picture would rigorously reveal to what extent ES cells form a collective entity in which they cooperate to survive and differentiate. Establishing such a quantitative, comprehensive picture may reveal that a large-scale (nonlocal) cooperation exists among differentiating ES cells. More generally, quantitatively establishing the "community size" and thereby a cell's degree of autonomy is a conceptual challenge that is relevant in many contexts, including for microbial communities [52] and for rigorously settling an open question of how exactly cell-cell communication may influence the efficiency of reprogramming adult cells into induced Pluripotent Stem Cells (iPSCs) [169].

The goal of our study is to use ES cell-culture as a test-bed to address this conceptual challenge - rigorously establish how autonomous and collective a cell is - by developing a systematic approach that integrates quantitative experiments and modelling. As a starting point, we examined how the overall behaviour of autonomously and collectively growing cells differ from each by modelling population growth ((Fig. 2.1)). Autonomous growth involves all cells growing with the same (constant) net growth rate (i.e., cell growth regardless of the initial number of cells) (Fig. 2.1A-C) and collective growth lets all cells' net growth rate depend on the concentration of a signal (e.g., a secreted factor) and thus the total number of cells that exist now (i.e., cell growth regardless of the initial number of cells) (Fig. 2.1D-F). From an outside (observer) perspective, one cannot immediately distinguish whether cell growth is autonomous or collective, let alone that it involves local or nonlocal communication among cells if it were collective. A distinct scenario is for cells that require starting above a threshold initial number of cells to enable collective growth (or else they become extinct) in a "switch-like" manner (Fig. 2.1G-I).

Revealing the existence of a "threshold" - which dictates a collective, "switch-like" behaviour - in a cell population may also disclose how cells spatiotemporally cooperate in their habitat. Therefore, we sought to explore whether ES-cell behaviour involves a (threshold-based) collective growth.

2.2. Results

2.2.1. Setup of ES-cell cultures and differentiation protocols

Practical experience often shows that seeding too few ES cells on a cell-culture dish causes suboptimal growths of cells in various types of cell-culture media. Although one usually seeds enough ES cells to keep many of them "*healthy*", it is unclear how many is "*too few*", what actually constitutes "*enough*" numbers of ES cells, whether or not there is a sharp threshold in the number of cells that separates the "*too few*" from the "*enough*" - and if so, what the underlying molecular mechanism is - and the area over which the cell density matters (e.g., # of cells / cm^2). Currently lacking is a systematic exploration of these issues, in which one precisely sets and varies the initial numbers of ES cells over a wide range and then studies the resulting growth of ES cells.

We posited that this phenomenon may be masking a community effect that might be mediated by a long-range communication. We systematically re-examined this phenomenon as our starting point. Specifically, we examined how mouse ES cells proliferate during self-renewal (pluripotency) and differentiation (exit of pluripotency) when they are sparsely scattered as near-single cells across a 10-cm diameter dish, at lower densities than is the standard for both self-renewal and differentiation conditions.

To do this, we first kept ES cells pluripotent (undifferentiated) by culturing them without any feeder cells and with Leukemia Inhibitory Factor (LIF) in either a serum-containing (FBS) or a serum-free (2*i*) medium. To initiate differentiation, we detached the pluripotent cells from dishes, resuspended them in PBS, counted their numbers in suspension (Supp. Fig. 2.7), and then randomly scattered a fewer-than-usual number of cells across a 10-cm diameter dish to obtain a desired population density (# of cells per cm^2 of dish area, from ~5 to ~15,000 cells / cm^2). This dish contained a "differentiation medium" (N2B27 [126] – see Materials and methods) which, lacking LIF, triggered the cells' exit from pluripotency (Fig. 2.2A).

With a wide-field microscope, we verified that this method of seeding led to virtually identical sizes of microcolonies (colony seeds) across all initial population densities on a plate at the start of differentiation (Fig. 2.2B). Even for some of the highest population densities examined, cells collectively covered less than 1% of the total plate area (Fig. 2.2B - bottom). Hence, any result that we will discuss below is not due to having highly confluent microcolonies or dishes. Two days after initiating differentiation, we added one of two inducers - Retinoic Acid (RA) or CHIR - to induce differentiation towards either a Neural Ectoderm (NE) lineage (with RA) or a Mesendoderm (ME) lineage (with CHIR) (Fig. 2.2A). An ES cell must first choose to enter either one of these two lineages before becoming any differentiated, somatic cell. We waited two days before adding the inducers because

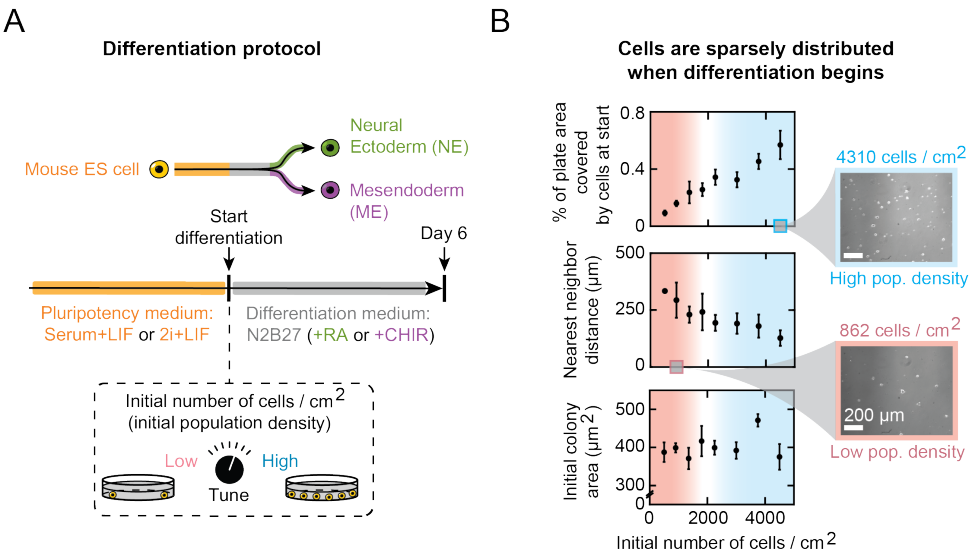

Figure 2.2: Protocol to differentiate sparsely distributed ES cells by tuning initial population density. (A) Differentiation protocol used in this study. See Materials and methods (Chapter 7). **(B)** As a function of initial number of cells seeded on a 10-cm diameter dish with 58 cm^2 surface area (i.e., initial population density): percentage of the dish area initially covered by microcolonies (top graph), distance to a microcolony's nearest neighbour on average (middle graph) and initial area of a microcolony on average (bottom graph). Microscope used to measure both. Blue shade indicates population expansion. Red shade indicates population extinction. Two example microscope images shown. Scale bar = 200 μm. n = 3; Error bars are s.e.m.

ES cells take at least two days to exit pluripotency by degrading their pluripotency factors such as Oct4 (Supp. Fig. 2.8) [119]. To not disturb any diffusible factors that mediate cell-cell communications, we did not shake or move the plates in any way during their days-long incubation and we discarded each plate after detaching all its cells to measure its population density.

We used two methods in parallel to confirm that ES cells are either pluripotent (undifferentiated) or differentiated (e.g., towards a NE lineage). First, a visual inspection of the morphology of ES-cell colonies often reveals whether it consists of differentiated cells or not (Fig. 2.3). A pluripotent ES cell appears as aggregated into tight colonies with the edges of the colonies as sharply distinct from the gelatin-coated surface area of the dish they are attached to. This phenomenon is reported in previous studies as well (e.g., [170]). Second, at the end of a differentiation experiment we used a flow cytometer to measure each ES cell's ability – after detaching them from dishes and resuspending them in PBS with 4% FBS – to express GFP driven by the *Sox1* promoter (a well-known, early marker in NE-lineage commitment as used previously [126]) (Fig. 2.4). In this way we obtained single-cell data that shows whether an ES cell expresses GFP or not; and therefore

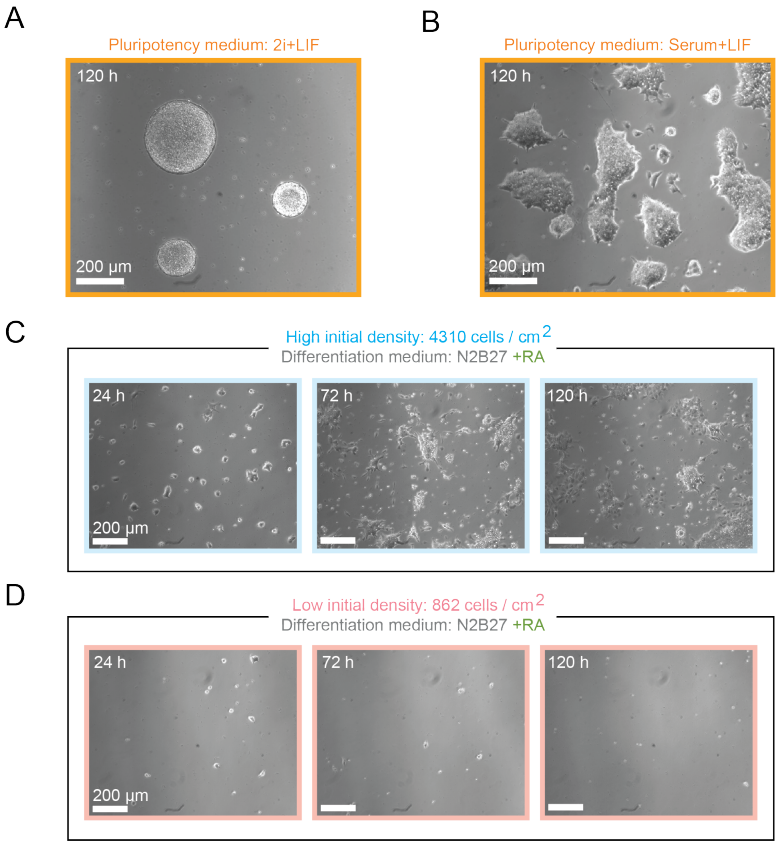

Figure 2.3: Example microscope images of pluripotent and differentiating ES cells. (A) Image of ES cells cultured for 5 days (120 hours) in 2*i*+LIF medium (pluripotency medium). Cells are aggregated in tight colonies (with distinctive edges). Scale bar = 200 μm. **(B)** Image of ES cells cultured for 5 days (120 hours) in serum+LIF medium (pluripotency medium). Cultures typically show few/no apoptotic bodies. Scale bar = 200 μm. **(C)** Time-lapse images of ES cells differentiating into Neural Ectoderm (NE) lineage and started at a high initial density (4310 cells/cm^2). Despite large, differentiated cell colonies, cultures typically show many apoptotic bodies (floating cell corpses). Scale bar = 200 μm. **(D)** Time-lapse images of ES cells differentiating into Neural Ectoderm (NE) lineage and started at a low initial density (862 cells/cm^2). Scale bar = 200 μm.

the percentage of an ES-cell population successfully differentiated towards a NE lineage.

Lastly, we confirmed that our differentiation protocol results in ES cells successfully expanding (≥10-fold in 6 days) and differentiating into a NE lineage (≥80% becoming Sox1-GFP positive), regardless of the use of serum (FBS) during self-renewal and regardless of the use of Retinoic Acid (RA) during differentiation. Our results are in agreement with established protocols [126, 146, 171].

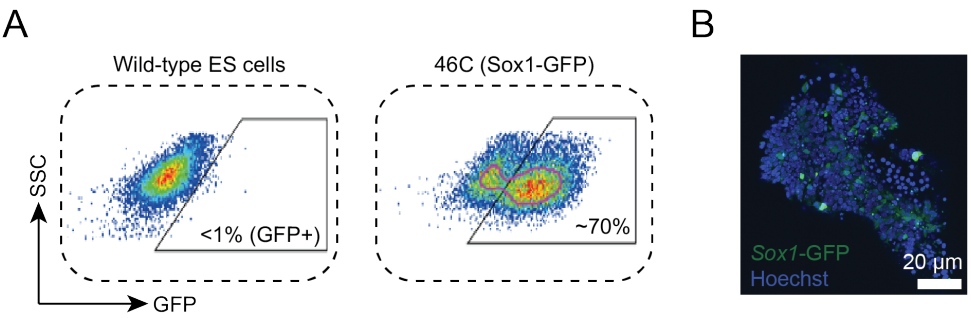

Figure 2.4: Quantitative method to identify percentage of 46C cell population successfully differentiated into Neural Ectoderm (NE) lineage. (A) FACS gating (trapezium shown) to determine % of ES cells differentiated into NE lineage through GFP driven by the *Sox1* promoter (NE marker). Control (wild-type ES cells, E14) gives negligible GFP-positive (+) cells. **(B)** Confocal microscopy image of 46C cells after 3 days in differentiation medium (N2B27). GFP (shown in green; driven by *Sox1* promoter) and Hoechst (shown in blue; DNA assay with 12 ng/mL Hoechst 33342) are shown. Scale bar = 20 μm.

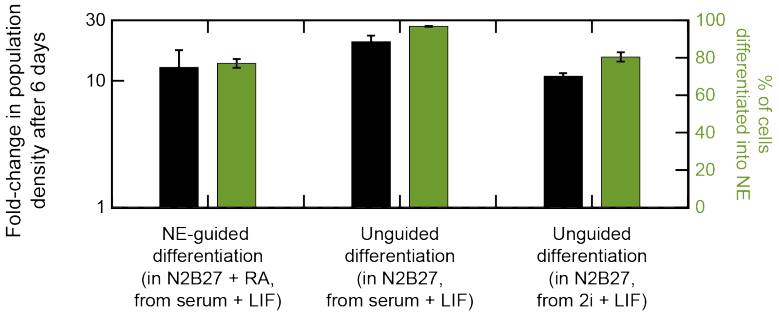

Figure 2.5: ES cells successfully grow and differentiate into Neural Ectoderm (NE) lineage, regardless of the use of serum during self-renewal and regardless of the use of Retinoic Acid (RA) during differentiation. We confirmed that our differentiation protocol results in ES cells successfully expanding and differentiating into the Neural Ectoderm (NE) lineage, regardless of the use of serum-(FBS)-based medium (serum + LIF) or serum-free medium (2*i* + LIF) during pluripotency prior to differentiation, and regardless of the use of N2B27 supplemented with or without Retinoic Acid (RA) (NE-guided or unguided differentiation, respectively). Data derived from 46C cells (*Sox1*-GFP) at initial densities of 3448 cells / cm^2 (left graph) and 8620 cells / cm^2 (middle and right graphs). n $\geq$ 3; error bars are s.e.m.

2.2.2. ES cells collectively grow with a density threshold during differentiation, but not during pluripotency

We first examined the NE-lineage commitment with RA using a cell line, denoted 46C, that expresses GFP driven by the *Sox1* promoter, which becomes expressed early in NE-lineage commitment. We found that cell populations that began with a sufficiently high density (above ~1700 cells / cm^2) grew towards the carrying capacity (Fig. 2.6A - top row) whereas populations that began with a sufficiently low density (below ~1700 cells / cm^2) approached extinction over six

days (Fig. 2.6A - bottom row). A population that nearly began with a "threshold density" (~1700 cells / cm^2) neither noticeably grew nor shrank during the first six days (Fig. 2.6A - middle row). But, sometime after, the population either suddenly grew towards the carrying capacity or shrank towards extinction (Supp. Fig. 2.9). Specifically, our method of using an ensemble of many dishes that all started with the same density revealed that two populations starting with the same near-threshold density could exhibit two distinct fates: one expanding and one becoming extinct (Supp. Fig. 2.9). Furthermore, using a flow cytometer to measure the percentage of cells expressing GFP over time revealed that higher initial population densities led to higher percentages of cells committing to the RA-induced NE-lineage after six days (Fig. 2.6A - right column).

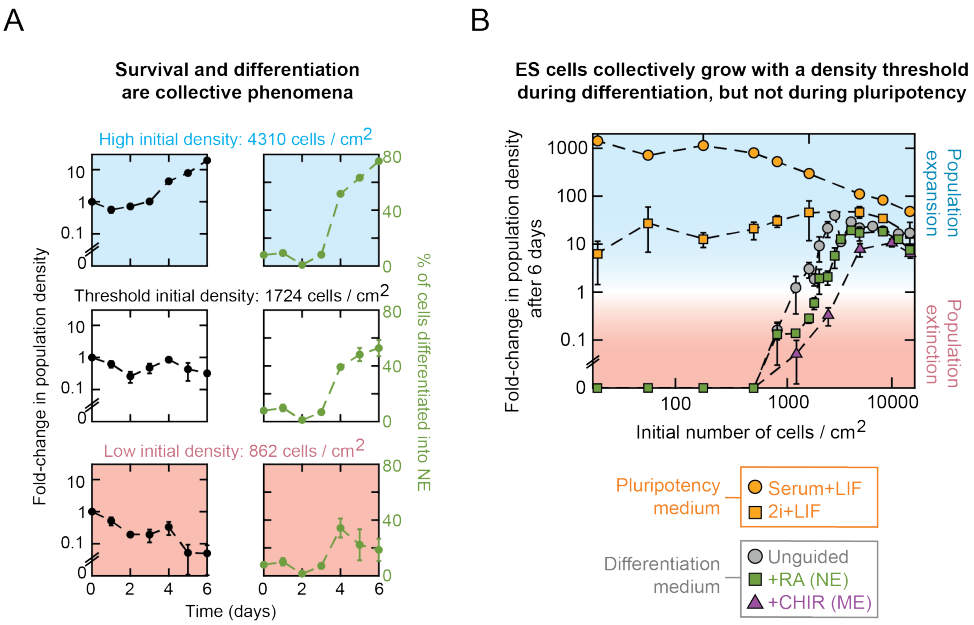

Figure 2.6: ES cells collectively grow with a density threshold during differentiation, but not during pluripotency. (A) Fold-change in population density (black) and % of cells entering Neural Ectoderm (NE) lineage (i.e., % of cells expressing Sox1-GFP) (green) as a function of time after RA-induced differentiation starts. Indicated above each row is the initial population density for the population shown in that row (See also Supp. Figs. 2.9, 2.10, 2.11). Data for 46C cells previously self-renewing in serum+LIF. n ≥ 3. Error bars are s.e.m. **(B)** As a function of initial population density, fold-change in population density after 6 days in pluripotency medium (orange) or one of three differentiation media (grey - N2B27 without any inducers; green - N2B27 with Retinoic Acid (RA) that induces NE-lineage differentiation; purple - N2B27 with CHIR that induces Mesendoderm (ME) lineage differentiation). Cell lines used: E14 (orange and grey), 46C (green), and Brachyury-GFP (purple). See Supp. Fig. 2.12 for all cell lines and media types. Blue shade indicates population expansion. Red shade indicates population extinction. n ≥ 3; Error bars are s.e.m.

We determined the "survival-versus-extinction" fate of a population for a wide range of starting densities (Fig. 2.6B). Importantly, we observed this phenomenon

for all three widely used ES-cell lines (E14, 46C [126], and Brachyury-GFP cell lines [172, 173]) (Fig. 2.6B and Supp. Figs. 2.10,2.11,2.12). We also observed this phenomenon occurring for all three possible lineage inductions: NE-lineage induction with RA (Fig. 2.6B - green and Supp. Figs. 2.10,2.11,2.12), ME-lineage induction with CHIR (Fig. 2.6B - purple and Supp. Fig. 2.12), and unguided differentiation (i.e., LIF removal without any inducers) (Fig. 2.6B - grey and Supp. Fig. 2.12). In all these different conditions, the threshold value that separates the initial population-densities that lead to survival from those that lead to extinction remained nearly identical. Mapping the survival-versus-extinction fate over a wide-range of initial population densities revealed that near the threshold density, the initial population density sharply determines the survival-versus-extinction fate, in a switch-like manner (Supp. Fig. 2.9): a mere two-fold difference in the initial density could mean extinction as opposed to the population surviving (e.g., ~1500 cells / cm^2 leads to extinction whereas ~3000 cells / cm^2 leads to population expansion towards the carrying capacity, despite both densities initially covering less than 1% of the plate area).

Our quantitative approach revealed the following notion: it is not that having more cells perhaps means "enhanced" growth; rather, we uncovered here that the entire population either becomes extinct or expands to the carrying capacity, with the outcome set by a relatively small difference in initial cell numbers. With mathematical modelling and further quantitative experiments, we will later show how this sharp, switch-like response to the initial population density arises.

In contrast to the differentiating cells, self-renewing ES cells did not show signs of collective growth with a density threshold in the wide range of population densities that we examined (~5 to ~15,000 cells / cm^2). Self-renewing populations of all initial densities expanded towards the carrying capacity, both in serum (Fig. 2.6B - orange circles) and in 2*i* (Fig. 2.6B - orange squares). Notably, cells scattered around the dish at densities as low as ~5 cells / cm^2 grew by ~1000 fold in six days (Fig. 2.6B - leftmost data points in orange). Therefore, we conclude that differentiating ES cells collectively grow with a size threshold (matches Fig. 2.1 - our mathematical model) whereas self-renewing ES cells do not.

Additionally, we found that initial density strongly dictates a population's rate of losing the pluripotency marker Oct4 (Supp. Fig. 2.8). A high-density population that is destined for surviving (expanding towards the carrying capacity) has ~20% Oct4-positive cells by day 4 of differentiation, whereas a low-density population destined for extinction still comprises ~70% Oct4-positive cells. These results complement our findings on differentiation efficiencies (Supp. Fig. 2.11).

In our experiments, every population started with microcolonies that were, on average, hundreds of microns apart from one another (Supp. Fig. 2.13). Crucially,

for each initial population density, we used time-lapse microscopy to measure the distance between every pair of colonies in a field-of-view (1.40 mm x 0.99 mm) and then, from these measurements, determined the distance between a colony and its nearest-neighbouring colony at the start of the time-lapse movie (i.e., at the start of pluripotency loss) (Fig. 2.3B). We found that whether a colony dies or not during the next four days and its growth rate were both independent of (uncorrelated with) the distance to the nearest-neighbouring colony for any of the initial population densities (Supp. Fig. 2.14).

2.3. Conclusions

As our starting point we asked ourselves the question: how do ES cells proliferate during pluripotency and differentiation for lower-than-usual initial densities (typically ~15,000 cells / cm^2 [171])? If the intuitive notion of "more cells mean enhanced growth" (i.e., a collective growth without a population-density threshold) were true, we would expect to observe an ES-cell population at any initial density to grow and expand toward the carrying capacity (i.e., survive). Intriguingly, this is not what we found. We discovered ES cells collectively grow (and survive) with a density threshold during differentiation, but not during pluripotency. Across a wide range of initial population density (yet still covering <1% of the cell-culture dish) we observed that a pluripotent ES-cell population of any initial density (ranging from ~5 to ~10,000 cells / cm^2) always survives and substantially expands (≥10 fold after 6 days). Differentiating cells, however, of which their initial population density starts below ~1700 cells / cm^2 become extinct over the course of 6 days whereas those that start above ~1700 cells / cm^2 survive and expand toward carrying capacity.

This collective, switch-like phenomenon is likely a manifestation of cooperativity as a result of cell-cell communication. Considering these results together, we reasoned that if cell-cell communication were responsible for above results, then it is likely a nonlocal communication (i.e., over many cell-lengths) that regulates the differentiating cells' proliferation and/or death. Since we observed the same phenomenon for all three lineage inductions and for all three different cell lines, for simplicity we will focus on the RA-induced differentiation of 46C cells previously self-renewing in serum+LIF.

As our next hypothesis (see Chapter 3) we tested whether this cell-cell communication is controlled by diffusible molecules that the cells themselves secrete and sense in their culture medium.

2.4. Supplementary Information

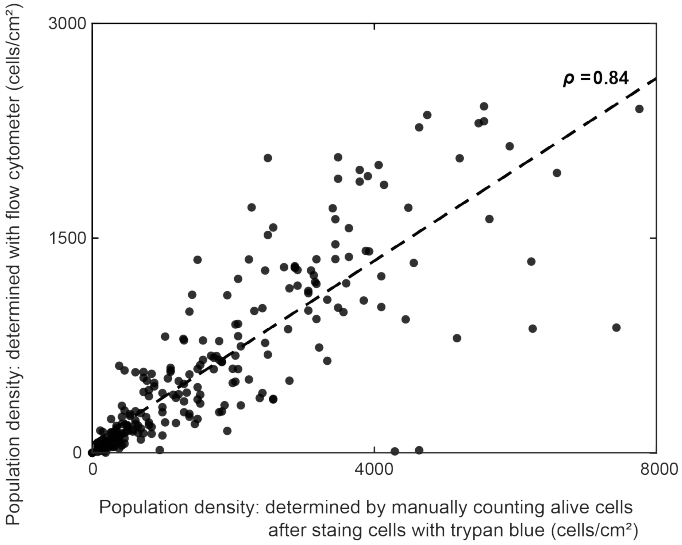

Figure 2.7: Two different methods of counting cells yield population densities that are directly proportional to each other (i.e., offset by a constant factor of order one) and in the same order of magnitude, thus affirming both methods for determining population densities. Each data point represents a single population whose density (# of cells / cm^2) was determined by two independent methods. Each axis represents a different method. As one method, we used a standard hemocytometer to count individual cells after subjecting the cells to the dye, trypan blue. Trypan blue penetrated only dead cells within the population. We counted the unstained (non-blue) cells with a hemocytometer to determine the resulting population density (# of cells / cm^2) of alive cells on a cell culture dish. As another method to determine the population density, we used a flow cytometer to count the number of cells (events) that belonged to a specified FSC-SSC gate. We set the FSC-SSC gate so that it captured alive cells while excluding dead cells. These two methods yielded cell counts - and thus the corresponding population densities - that were directly proportional to one another, as indicated by a high Pearson correlation coefficient (black line; $\rho = 0.84$). The proportionality factor is on the order of one, meaning that, for the same population, the two methods yield numbers that are in the same order of magnitude as the population density. Given this result, throughout our study, we primarily counted cells manually (i.e., with trypan blue solution) and used the flow cytometer when this was not possible. Specifically, we used the flow cytometer to count populations that had very few cells such as those near extinction (i.e., populations whose fold-change in density was near or below 0.1 after some days).

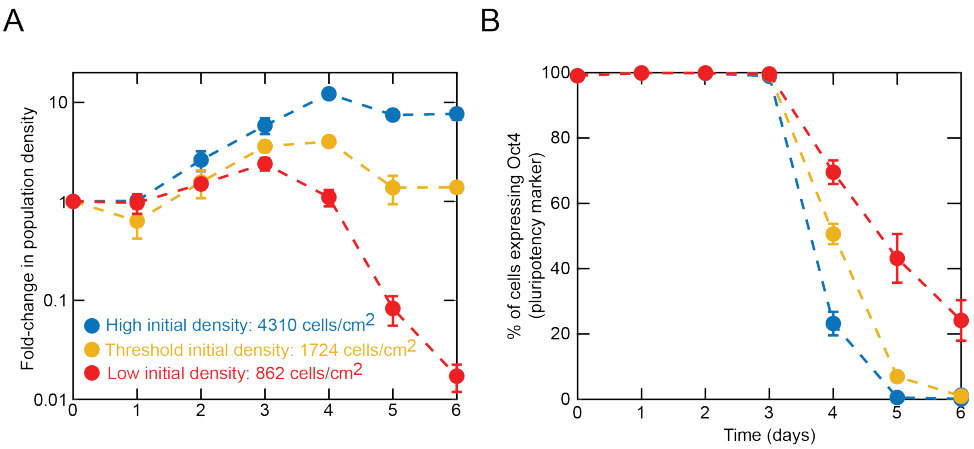

Figure 2.8: Initial population density determines the rate of loss of the pluripotency marker Oct4 during differentiation. Data shown for *Oct4*-GFP cell line (a kind gift from Austin Smith, also see [116, 174]). This cell line has the *Oct4* promoter controlling GFP expression. Different colors represent different initial population densities as indicated in the legend (4310, 1724, and 862 cells / cm^2). For each differentiation, we took the pluripotent cell line (previously cultured in 2*i*+LIF) and then started differentiation with the indicated initial population densities, adding Retinoic Acid (RA) into N2B27 medium after 2 days (i.e., on day 2). As seen here, the Oct4 degradation (as measured by the % of cells expressing GFP) during differentiation, and therefore the loss of pluripotency depends on the initial population density. n = 3; error bars are s.e.m. On day 4 of differentiation high-density populations (shown in blue) have ~20% *Oct4*-GFP positive cells whereas low-density populations (shown in red) still have ~70% *Oct4*-GFP positive cells. Intriguingly, on day 5 nearly-extinct low-density populations still comprise ~50% *Oct4*-GFP positive cells, whereas high-density populations (at carrying capacity) have virtually none. These results complement our findings on differentiation efficiencies (Supp. Fig. 2.11).

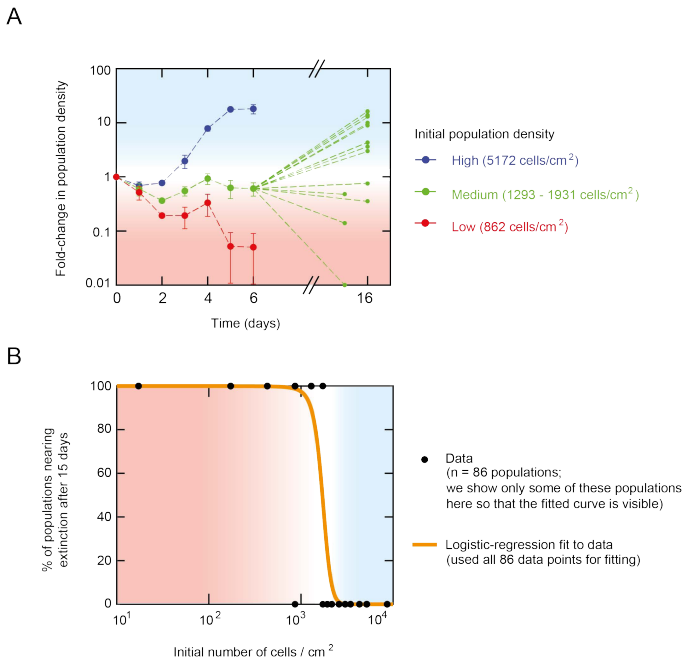

Figure 2.9: Differentiating populations that start with a (near) "threshold density" (~1700 cells/cm^2) neither expand nor shrink during the first 6 days. But, after more days, these populations either expand towards the carrying capacity or shrink towards extinction in a stochastic manner (i.e., two populations of the same starting density can have two different fates (one survives and one becomes extinct)). Data for 46C cells (i.e., cells that have *Sox1* promoter controlling GFP expression) differentiating toward NE lineage in N2B27+RA, previously self-renewing in serum+LIF. Note that Sox1 is a marker of NE lineage. **(A)** Blue: populations that started with a sufficiently high density (5172 cells/cm^2) all grew towards the carrying capacity. Red: populations that started with a sufficiently low density (862 cells/cm^2) became extinct within the first 6 days. Green: populations that started near a "threshold density" (between 1293 and 1931 cells/cm^2) neither grew or shrank in the first 6 days. However, by 15-16 days after removing LIF (i.e., beginning differentiation), some of these populations reached the carrying capacity (i.e., population density increased by ~10-folds) while some others became extinct (i.e., population density became ~0.1-fold or less than its starting value). Still, some populations maintained nearly the same density for these 15-16 days (i.e., green curves with fold change of nearly one after 15-16 days). Thus, populations having the same initial density can have distinct fates: some would become extinct and some would survive (i.e., the fate is stochastically determined). For all the data shown for the first six days, n = 3 and error bars are s.e.m. Each green data point, taken 15-16 days after triggering differentiation, represents a single population (to show the stochasticity) rather than being averaged over multiple populations. They thus do not show error bars. **(B)** To quantify the stochastic nature of the survival-versus-extinction fate for populations that start with a near-threshold density (green data in (A)), we measured the fold-change in population density for 86 populations that collectively spanned a wide range of initial densities (black points). To each population, we either assigned a value of zero if it eventually grew towards the carrying capacity (i.e., fold-change of larger than 1) or a value of one if it eventually approached extinction within the first 16 days of differentiation. Then, we performed a logistic regression on these black data points by fitting a logistic function, $\rho(x) = \frac{1}{1+e^{-(\beta_0+\beta_1 x)}}$ (orange curve). Consequently, $\rho(x)$ represents the probability that a population approaches extinction by 15-16 days after differentiation began. By fitting, we found β_1 = -8.7856 ± 0.8780 with a p-value of 3.76 x 10^{-25} according to the Wald test. This logistic regression is the simplest model (null model) that we can have for describing the probability of becoming extinct without any information about the mechanisms that determine the survival-versus-extinction fate. Later, we will introduce a mechanistic model that replaces this logistic regression fit (see Chapter 6).

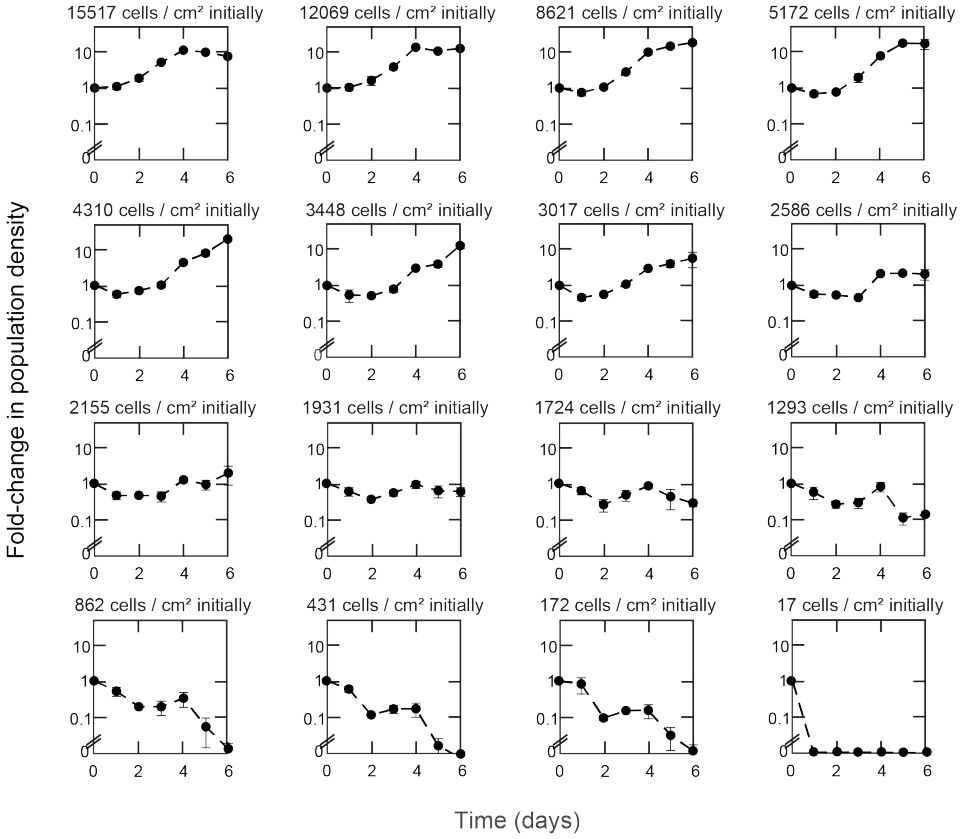

Figure 2.10: Population growth during differentiation towards Neural Ectoderm (NE) lineage for a wide range of starting population densities. Data shown for populations of 46C cells which have *Sox1* promoter driving GFP expression. 46C cells (previously self-renewing in serum+LIF) are undergoing Retinoic Acid (RA) induced differentiation (N2B27+RA) towards the NE lineage (see Material and methods). We triggered pluripotency exit to begin each time course shown here. Each box shows the population dynamics for a different starting population-density (indicated above each box). Each box shows the fold-change in population density (vertical axis) as a function of the time passed since triggering differentiation (horizontal axis). $n \geq 3$ for each data point. Error bars are s.e.m.

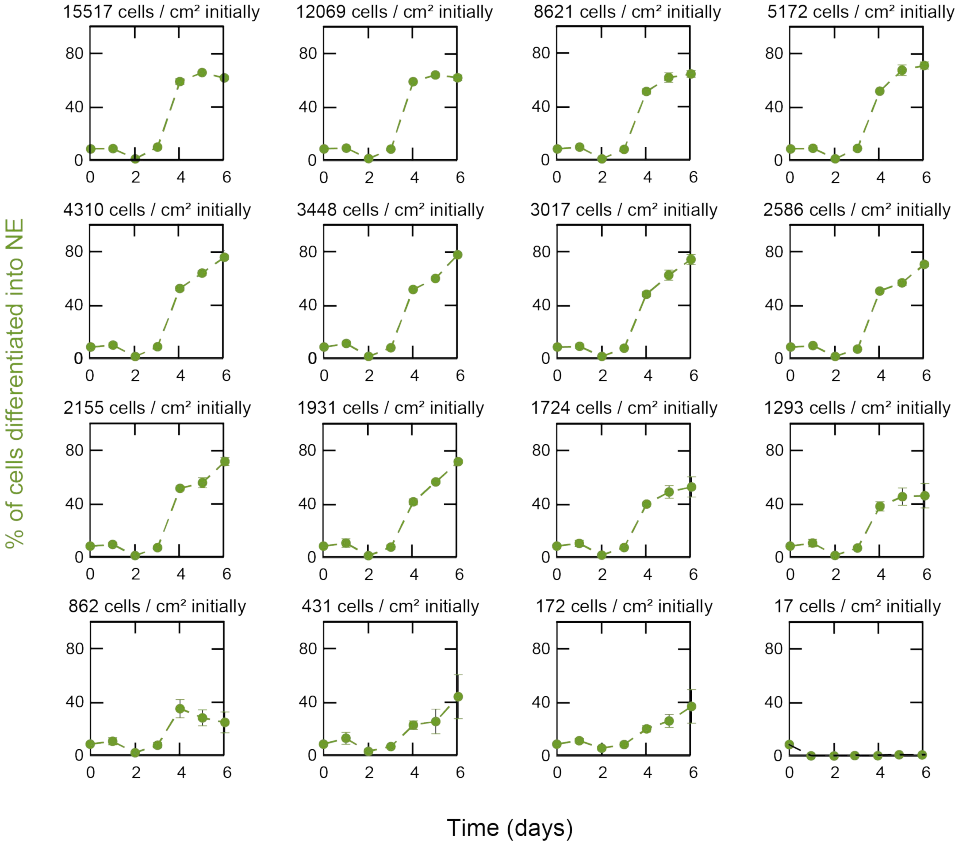

Figure 2.11: Populations with higher initial densities achieve a higher differentiation efficiency (% of cells successfully entering Neural Ectoderm (NE) lineage. Retinoic Acid (RA) induced differentiation towards the NE-lineage by 46C cell-line populations. The 46C cell line has *Sox1* promoter driving GFP expression. Sox1 - and thus GFP - is expressed only when the cell enters the NE lineage (see Material and methods). We triggered pluripotency exit to begin each time course (see data as shown in Supp. Fig. 2.12). Each box shows the differentiation efficiency for a different starting population-density (indicated above each box). On each day, we collected all cells from a cell-culture plate and then flowed them into a flow cytometer to measure the percentage of alive cells in the population that expressed GFP (i.e., percentage of cells that expressed Sox1 - a marker of NE-lineage commitment) (see Materials and methods). Differentiation efficiency reached a maximum 80% for populations that started above the threshold density of 1700 cells/cm^2. Differentiation efficiency was below 50% for populations that began with a below-threshold density. n $\geq$ 3; error bars are s.e.m.

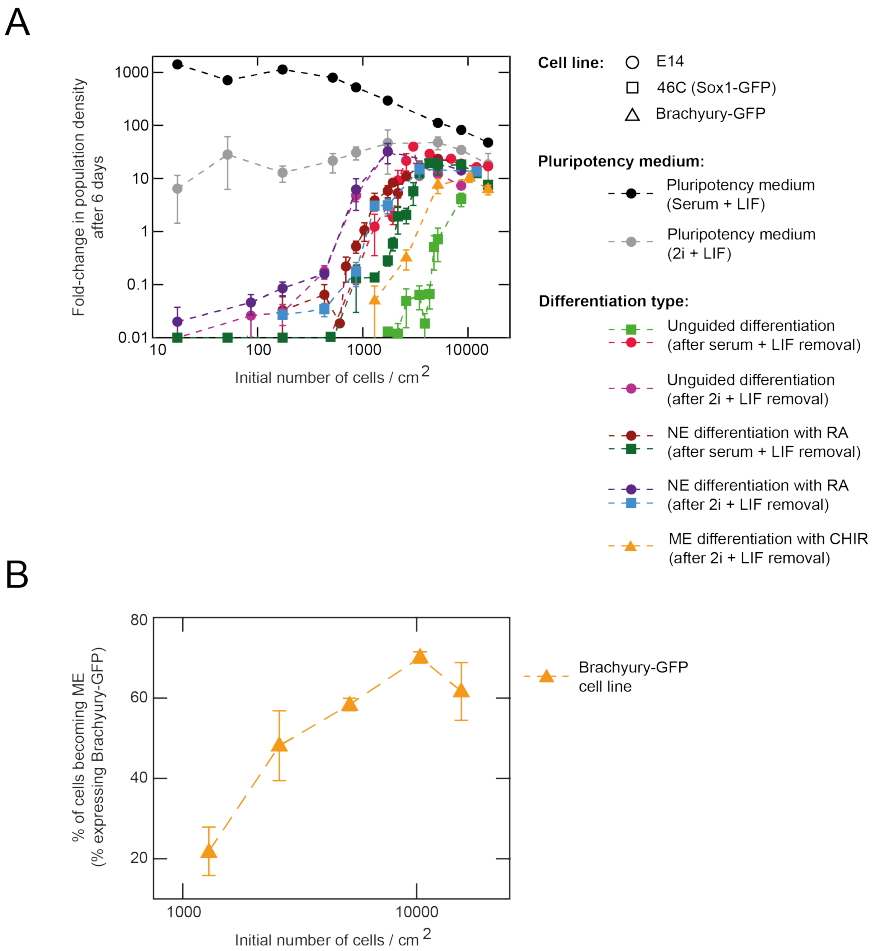

Figure 2.12: Different cell lines and multiple types of differentiation all exhibit the same phenomenon: differentiating population's initial density determines its survival-versus-extinction fate. **(A)** Data shown for three different cell lines: E14 (circles), 46C (squares), and *Brachyury*-GFP (triangles). The 46C cells have a *Sox1* promoter controlling their GFP expression (Sox1 is a marker of the Neural Ectoderm (NE) lineage). The *Brachyury*-GFP cells have a *Brachyury* promoter controlling their GFP expression (gift from V. Kouskoff and described in [172, 173]. Brachyury is a marker of mesendoderm (ME) lineage. Different colors represent different types of cell-culture media as indicated in the legend. For each differentiation, we took one of the three cell lines that were kept pluripotent with LIF in either a serum-based medium or a serum-free (*2i*) medium. The three types of differentiations are: unguided differentiation in which no inducer was added after triggering pluripotency loss, NE differentiation in which we added Retinoic Acid (RA), and ME differentiation in which we added the small molecule, CHIR (see Materials and methods). As seen here, regardless of the cell line and differentiation type, a differentiating population's initial density determined its survival-versus-extinction fate. **(B)** After four days of CHIR-induced differentiation, we used a flow cytometer to measure the percentage of the *Brachyury*-GFP cells that expressed GFP (i.e., percentage of cells in a population that entered the ME lineage [119]. As with the 46C cells that differentiated towards the NE lineage (Supp. Fig. 2.13), populations of *Brachyury*-GFP cells that start with higher densities have higher differentiation efficiencies (larger percentages of cells entering the ME lineage). For both (A) and (B): n = 3; error bars are s.e.m.

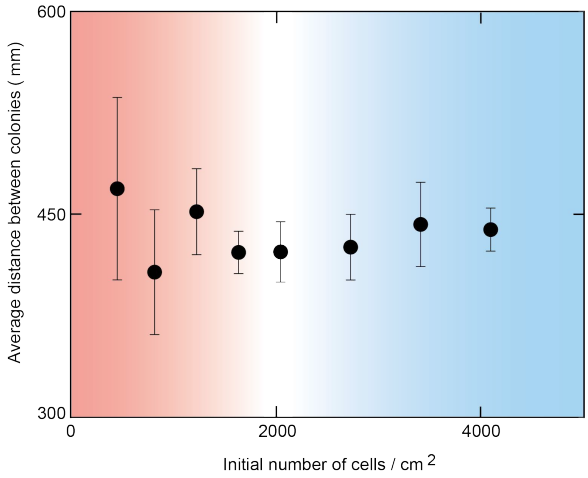

Figure 2.13: For every population density, microcolonies are hundreds of microns apart from each other when differentiation begins. Data shown for E14 cells in unguided differentiation (N2B27), previously self-renewing in serum+LIF. We scattered a desired number of cells across a 6-cm diameter dish containing N2B27 to trigger pluripotency loss. Then, we used a wide-field microscope to locate and image the microcolonies in seventeen fields of view. Each field of view has a dimension of 1.40 mm x 0.99 mm. From these images, we determined the distance between every pair of colonies that resided in the same field of view. Then, we averaged these distances (averaging over all pairs of colonies from all seventeen fields of view per dish). The resulting, average distance between colonies is plotted here as a function of the initial population density. As shown here, for a wide range of initial population densities, the average distance between microcolonies were virtually identical (~450 μm). Each cell has a diameter of ~10 μm, meaning that microcolonies, if they resided in the same field of view, were hundreds of microns apart (45 cell-diameters apart). n = 3 dishes for each initial population density; error bars are s.e.m.

A way to understand why the average colony-colony distance is nearly independent of the initial population density is that the dish area is much larger than can be covered by the cells, even for the high-density populations (at most 1% of dish area is covered by the cells, as one can also check by a back-of-envelope calculation). In short, the vast difference in length-scale between individual cells and the plate area leads to above result. Given this, more informative metric is actually the distance between a colony and its nearest-neighboring colony (see Supp. Fig. 2.14).

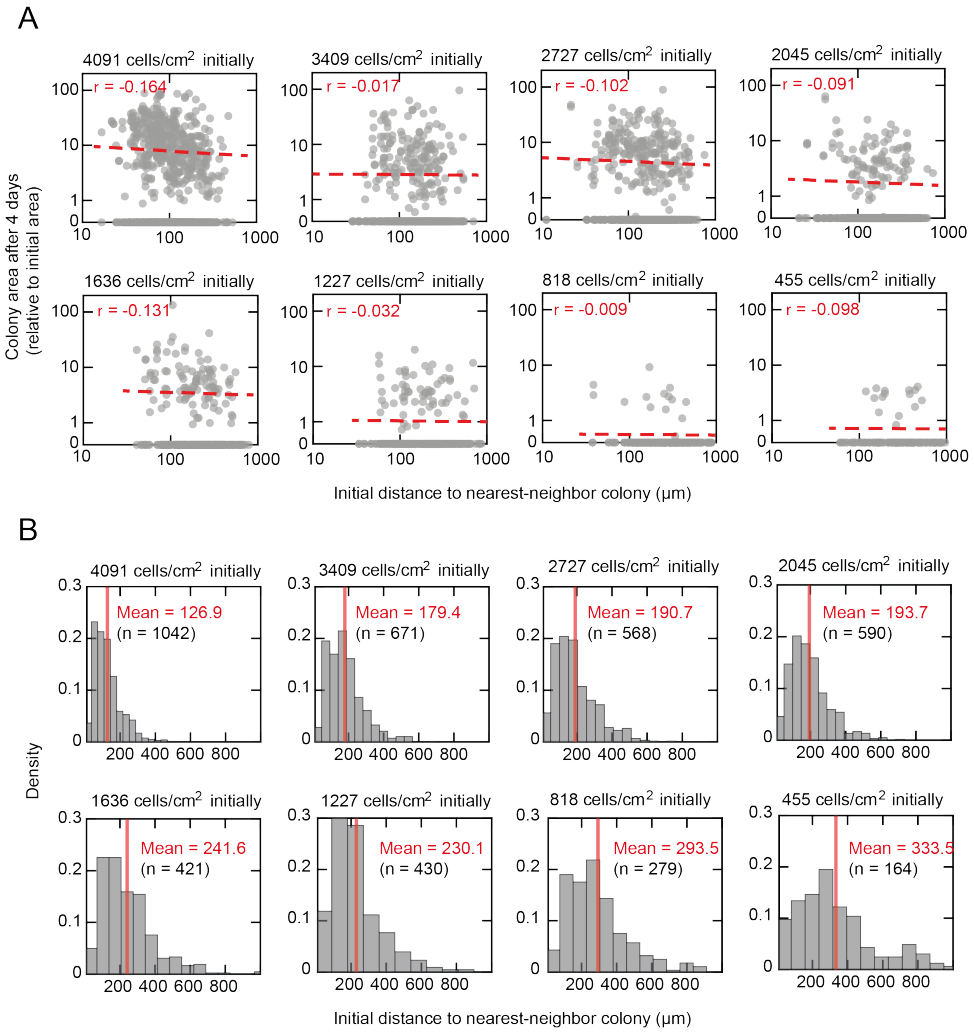

Figure 2.14: Growth and survival of differentiating cells do not depend on the distance between nearest-neighboring colonies for any initial population density. Data for E14 cells undergoing unguided differentiation (i.e., no inducers such as RA), previously self-renewing in serum+LIF. We scattered a desired number of cells across a 6-cm diameter dish containing N2B27 to initiate exit from pluripotency. Then, we used a wide-field microscope to locate and image the microcolonies in seventeen fields of view (see Materials and methods). Each field of view has a dimension of 1.40 mm x 0.99 mm. From these images, we determined the distance between every pair of colonies that resided in the same field of view. From these measurements, we found the smallest distance (i.e., distance from one colony to its nearest-neighboring colony). We did this for each colony in a field of view. The resulting, nearest-neighboring distance for each colony is plotted here as a function of the initial population density. Each grey point represents the final area (after 96 hours) of a colony relative to its initial area as a function its distance to its nearest neighbor (at the start of the time-lapse movie). If a colony died during the time-lapse, then we assigned it a value of zero as the fold-change in its area. Each box shows the fold-change in the colony area (vertical axis) as a function of the distance from colony to its nearest neighbor (horizontal axis) for 17 fields of view and a specific population density. Dashed curves in each box denote the Pearson correlation with the Pearson correlation coefficient r in each box. There is virtually no correlation between a colony's final area (and whether it dies or not) and its initial, nearest-neighbor distance, for any starting population density. These results strongly indicate that the presence of a nearby colony does not predict whether a colony survives or not and also does not predict how fast each colony grows during differentiation.

3

Nonlocal communication determines collective survival

Parts of this chapter are also reported in Daneshpour et al. [2]

3.1. Introduction

We found that survival and differentiation are collective phenomena in differentiating Embryonic Stem (ES) cells. Moreover, we discovered that this phenomenon exhibits a striking feature: in fact, the whole population's survival-vs-extinction fate critically depends - that is, in a switch-like manner - on its density at the start of differentiation. We sought to determine whether the collective survival is due to cells secreting and sensing each other's survival-promoting factors to cooperate by communicating and, if so, to determine the spatial range of this communication.

3.2. Results

3.2.1. Secreted molecules decide collective survival in the first 3 days of differentiation

We hypothesized that differentiating cells secrete at least one factor ("survival factor") and that cells sensing this factor have an increased chance of replicating. This would lead to a collective growth. If this hypothesis is true, then collecting medium from a high-density population (5172 cells / cm^2) would pool together the survival factor from everywhere in the dish. Then, giving this conditioned medium to a low-density population (862 cells / cm^2) that was bound for extinction should now rescue that population from extinction (Figs. 3.1).

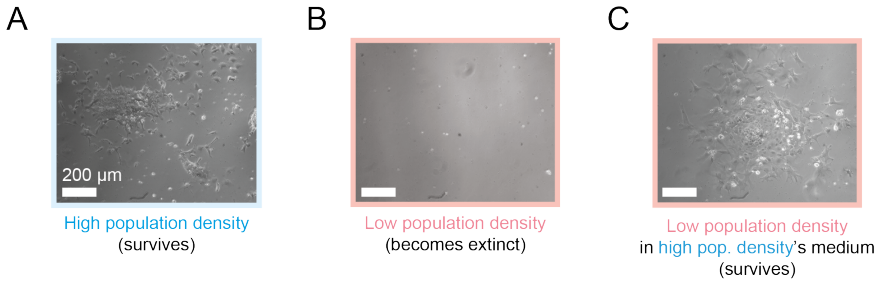

Figure 3.1: Triggering collective survival with conditioned media reveals extracellular survival-promoting factors. Microscopy images (day 6 of differentiation) for 46C cells (previously self-renewing in serum+LIF) induced to enter Neural Ectoderm (NE) lineage with Retinoic Acid. **(A)** High-density population (5172 cells / cm^2) showing expanded cell colonies. Scale bar is 200 μm. **(B)** Low-density population (862 cells / cm^2) after becoming extinct (with a few floating cell corpses). Scale bar is 200 μm. **(C)** Low-density population (862 cells / cm^2) showing expanded cell colonies after replacing its medium on day 2 with a 2-day-old medium of a high-density population (from (A)) and then leaving alone the population in this pre-conditioned until day 6 for imaging. Scale bar is 200 μm.

We systematically examined the effects of giving populations a conditioned medium in two ways (Figs. 3.2A). In one method (Figs. 3.2A - labelled "1"), we collected the high-density population's medium after X days of differentiation (Fig. 3.1A) and then, in it, initiated differentiation of low-density population (Fig. 3.1B). In this

"day X to day 0" transfer, the low-density population was rescued from extinction if and only if X was 2, 3, or 4 (Fig. 3.2B - left column: black bars show ~4-fold change in population density for X = 2, 3, and 4). If X was 5, then the low-density population was barely saved. If X was 1 or 6, the low-density population still went extinct. These results are consistent with the survival factors either not yet being secreted after 1 day or needing ~2 days to accumulate to a sufficient concentration and degrading over time such that there is not enough of them to rescue populations after ~5 days of differentiation.

As another method (Figs. 3.2A - labelled "2"), we collected the medium of the high-density population X days after beginning differentiation and then transplanted in it a low-density population that was already differentiating, before being transplanted, for the same number of days (X days). In this "day X to day X" transfer, the low-density population was rescued from extinction if and only if the X was 2 or 3 (Fig. 3.2B - right column: black bars: show fold-change in population density which is ~4-fold for X = 2 and just above 1-fold for X = 3). These results are consistent with differentiating cells no longer responding to the survival factors from the third day of differentiation onwards and thus they proceed to extinction.

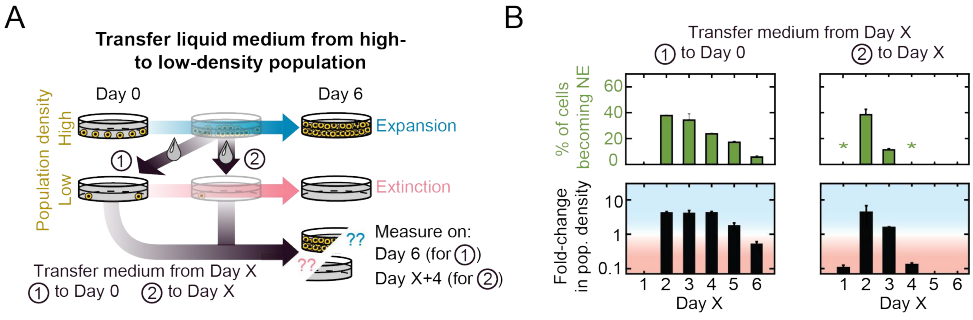

Figure 3.2: Survival-vs-extinction fate is sealed in first 3 days by secreted factor(s). (A) Over 6 days, high-density population (5172 cells / cm^2) expands (top: blue arrow) and low-density population (862 cells / cm^2) approaches extinction (middle: pink arrow). Two methods shown for replacing medium of the low-density population by that of the high-density population. Method (labeled "1"): replace initial medium of low-density population with the medium from X-days-old high-density population. Method 2 (labeled "2"): replace medium of X-days-old low-density population with that of X-days-old high-density population. **(B)** Results of two experiments described in (A). Left column for method 1 and right column for method 2. Data for 46C cells (previously self-renewing in serum+LIF) induced to enter Neural Ectoderm (NE) lineage with N2B27+RA. As a function of Day X, green bars show percentage of cells in population becoming NE (expressing *Sox1*-GFP) and black bars show fold-change in population density. Blue and red shades indicate population expansion and extinction, respectively. Asterisks indicate too few cells for reliable measurement on flow cytometer (less than 0.1-fold change in population density). Error bars are s.e.m.; n = 3.

3.2.2. Multiscale analysis excludes local communication accounting for collective survival during differentiation

The existence of cell-state promoting factors that are secreted by *in vitro* cultured cells is the starting point of our work. We argued that giving conditioned media to cells does not establish any range of communication between the cells. This is because in the practice of giving conditioned media involves pooling together all secreted factors from everywhere on a dish, uniformly mixing them, and then giving this uniform mixture to cells on a new dish. Doing so destroys all spatial information such as which cell is talking to which other cells on the original dish. Conditioned media establish existence of secreted signals but not their range. This is why our scientific quest for quantitatively understanding cell-cell communication in ES cells can not stop at Fig. 3.2B, but only begins now.

To determine the spatial scale of communication required for collective survival during differentiation (i.e., how far the secreted molecules effectively diffuse), we used a wide-field microscope to continuously track and measure the area of individual microcolonies in a population in multiple, millimeter-scale (1.40 mm x 0.99 mm) field-of-views on each dish. We analyzed microcolonies by using custom-built image segmentation (Fig. 3.3 and see Materials and methods).

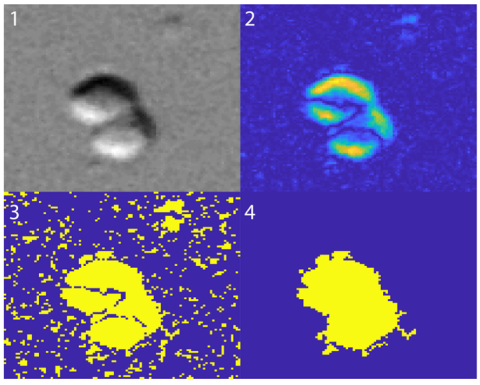

Figure 3.3: Image segmentation process to identify and track microcolonies and their respective area over 4 days of differentiation. (1) Brightfield image of microcolony. (2) Deviation of each pixel value with respect to the mean pixel value. (3) Binary image based on thresholding. (4) After removing noise and filling the edges.

We found that the area of a colony was an accurate proxy for the number of cells in the colony, leading to the fold-change in number of cells over time (Fig. 2.6B) closely matching the fold-change in colony area over the same duration (Supp. Fig. 3.8). From the resulting time-lapse movies, we sought to determine at the level of individual microcolonies whether "locality" - such as a microcolony's size, the number of its surrounding neighbours, the distance to its neighbours and its

motility - dictates a microcolony's survival, and eventually the collective survival at the level of the population on a dish. In other words, we sought to determine whether there is a correlation between a microcolony's local characteristics and its survival (Fig. 3.4).

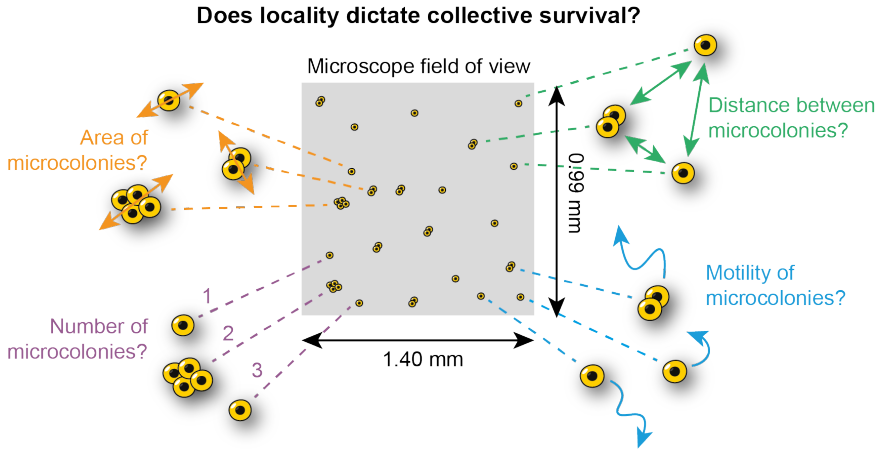

Figure 3.4: In search of local characteristics of microcolonies dictating the collective survival during differentiation. We sought to determine any correlation between ES-cell microcolonies' local characteristics when differentiation begins - such as area of microcolonies (orange), number of microcolonies in a field of view (purple), distance between microcolonies and their nearest neighbour (green) and motility of microcolonies (blue) - and their end survival within a large field of view (1.40 x 0.90 mm).

As a first step, we sought to answer whether any cell-cell communication within a microcolony (Fig. 3.5A - orange arrows) or any communication between nearby microcolonies - defined as being in the same ~1-mm^2 field of view (Fig. 3.5A - purple arrows) - could account for the population's survival-versus-extinction fate.

We tracked the area of each microcolony over 4 days of differentiation in N2B27 without any inducer such as RA (Fig. 3.5B and Supp. Fig. 3.8). Most microcolonies started with one or a few cells (see Fig. 2.2B), as indicated by the distribution of their initial areas (Fig. 3.5C - horizontal axis). Using the variations in the initial microcolony sizes, we found virtually no correlation between the final area of a colony after 4 days of differentiation and its initial area, for both high-density (e.g., 2857 cells / cm^2) and low-density (e.g., 857 cells / cm^2) populations (Fig. 3.5D; see Supp. Fig. 3.9 for all population densities). In Chapter 8 we show with a mathematical model that initial colony area, diffusion length of secreted factors and the cells' response threshold collectively dictate a microcolony's survival (Fig. 8.5). In light of that model and our experimental results presented here, simple forms of intra-colony communication - each cell secreting a molecule whose intra-colony concentration is high enough to rescue the colony if the colony starts with enough cells - cannot account for the fate of the population on that dish.

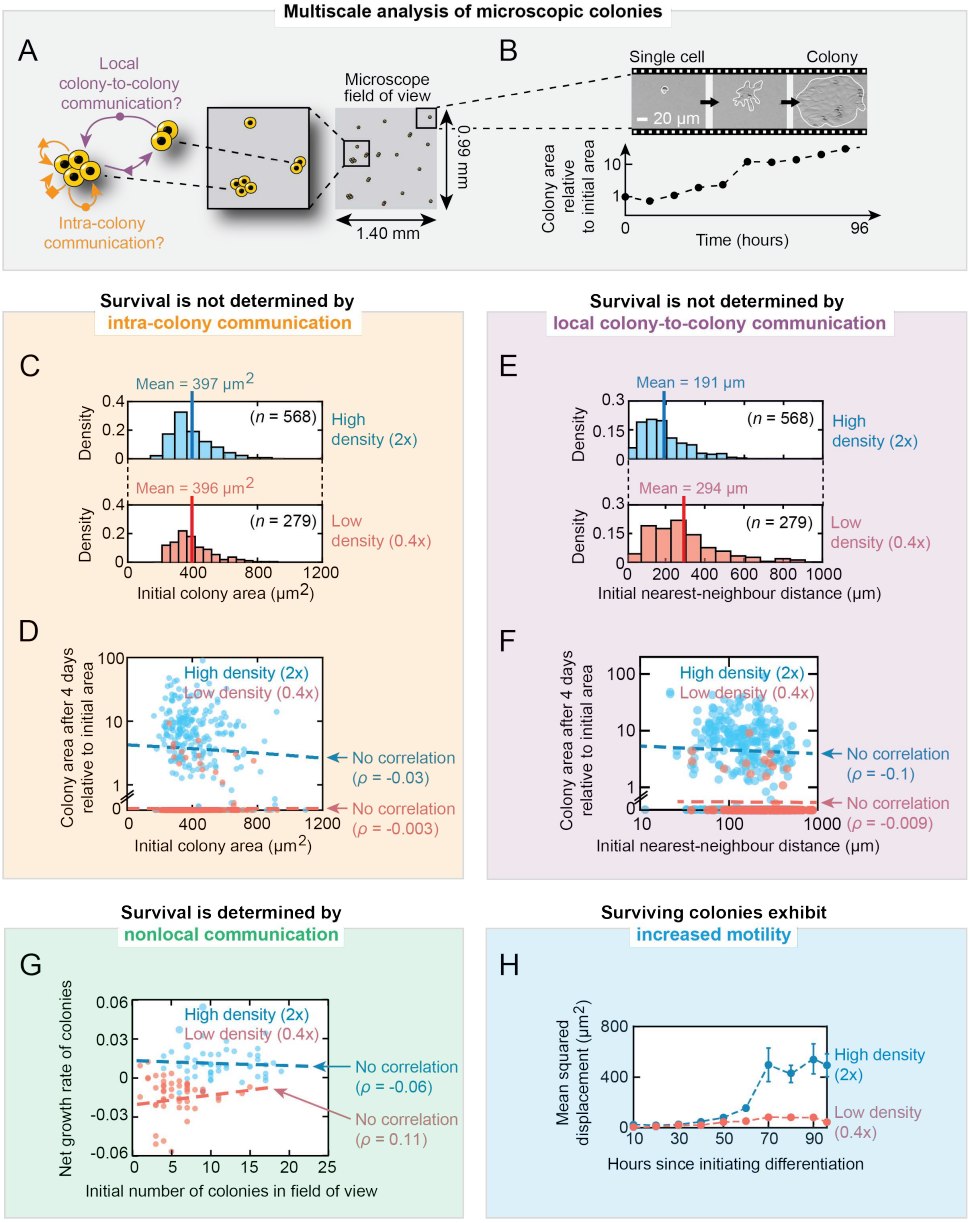

Figure 3.5: Local communication occurring below a millimeter scale cannot account for collective survival. (A) Two modes of communication to exclude as possible mechanisms that control population's survival-versus-extinction fate by using time-lapse microscopy. Each field of view in microscope is 1.40 mm x 0.99 mm. **(B)** Example of 96-hour time-lapse movie that tracks growth of a microcolony (subregion of a field-of-view shown). Scale bar = 20 μm. See also Supp. Fig. 3.8.
(*Caption continued on next page.*)

Figure 3.5 ***(previous page)*****: (C)** Histogram of initial colony areas for two initial population densities: "High density (2x)" (shown in blue) represents 2857 cells / cm^2 (population survives and expands towards the carrying capacity) and "Low density (0.4x)" (shown in red) represents 857 cells / cm^2 (population becomes extinct). Data from 3 x 17 fields of view are shown for E14 cells in N2B27 (unguided differentiation) after self-renewing in serum+LIF. Also see Supp. Fig. 3.9 for all population densities. Shown are the means of the histograms and the sample size (n = total number of colonies in all fields of view). **(D)** Same legend as described in (C). Each blue dot (n = 568) represents a microcolony from the high-density population and each red dot (n = 279) represents a microcolony from the low-density population. Area of each microcolony after 4 days of differentiation normalized by its initial area (vertical axis) versus its initial area (horizontal axis). Blue line: linear regression with ρ = -0.03. Red line: linear regression with ρ = -0.003. See Supp. Fig. 3.9 for all population densities. **(E)** Histogram of initial nearest-neighbour distances of microcolonies for two initial population densities. Same legend as described in (C). Data from 3 x 17 fields of view are shown for E14 cells in N2B27 (unguided differentiation) after self-renewing in serum+LIF. Also see Supp. Fig. 2.14 for all population densities. Shown are the means of the histograms and the sample size (n = total number of colonies in all fields of view). **(F)** Blue and red data points represent the exact same microcolonies as in (D) but now showing microcolony's area after 4 days of differentiation normalized by its initial area (vertical axis) versus its initial nearest-neighbour distance (horizontal axis). Blue line: linear regression with ρ = -0.1. Red line: linear regression with ρ = -0.009. See Supp. Fig. 2.14 for all population densities. **(G)** Blue and red data points represent the exact same microcolonies as in (D) and (F) but now showing microcolony's net growth rate (vertical axis) versus the initial number of microcolonies in the ~1-mm^2 field-of-view that contains the colony (horizontal axis). Blue line: linear regression with ρ = -0.06. Red line: linear regression with ρ = 0.11. See Supp. Fig. 3.10 for all population densities. Also see Supp. Fig. 3.7 for experiments that show that the distance between one colony and its nearest-neighboring colony does not determine the colony's survival and its growth rate. **(H)** Blue and red data points represent the exact same microcolonies as in (D-G) but now showing microcolony's mean squared displacement (measure for motility relative to XY coordinates (positions) of microcolonies at the start of differentiation) versus time during a 96-hours time-lapse movie. See Supp. Fig. 3.11 for full details of calculation and for all population densities. Error bars are s.e.m. (n = 3).

To be clear, this does not mean that there is absolutely no intra-colony communication. But our analysis here suggests that local (intra-colony) communication cannot be determining whether the entire population survives or not. In Chapter 8 we will also explain why, if secreted molecules are indeed responsible for collective survival, a larger colony does not automatically need to have a higher probability of surviving due to a higher concentration of these molecules accumulating in the colony (i.e., analyzing reaction-diffusion equation will show that molecules that diffuse far away does not create a sharp local gradient around a secreting cell).

Although the nearest-neighbour distances of microcolonies at the start of differentiation change by a mere two fold when changing the initial density from low (extinction) to high (survival) (Fig. 3.5E; see also Supp. Fig. 2.14), we found that whether a colony grows/dies or not during the next four days is independent of (uncorrelated with) the distance to the nearest-neighbouring colony (Fig. 3.5F).

Furthermore, a microcolony's growth rate – a rate at which a microcolony's area grows in the time-lapse movies - was virtually uncorrelated with the total number of microcolonies in its ~1-mm^2 field of view (Fig. 3.5G; see Supp. Fig. 3.10 for all population densities). Hence, the number of microcolonies in a 1-mm^2 region does

not dictate whether or not any of the cells in that region survive and their growths.

To see what the results in Fig. 3.5E-G imply, consider two separate ~mm^2-scale fields of view - one from a high-density population and another from a low-density population - that appear virtually identical because both initially have the virtually the same number and distribution of microcolonies. Yet, the field from the high-density population would have microcolonies subsequently expanding while the field from the low-density population would have microcolonies subsequently dying. Hence, a ~mm^2-scale field of view contains insufficient information: there is no local characteristic of microcolonies that we can extract from a field of view for predicting whether the microcolonies in the field will expand or die.

Intriguingly, we found that microcolonies from a high-density population become increasingly motile (starting ~60 hours after initiating differentiation in Fig. 3.5H) on the surface of the dish relative to their positions at the start of differentiation (i.e., the initial location where the cells settled when seeded) whereas extinction-bound microcolonies from a low-density population show no (change in) motility during the four days of differentiation (also see Supp. Fig. 3.11 for all population densities and for more details). We did not further explore whether motility merely correlates with or actually contributes to (causes) survival. If we were to speculate, then we hypothesize that increased motility (after ~3 days of differentiation (Fig. 3.5H)) is the result of nonlocal communication first since collective survival is decided early during differentiation (primarily, after 2 days of differentiation (Fig. 3.2B)).

Taken together, the time-lapse movies suggest that nonlocal communication, by means of long-range (beyond ~mm^2-scale) diffusing molecules, dictate the differentiating population's survival-versus-extinction fate.

3.2.3. Survival factor is stable for days and light enough to enable nonlocal communication

If secreted molecules mediate nonlocal communication, then their characteristic diffusion lengths are set accordingly. Solving the reaction-diffusion equation reveals that a molecule's diffusion length is $\sqrt{D\tau}$, where D is the diffusion constant and τ is the half-life of the molecule (see Chapter 6). D is proportional to the molecular weight. Later on, we place lower and upper bounds on the molecular weight(s) of the secrete molecule(s) (see Chapter 5).

Using Stokes-Einstein relation, we could calculate the diffusion constant D directly from a molecular weight (see Chapter 6). For the argument outlined below, we assumed that the survival factor was ~100 kDa (leaning on the side of being conservative, but which is nearly the maximum possible value we experimentally confirmed (see Chapter 5)). Since the diffusion length λ is $\sqrt{D\tau}$, we assumed vari-

ous values of τ (from minutes to days), calculated the corresponding λ, and then plugged this value into the solution to the reaction-diffusion equation to obtain the steady-state concentration profile for various τ (Fig. 3.6A). These calculations revealed that when the half-life τ is several days (e.g., 2 days), a cell can create a substantial concentration of the survival molecule (at least ~25% of maximal possible concentration) several millimeters away (Fig. 3.6A).

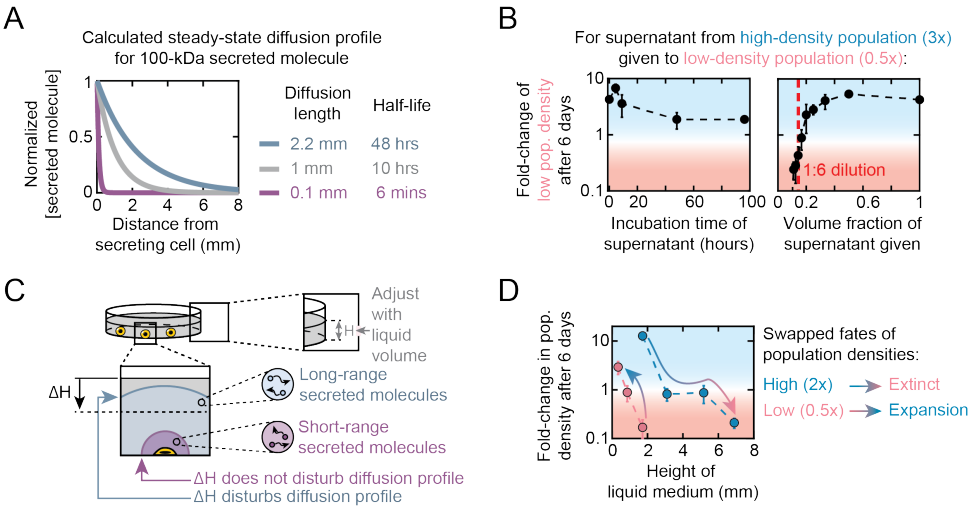

Figure 3.6: Survival-promoting molecule is stable for days and is light enough to enable nonlocal communication. (A) Calculated diffusion profiles (steady state) for secreted molecules (~100 kDa molecular weight) with three different half-lives (τ) and diffusion lengths (λ). We used the steady-state solution (equation 6.8 in Chapter 6) of the 3D reaction-diffusion equation (equation 6.7 in Chapter 6) to plot the normalized concentration of secreted molecules, assuming spherical cells of certain radius (typically ~7.5 μm) that secrete molecules along the axial direction (distance from secreting cells) at a constant rate equally in all directions. We used Stokes-Einstein relation for diffusing spherical particles (assumption for secreted molecules) to estimate the diffusion constant D for a 100-kDa secreted molecule (overestimation; see Chapter 5) to determine the secreted molecule's diffusion length $\lambda = \sqrt{D\tau}$. See full details and derivation in Chapter 6. Plotted are half-lives τ = 6 mins, 10 hrs and 48 hrs (2 days). Even with an overestimated molecular weight, secreted molecules with days-long diffusion lengths (here, 48 hours) have millimeters-long diffusion lengths (here, 2.2 mm). **(B)** Experimental confirmation of days-long stability of secreted molecules. We sought to infer the (effective) half-lives of all secreted molecules important for determining the survival-vs-extinction fate of a population. To do so, we took a high-density population's (5172 cells / cm^2) medium (supernatant) 2 days after initiating their unguided differentiation in N2B27 medium and then aged this conditioned medium in a incubator for a duration given in the horizontal axis. After incubating the conditioned medium, we transplanted in it a low-density population (862 cells / cm^2; usually bound to extinction) 2 days after initiating its unguided differentiation and then counted its resulting expansion after 4 days. In a similar experiment, we took the high-density population's supernatant and then made serial dilutions (volume fractions) of it with fresh medium before given it to a low-density population. See Supp. Fig. 5.13 for detailed explanation. The results show that ageing the secreted molecules for 96 hours (4 days) still results in a rescue from extinction after transferring them to the low-density population and that given the "1:6 dilution" required to dilute enough secreted molecules to no longer rescue populations from extinction...
(*Caption continued on next page.*)

Figure 3.6 ***(previous page)*****:** ...we can infer that the total pool of secreted molecules must have an effective half-lives of at least 2 days (see caption of Supp. Fig. 5.13 for derivation). The fold-change achievable does decrease as the medium's age increases, from ∼4-fold (for unaged medium) to ∼2-fold (for medium aged for 96 hours). Error bars are s.e.m.; n = 3. **(C)** Diffusion profile (volume filled by diffusing molecules) for molecule that diffuses far (blue region) and molecule that diffuses short range (purple region). Cell, in yellow, that secretes both molecules in all (also axial) directions is adhered to the dish bottom. △H is change in liquid height along axial direction. H is the total height of liquid medium that we tune in (D). **(D)** Results of experiment described in (C). Fold-change in population density of 46C cells after 6 days of differentiation into NE lineage, as a function of the height of the liquid medium ("H" in (C)). Red points are for low-density population (initially 862 cells / cm^2) and blue points are for high-density population (initially 3448 cells / cm^2). Error bars are s.e.m.; n = 3.

We experimentally confirmed that survival factors in the supernatant of a high-density population are stable enough to live for several days without diminishing survival-promoting effects. Specifically, we took the supernatant of a high-density population (5172 cells / cm^2), incubated the supernatant without any cells at 37^{o}C for various durations (up to four days), and then transplanted a low-density population (862 cells / cm^2) into this aged supernatant. Six days afterwards, the low-density population nearly doubled in density, which was about half of the ∼4-fold growth in a ∼4-hours-aged supernatant (Fig. 3.6B - left graph shows minor decrease over days). In another experiment, we diluted the fresh supernatant from the high-density population by various amounts into fresh N2B27 without ageing it, and then incubated the low-density population in the diluted supernatant. In the undiluted supernatant, the low-density population grew by ∼4-fold whereas it grew by ∼2-fold in a fresh medium that contained only 25% of the supernatant (Fig. 3.6B - plateau in the right graph). This result and the 4-day-old supernatant experiment establish that the half-life of the survival factor (the indispensable survival factor if there is more than one specie) must be at least two days. Indeed, a shorter than two days of half-life would lead to the 4-days-old supernatant having less than 25% of the supernatant causes the low-density population to grow by less than 2-fold. In fact, in media containing 1/6 or less of the supernatant, the low-density population went extinct (Fig. 3.6B - left of vertical red line in the right graph).

To verify the long-range diffusion in a different way, we considered the following: changing the height of the liquid-culture medium by millimeters would disturb the molecule's concentration profile if the molecule can travel by millimeters in the first place (Fig. 3.6C - blue dome) but not if the molecule's diffusion length is less than a millimeter (Fig. 3.6C - purple dome). For example, decreasing the medium height, which is ∼2-mm above the cells (dish bottom) in our experiments so far (i.e., for a 10-mL culture medium in a 10-cm diameter dish), would lower the "ceiling" (top of liquid). If the secreted molecule can travel the ∼2-mm distance, then it would now concentrate more at the bottom of the dish (on the cells) due to

the decreased ceiling (Fig. 3.6C). Conversely, increasing the liquid height would let the molecule escape further away from the secreting cells and thereby concentrate less around the cells, given that the molecule can diffuse beyond the ~2-mm distance. Changing the liquid height would not change the initial population-density (# of cells attached per area of the dish bottom). In accordance with this line of reasoning, a low-density population (862 cells / cm^2) was rescued and grew towards the carrying capacity when we decreased the liquid height to ~0.3-mm whereas it became extinct if the liquid height was the usual ~2-mm (Fig. 3.6D - pink points). Conversely, a high-density population (3448 cells / cm^2) became extinct if the liquid height was ~7-mm but survived if the height was ~5-mm or ~2-mm, with a faster growth in a ~2-mm height than in a ~5-mm height (Fig. 3.6D - blue points; also Supp. Fig. 3.12 for percentages of cells that differentiated as a function of liquid height). Hence, differentiating cells communicate through survival factor(s) that travel over a distance of at least ~5 to ~7-mm (near centimeter).

3.3. Conclusions

Together, these results reinforce the conclusion that ES cells nonlocally communicate, by secreting diffusive factors that spread over at least several millimeters (Fig. 3.7), and that determine the population's survival-vs-extinction fate during differentiation.

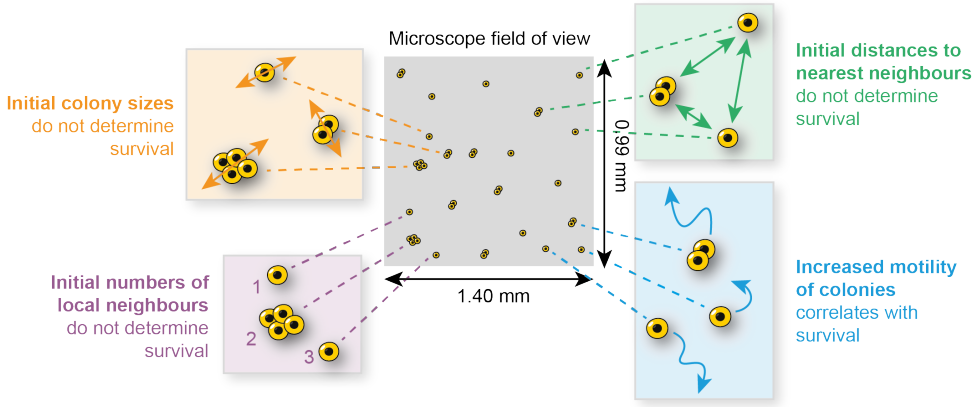

Figure 3.7: Nonlocal communication determines collective survival during differentiation. We found virtually no correlation between a microcolony's growth (and whether it dies or not) and any of that microcolony's local characteristics: initial colony size (orange), initial number of colonies (local neighbours) in a ~mm^2-scale field (purple), and initial distance to colony's nearest neighbour (green). Additionally, we found that microcolonies of a surviving population (high initial density) show increased motility from the third day of differentiation onwards (blue), most likely after determining their collective survival with nonlocal communication 2 days after initiating their differentiation.

With the diffusion length being at least several millimeters, we can effectively as-

sume that the survival factor is well mixed. This also justifies our stochastic model (that assumes a uniform concentration for the survival factor) which we will introduce in Chapter 6. As a further proof of the survival factor being essentially well mixed, in another experiment, we widely varied both the initial population-density (setting the strength of cooperativity) and the liquid-medium height (setting the confines of the cells' habitat). We will discuss these results - in light of our stochastic model - in Chapter 6 as well. Next, we sought to determine what intracellular pathways the secreted molecules control. In turn, this may help us identifying at least one secreted molecule.

3.4. Supplementary Information

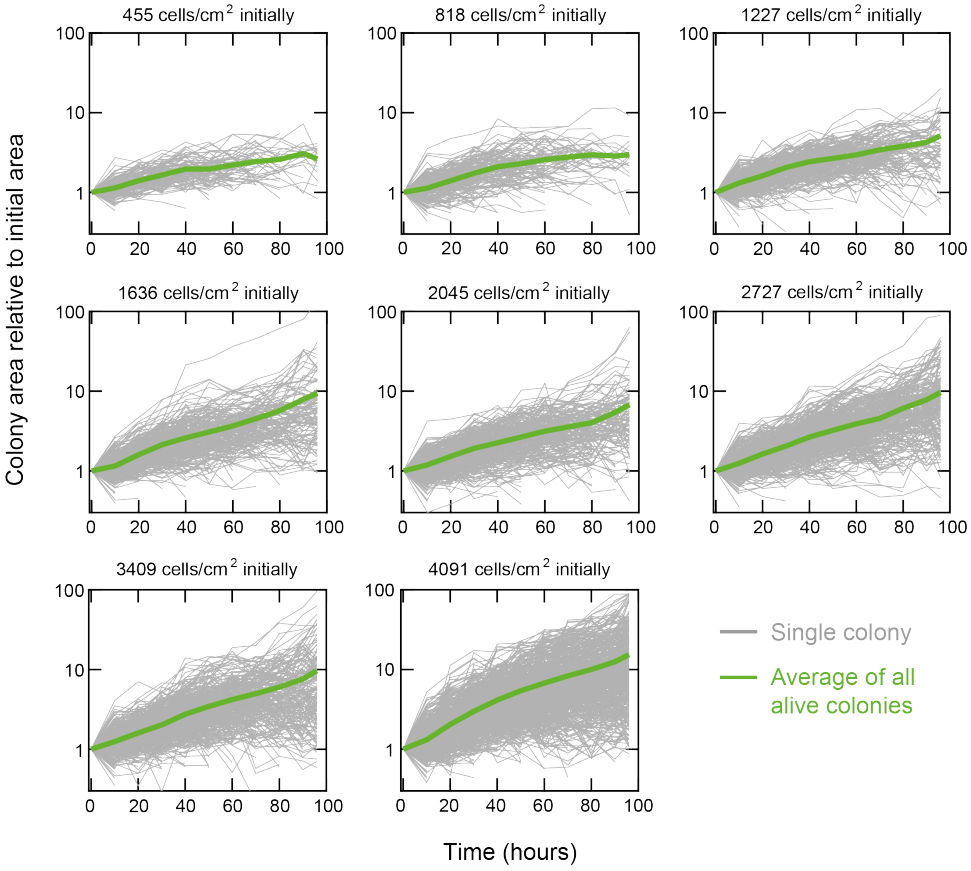

Figure 3.8: Time-lapse microscopy over 4 days reveals the growth rate of each microcolony for a wide range of initial population densities. Data shown for E14 cells in N2B27 (unguided differentiation) without any inducer such as Retinoic Acid, after self-renewing in serum+LIF. We used a wide-field microscope to image and measure the area of each microcolony over four days (each grey curve). During the four days, we measured the area of a given microcolony every 10 hours (see Materials and methods). Each box shows the fold-change in the colony area (vertical axis) as a function of the time passed since triggering differentiation (horizontal axis) for different starting population densities. In these movies, we observed both growing and dying colonies. For the colonies that died, the grey curves abruptly end, at the last time frame in which they were alive and before the end of the four-day period. The dying colonies visibly stood out as they typically displayed apoptotic bodies or lifted off the plate and thus disappeared from the focal plane. At each time frame, we computed the average area of all living colonies (green curve) from which we can extract the average growth rate of a colony for each population density (used for a model that we will introduce later in Chapter 6).

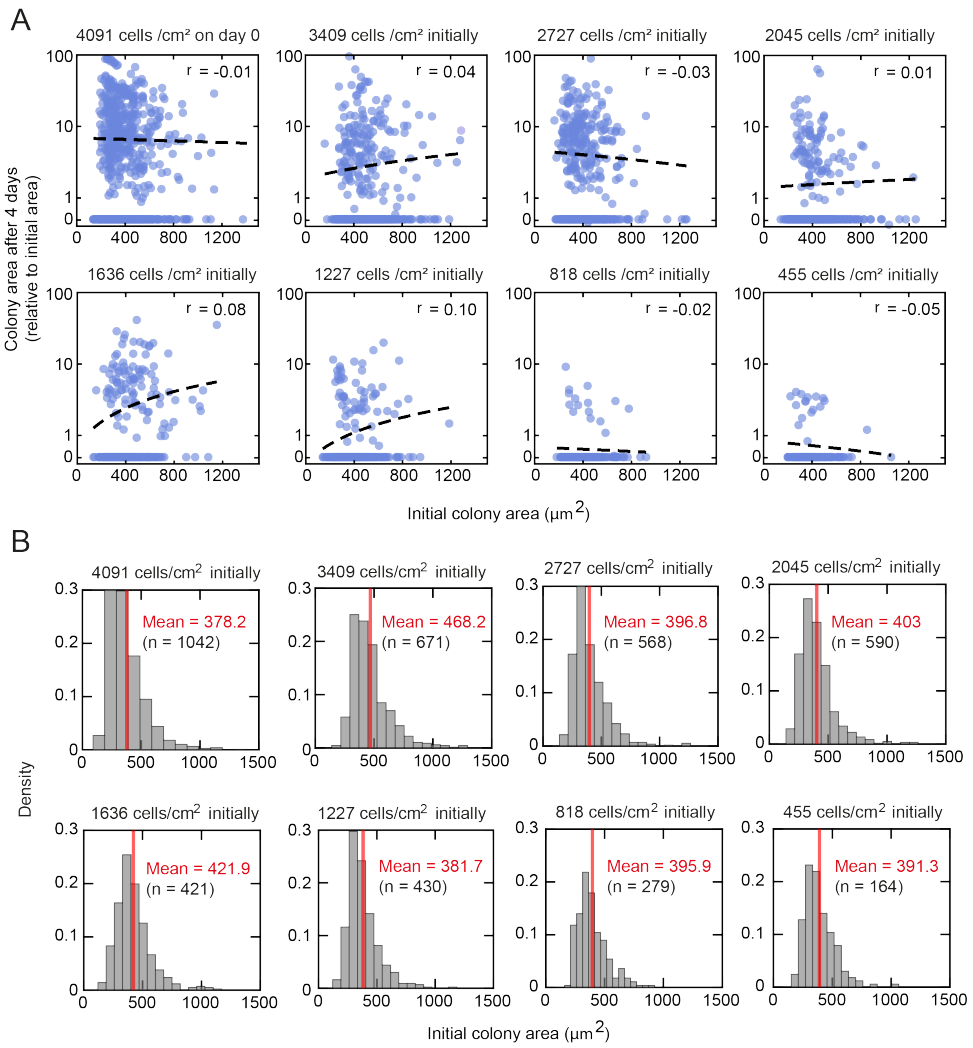

Figure 3.9: Growth and survival of differentiating cells within a colony do not depend on how many cells are initially in the colony (i.e., colony area) for any population density. (A) Data shown for E14 cells in N2B27 (unguided differentiation) without any inducer such as Retinoic Acid, after self-renewing in serum+LIF. Same protocol as in Supp. Fig. 3.8. We used a time-lapse microscope to measure the colony area during four days of differentiation. Each blue point represents the final area (after 96 hours) of a colony relative to its initial area (i.e., fold-change in colony area compared to the initial area). If a colony died during the time-lapse (spotted as explained in caption for Supp. Fig. 3.8), then we assigned it a value of zero as the fold-change in its area. Each box shows the fold-change in the colony area (vertical axis) as a function of the initial colony area (horizontal axis) for 17 fields of view and a specific population density. Dashed curves in each box denote the Pearson correlation with the correlation coefficient ρ in each box. There is virtually no correlation between a colony's final area (and whether it dies or not) and its initial area, for any starting population density. These results suggest that the initial area of a microcolony – which in turn is set by the number of cells in a microcolony – does not predict whether any cells in the colony survive or not and also does not predict how fast each cell grows during differentiation. **(B)** Same data as in (A). Shown are the means (red vertical lines) and the sample size (n) as the number of microcolonies (dots in (A)) in all 3 x 17 fields of view per initial population density we analyzed.

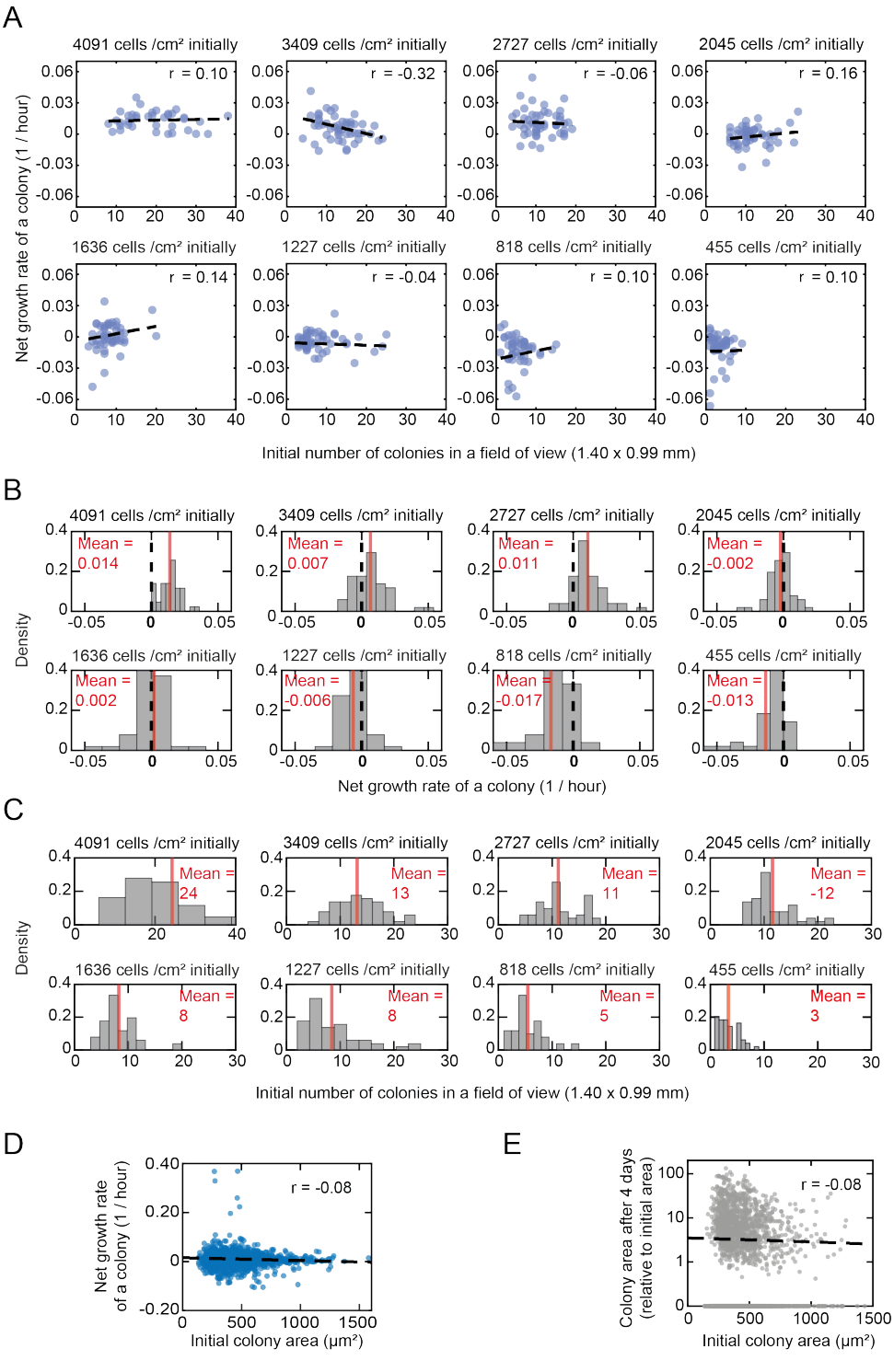
A
4091 cells /cm² initially
r = 0.10
3409 cells /cm² initially
r = -0.32
2727 cells /cm² initially
r = -0.06
2045 cells /cm² initially
r = 0.16
1636 cells /cm² initially
r = 0.14
1227 cells /cm² initially
r = -0.04
818 cells /cm² initially
r = 0.10
455 cells /cm² initially
r = 0.10
Net growth rate of a colony (1 / hour)
Initial number of colonies in a field of view (1.40 x 0.99 mm)
B
4091 cells /cm² initially
Mean = 0.014
3409 cells /cm² initially
Mean = 0.007
2727 cells /cm² initially
Mean = 0.011
2045 cells /cm² initially
Mean = -0.002
1636 cells /cm² initially
Mean = 0.002
1227 cells /cm² initially
Mean = -0.006
818 cells /cm² initially
Mean = -0.017
455 cells /cm² initially
Mean = -0.013
Density
Net growth rate of a colony (1 / hour)
C
4091 cells /cm² initially
Mean = 24
3409 cells /cm² initially
Mean = 13
2727 cells /cm² initially
Mean = 11
2045 cells /cm² initially
Mean = -12
1636 cells /cm² initially
Mean = 8
1227 cells /cm² initially
Mean = 8
818 cells /cm² initially
Mean = 5
455 cells /cm² initially
Mean = 3
Density
Initial number of colonies in a field of view (1.40 x 0.99 mm)
D
r = -0.08
Net growth rate of a colony (1 / hour)
Initial colony area (µm²)
E
r = -0.08
Colony area after 4 days (relative to initial area)
Initial colony area (µm²)

Figure 3.10 ***(preceding page)*****: Net growth rate of a colony does not depend on how many cells are in the colony (i.e., colony area) for any population density.** Data shown for E14 cells in N2B27 (unguided differentiation) without any inducer such as Retinoic Acid, after self-renewing in serum+LIF. Same protocol as in Supp. Fig. 3.8. **(A)** We fitted an exponential function, Area(t) = $A_0 exp(\mu t)$, to each grey trace shown in Supp. Fig. 3.8 (i.e., we estimated colony area as exponentially growing as a function of time). From this fit, we determined net growth rate μ for each colony (i.e., for every grey trace shown in Supp. Fig. 3.8). For a given colony, we determined its net growth rate and the initial number of colonies that resided in the same field of view. Each blue point shows the data for a single colony. The net growth rate is positive ($\mu > 0$) if the colony grew over the four days of differentiation whereas it is negative ($\mu < 0$) or zero if the colony died (i.e., shrank or did not grow after which it often detached from the plate and thus disappeared from the field of view). Each box shows a colony's net growth rate (vertical axis) as a function of the initial number of colonies that resided in the same field of view (horizontal axis) for a specific population density. We analyzed 17 fields of view for each starting population density. Dashed lines in each box shows the Pearson correlation with the correlation coefficient ρ denoted in each box. Here we see that how fast a colony grows - and whether it survives or dies - is virtually uncorrelated with how many other colonies there are in its ~1 mm x 1 mm neighborhood. **(D)** There is virtually no correlation between a colony's net growth rate and its initial area, as shown here. Data points come from many different, initial population densities and pooled together here. Dashed line shows the Pearson correlation with the correlation coefficient ρ= -0.08. **(E)** There is virtually no correlation between a colony's fold-change in colony area relative to its initial area and its initial area, as shown here. Data points come from many different, initial population densities and pooled together here. Dashed line shows the Pearson correlation with the correlation coefficient ρ= -0.01.

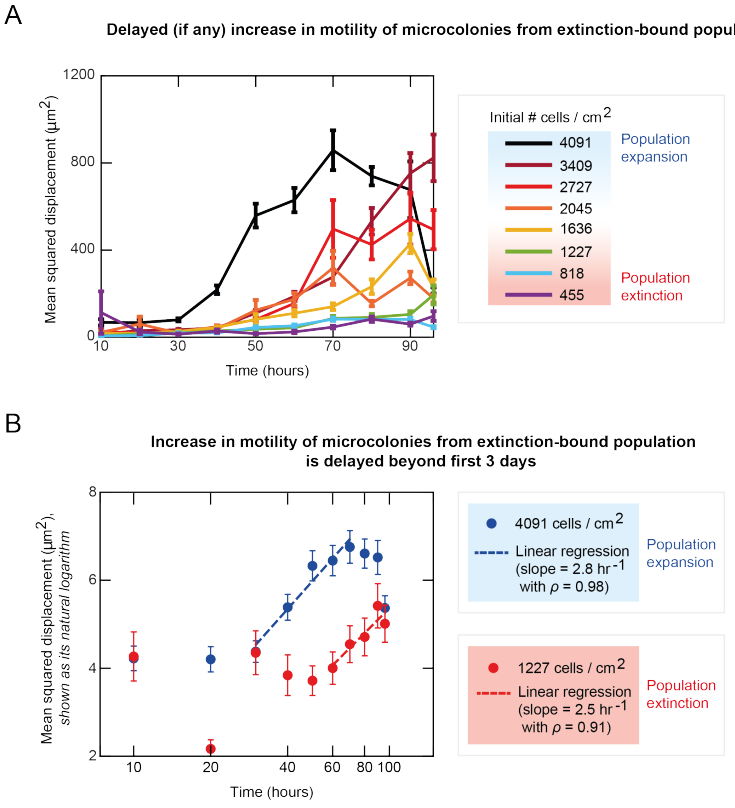

Figure 3.11 ***(preceding page)*****: No significant change in motility of microcolonies from extinction-bound population in first 3 days of differentiation.** Data shown for E14 cells in N2B27 (unguided differentiation) without any inducer such as Retinoic Acid, after self-renewing in serum+LIF. We used a wide-field microscope to image and measure the area of each microcolony over four days (see Supp. Fig. 3.8). During the four days, we measured the area of a given microcolony in each field of view (dimension 1.40 x 0.99 mm; total of 17 fields of view for each plate) with 10-hour intervals (see Materials and methods). To locate each microcolony in time we determined the x-coordinates and the y-coordinates of the micrcolony's area's centroid. From the trajectory of a centroid we computed the Mean Squared Displacement (MSD) which is a common measure to determine the spatial extent of a particle's motion (random or directed) [175, 176]. The Mean Square Displacement MSD(τ) for particle's 2-dimensional trajectory is determined by MSD(τ) = $< \triangle\vec{r}^2 > = < [\vec{r}^2(t+\tau) - \vec{r}^2(t)]^2 > = < [x(t+\tau) - x(t)]^2 + [y(t+\tau) - x(t)]^2 >$, where $\vec{r}(t)$ denotes the particle's position in 2D space (with x-coordinates and y-coordinates) at time t, and τ is the time interval between two positions the particle takes in order to compute the displacement $\triangle\vec{r}(\tau) = \vec{r}(t+\tau) - \vec{r}(t)$. The average as denoted by $< ... >$ indicates a time average. Here we set a particle's position equal to the microcolony's area's centroid. For a pure 2-dimensional random (i.e., Brownian) motion in liquid we expect the MSD(τ) $\propto \tau$ (where the proportionality constant is exactly equal to $4D$, with D being the microcolony's diffusion coefficient). **(A)** Plotted are the MSD for microcolonies (each with its own trajectory) from each initial population density (see legend). Shown are the ensemble averages over all trajectories. Error bars are s.e.m. Expanding populations (above ~1700 cells / cm^2) show an increase in MSD in first 3 days of differentiation whereas extinction-bound populations (below ~1700 cells / cm^2) have rather flat MSD over four days. For the legend, blue and red shades indicate population expansion and extinction, respectively. **(B)** Shown is the MSD (as its natural logarithm) versus time (as its natural logarithm) for microcolonies from an expanding population (in blue - 4091 cells / cm^2) and an extinction-bound population (in red - 1227 cells / cm^2). Same data as shown in (A). A linear regression indicates a time-interval where the MSD increases linearly. For the expanding population this linear relation starts after ~30 hours during differentiation whereas for the extinction-bound population this starts after ~70 hours during differentiation. Error bars are s.e.m. For the legend, blue and red shades indicate population expansion and extinction, respectively. Together, these results indicate that microcolonies from extinction-bound populations show no significant change in motility in first 3 days of differentiation. These first ~3 days define a time window for which we also found populations determine their survival-vs-extinction fate by secreting diffusive factor(s) (see Fig. 3.2)

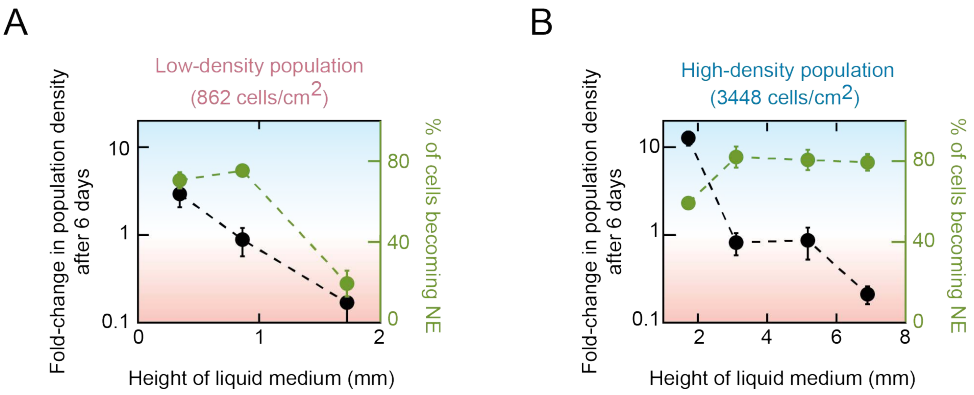

Figure 3.12: Changing the height of the cell-culture medium over several millimeters alters the survival-versus-extinction fate of the population on the bottom of the cell-culture dish. Data shown for 46C cells in N2B27+RA (NE-guided differentiation) with the inducer Retinoic Acid (RA), after self-renewing in serum+LIF. Black data points are duplicates of the data shown in Fig. 3.6 and they indicate the fold change in the population density (relative to the initial population density) as a function of the liquid-medium height above the cells. Green data points indicate the percentage of the cells that expressed GFP (i.e., Sox1 - a marker for NE lineage), which we measured with a flow cytometer, as a function of the liquid height above the cells. In our study, we used a 10-mL liquid medium (e.g., in Figs. 2.2-2.6) unless we explicitly state that we used a different volume (e.g., in Fig. 3.6 and here). A 10-mL liquid has a height that is just below ~2 mm in a 10-cm diameter dish. **(A)** Data for a differentiating population that starts with a low density (862 cells / cm^2). In a 10-mL liquid, this population becomes extinct (last data point, at ~2-mm liquid height). From the smallest to the largest liquid height, the data correspond to 2 mL, 5 mL, and 10 mL liquid media. **(B)** Data for a differentiating population that starts with a high density (3448 cells / cm2). In a 10-mL liquid, this population survives and grows towards the carrying capacity (first data point, at ~2-mm height). From the smallest to the largest liquid height, the data correspond to 10 mL, 20 mL, 30 mL, and 40 mL liquid media. (A) shows that we can rescue a low-density population - it survives - if we decrease the liquid height by 50% or more from the usual, ~2-mm. (B) shows that we can drive a high-density population to barely survive or become extinct if we increase the liquid height by a 2-fold or more. Altogether, these results exclude local communication. They suggest that the key secreted molecules diffuse over at least several millimeters to control a population's survival-vs-extinction fate.

4

Nonlocal communication requires YAP1 activity

Parts of this chapter are also reported in Daneshpour et al. [2]

4.1. Introduction

Given that a macroscopic range (near-centimeter scale) of communication dictates survival or death of the entire ES-cell population in a switch-like manner, we next examined the mechanism of action of the secreted molecules. In the next two chapters we devoted our efforts to ultimately identifying the responsible survival factor. The existence of a "population-density threshold" - above which extinction-bound ES cells become bound to surviving and expanding toward the carrying capacity while differentiating - suggests that initial population-density (secreted molecules) controls molecular components of signalling pathways to activate survival mechanisms (i.e., genes) in high-density populations but not low-density populations.

4.2. Results

4.2.1. Transcriptome analysis reveals increased YAP1 activity for collective survival during differentiation

To systematically identify what category of genes are primarily activated/repressed as population-density increases, we first performed RNA sequencing (RNA-Seq) to reveal the presence and abundance of RNA (gene expression) in ES-cell populations of high (5172 cells / cm^2), medium (1931 cells / cm^2) and low (862 cells / cm^2) initial density (Fig. 4.1 and Supp. Figs. 4.6-4.7). The high-density populations survive and expand towards the carrying capacity while the low-density populations become extinct during differentiation. The medium-density population was near the density threshold and it neither expanded nor shrank to extinction over six days. For each density, we collected and lysed 46C cells that were differentiating for two days in N2B27 because this is when the growth-dynamics of a surviving population begins to be distinguishable from that of an extinction-bound population (Fig. 2.6A and Fig. 3.2B).

We found that the high-density population, compared to the low-density population, showed significant enrichments in genes that are involved in multicellular processes, cell-cell signalling, neurological processes, and cell adhesion (Fig. 4.6). More specifically, compared to the low-density population, the high-density population had higher expression of genes that YAP1 directly or indirectly activates (e.g., *Cyr61* and *Amotl2*) and lower expression of genes that YAP1 directly or indirectly downregulates (e.g., *Angptl4* and *Tmem79*) (Fig. 4.1 and Supp. Fig. 4.7) [177–184]. YAP1 is a key component of the widely conserved Hippo signalling pathway and a master regulator of transcription for genes that control cell proliferation, apoptosis, and differentiation (Supp. Fig. 4.6) [177, 178, 185, 186]. YAP1 is primarily known for being regulated by cell-cell contact-mediated signalling [187]. But recent studies are beginning to show that YAP1 controls survival in a non-cell

autonomous manner by cells that secrete diffusible signals such as Cyr61 [178, 188]. Altogether, these results suggest that YAP1 becomes more active in populations that begin with higher densities.

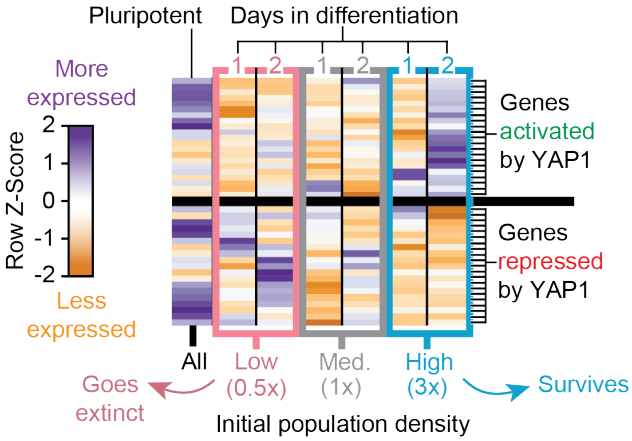

Figure 4.1: YAP1 targets are more activated / repressed as population density increases. Heat map showing transcriptome-wide changes in 46C cells during unguided differentiation (N2B27) (after self-renewing in serum+LIF) in low-density population (862 cells / cm^2; enclosed in pink box), near-threshold (medium-density) population (1931 cells / cm^2; enclosed in grey box), and high-density population (5172 cells / cm^2; enclosed in blue box). Leftmost column shows data for self-renewal (pluripotent) population before differentiation begins (labeled "All" since every population starts as this population before differentiation). Each column of differentiating population shows data for 1 day after (labeled "1") or 2 days after (labeled "2") starting differentiation. Each row shows a different gene, each of which are either activated (21 genes) or repressed (19 genes) by YAP1, either directly or indirectly. Supp. Fig. 4.7 lists all genes. Color represents row Z-score: a measure of by how much a gene's expression level for a given condition deviates from that gene's expression level averaged across all different conditions (i.e., different populations and days). Purple represents a positive row Z-score (more expressed than average). Orange represents a negative row Z-score (less expressed than average). Data based on 3 biological replicates.

4.2.2. Collective survival only occurs under active YAP1 in first two days of differentiation

The RNA-Seq results suggest that YAP1, as a master regulator, becomes more active in populations that begin with higher densities (Fig. 4.1). Therefore, we focused on YAP1's role in determining collective survival during differentiation. YAP1 exists in either a phosphorylated or a dephosphorylated form (Fig. 4.2A). YAP1 is inactive when it is phosphorylated and active when it is unphosphorylated. The dephosphorylated (active) YAP1 enters the cell nucleus to transcriptionally regulate numerous genes, including anti-apoptotic (e.g., *Bcl2*) and YAP1-specific cell-signaling (e.g., *Cyr61*) genes.

To determine if and when active YAP1 is required for collective survival, we inhibited any active YAP1 inside cells with verteporfin (VP), which is a well-characterized

permeable small-molecule inhibitor of YAP1 [177, 189] (Fig. 4.2A).

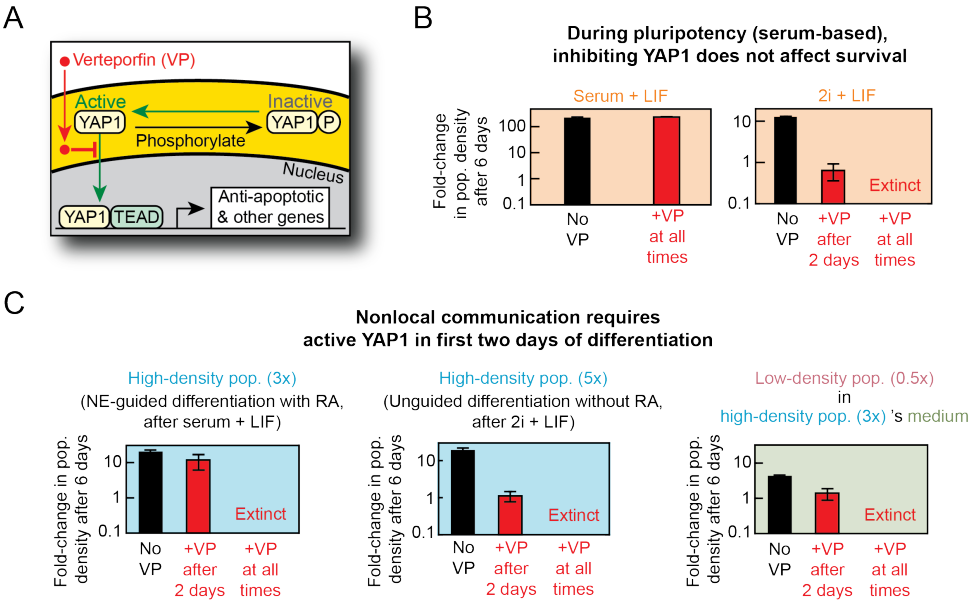

Figure 4.2: Nonlocal communication requires active YAP1 for survival in first 2 days of differentiation, but not during serum-based pluripotency. (A) YAP1 exists as either phosphorylated (labeled "P") or dephosphorylated. Verteporfin (VP) inhibits active (dephosphorylated) Yap1 from entering the nucleus and regulating target gene expression. **(B)** Fold-change in population density (46C cells) after 6 days in either serum-based (serum+LIF) (left graph) or serum-free (2*i*+LIF) (right graph), pluripotency media. Red bars is for populations either incubated continuously or after 2 days with 1-μM verteporfin (VP) in DMSO until day 6. Black bar is for populations without VP but with the same amount of DMSO as control. All populations started at 862 cells / cm^2. Error bars are s.e.m.; n = 3. **(C)** Fold-change in population density for high-density population (5172 cells / cm^2 ("3x") or 8620 cells / cm^2 ("5x") initially, in blue box) and low-density population that was rescued with medium of 2-days-old high-density population (862 cells / cm^2 initially, in green box) after 6 days of differentiation towards NE-lineage. Data for 46C cells differentiating en previously self-renewing as indicated above the graphs. For the right graph (green box), 46C cells were previously self-renewing in serum+LIF. Results are for either NE-guided (with Retinoic Acid (RA)) or unguided (only N2B27) differentiation, and for cells previously propagated in serum-based (FBS) or serum-free (2i), pluripotency medium. Black bar: Verteporfin (VP) was always absent. Red bar in middle of each box: VP was added to medium after the first two days. Third column of each box shows absence of cells (extinction) when VP was present from the start of differentiation. Error bars are s.e.m.; n = 3.

When we added 1 μM of VP in the medium (serum+LIF) of self-renewing cells, populations grew normally to the carrying capacity (Fig. 4.2B - left graph denoted "Serum + LIF"). In N2B27 with Retinoic Acid (RA), keeping 1 μM of VP from the start of differentiation (day 0) drove a high-density population (5172 cells / cm^2) to extinction (Fig. 4.2C - "+VP at all times" in blue box of left graph). But, in N2B27 with RA, adding 1 μM of VP after two days did not hinder the high-density population's growth: the population grew to nearly reach the carrying capacity in six days as usual (Fig. 4.2C - "+VP after 2 days" in blue box of left graph). This

population behaved as if VP were never present. We obtained the same results when we added VP to N2B27 without RA (Fig. 4.2C - middle graph).

A low-density population (862 cells / cm^2), as shown before, survives and grows in differentiation medium (N2B27) taken from a 2-days-old, high-density population (Fig. 4.2C - "No VP" in green box of right graph). Adding 1 μM of VP at the time of the medium transfer (start of differentiation) causes the low-density population to become extinct (Fig. 4.2C - "+VP at all times" in green box of right graph). In contrast, adding the VP two days after the medium transfer causes the low-density population to survive and grow, albeit more slowly compared to the situation in which VP was never present (Fig. 4.2C - "+VP after 2 days" in green box of right graph).

Altogether, these results establish that the putative nonlocal communication requires YAP1 to be activatable to save a differentiating population from extinction during the first 2 days of differentiation.

4.2.3. Nonlocal communication activates YAP1 targets including anti-apoptotic processes

To confirm that YAP1 is crucial for the nonlocal communication and collective survival, we used phospho-ELISA to measure the amount of phosphorylated (inactive) YAP1 in cells for various initial population densities. The phoshpo-ELISA specifically detected phosphorylation at Ser397, one of the primary phosphorylation sites of YAP1 for the mouse [185, 190]. For each initial population density, we measured the amount of inactive YAP1 per cell, three days after starting differentiation. We also measured the amounts of inactive YAP1 per cell in populations that were self-renewing at various densities (Supp. Fig. 4.8). Note that we did not measure the total amount of YAP1. But we can still compare the levels of inactive YAP1 between the different populations because our RNA-Seq established that differentiating populations of different initial densities all expressed nearly the same level of *YAP1* (Supp. Fig. 4.8).

In a low-density population (862 cells / cm^2) that was headed for extinction, cells had nearly the same amount of inactive YAP1 as the self-renewing cells of the same density (Fig. 4.3A - first bar (pink); and in Supp. Fig. 4.8). In a high-density population (5172 cells / cm^2) cells had about half as much inactive YAP1 (i.e., double the amount of active YAP1) compared to the cells in the extinction-bound, low-density population (Fig. 4.3A - second bar (blue); and in Supp. Fig. 4.8). In the low-density population that was rescued by a conditioned medium taken from a 2-days-old, high-density population, cells also had about half as much inactive YAP1 (i.e., double the amount of active YAP1) compared to the cells in the extinction-bound, low-density population (Fig. 4.3A - third bar (green); and in Supp. Fig.

4.8).

These results establish that, after exiting pluripotency (day 3), cells of surviving populations have less inactive (i.e., more active) YAP1 than cells of extinction-bound populations, consistent with active YAP1 being required for populations to survive pluripotency exit (Fig. 4.2C).

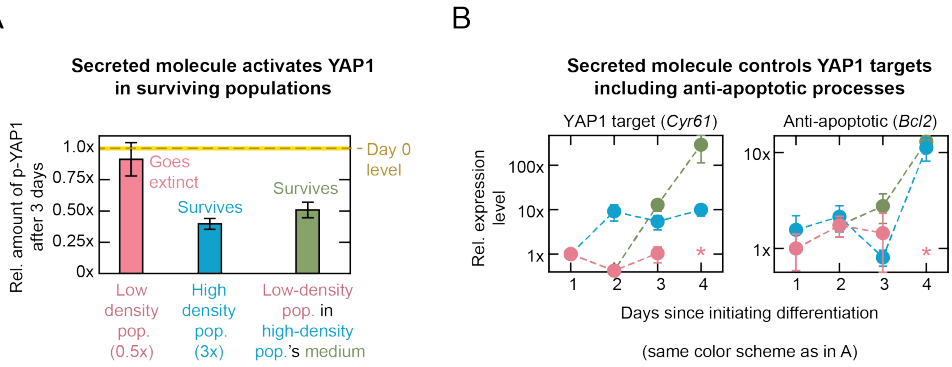

Figure 4.3: Nonlocal communication increases YAP1 activity and promotes anti-apoptotic process during differentiation. (A) ELISA measurements showing amounts of YAP1 protein phosphorylated at Ser397 (inactive YAP1) (see Materials and methods and also Supp. Fig. 4.8). Vertical axis shows the relative amount of inactive YAP1: the level of inactive YAP1 for a differentiating population divided by the amount of inactive YAP1 for a pluripotent population that has the same cell numbers as the differentiating population at the time of lysing the cells for ELISA. Values are for 46C cells, 3 days after starting differentiation towards NE lineage. Pink: low-density population (862 cells / cm^2 initially). Blue: high-density population (5172 cells / cm^2 initially). Green: low-density population rescued after two days by medium from a 2-day-old high-density population. Error bars are s.e.m.; n = 3. **(B)** *Cyr61* (direct YAP1 target) and *Bcl2* (anti-apoptotic gene) expression levels over time after initiating differentiation towards NE lineage. Data obtained from 46C cells in N2B27+RA after self-renewing in serum+LIF. Same color scheme as in (A). Also see Supp. Fig. 4.9. On each day, we first normalized a population's gene expression level by that population's *Gapdh* level (housekeeping gene). Afterwards, plotted on the vertical axis, we divided each population's *Gapdh*-normalized gene expression level on a given day by the *Gapdh*-normalized value for a one-day-old low-density population (whose value is thus "1x" here). Error bars are s.e.m.; n = 3.

By measuring the expression levels of genes that YAP1 transcriptionally regulates, we found that *Bcl2*, an anti-apoptotic gene known to be activated by YAP1 [177], was upregulated in all populations that survived (either by themselves or rescued by conditioned medium) whereas it remained low in population that went extinct. Specifically, with reverse transcription quantitative real-time PCR (RT-qPCR), we measured *Bcl2* and other targets of YAP1 in three populations: a low-density population (862 cells / cm^2: Fig. 4.3B - pink), a high-density population (5172 cells / cm^2: Fig. 4.3B - blue), and a low-density population cultured in the supernatant of a high-density population (Fig. 4.3B - green). Of these, only the low-density population became extinct and maintained relatively low, basal levels of *Bcl2* expression that remained unchanged over days (Fig. 4.3B - pink in the right graph). The other two populations, after 2-3 days, began to increase their *Bcl2* expression

level by up to 10-fold (Fig. 4.3B - right graph). Importantly, we also found that the only two, surviving populations had upregulated *Cyr61*, a well-known (direct) target of YAP1 [178, 188], after 2-3 days of beginning differentiation (Fig. 4.3B - left graph). This supports the claim that the *Bcl2* upregulation is most likely due to YAP1's direct regulation (see Supp. Fig. 4.9 for other YAP1-mediated genes that we studied).

Finally, we also observed that the protein level of active caspase-3, a well-known apoptosis executioner [177] (also see Chapter 8 for more detailed explanation about the role of caspases in apoptosis), was ~2-fold higher in the low-density population than in the high-density and rescued populations (Fig. 4.3 and Supp. Fig. 4.10).

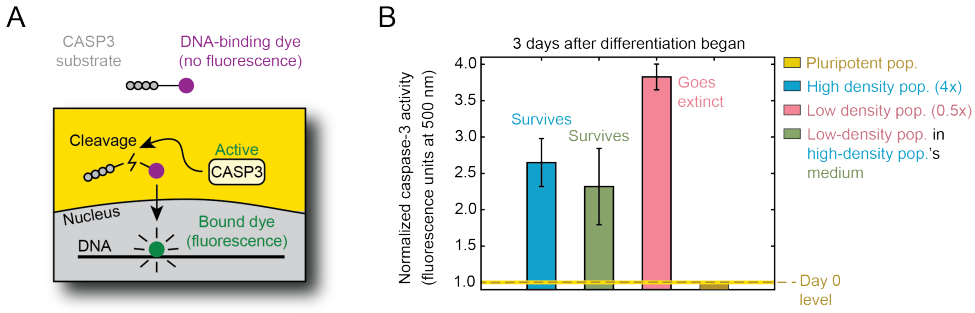

Figure 4.4: Increased caspase-3 (apoptosis executioner) activity for extinction-bound populations. **(A)** We sought to examine the activity of a well-known, pro-apoptotic marker (caspase-3) in populations that are either extinction-bound or surviving. We used a membrane-permeable, DNA-dye-based assay (NucView 488 Caspase-3 Assay Kit for Live Cells). This assay measured the amounts of active caspase 3/7 inside cells. **(B)** Data shown for E14 cells differentiating in N2B27+RA (NE lineage) and previously self-renewing in serum+LIF. We examined active caspase-3 levels in four different populations: (1) high-density population (6896 cells / cm^2 – blue bar); low-density population (517 cells / cm^2 – pink bar); (3) low-density population that was rescued from extinction by transplanting it, after two days, into the high-density population's medium (green bar); and (4) pluripotent E14 cells before we induced the differentiation (yellow bar). After 3 days of differentiation, we collected the cells from each of these populations, mixed them with the DNA-dye according to the manufacturer's protocol, and then measured the resulting fluorescence at 500 nm in single cells with a flow cytometer. Plotted here are the geometric means of the fluorescence for each population (also see Supp. Fig. 4.10). Higher fluorescence means increased caspase-3 activity. We normalized the values to the fluorescence level of the pluripotent population (yellow bar), as indicated by the dashed line. n = 3; Error bars are s.e.m. These results show that all differentiating populations have upregulated levels of caspase-3 relative to the pluripotent populations. However, the nonlocal communication causes populations to have less increased caspase-3 activities compared to extinction-bound populations.

Combined, these results establish that low-density (extinction-bound) populations have elevated apoptotic activities that are not countered by anti-apoptotic activities whereas surviving (high-density or rescued) populations have elevated anti-apoptotic activities that are not countered by apoptotic activities.

4.3. Conclusions

We discovered that nonlocal communication - which is crucial to deciding collective survival during differentiation - requires and increases YAP1 activity in the surviving populations.

We used three complementary methods to establish the involvement of YAP1. In one, using RNA-Seq and RT-qPCR, we show that (high-density or rescued) populations that survive express high amounts of YAP1-activated genes such as *Cyr61* and *Amotl2*. In another, using a small-molecule inhibitor, we show we can drive surviving populations towards extinction by blocking active YAP1 during the first 2 days of differentiation. Finally, we show that extinction-bound populations have higher amounts of inactive YAP1 (phosphorylated YAP1) compared to surviving populations. As a result, extinction-bound populations do not have upregulated levels of anti-apoptotic genes (such as *Bcl2*) but instead have higher amounts of apoptosis executioner proteins (active caspase-3).

Therefore, nonlocal communication through secreted molecules controls anti-apoptotic processes only for populations bound to surviving the process of differentiation (Fig. 4.5).

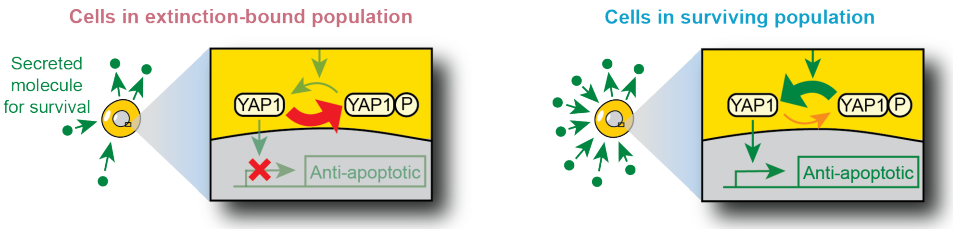

Figure 4.5: YAP1-based mechanism for determining collective survival during differentiation. Conclusions from the results in Figs. 4.1-4.4. Diagrams show how secreted molecules activate the transcription regulator YAP1. As a result, but in contrast with cells in surviving population (right cartoon), cells in extinction-bound populations fail to activate anti-apoptotic activities (left cartoon).

4.4. Supplementary Information

(see next page)

A

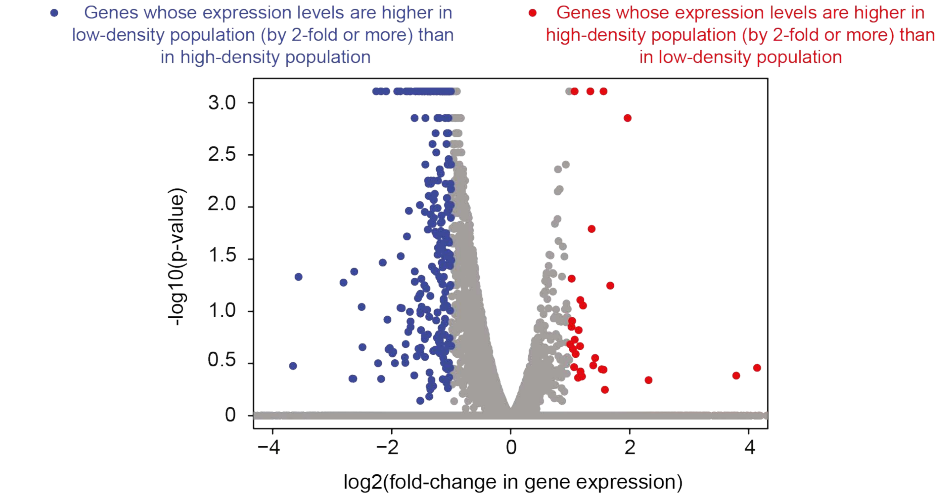
Genes whose expression levels are higher in low-density population (by 2-fold or more) than in high-density population
Genes whose expression levels are higher in high-density population (by 2-fold or more) than in low-density population
-log10(p-value)
log2(fold-change in gene expression)

B

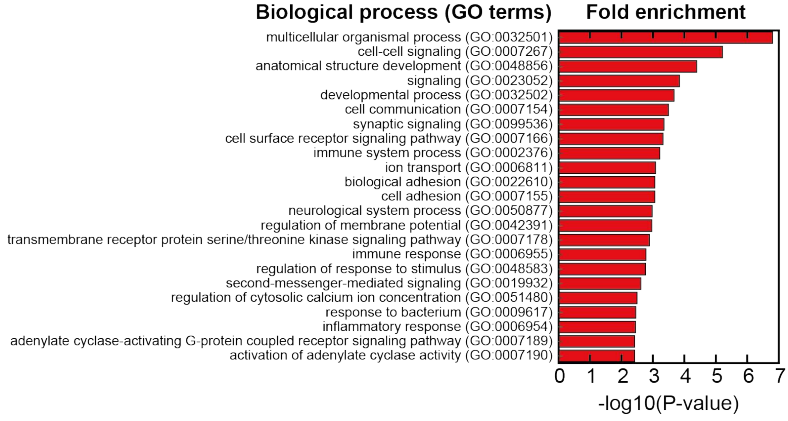
Biological process (GO terms)
Fold enrichment
multicellular organismal process (GO:0032501)
cell-cell signaling (GO:0007267)
anatomical structure development (GO:0048856)
signaling (GO:0023052)
developmental process (GO:0032502)
cell communication (GO:0007154)
synaptic signaling (GO:0099536)
cell surface receptor signaling pathway (GO:0007166)
immune system process (GO:0002376)
ion transport (GO:0006811)
biological adhesion (GO:0022610)
cell adhesion (GO:0007155)
neurological system process (GO:0050877)
regulation of membrane potential (GO:0042391)
transmembrane receptor protein serine/threonine kinase signaling pathway (GO:0007178)
immune response (GO:0006955)
regulation of response to stimulus (GO:0048583)
second-messenger-mediated signaling (GO:0019932)
regulation of cytosolic calcium ion concentration (GO:0051480)
response to bacterium (GO:0009617)
inflammatory response (GO:0006954)
adenylate cyclase-activating G-protein coupled receptor signaling pathway (GO:0007189)
activation of adenylate cyclase activity (GO:0007190)
-log10(P-value)

C

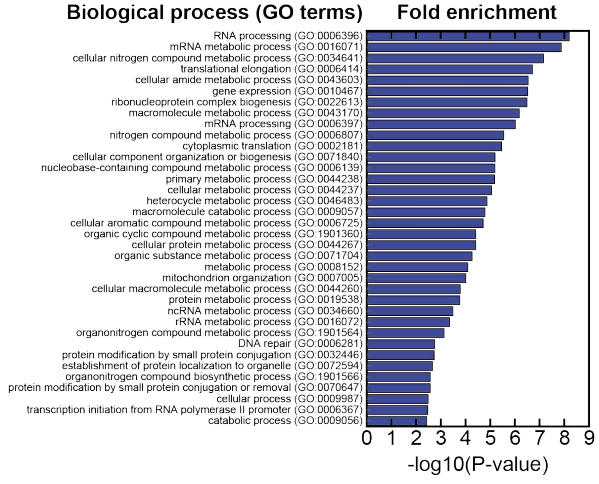
Biological process (GO terms)
Fold enrichment
RNA processing (GO:0006396)
mRNA metabolic process (GO:0016071)
cellular nitrogen compound metabolic process (GO:0034641)
translational elongation (GO:0006414)
cellular amide metabolic process (GO:0043603)
gene expression (GO:0010467)
ribonucleoprotein complex biogenesis (GO:0022613)
macromolecule metabolic process (GO:0043170)
mRNA processing (GO:0006397)
nitrogen compound metabolic process (GO:0006807)
cytoplasmic translation (GO:0002181)
cellular component organization or biogenesis (GO:0071840)
nucleobase-containing compound metabolic process (GO:0006139)
primary metabolic process (GO:0044238)
cellular metabolic process (GO:0044237)
heterocycle metabolic process (GO:0046483)
macromolecule catabolic process (GO:0009057)
cellular aromatic compound metabolic process (GO:0006725)
organic cyclic compound metabolic process (GO:1901360)
cellular protein metabolic process (GO:0044267)
organic substance metabolic process (GO:0071704)
metabolic process (GO:0008152)
mitochondrion organization (GO:0007005)
cellular macromolecule metabolic process (GO:0044260)
protein metabolic process (GO:0019538)
ncRNA metabolic process (GO:0034660)
rRNA metabolic process (GO:0016072)
organonitrogen compound metabolic process (GO:1901564)
DNA repair (GO:0006281)
protein modification by small protein conjugation (GO:0032446)
establishment of protein localization to organelle (GO:0072594)
organonitrogen compound biosynthetic process (GO:1901566)
protein modification by small protein conjugation or removal (GO:0070647)
cellular process (GO:0009987)
transcription initiation from RNA polymerase II promoter (GO:0006367)
catabolic process (GO:0009056)
-log10(P-value)

Figure 4.6 *(preceding page)*: Enrichment analysis of RNA-Seq data reveals that high-density populations, compared to low-density populations, have higher levels of processes (GO terms) such as multicellular organismal processes, cell-cell signaling, neurological system processes, and cell adhesion. We identified possible, intracellular pathways that the secreted molecules control by performing a transcriptome-level profiling (RNA-Seq) to examine differentially expressed genes. For this, we used Retinoic Acid (RA) to cause 46C cells to differentiate towards the Neural Ectoderm (NE) lineage in N2B27+RA after self-renewing in serum+LIF. We performed RNA-Seq on populations of three different starting densities: (1) a low-density (862 cells/cm^2) population that becomes extinct; (2) a high-density (5172 cells/cm^2) population that grows towards the carrying capacity; and (3) a medium-density (1931 cells/cm^2) population that is near the threshold density. For RNA-Seq, we collected all cells from these populations on the first and second days after triggering differentiation. We also collected cells that were kept pluripotent in a serum-based pluripotency medium (FBS with LIF) as a comparison. We analyzed the resulting transcriptome expression levels (FPKMs) for each gene by focusing on gene-expression levels that differed by more than 2-folds between the high- and low-density populations. **(A)** Volcano plot. Each grey dot represents a single gene. The horizontal axis shows the relative expression level: the expression level of the high-density population divided by the expression level of the low-density population. The vertical axis shows the p-value of the statistical test performed in Cufflinks (see Materials and methods). Genes that are more highly expressed by the high-density population than the low-density population, by 2-folds or more, are shown as red points. Genes that are more highly expressed by the low-density population than the high-density population, by 2-folds or more, are shown as blue points. **(B)** Enrichment analysis for genes that are more highly expressed by the high-density population than the low-density population by 2-folds or more (red data points in (A)). We used PANTHER and a custom MATLAB script to examine which GO terms (biological processes) are enriched and determine the corresponding significance (p-value) of the enrichment. We list here the enriched GO terms with their GO-term numbers. This plot shows that GO terms such as "multicellular organismal processes", "cell-cell signaling", "neurological system processes" and "cell adhesion" have some of the highest fold enrichments. **(C)** Enrichment analysis for genes that are more highly expressed by the low-density population than the high-density population by 2-folds or more (blue data points in (A)). We list here the enriched GO terms with their GO-term numbers. This plot shows that GO terms such as "RNA processing" and "macromolecule catabolic processes" have some of the highest fold enrichments. See also Supp. Fig. 4.7 for further analyses of the RNA-Seq dataset.

A

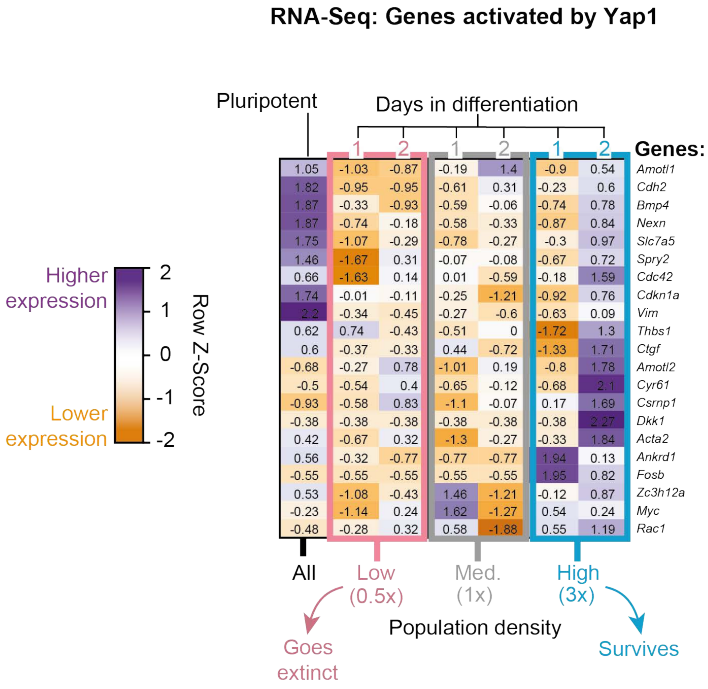
RNA-Seq: Genes activated by Yap1
Pluripotent
Days in differentiation
1 2 1 2 1 2
Genes:
1.05 -1.03 -0.87 -0.19 1.4 -0.9 0.54 Amotl1
1.82 -0.95 -0.95 -0.61 0.31 -0.23 0.6 Cdh2
1.87 -0.33 -0.93 -0.59 -0.06 -0.74 0.78 Bmp4
1.87 -0.74 -0.18 -0.58 -0.33 -0.87 0.84 Nexn
1.75 -1.07 -0.29 -0.78 -0.27 -0.3 0.97 Slc7a5
1.46 -1.67 0.31 -0.07 -0.08 -0.67 0.72 Spry2
0.66 -1.63 0.14 0.01 -0.59 -0.18 1.59 Cdc42
1.74 -0.01 -0.11 -0.25 -1.21 -0.92 0.76 Cdkn1a
2.2 -0.34 -0.45 -0.27 -0.6 -0.63 0.09 Vim
0.62 0.74 -0.43 -0.51 0 -1.72 1.3 Thbs1
0.6 -0.37 -0.33 0.44 -0.72 -1.33 1.71 Ctgf
-0.68 -0.27 0.78 -1.01 0.19 -0.8 1.78 Amotl2
-0.5 -0.54 0.4 -0.65 -0.12 -0.68 2.1 Cyr61
-0.93 -0.58 0.83 -1.1 -0.07 0.17 1.69 Csrnp1
-0.38 -0.38 -0.38 -0.38 -0.38 -0.38 2.27 Dkk1
0.42 -0.67 0.32 -1.3 -0.27 -0.33 1.84 Acta2
0.56 -0.32 -0.77 -0.77 -0.77 1.94 0.13 Ankrd1
-0.55 -0.55 -0.55 -0.55 -0.55 1.95 0.82 Fosb
0.53 -1.08 -0.43 1.46 -1.21 -0.12 0.87 Zc3h12a
-0.23 -1.14 0.24 1.62 -1.27 0.54 0.24 Myc
-0.48 -0.28 0.32 0.58 -1.88 0.55 1.19 Rac1
All
Low (0.5x)
Med. (1x)
High (3x)
Goes extinct
Population density
Survives
Higher expression
Lower expression
Row Z-Score
2
1
0
-1
-2

B

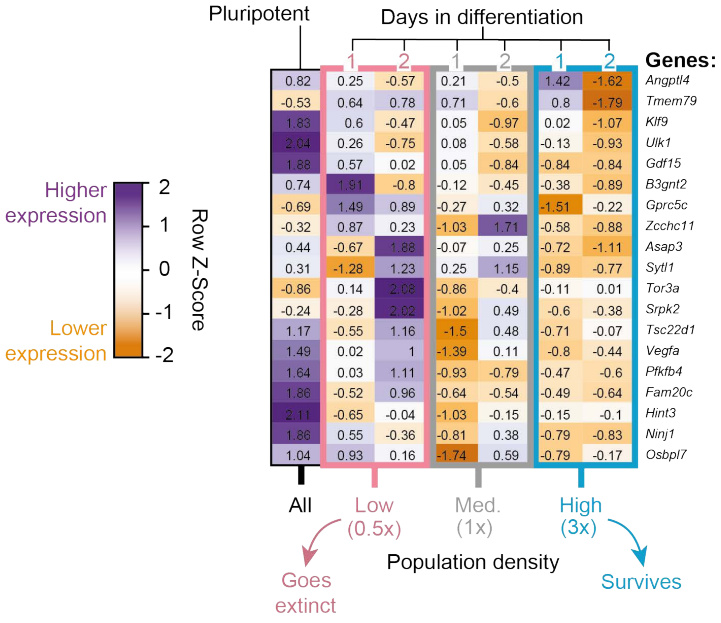
RNA-Seq: Genes repressed by Yap1
Pluripotent
Days in differentiation
1 2 1 2 1 2
Genes:
0.82 0.25 -0.57 0.21 -0.5 1.42 -1.62 Angptl4
-0.53 0.64 0.78 0.71 -0.6 0.8 -1.79 Tmem79
1.83 0.6 -0.47 0.05 -0.97 0.02 -1.07 Klf9
2.04 0.26 -0.75 0.08 -0.58 -0.13 -0.93 Ulk1
1.88 0.57 0.02 0.05 -0.84 -0.84 -0.84 Gdf15
0.74 1.91 -0.8 -0.12 -0.45 -0.38 -0.89 B3gnt2
-0.69 1.49 0.89 -0.27 0.32 -1.51 -0.22 Gprc5c
-0.32 0.87 0.23 -1.03 1.71 -0.58 -0.88 Zcchc11
0.44 -0.67 1.88 -0.07 0.25 -0.72 -1.11 Asap3
0.31 -1.28 1.23 0.25 1.15 -0.89 -0.77 Sytl1
-0.86 0.14 2.08 -0.86 -0.4 -0.11 0.01 Tor3a
-0.24 -0.28 2.02 -1.02 0.49 -0.6 -0.38 Srpk2
1.17 -0.55 1.16 -1.5 0.48 -0.71 -0.07 Tsc22d1
1.49 0.02 1 -1.39 0.11 -0.8 -0.44 Vegfa
1.64 0.03 1.11 -0.93 -0.79 -0.47 -0.6 Pfkfb4
1.86 -0.52 0.96 -0.64 -0.54 -0.49 -0.64 Fam20c
2.11 -0.65 -0.04 -1.03 -0.15 -0.15 -0.1 Hint3
1.86 0.55 -0.36 -0.81 0.38 -0.79 -0.83 Ninj1
1.04 0.93 0.16 -1.74 0.59 -0.79 -0.17 Osbpl7
All
Low (0.5x)
Med. (1x)
High (3x)
Goes extinct
Population density
Survives
Higher expression
Lower expression
Row Z-Score
2
1
0
-1
-2

Figure 4.7 *(preceding page)*: RNA-Seq analysis reveals that YAP1 becomes more active in populations that start with higher densities. Same RNA-Seq dataset as in Supp. Fig. 4.6. YAP1 is a key component of the Hippo signaling pathway that is important for cell proliferation and apoptosis. We zoomed into YAP1-related genes in our RNA-Seq dataset because the analysis of enriched GO terms (Supp. Fig. 4.6) revealed several YAP1-related genes prominently participating in the "cell adhesion" processes (one of the top enriched GO terms). Details of the RNA-Seq are in the caption for Supp. Fig. 4.6. In brief, we performed RNA-Seq on populations of three different starting densities: (1) a low-density (862 cells/cm^2) population that becomes extinct; (2) a high-density (5172 cells/cm^2) population that grows towards the carrying capacity; and (3) a medium-density (1931 cells/cm^2) population that is near the threshold density. For RNA-Seq, we collected all cells from these populations on the first and second days after triggering differentiation. We also collected cells that were kept pluripotent in a serum-based pluripotency medium (FBS with LIF) as a comparison. We analyzed the expression levels (FPKMs) by classifying genes into two groups: (1) genes that are activated by YAP1; and (2) genes that are repressed by YAP1 [177–184]. For each gene, we compute its mean expression level μ by averaging the its expression level across all experimental conditions (i.e., across all densities and days). Afterwards, we determined the row Z-score for each gene and experimental condition, which is a measure of by how much a gene's expression level in a given experimental condition deviates from the mean expression level (μ) for that gene. A gene that is more highly expressed has a high row Z-score (close to ~ 2) and is indicated as a shade of purple in the heatmaps here. A gene that is more lowly expressed has a low row Z-score (close to -2) and is indicated as a shade of orange in the heatmaps here. **(A)** Heat map that shows the row Z-score for each gene (each row) and each experimental condition (each column). These genes are known to be either directly or indirectly activated by Yap. We observed that these genes, including *Cyr61* and *Amotl2*, were more highly expressed (purple color) by the higher-density populations than the lower-density populations, suggesting that YAP1 is more active in higher-density populations. **(B)** Heat map that shows the row Z-scores for each gene (each row) and each experimental condition (each column). These genes are known to be either directly or indirectly repressed by YAP1. We observed that these genes, including *Angptl4* and *Tmem79*, were more highly expressed (purple color) by lower-density populations than the higher-density populations. Taken together, the results here (A-B) are consistent with YAP1 becoming more active in higher-density populations.

A

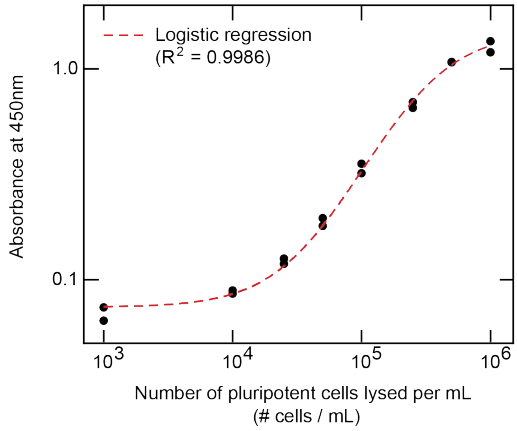
Logistic regression
(R^2 = 0.9986)
Absorbance at 450nm
1.0
0.1
10^3
10^4
10^5
10^6
Number of pluripotent cells lysed per mL
(# cells / mL)

B

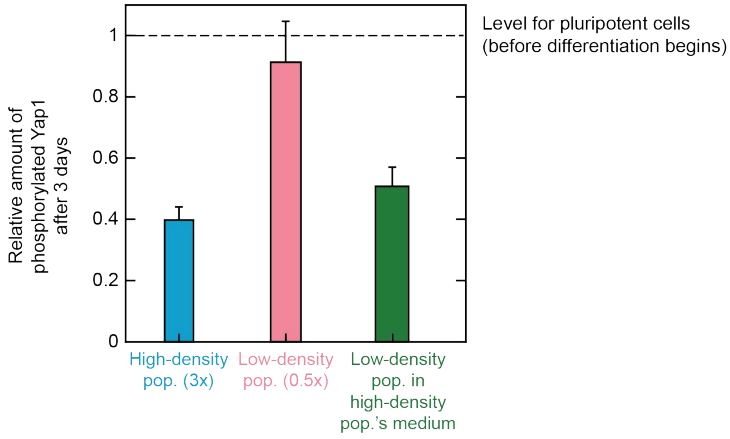
Relative amount of phosphorylated Yap1 after 3 days
1
0.8
0.6
0.4
0.2
0
Level for pluripotent cells
(before differentiation begins)
High-density pop. (3x)
Low-density pop. (0.5x)
Low-density pop. in high-density pop.'s medium

C

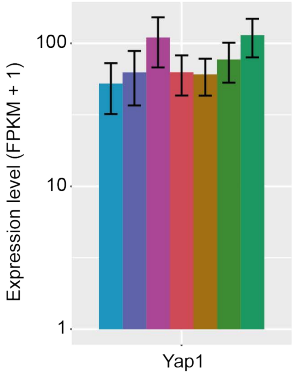
Expression level (FPKM + 1)
100
10
1
Yap1

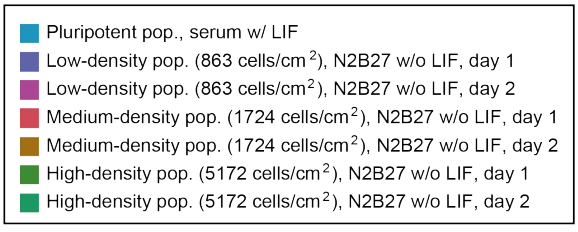
Pluripotent pop., serum w/ LIF
Low-density pop. (863 cells/cm^2), N2B27 w/o LIF, day 1
Low-density pop. (863 cells/cm^2), N2B27 w/o LIF, day 2
Medium-density pop. (1724 cells/cm^2), N2B27 w/o LIF, day 1
Medium-density pop. (1724 cells/cm^2), N2B27 w/o LIF, day 2
High-density pop. (5172 cells/cm^2), N2B27 w/o LIF, day 1
High-density pop. (5172 cells/cm^2), N2B27 w/o LIF, day 2

Figure 4.8 ***(preceding page)*****: Populations that survive differentiation have more active (dephosphorylated) YAP1 compared to populations that become extinct during differentiation.** To determine how the YAP1 activity may be determined by the population density, we performed ELISA that specifically detects inactive (phosphorylated) YAP1 - YAP1 phosphorylated at Ser397, which is a primary phosphorylation site [185, 186] (see Material and methods). **(A)** Standard curve for the ELISA. Here we lysed pluripotent populations of various densities and then measured the amount of phosphorylated YAP1 in each lysate - this yields an optical absorbance value at 450 nm (black points). Duplicates for each lysate are shown. Red curve is the logistic fit function: $f(x) = D + \frac{A-D}{1+(\frac{x}{C})D}$, with A, B, C and D are fit constants and x is the number of cells lysed per mL. Results: $A = 0.074$, $B = 1.418$, $C = 2.95 \times 10^5$ and $D = 1.502$ with an $R^2 = 0.9986$. **(B)** We performed ELISA on the 46C cells that were induced to differentiate towards the Neural Ectoderm (NE) lineage in N2B27+RA after self-renewing in serum+LIF. We examined three populations: (1) high-density population (5172 cells/cm^2); (2) low-density population (862 cells/cm^2); and (3) low-density population that we rescued from extinction by transplanting it, after two days, into the high-density population's medium. For each population, we measured its level of phosphorylated (inactive) YAP1 three days after starting differentiation and then normalized this level to the level present in pluripotent cells of the same density (shown in (A)). This yielded a "relative abundance" for each of the three populations. Compared to the pluripotent cells of equivalent density, cells of the low-density population (pink bar) had ~10% fewer inactive YAP1 whereas cells of the high-density population (blue bar) had ~60% fewer inactive YAP1 than the pluripotent population of the same density. Cells of the rescued low-density population (green bar) had ~50% (green bar) less inactive YAP1 than pluripotent populations of the same density. Together, these results establish that, after exiting pluripotency, cells of surviving populations have more active (dephosphorylated) YAP1 than cells that head towards extinction. **(C)** Expression level of YAP1 from RNA-Seq dataset. Legend shows different conditions. Note that on each day, the low-density (862 cells/cm^2 initially) and the high-density (5172 cells/cm^2 initially) populations have virtually the same YAP1 expression level. Thus, we can compare the amounts of inactive (phosphorylated) YAP1 between the low- and high-density populations in Fig. 4.3A (i.e., since both populations have (nearly) the same total level of YAP1, we would be subtracting the amount of inactive YAP1 from the same value for both populations to get the amount of active YAP1). Medium-density (1931 cells/cm^2 initially) population starts with the near-threshold density. n = 3 for all plots; Error bars are s.e.m.

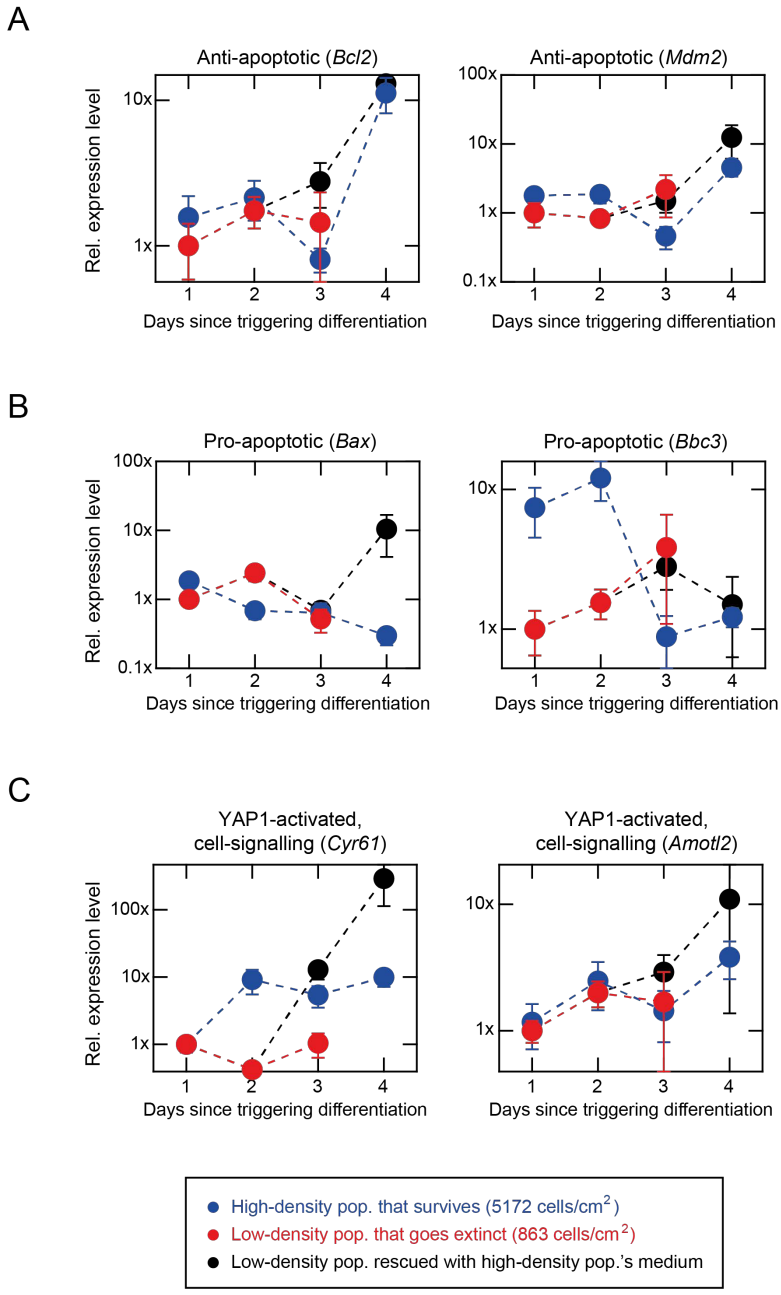
A
Anti-apoptotic (Bcl2)
Anti-apoptotic (Mdm2)
Rel. expression level
10x
1x
100x
0.1x
1
2
3
4
Days since triggering differentiation
B
Pro-apoptotic (Bax)
Pro-apoptotic (Bbc3)
C
YAP1-activated, cell-signalling (Cyr61)
YAP1-activated, cell-signalling (Amotl2)
High-density pop. that survives (5172 cells/cm2)
Low-density pop. that goes extinct (863 cells/cm2)
Low-density pop. rescued with high-density pop.'s medium

Figure 4.9 *(preceding page)*: High-density populations and rescued low-density populations (rescued by high-density population's medium) eventually have elevated anti-apoptotic pathway activities (e.g., expressions of *Bcl2* and *Mdm2* genes, which are controlled by YAP1), and elevated YAP1-controlled cell-signaling activities (e.g., expressions of *Cyr61* and *Amotl2*). With real-time quantitative PCR (primers in Materials and methods), we measured anti-apoptotic, pro-apoptotic, and YAP1-mediated cell-signaling genes over the course of differentiation. Normalization of expression values: for each gene g, we first divided its expression level by the expression level of *Gapdh*, resulting in a value N_g. For each population, we divided its N_g by the low-density population's N_g on day 1 to get the final, normalized expression level μ which is plotted in here in all graphs. Thus, "1x" is the expression level of the low-density population on the first day after starting differentiation. **(A)** Expression levels of two anti-apoptotic genes, *Bcl2* (left graph) and *Mdm2* (right graph). Data for *Bcl2* is a replicate of the data shown in Fig. 4.3B which we show here for comparison with *Mdm2*. Both *Bcl2* and *Mdm2* show increased expressions (more anti-apoptotic) for high-density population (blue) and low-density population that was rescued by the medium of the high-density population after the 2nd day (black). Low-density population that goes extinct (red) shows nearly constant, low expression level of both genes. No data for 4th day is shown for the low-density population because it becomes extinct after the 3rd day (there were already barely any cells left for the 3rd day data shown here). **(B)** Expression levels of two pro-apoptotic genes - *Bax* (left graph) and *Bbc3* (right graph). Color scheme is the same as in (A). The high-density population initially has a higher *Bbc3* expression than the low-density population but eventually down-regulates and has lower *Bbc3* expression than the low-density population. The low-density population, in turn, gradually increases its *Bbc3* expression over time, up to the moment of extinction ($\sim$ day 3). Note that the rescued low-density population keeps its *Bbc3* expression level low, past day 2 (which is when it receives the medium from a high-density population) and has nearly same low *Bbc3* expression as the high-density population after being rescued. Note that differentiation is known to increase expression of apoptotic genes. **(C)** Expression levels of two cell-signaling genes that are upregulated by YAP1, *Cyr61* (left graph) and *Amotl2* (right graph). Only the high-density and the rescued low-density populations gradually increase the expression levels of both genes whereas the low-density population that heads towards extinction (red) maintains a nearly constant, low expression of both genes (consistent with our findings in Figs. 4.1-4.2-4.3 that secreted factors that are abundant for high-density populations increase YAP1 activity (and thus upregulate expression of *Cyr61* and *Amotl2*). In all the plots, n = 3; Error bars are s.e.m.

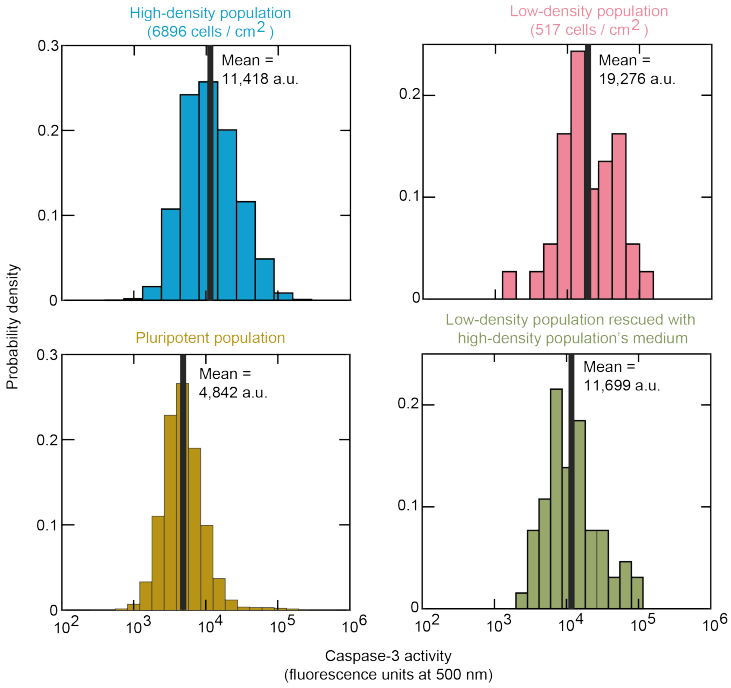

Figure 4.10: Pro-apoptotic caspase-3 activity (histograms) is higher in low-density populations than in high-density and rescued low-density populations. We sought to examine the activity of a well-known, pro-apoptotic marker (caspase-3) in populations that are either extinction-bound or surviving. We used a membrane-permeable, DNA-dye-based assay (NucView 488 Caspase-3 Assay Kit for Live Cells). This assay measured the amounts of active caspase 3/7 inside cells. Data shown for E14 cells that were induced to differentiation towards the Neural Ectoderm (NE) lineage by Retinoic Acid (RA). We examined caspase-3 levels in four different populations: (1) high-density population (6896 cells/cm^2 – blue histogram); low-density population (517 cells/cm^2 – pink histogram); (3) low-density population that was rescued from extinction by transplanting it, after two days, into the high-density population's medium (green histogram); and (4) pluripotent E14 cells before we induced the differentiation (yellow histogram). After 3 days of differentiation, we collected the cells from each of these populations, incubated them with the DNA-dye according to the manufacturer's protocol, and then measured the resulting fluorescence at 500 nm in single cells with a flow cytometer (see Materials and methods). Also indicated here (with vertical, black line) are the geometric means of the fluorescence for each population. Higher fluorescence means higher caspase-3 activity. Shown here are single replicates (as examples) from which the means are based on 3 biological replicates and shown in Fig. 4.4B. These histograms show that all differentiating populations upregulated levels of caspase-3 activity relative to the pluripotent populations. Thus, the nonlocal communication causes populations to have less caspase-3 activities than extinction-bound populations.

5

Secreted FGF4 mediates nonlocal communication through YAP1

Parts of this chapter are also reported in Daneshpour et al. [2]

5.1. Introduction

There may be more than one survival factor. We sought to find at least one of them which - according to our findings so far - should be stable for days and light enough to mediate a nonlocal communication as well as activate YAP1-based anti-apoptotic activities.

5.2. Results

5.2.1. Secreted molecules have molecular weights in the range of 25 to 300 kDa

To narrow down our search, we first sought to place lower and upper bounds on the molecular weight of secreted molecules that trigger collective survival. We flowed the differentiation medium (supernatant) of a 2-days-old high-density population (5172 cells / cm^2) through a membrane filter that captures all molecules that are larger (heavier) than the membrane's "filter size" which is specified in the units kilodaltons (kDa). Importantly, none of the filters captured any ingredients of the fresh (unconditioned) N2B27 essential for ES-cell growth [191] (we also confirmed this experimentally - see Supp. Fig. 5.6). The supernatant that passed through the membrane contains only the molecules that are smaller than the filter size [191] (Supp. Fig. 5.6 and see Materials and methods). Into this filtered supernatant, we transplanted a 2-days-old, low-density population (862 cells / cm^2) (Fig. 5.1A - top). The filtered supernatant, containing all molecules that are smaller than the filter size, could only rescue the low-density population from extinction if and only if the filter size was 50 kDa or larger (Fig. 5.1B - top graph). This puts a lower bound on the molecular weight.

In a second experiment, we filtered the supernatant, took all the molecules that were captured in the membrane, and then dissolved these into a fresh N2B27. This medium, containing all molecules that are larger than the filter size, rescued the low-density population from extinction if and only if the filter size was 100 kDa or less (Fig. 5.1B - bottom graph graph). Moreover, supernatant containing all molecules larger than 100 kDa, but not larger than 300 kDa, also rescued the low-density population from extinction. With control experiments, we determined that the filters make some errors in filtering molecules such that molecules that were lighter or heavier by ~50% of the filter size were passed through or captured by the filter membrane (Fig. 5.1C).

These results establish that the lowest possible molecular weight of survival molecule(s) is ~25 kDa (i.e., ~50% of the 50-kDa minimum mentioned above). Therefore, the secreted molecules are most likely large proteins (~25 kDa and larger), rather than metabolites (typically <1.5 kDa), and that there is a possibility that there are at least two species of secreted molecules.

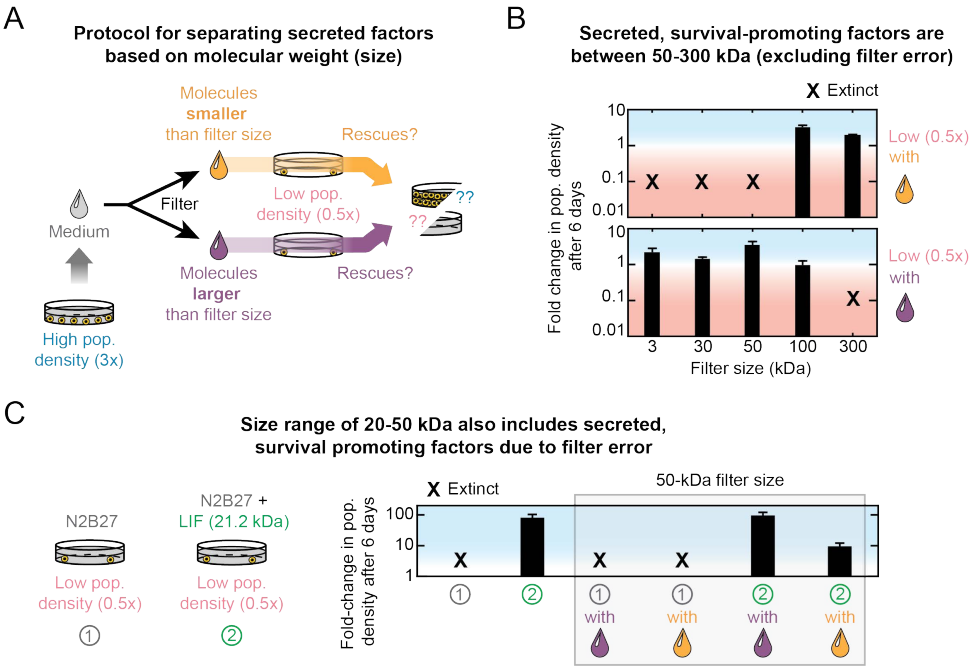

Figure 5.1: Collective survival is mediated by secreted molecules in the range of 25 to 300 kDa. (A) Protocol for separating secreted molecules based on their molecular weights, through membrane-based filters (see Materials and methods). Data for 46C cells differentiating in N2B27+RA after self-renewing in serum+LIF. Grey arrow: medium is first taken from a high-density population (5172 cells / cm^2 initially). We then run the medium through a membrane filter of a certain filter (pore) size, resulting in splitting of medium in two parts (splitting black arrows): one part (orange) contains all molecules that are smaller than the filter size (in kDa) and a low-density population (862 cells / cm^2 initially) is then incubated in this medium to see if it expands or becomes extinct (orange arrow). The other part of the filtered medium (purple) contains all molecules that are larger than the filter size (in kDa). Same procedure is carried out with this medium (purple arrow) as with the medium containing all the lighter molecules. Full details in Materials and methods. **(B)** Results of experiment described in (A). Top graph: fold change in density of the low-density population (vertical axis) that was incubated in the medium which contained either molecules smaller than the filter size (top graph) or larger than the filter size (bottom graph). Filter size is indicated on the horizontal axis. Cross ("X") indicates that the population went extinct (i.e., fold change below 0.01). Blue shade indicates population expansion and red shade indicates population extinction. Error bars are s.e.m.; n = 3. **(C)** Results of control experiment to estimate the error in filtering (with 50-kDa filter size) N2B27 (unguided differentiation) supplemented with recombinant LIF (21.2 kDa) on day 0. Same procedure is carried out with this medium regarding the >50kDa-molecule (purple) and <50kDa-molecule (orange) medium parts. Cross ("X") indicates that the population went extinct (i.e., fold change below 0.01). Error bars are s.e.m.; n = 3.

5.2.2. FGF signaling is necessary to avoid population extinction

To identify at least one of the secreted molecules, we further analyzed our RNA-Seq dataset on high-density (5172 cells / cm^2), medium-density (1931 cells / cm^2), and low-density populations (862 cells / cm^2) (Supp. Figs. 4.6-4.7). In this RNA-Seq dataset, we identified 11 genes encoding secreted molecules whose

weights were within the weight-range identified by the filters (Supp. Fig. 5.15). Of these, the ~22-kDa FGF4 and ~29-kDa FGF5 (two well-characterized members of the Fibroblast Growth Factor family) had molecular weights that are close to the ~25-kDa lower limit that we established before. Our RNA-Seq dataset also showed that cells highly expressed FGF4, FGF5, and several FGF receptors (FGFRs) during the crucial, first two days of differentiation - the time window in which rescuing a population from extinction is still possible (Supp. Fig. 5.7).

As a next step, we tested whether FGFs are important for determining a population's survival-versus-extinction fate by blocking FGFRs. For this, we incubated various differentiating populations with PD173074 which is a well-characterized, small-molecule inhibitor of FGFRs [133, 192] (Fig. 5.2). Inhibiting FGFRs continuously for 6 days drove every population towards extinction, including those with densities higher than the threshold value (~1700 cells / cm^2) (Fig. 5.2 - bottom graph).

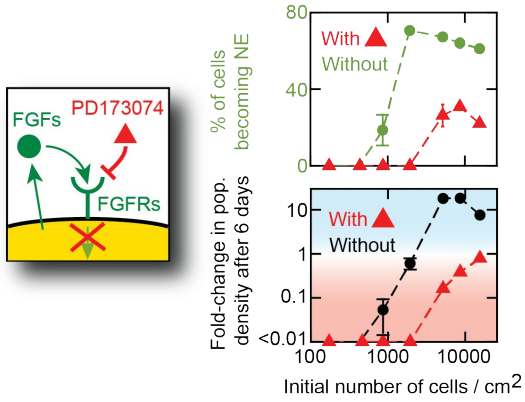

Figure 5.2: Blocking FGF receptors reduces population growth and differentiation efficiency. Cartoon shows PD173074, a well-characterized small-molecule inhibitor of FGF receptors [133, 192]. Fold-change in population density (bottom graph) and percentage of populations that enter NE lineage (top graph), both measured 6 days after differentiation began and as a function of initial population density. Data for 46C cells differentiating in N2B27+RA after self-renewing in serum+LIF. Red data points in both graphs are for populations that were incubated with 2 μM (1056 ng/mL) of PD173074 from the start of differentiation. PD173074 was dissolved in DMSO. Thus, as a control, black and green points are for populations without PD173074 but with the same amount of DMSO (volume per volume) as the populations represented by red data points. Blue shade indicates population expansion and red shade indicates population extinction. Error bars are s.e.m.; n = 3.

Interestingly, with the FGFRs blocked, having a higher initial density enabled staving off extinction for a longer time: fold-change in population density was closer to but still below one after 6 days for populations with higher initial densities (Fig. 5.2 - bottom graph). This suggests that even if FGFs turn out to be one of the major autocrine-signaling factors that determine a population's survival, there are other factors (non-FGFs) that promote a population's survival (i.e., higher-

density populations would accumulate more of these factors than lower-density populations). This is consistent with the possibility that there may be at least two survival-promoting factors (Fig. 5.1B). Yet, it is important to note that none of the high-density populations expanded - their fold-changes were either far or just below one after 6 days of continuous blockage of FGFRs. This means that FGF-signaling is crucial for population expansion. The FGFR-blockage also drastically decreased the percentage of cells that entered the NE-lineage (expressed GFP) for all populations (Fig. 5.2 - top graph).

These results indicate that FGF signaling, likely involving the highly expressed FGF4 or FGF5, is crucial for determining a population's survival-versus-extinction fate. Of the two FGFs that we found to be highly expressed - FGF4 and FGF5 - we will focus on FGF4, which is one of the most well-studied members of FGF family.

5.2.3. Adding sufficiently high concentrations of FGF4 prevents population extinction

We obtained recombinant versions of each of the 11 molecules that we identified as candidate secreted molecules, including recombinant FGF4 and FGF5 (see Materials and methods). We then incubated a low-density population in 11 different N2B27 media, each containing just one of the 11 molecules (Fig. 5.3).

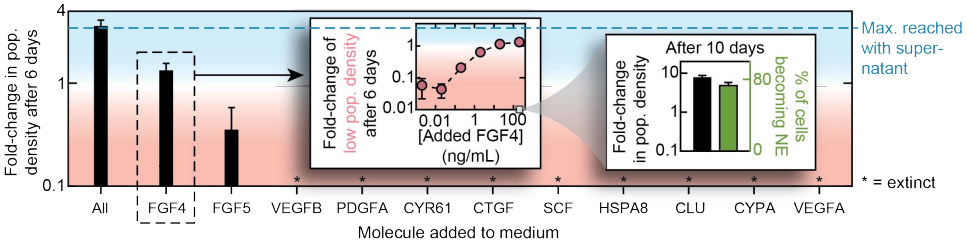

Figure 5.3: Sufficiently high concentrations of FGF4 rescues populations from extinction. Using the minimum molecular weight of the survival-promoting secreted molecules (~25 kDa) (Fig. 5.1) and our RNA-Seq data set (Supp. Fig. 5.15), we identified and screened 11 potentially secreted factors (see Supp. Fig. 5.15 for their molecular weights). We tested whether supplementing N2B27 (unguided differentiation) with each recombinant protein separately at a high concentration rescues a low-density population (862 cells / cm^2) from extinction. Data are for 46C cells differentiating in N2B27+RA supplemented with each recombinant molecule (listed along horizontal axis), after self-renewing in serum+LIF. We also tested various combinations of these 11 factors. See all details in the caption of Supp. Fig. 5.16. Main graph: combining all 11 factors ("All") resulted in the expansion of the low-density population virtually equal the expansion achieved by transplanting the low-density population into a high-density population's medium (i.e., ~3-fold; blue dashed line). None but FGF4 and FGF5 resulted in the expansion of the population above a fold-change of 0.1 after 6 days. Middle graph: fold-change in density of a differentiating population, after 6 days in medium containing FGF4 that we added. Horizontal axis shows the concentration of human differentiation. Horizontal dashed line shows the maximum fold-change in density obtained in our study, which occurs when the same low-density population is rescued by a filtered medium (in Fig. 5.1B).
(*Caption continued on next page.*)

Figure 5.3 ***(previous page)*****:** Right graph: fold change in population density and percentage of cells entering NE lineage (*Sox1*-GFP expressing cells), both measured 10 days after differentiation begins in presence of 200-ng/mL recombinant mouse FGF4 that we added at the start of differentiation. All error bars are s.e.m.; n = 3.

Of these, only FGF4 the low-density population from extinction, leading to ~2-fold growth in six days (Fig. 5.3 - second bar). Notably, FGF5 alone did not rescue the population but the population approached extinction more slowly than any of the nine other molecules (Fig. 5.3 - third bar). Intriguingly, adding all 11 molecules into N2B27 causes the most growth: the low-density population was rescued from extinction and grew by ~4-fold in six days, which is almost equal to the maximum possible growth seen in our medium-transfer experiments (Supp. Fig. 5.16). This suggests that FGF4's rescuing ability is enhanced by some of the ten other molecules. Incubating the low-density population in N2B27 with different amounts of FGF4 showed that the rescue from extinction requires FGF4 of at least ~2 ng/mL, which equals to ~0.13 nM (Fig. 5.3 - middle inset). The low-density population, incubated in N2B27 supplemented with 200 ng/mL of recombinant FGF4, grew by ~10-fold after ten days and about ~80% of the cells had differentiated into the NE lineage (Fig. 5.3 - right inset).

These results establish that FGF4 alone is sufficient for rescuing the low-density population from extinction.

5.2.4. High-density populations accumulate detectable concentrations of extracellular FGF4 in two days

Adding a recombinant form of FGF4, by hand, into the differentiation medium rescues low-density populations from extinction. An important, remaining question is whether differentiating cells secrete and accumulate FGF4 themselves during the first two days in which a population's survival-versus-extinction fate is determined. Consistent with our RNA-Seq dataset, we found with RT-qPCR that pluripotent cells and differentiating cells, during the first 2 days of differentiation, indeed express *FGF4* and FGF receptors (*FGFR1-4*) (Supp. Fig. 5.8). Studies typically assume that cells that express *FGF4* also secrete it. But for our purpose, we need to directly detect extracellular FGF4. Specifically, rather than the absolute concentration of extracellular FGF4, we are interested in seeing whether and how fast the concentration of extracellular [FGF4] increases over time during differentiation. Hence, we decided to use ELISA to measure the fold change in the concentration of extracellular FGF4 during the first 2 days of differentiation.

To do so, we measured the concentration of extracellular FGF4 relative to that of a highly confluent population of pluripotent cells for comparison. The latter is

expected to have a high concentration of extracellular FGF4, based on previous studies' finding that pluripotent ES cells highly express *FGF4* [133, 136]. Normalizing all our ELISA measurements of FGF4 concentration by that of the pluripotent population also makes our result interpretable in the event that ELISA does not detect 100% of all FGF4s that are secreted (e.g., due to antibodies not binding to all their targets) (see Supp. Fig. 5.9 for validations of these justifications).

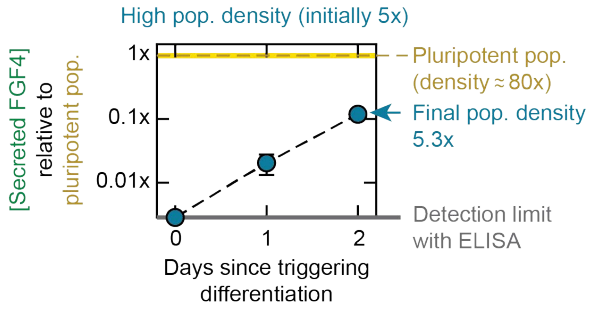

Figure 5.4: High-density populations accumulate extracellular [FGF4]. ELISA measurements of concentrations of extracellular [FGF4] in conditioned medium of a high-density population (8620 cells / cm^2 initially) during unguided differentiation (blue points). Data for 46C cells differentiating in N2B27 after self-renewing in serum+LIF. Vertical axis shows FGF4 concentration relative to that of a ~80% confluent pluripotent population (denoted "1x" and marked with yellow horizontal line). 80% confluency equals ~8 x 10^6 cells in 10-cm diameter dish. Lower detection limit of the ELISA assay is indicated (in grey). See Supp. Fig. 5.9 for ELISA standard curves and detailed explanation. Error bars are s.e.m.; n = 3.

With these justifications in mind, we used ELISA to measure the concentration of extracellular FGF4 in the medium of a high-density population ("5x" = 8620 cells / cm^2) during the first two days of differentiation (Fig. 5.4 and Supp. Fig. 5.9). We also used ELISA to measure the concentration of extracellular FGF4 in the medium of a highly confluent population of pluripotent cells (population density of ~80x) (Fig. 5.4 - yellow line). The differentiation medium did not initially have any detectable amounts of FGF4 (Fig. 5.4 - "day 0"). However, we detected [FGF4] increasing from zero (undetectable) to an appreciable amount in the first two days of differentiation in N2B27 (Fig. 5.4 - blue points). The final concentration of FGF4 that we detected after two days was ~10 times less than the FGF4 detected after two days in the self-renewal medium (serum+LIF) of a highly confluent population (~16 times more cells than the differentiating population) (Fig. 5.4 - yellow line) (also see Supp. Fig. 5.9 and Materials and methods for details of ELISA and rationale behind normalizing the concentration).

Consistent with FGF being secreted and detected, we found earlier with RT-qPCR that differentiating cells indeed express *FGF4* and FGF receptors (*FGFR1-4*) during the first two days (Supp. Fig. 5.8).

5.2.5. Nonlocal communication uses FGF4 and YAP1 to determine collective survival

So far, our findings (Figs. 5.1-5.4) establish that FGF signaling is necessary and that the secreted FGF4 alone is sufficient for determining whether a population survives or becomes extinct. Crucially, to further support this claim, we sought to confirm that differentiating cells collectively activate YAP1 and related anti-apoptotic activities by nonlocal communication with FGF4. For this, we rescued a low-density population by adding a high concentration of recombinant FGF4 into its medium, and then with ELISA found that the rescued cells had nearly identical, high level of activated (dephosphorylated) YAP1 as a high-density population and a low-density population that was rescued by the medium of a high-density population (Supp. Fig. 5.10). Moreover, these FGF4-rescued cells of the low-density population increased their expressions of anti-apoptotic (*Bcl2*) and cell-signaling (*Cyr61*) genes that YAP1 regulates (Supp. Fig. 5.11), just like the cells that were rescued with the medium conditioned by a high-density population.

We confirmed that FGF4's half-life and molecular weight (diffusion constant) together yield diffusion length that is at least several millimeters to enable nonlocal communication. Specifically, we first determined that extracellular FGF4 (secreted) in N2B27 without any cells does not measurably degrade for three days at 37°C (standard incubation temperature for our cell cultures) (Supp. Fig. 5.12). Moreover, in another experiment, we took the medium of a high-density population and then incubated it at 37°C without any cells for four days. After four days, this medium still rescued a low-density population from extinction, with the low-density population growing by nearly the same amount as they do in fresh (unaged) conditioned medium from the high-density population (Supp. Fig. 5.13). Thus, the extracellular FGF4, contained in the total pool with possibly other molecules secreted by the high-density population, is stable for at least 3 days. With FGF4's relatively small molecular weight (~22 kDa), we used the Stokes-Einstein relation to compute FGF4's diffusion constant D. The diffusion length is $\sqrt{D\tau}$, where τ is the half-life deduced above. Using the values obtained, we found that FGF4 diffuses over several millimeters (see Chapter 6). As a confirmation of the fact that diffusion is the primary means of spreading secreted molecules in our culture conditions, we used a microscope to make a time-lapse movie in which a droplet of dye (i.e., a visible diffusible molecule of a known molecular weight) spreads in N2B27 without any cells at 37°C (Supp. Fig. 5.14; also see Chapter 6). By analyzing how fast the boundary of the circular droplet spreads, we found that diffusion alone, without any other mechanism such as liquid convection, quantitatively accounts for the (nonlocal) spreading. Thus, secreted molecules, including FGF4, would spread by diffusion rather than convection between cells.

While FGF4 is sufficient and FGF signaling is necessary for a population to deter-

mine its survival-versus-extinction fate, our experiments also show that additional, secreted molecules likely also contribute to determining a population's collective survival. As an illustration of this, note that a low-density population can expand by ~3-fold in a filtered medium taken from a high-density population (Fig. 5.1B) whereas it barely expands even after 6 days in a high concentration of added recombinant FGF4 (but it does expand by ~10-fold after 10 days (Fig. 5.3)). Hence, the filtered medium may contain survival-promoting factors other than FGF4.

Aside from FGF4 and FGF5, our RNA-Seq dataset revealed nine other autocrine-signaling molecules that are known to regulate cell proliferation and/or death such as VEGFB and CYPA (Supp. Fig. 5.15; we also detected secreted CYPA with mass spectrometry). But adding recombinant versions of any of these nine molecules, either one-by-one or in combinations, did not result in rescuing of a low-density population (Supp. Fig. 5.16) or to a larger extent than the rescue with recombinant FGF4 alone. These results establish that being an autocrine-signaling molecule that controls cell proliferation and/or death - a knowledge typically derived without examining the molecule's diffusion length and the extent of self- and neighbor-communication - does not mean that it participates in determining a population's survival.

5.3. Conclusions

We found that cooperatively amassing secreted FGF4 is sufficient and FGF signaling is necessary for preventing extinction of an ES-cell population during differentiation (Fig. 5.5).

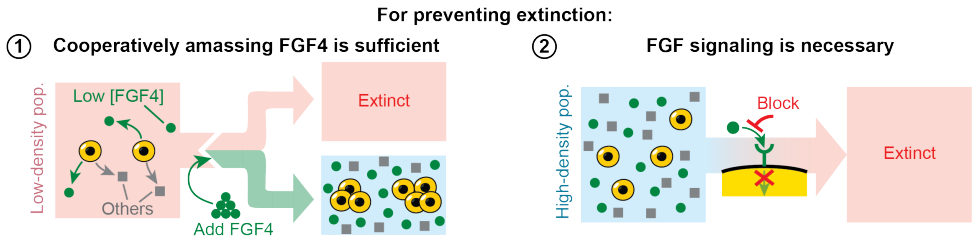

Figure 5.5: Suggested mechanism for FGF4 and FGF signaling controling ES-cell population's survival-vs-extinction fate during differentiation. Conclusions from experiments in Fig. 5.1-5.4. Left cartoon: gathering enough extracellular FGF4 is sufficient to prevent population extinction and this occurs for populations that start with sufficiently high densities. Equivalently, adding enough FGF4 to medium of low-density population alone is sufficient for preventing extinction. Right cartoon: FGF signaling is necessary for recuing a low-density population from extinction.

5.4. Supplementary Information

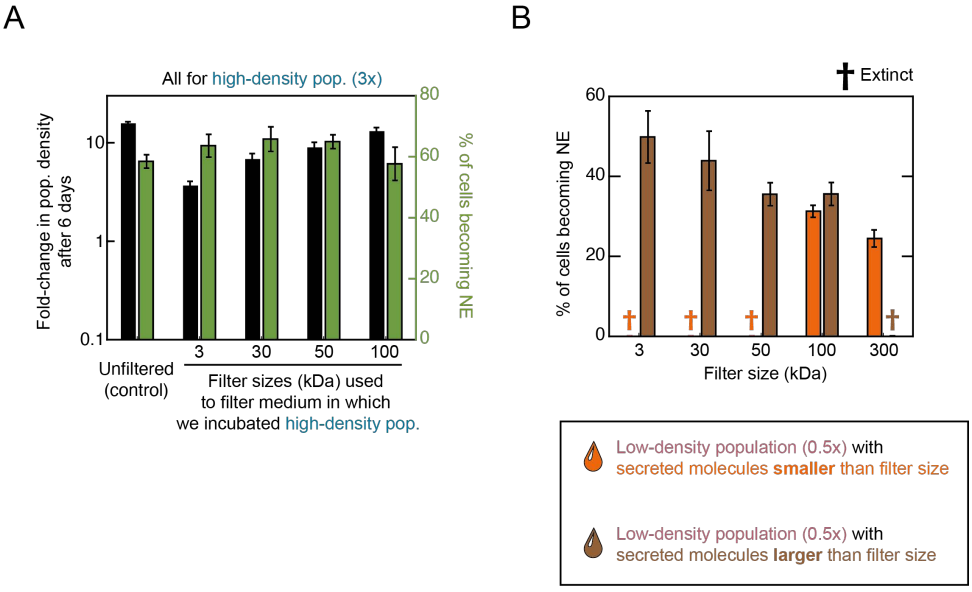

Figure 5.6: Filtering culture medium does not eliminate media components that are essential for cell growth. We used commercial, membrane-based filters of various sizes (Fig. 5.1, see Materials and methods). Data for 46C cells differentiating in N2B27+RA after self-renewing in serum+LIF. **(A)** To check that the filters do not remove any essential media components for cell growth, we filtered the medium of a high-density population with filters of various sizes, after two days of differentiation. We then took the filtered medium (medium that passed through the filter and thus containing all molecules that are smaller than the filter size), and gave it back to the same high-density population. We incubated the population for four days in this medium. On the last day, we measured the fold-change in population density (black bars) and the percentage of cells becoming NE (green bars). As a control, we also measured the fold-change in population density after six days of growth in unfiltered medium (first black and green bars). Since all black bars have nearly the same height as do all the green bars, we can conclude that none of the filters catch any ingredients in the cell-culture medium that are essential for cell growth (e.g., vitamins and other components which are already present in the medium from the beginning of cell culture, rather than secreted by cells). **(B)** We cultured a low-density population (862 cells / cm^2) in a medium from a high-density population (5172 cells / cm^2) that went through the filter (orange bars). This medium has all molecules that are smaller than the filter size. We also cultured the low-density population in a medium that contained all the molecules that are larger (heavier) than the filter size (brown bars), which we captured by flowing the high-density population's medium through the filter. We used a wide range of filter sizes (horizontal axis). The bars show the percentages of cells entering the NE after being cultured in the filtered medium. Crosses indicate that the population became extinct in the filtered medium. The corresponding fold-changes in population density are shown in Fig. 5.1B

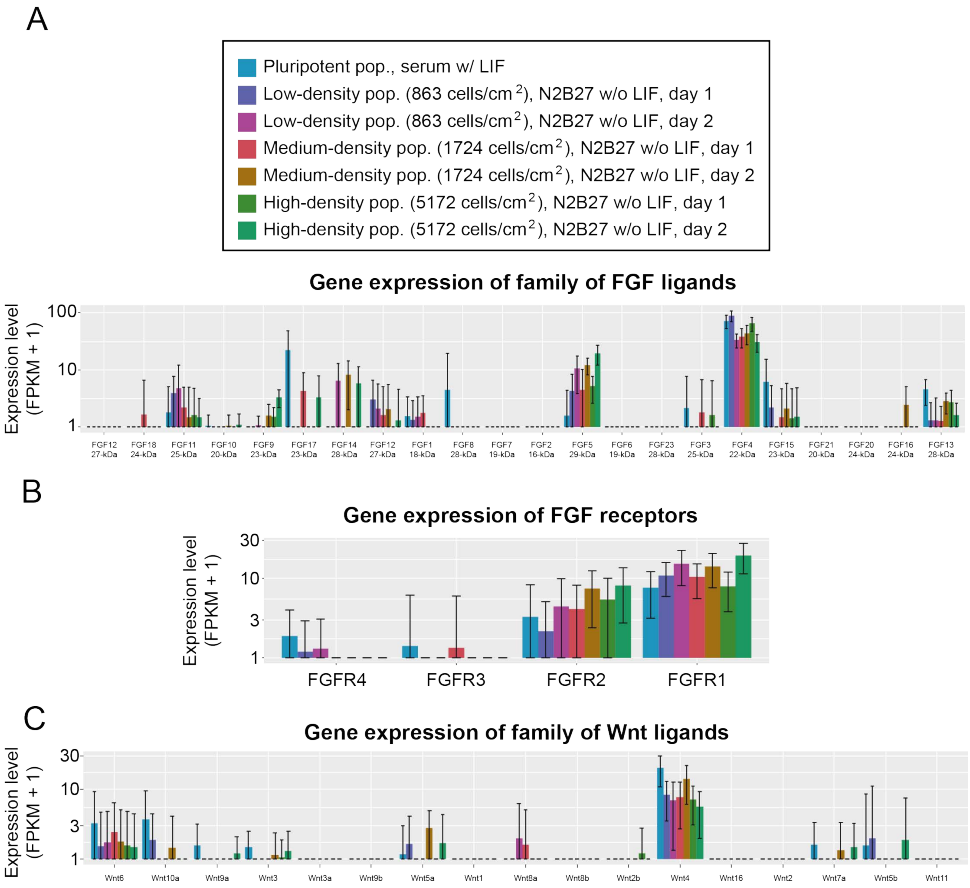

Figure 5.7: RNA-Seq dataset: Expression levels of 22 FGF ligands, 4 FGF receptors (FGFR) and 17 Wnt ligands. We performed RNA-Seq to measure the expression levels of 22 FGF ligands (A), 4 FGF receptors (FGFR) (B) and 17 Wnt ligands (C). Data for 46C cells differentiating in N2B27 after self-renewing in serum+LIF.. We performed RNA-Seq on four populations: (1) pluripotent population prior to differentiation; (2) low-density (862 cells / cm^2) population; (3) high-density (5172 cells / cm^2) population; and (4) medium-density (1724 cells / cm^2) population that is near the threshold density. For the three differentiating populations, we collected their cells on the first and second day after triggering differentiation. **(A)** Expression levels of all FGF ligands. Shown are the following genes: *FGF1-8*, *FGF20-21* and *FGF23*. Below each gene name is the corresponding molecular weight in kDa. Note that *FGF4* expression prominently stands out among all the FGFs. **(B)** Expression levels of all FGF receptors (FGFRs). Shown are the following genes: *FGFR1-4*. Below each gene name is the corresponding molecular weight in kDa, according to two online resources: Uniprot ([193]) and ExPASy ([194]). n = 3 for all plots; Error bars are s.e.m. **(C)** Expression levels of Wnt ligands. Shown are the following genes: *Wnt6*, *Wnt10a*, *Wnt9a*, *Wnt3*, *Wnt3a*, *Wnt9b*, *Wnt5a*, *Wnt1*, *Wnt8a*, *Wnt8b*, *Wnt2b*, *Wnt4*, *Wnt16*, *Wnt7a*, *Wnt5b and Wnt11*. None of the Wnt genes prominently stand out, except for *Wnt4* which still has an order of magnitude lower expression relative to *FGF4* expression. n = 3 for all plots; Error bars are s.e.m.

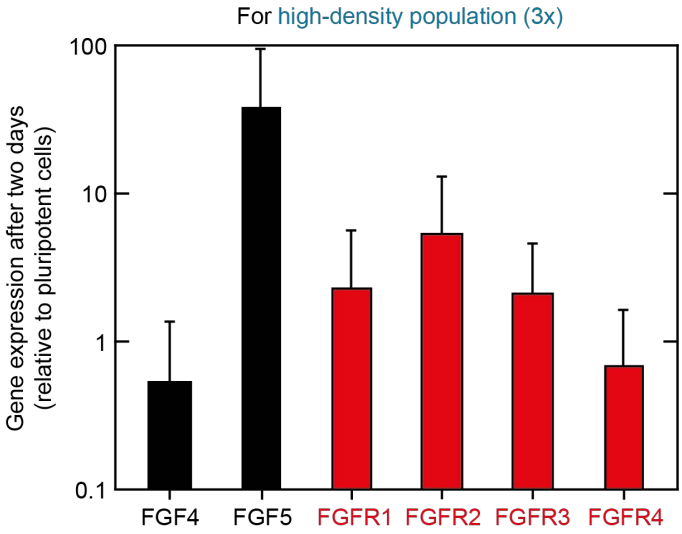

Figure 5.8: Differentiating populations express *FGF4*, *FGF5* and all four FGF receptor genes during the first 2 days of differentiation. We used real-time quantitative PCR (RT-qPCR) to measure the expression levels of all four receptors (*FGFR1-4*) of Fibroblast Growth Factors (FGFs) and the expression levels of the two FGFs, *FGF4* and *FGF5* (primers in Materials and methods). Data for 46 cells differentiating in N2B27 after self-renenwing in serum+LIF. We examined a high-density population (5172 cells / cm^2) after two days of differentiation. We normalized the resulting expressions of a gene relative to that of the housekeeping gene, *Gapdh* of the same population, and then further normalized the resulting value to the pluripotent population's normalized expression level (similar to the procedure described in the caption for Supp. Fig. 4.9). Thus, a given gene's expression level is compared to the pluripotent population's expression level for that gene. Normalized expression levels of *FGF4* and *FGF5* (in black) and *FGFR1-2* (in red). n = 3; Error bars are s.e.m. Altogether, these results show that *FGF4*, *FGF5* and *FGFR1-2* are expressed – and some more so than the pluripotent population (i.e., expression value greater than 1) – during the first 2 days in which ES cells exit pluripotency.

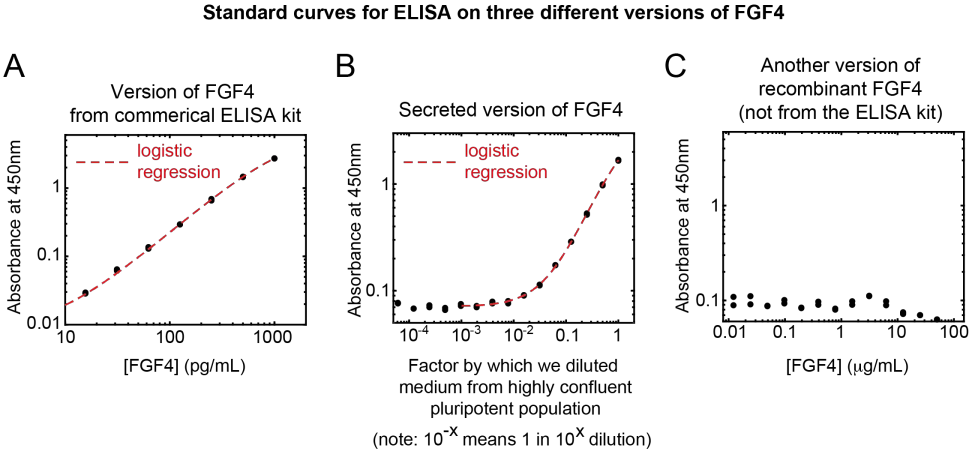
Standard curves for ELISA on three different versions of FGF4
A
Version of FGF4
from commerical ELISA kit
logistic
regression
Absorbance at 450nm
[FGF4] (pg/mL)
B
Secreted version of FGF4
logistic
regression
Absorbance at 450nm
Factor by which we diluted
medium from highly confluent
pluripotent population
(note: 10-X means 1 in 10X dilution)
C
Another version of
recombinant FGF4
(not from the ELISA kit)
Absorbance at 450nm
[FGF4] (μg/mL)

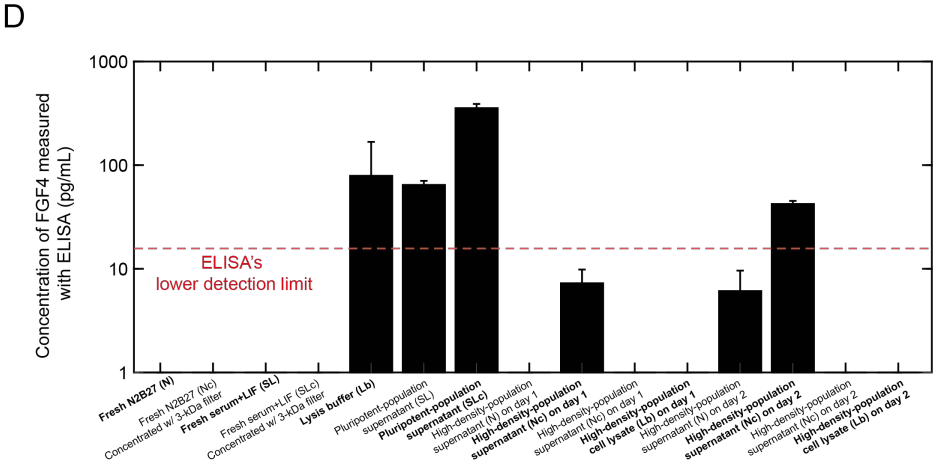
D
Concentration of FGF4 measured
with ELISA (pg/mL)
ELISA's
lower detection limit
Fresh N2B27 (N)
Fresh N2B27 (Nc)
Concentrated w/ 3-kDa filter
Fresh serum+LIF (SL)
Fresh serum+LIF (SLc)
Concentrated w/ 3-kDa filter
Lysis buffer (Lb)
Pluripotent-population
supernatant (SL)
Pluripotent-population
supernatant (SLc)
High-density-population
supernatant (N) on day 1
High-density-population
supernatant (Nc) on day 1
High-density-population
supernatant (N) on day 1
High-density-population
supernatant (Nc) on day 1
High-density-population
cell lysate (Lb) on day 1
High-density-population
supernatant (N) on day 2
High-density-population
supernatant (Nc) on day 2
High-density-population
supernatant (Nc) on day 2
High-density-population
cell lysate (Lb) on day 2

Figure 5.9 *(preceding page)*: Cells secrete and extracellularly accumulate appreciable amounts of FGF4 during the first 2 days of differentiation. We performed ELISA that detects mouse FGF4. **(A)** Standard curve based on a recombinant mouse FGF4 that came with the commercial ELISA kit. Note that this FGF4 is not necessarily the same version as the FGF4 that our cells secrete. Each measurement (absorbance at 450 nm) was done in duplicate (black data points). Then, we performed a logistic regression on the data by fitting a 4-parameter logistic function (red curve): $f(x) = D + \frac{A-D}{1+(\frac{x}{C})^B}$, where A, B, C and D are constant coefficients and x is the known concentration of the recombinant mouse FGF4 that we added. We found: $A = 0.0084$, $B = 1.313$, $C = 1312$ and $D = 6.59$. **(B)** Standard curve based on the version of FGF4 that pluripotent cells secrete into their medium. We first concentrated the medium taken from a highly confluent (~80% confluent) pluripotent population with a 3-kDa filter and then performed ELISA on serially diluted fractions of this concentrated medium. Each measurement (absorbance at 450 nm) was done in duplicate (black points). Then, we performed a logistic regression on the black data points by fitting a 4-parameter logistic function (red curve): $f(x) = D + \frac{A-D}{1+(\frac{x}{C})^B}$), where A, B, C and D as constant coefficients and x as amount of lysed, pluripotent cells (day 0). We found: $A = 0.07123$, $B = 1.184$, $C = 1.407$ and $D = 4.069$. The standard curve shows that pluripotent ES cells secrete a version of FGF4 that our ELISA can detect. Moreover, it also shows a limitation of our ELISA: the assay can only detect sufficiently high concentration of FGF4 as seen by the fact that it cannot detect any FGF4 in a 1:100 dilution of a concentrated medium taken from a highly confluent ES cells. **(C)** Standard curve based on recombinant mouse FGF4 from a different manufacturer (not from the ELISA kit) that we could add to the cell-culture medium to rescue low-density populations. Each measurement (absorbance at 450 nm) was done in duplicates (black points). As seen here, the ELISA cannot detect any amounts of this version of FGF4, even when its concentration is 100-folds higher than the highest concentration - of the version supplied by the ELISA kit - that we used in (A). The three standard curves (A-C) show that ELISA is highly sensitive to the form of FGF4 - we used three different forms in each of (A-C). The two versions of FGF4 that are not supplied by the ELISA kit (B-C) are detected with lower efficiency than the version supplied by the kit (A). **(D)** ELISA measurements of secreted FGF4 (in pg/mL) in various conditions (indicated with labels on the horizontal axis). We detected abundant FGF4 in the pluripotency medium (~500 pg/mL). We also performed ELISA on 46C cells that were induced in N2B27+RA to differentiate towards the Neural Ectoderm (NE) lineage with Retinoic Acid (RA) after self-renewing in serum+LIF (see Materials and methods). In the medium of the high-density population (8620 cells / cm^2) after two days of differentiation, we detected ~50 pg/mL of FGF4. After 1 day of differentiation, the medium of the high-density population did not contain any detectable amounts of FGF4. Hence, high-density populations take 2 days to accumulate appreciable (detectable) amounts of FGF4.

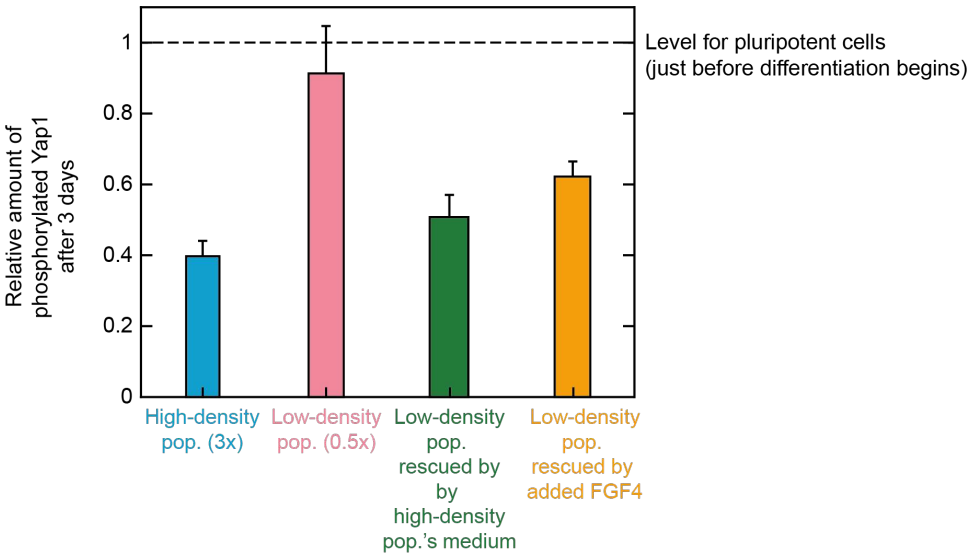

Figure 5.10: Low-density population rescued by added recombinant FGF4 in the medium has similar, high level of active (dephosphorylated) YAP1 level as high-density population and a low-density population that was rescued by the medium of the high-density population. We performed ELISA that measured the phosphorylated YAP1 levels in 46C cells that were induced to differentiate in N2B27+RA towards the Neural Ectoderm (NE) lineage by Retinoic Acid (RA) after self-renewing in serum+LIF. The first three bars (blue, pink, and green) are the same data shown in Supp. Fig. 4.8 and are shown here for comparison with the orange bar. Orange bar shows the level of inactive (phosphorylated) YAP1 level for a low-density population that was rescued by a high concentration of recombinant FGF4 that we added into its medium. n = 3; Error bars are s.e.m.

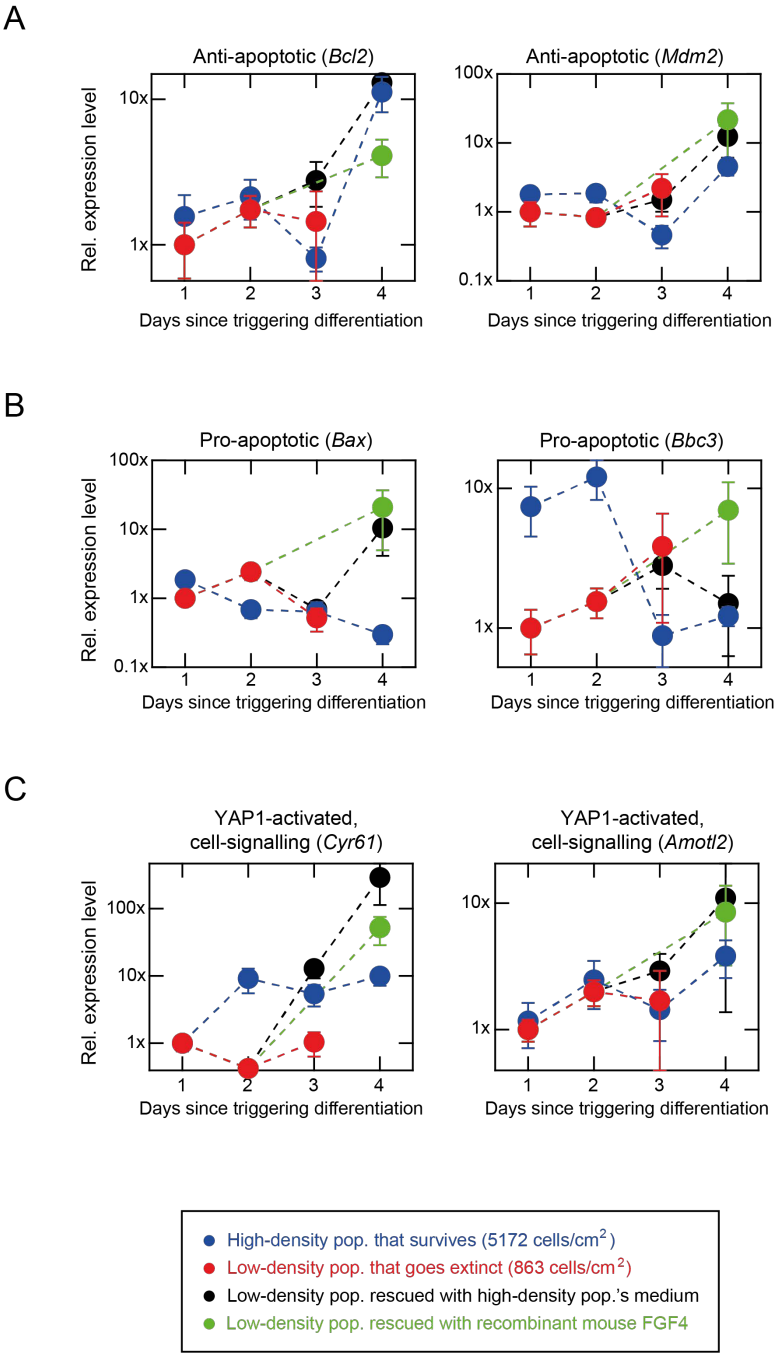
A
Anti-apoptotic (Bcl2)
Anti-apoptotic (Mdm2)
Rel. expression level
10x
1x
100x
0.1x
1
2
3
4
Days since triggering differentiation
B
Pro-apoptotic (Bax)
Pro-apoptotic (Bbc3)
C
YAP1-activated, cell-signalling (Cyr61)
YAP1-activated, cell-signalling (Amotl2)
High-density pop. that survives (5172 cells/cm2)
Low-density pop. that goes extinct (863 cells/cm2)
Low-density pop. rescued with high-density pop.'s medium
Low-density pop. rescued with recombinant mouse FGF4

Figure 5.11 ***(preceding page)*****: Low-density populations that are rescued from extinction with recombinant mouse FGF4 activate anti-apoptotic pathways (e.g.,** ***BCL2*** **and** ***MDM2*** **genes) and YAP1-controlled targets (e.g.,** ***CYR61*** **and** ***AMOTL2*** **genes).** The RT-qPCR data shown in blue, red, and black are the same as the data shown in Supp. Fig. 4.9. We show them here again for comparison with the green data points. Green data points are for a low-density population that we rescued by adding 200 ng/mL of recombinant mouse FGF4 to its medium, just after two days into differentiation (hence the data points for "day 1" and "day 2" are the same as the red data points). Expression levels of (**A**) anti-apoptotic genes, (**B**) pro-apoptotic genes, and (**C**) YAP1-activated cell-signaling genes measured with RT-qPCR. Primers are listed in Materials and methods. In all the plots, n = 3; Error bars are s.e.m.

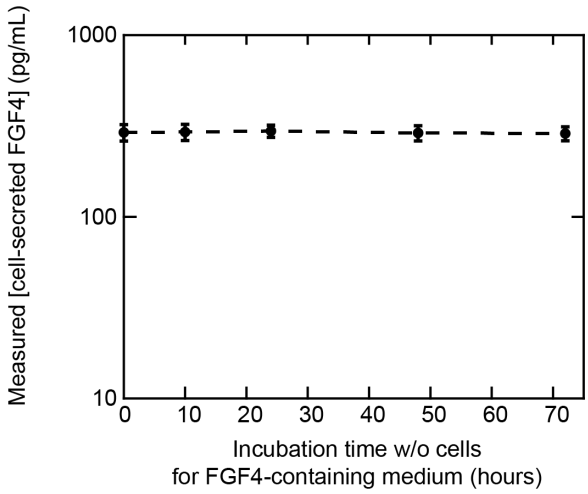

Figure 5.12: Secreted FGF4 shows no appreciable degradation for 3 days at 37°C in liquid medium. Determining the degradation rate of FGF4 that cells secrete tells us whether FGF4 can diffuse by millimeters or not, through the Stokes-Einstein relation (see Chapter 6). We performed ELISA that targets FGF4 (see Chapter 6) to determine the concentrations of secreted FGF4 when incubated without cells in liquid medium. For this, we used a 3-kDa filter to concentrate the pluripotency medium (serum+LIF) taken from a confluent population of 46C cells. Then we incubated the medium without any cells in a 37°C incubator for the hours indicated on the horizontal axis. We then took it out of the incubator and performed ELISA on it to measure the remaining [FGF4]. We observed that after incubating for 72 hours (3 days), the initial concentration of the secreted FGF4 was not appreciably degraded. This result suggests that the concentration of secreted FGF4, by itself and in the absence of cells, is stable over at least 3 days and thus – according to the Stokes-Einstein relation – can diffuse over millimeters (see Chapter 6).

A

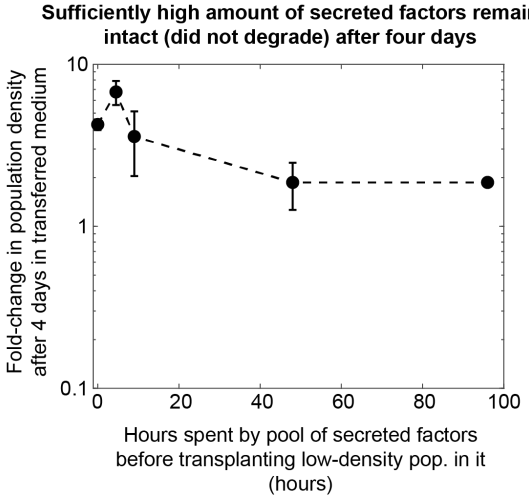

● Medium taken from high-density population and then aged in incubator for duration given in the horizontal axis, before incubating low-density population in it

B

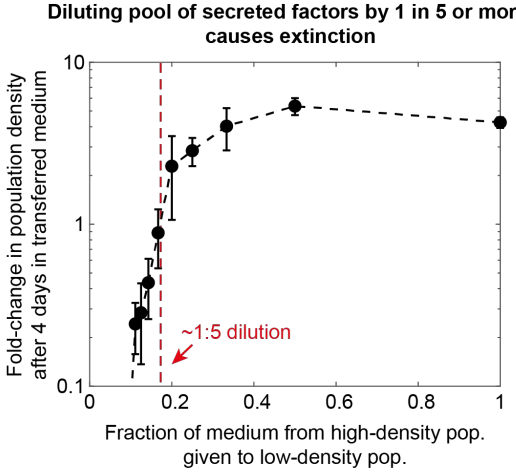

● Low-density population incubated in diluted medium of high-density population

(dilution indicated in horizontal axis)

(Note: 0.1 means 1 in 10 dilution of the high-density pop.'s medium into fresh medium)

Figure 5.13 ***(preceding page)*****: Secreted factors that control differentiating population's survival-vs-extinction fate have a combined, effective half-life of at least 2 days.** According to the reaction-diffusion equation, molecules of ∼100 kDa in an aqueous environment need to have a half-life of at least ∼12 hours to have a diffusion length that is over 1 mm (see Chapter 6). We sought to infer the half-lives of all the secreted molecules that are important for determining the survival-versus-extinction fate of a population. What is important is actually not the individual half-life of each molecule but rather the effective half-life of all molecules combined. Note that we established that more than one secreted factor determines the survival-versus-extinction fate of a population (Fig. 5.1B). To determine the effect half-life of all molecules combined, we used 46C cells that were induced in N2B27+RA to differentiate towards the Neural Ectoderm (NE) lineage with Retinoic Acid (RA) after self-renewing in serum+LIF. We used two populations: (1) high-density population (5172 cells / cm^2); and (2) low-density population (862 cells / cm^2). Combining the results of (A) and (B) enabled us to infer the lower bound on the effective half-life, as we now explain. **(A)** After 2 days of differentiation with N2B27, we transferred the high-density population's medium to an empty plate that had no cells. We incubated the medium without any cells in a 37°C incubator for various amounts of time before transferring it to a low-density population that was just ending its second day of differentiation. After 4 days of incubation in the transferred medium (so a total of 6 days of differentiation), we measured the fold-change in density of the low-density population (black points). We plotted the results here as a function of the amount of time the medium spent in the incubator without any cells before we transferred it to the low-density population. The result shows that ageing the medium for 96 hours in 37°C before transferring it to the low-density population still results in rescuing of the low-density population (fold change in population density > 1). The fold-change achievable does decrease as the medium's age increases, from ∼4-fold (for unaged medium) to ∼2-fold (for medium aged for ∼96 hours). n = 3; error bars are s.e.m. **(B)** In a parallel experiment, we took the medium of the high-density population after two days of differentiation. Then, we diluted it by different amounts into a fresh differentiation medium (one that never harbored any cells). We incubated a 2-days-old low-density population into the diluted medium and then measured the fold-change in its density after four days (so a total of 6 days of differentiation). Plotted here is the fold-change in the population density as a function of how much of the medium from the high-density population was mixed with the fresh medium (e.g., 0.2 on the horizontal axis means a dilution by 1 in 5). The red line shows the maximum dilution that is allowed for still rescuing the low-density population. Any higher dilution causes the low-density population to have a fold-change in density that is less than one. The factor of ∼1:5 required to dilute high-density population's medium with fresh medium before it is no longer able to rescue a low-density population from becoming extinct happens to be the ∼same factor one gets for the ratio between the low- and high-population density (i.e., 862 / 5172 = 1 / 6). n = 3; error bars are s.e.m. Combining the results of (A) and (B), we can conclude that more than 1/5 of the secreted molecules remain in the medium after four days of ageing in (A) since, for otherwise, the results in (B) tell us that the fold-change in (A) for medium that was aged for 96 hours should be less than 1, which is not the case. In fact, using the same reasoning, we can say that the effective, combined half-life of the secreted molecules is at least two days. To see, this, note that a half-life of one day would mean that after four days, we would have 1/16 of the molecules degraded after four days since $1/2^4 = 1/16$. But $1/16 < 1/5$, which would mean that the low-density population should have become extinct in the medium that we aged for 96 hours in (A). This is not the case. Repeating the calculation by assuming that the effective, combined half-life is two days leads to: $1/2^2 = 1/4 > 1/5$, which is consistent with the data in (A). In summary, the effective, combined half-life of the secreted molecules is at least two days.

A

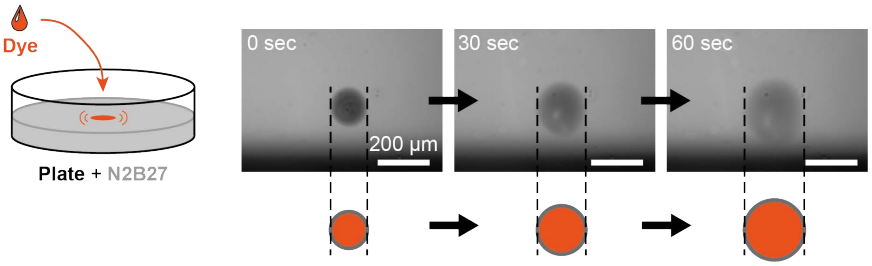
Dye
Plate + N2B27
0 sec
30 sec
60 sec
200 μm

B

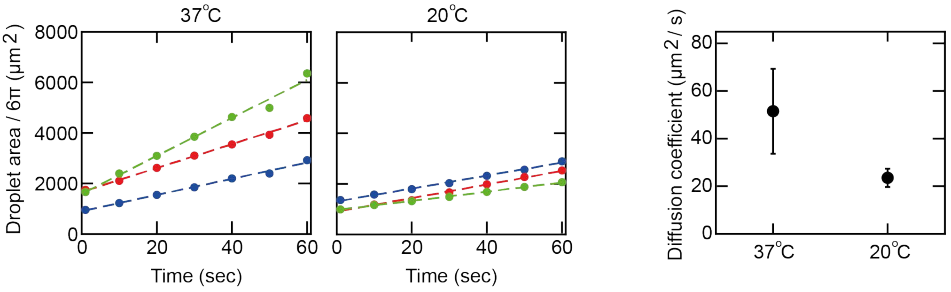
37°C
20°C
Droplet area / 6π (μm 2)
8000
6000
4000
2000
0
0
20
40
60
Time (sec)
Diffusion coefficient (μm 2 / s)
80
60
40
20
0
37°C
20°C

C

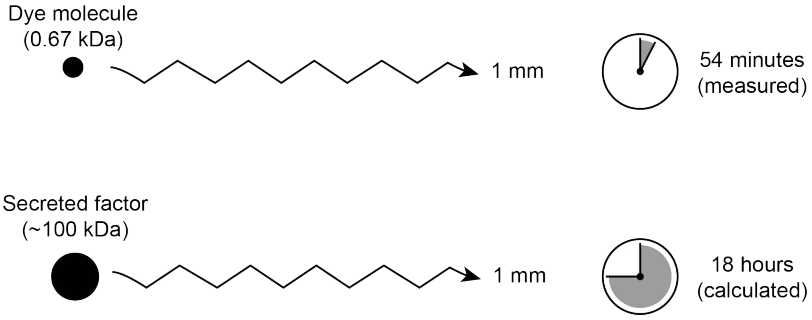
Dye molecule
(0.67 kDa)
1 mm
54 minutes
(measured)
Secreted factor
(~100 kDa)
1 mm
18 hours
(calculated)

Figure 5.14 *(preceding page)*: Diffusion alone, without any other mechanism of transport, explains the long-range (millimeters-scale) spreading of secreted survival-promoting factors. To further support the idea that diffusion alone spreads the cell-secreted factors in our experiments, we determined how fast a droplet of a dye molecule of a known molecular weight spreads in a differentiation medium without any cells, under the same incubation conditions as our cell cultures. **(A)** We used a gel loading dye (DNA Gel Loading Dye 6X, Thermo Scientific, #R0611) which consists of two molecules: bromophenol blue (669.96 Da) and xylene cyanol (538.61 Da). For simplicity, our calculations below will assume that the dye consists of only the heavier molecule, bromophenol blue. We injected a single, 0.5-μL droplet of the dye at the center of a 6-cm diameter plate that contained 5-mL of transparent N2B27 medium, either at room temperature (20°C) or pre-warmed at 37°C. We used a wide-field microscope to make a time-lapse movie with a bird's eye view and snapshots every 10-seconds. Three snapshots (at 0, 30 and 60 seconds; all done at 37°C) of a single droplet of the dye shows the droplet expanding. Scale bar = 200 μm. **(B)** We determined the diffusion constant D of the dye in two ways: using the time-lapse movie and from theory. In the plots, three different colors represent three independent experiments. To determine D from the movies, we tracked the visible droplet boundary over time in a movie to plot the droplet area over time (shown in the two plots here at 37°C and 20°C). As shown, the droplet area linearly increased over time, which is consistent with pure diffusion (pure Brownian motion) since the area of a droplet is proportional to the mean squared displacement of a particle. Specifically, for a particle that undergoes a pure three-dimensional diffusion (Brownian motion), its mean squared displacement $< R^2 >$ at time t is: $< R^2 >= 6Dt$. Let A be the 2-dimensionally projected area of the droplet. Then, $< R^2 >= \frac{A}{\pi}$ and hence, $D = \frac{A}{6} = \frac{A_{slope}}{6\pi}$, where A_{slope} is the slope of the linear fits to the droplet area as shown in the two plots here. From these fits, the experimentally determined diffusion constants D_{exp} at 37°C and 20°C are 51.5 ± 17.8 μm^2/s and 23.5 ± 3.9 μm^2/s respectively (n = 3; error bars are s.e.m.). As a comparison, we determined the diffusion constant D from theory - via the Stokes-Einstein relation which states, $D = \frac{kT}{6\pi\eta r_{dye}}$ where k is the Boltzmann constant, T is temperature, η is the medium's dynamic viscosity, and r_{dye} is the radius of the dye molecule. For water, η = 0.000692 kg/m·s at 37°C and η = 0.001003 kg/m·s at 20°C (from BioNumbers ([195])). We conservatively estimated r_{dye} by noting that bromophenol blue consists of ~10 carbon-carbon bonds which would mean that the dye molecule's diameter is 10 x 0.126 nm. For simplicity, we assume that r_{dye} = 1 nm. The Stokes-Einstein equation then states that the dye's diffusion constants D_{theory} at 37°C and 20°C are 328.1 μm^2/s and 214.0 μm^2/s respectively. Hence, $D_{exp} < D_{theory}$. The fact that our analysis relies on the visible (by eye) boundary of the expanding droplet would underestimate the D_{exp} since the dye must be spreading at least as fast as the boundary does. More importantly, if there were significant convection currents in the liquid medium, then D_{exp} would be much larger than the measured value. This argues against there being any significant liquid convection in our cell-culture media. In other words, the dye-based experiment strongly indicates that cell-secreted survival-promoting factors spread out by pure diffusion rather than by convection currents which, according to the dye, are negligible in our cell-culture conditions. Furthermore, note that $\frac{D_{exp}(37°C)}{D_{exp}(20°C)}$ = ~2.2x and $\frac{D_{theory}(37°C)}{D_{theory}(20°C)}$ = ~1.5x; the experimental and theoretical values for pure diffusion closely match (proportional to a factor on the order of one). **(C)** Based on Brownian motion in 3 dimensions with the experimentally determined diffusion constant, the dye molecule has a mean squared displacement of $< R^2 >$ = 1 mm^2 after $t_{dye} = \frac{R^2}{6D}$ = 54 minutes (with $D = D_{exp}(dye, 37°C)$ = 51.5 μm^2/s). The same calculation, but now based on the Stokes-Einstein relation estimate of the diffusion constant would yield t_{dye}= 8.5 minutes for a 1 mm^2 mean squared displacement (with $D_{theory}(dye, 37°C)$= 328.1 μm^2/s). Hence the theory predicts a faster spreading of dye than experimentally observed - again, arguing against liquid convection or any other mechanism besides diffusion helping to spread the dye. A secreted molecule of 100 kDa would have a mean squared displacement of 1 mm^2 after time, $t_{secreted} = \frac{<R^2>}{6D_{secreted}} = \frac{<R^2>\cdot r_{secreted}}{6\cdot D_{exp}(dye,37°C)\cdot r_{dye}}$ = 18 hours, where we estimate the radius of the molecule to be $r_{secreted}$= 20 nm (see Chapter 6). Hence the two days taken to observe appreciable amount of FGF4 and other survival-promoting factor(s) traveling millimeters and accumulating is consistent with the $t_{secreted}$ calculated here (i.e., if $t_{secreted}$ were much larger than two days, then we should not be observing the survival-factors travelling by millimeters within two days).

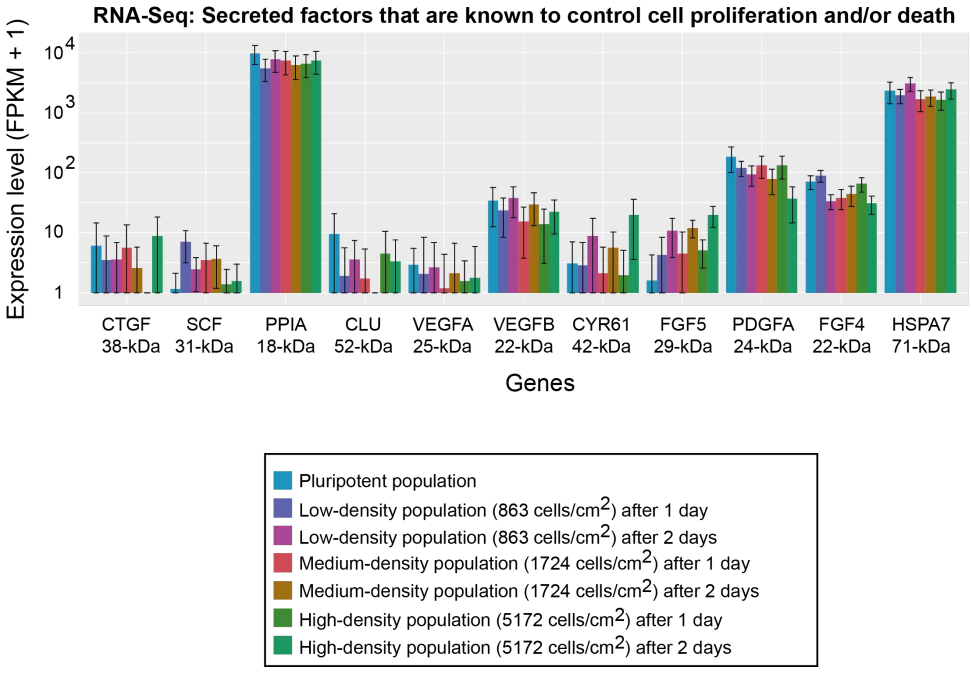

Figure 5.15: RNA-Seq dataset: Expression levels of 11 (candidate) secreted molecules that are known to control cell proliferation. To identify secreted factors other than FGF4 that might contribute to determining a population survival, we performed RNA-Seq to detect expression of any secreted factors that are known to control cell proliferation and/or death. Data shown for 46C cells induced in N2B27+RA to differentiate towards the Neural Ectoderm (NE) lineage with Retinoic Acid (RA) after self-renewing in serum+LIF. We performed RNA-Seq on four populations: (1) pluripotent population prior to differentiation; (2) low-density (862 cells / cm^2) population; (3) high-density (5172 cells / cm^2) population; and (4) medium-density (1724 cells / cm^2) population that is near the threshold density. For the three differentiating populations, we collected their cells on the first and second day after triggering differentiation. Expression levels (FPKMs) of secreted factors that are known to control proliferation and/or apoptosis in ES cells and that fall within the range of molecular weights that the membrane-filter experiments identified (~25–300 kDa with ±50% error) (Fig. 5.1). Shown are the following genes: *CTGF*, *SCF*, *PPIA* (also known as *CYPA*), *CLU*, *VEGFA*, *VEGFB*, *CYR61*, *FGF5*, *PDGFA*, *FGF4* and *HSPA8*. Below each gene name is the molecule's weight (kDa) according to two online resources: Uniprot ([193]) and ExPASy ([194]). n = 3 for all plots; Error bars are s.e.m.

A

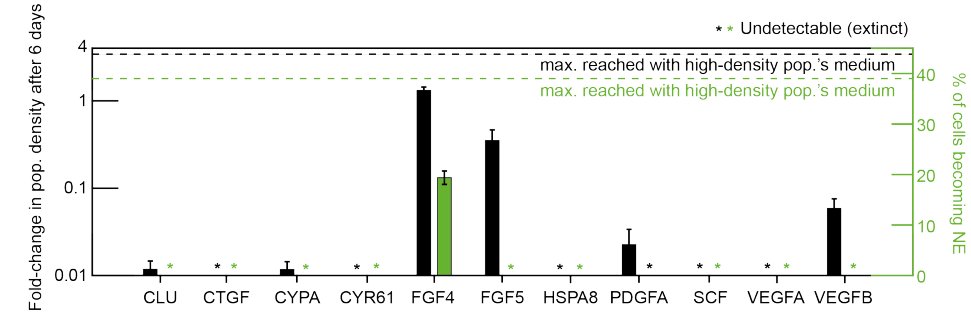

	CLU	CTGF	CYPA	CYR61	FGF4	FGF5	HSPA8	PDGFA	SCF	VEGFA	VEGFB
11-molecule mix:	X	X	X	X	X	X	X	X	X	X	X
6-molecule mix:			X		X	X	X	X			X
4-molecule mix:					X	X		X			X
2-molecule mix:					X	X					

B

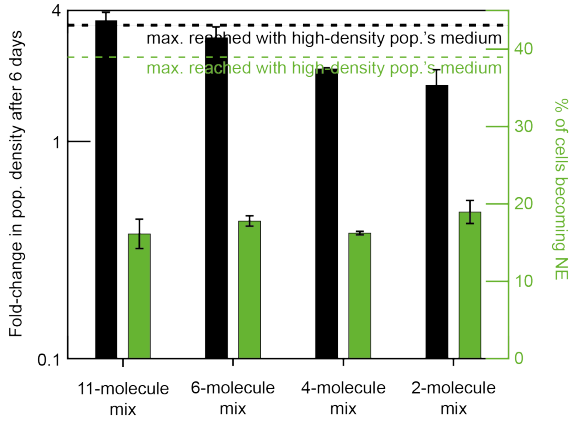

5

Figure 5.16 ***(preceding page)*****: Out of all the extracellular factors that we added one-by-one into differentiation medium, only FGF4 rescues low-density populations from extinction.** The RNA-Seq dataset (Supp. Fig. 5.15) revealed that 11 secreted molecules that are known to control cell proliferation/and or death were highly expressed in differentiating, high-density populations. We thus reasoned that one or combinations of these factors may be the secreted molecule(s) that determine the survival-versus-extinction fate of a population. **(A)** We tested these molecules by adding them one-by-one into the medium of a low-density population (862 cells / cm^2) that would ordinarily become extinct. We used 46C cells that were induced in N2B27+RA to differentiate towards the Neural Ectoderm (NE) lineage with Retinoic Acid (RA) after self-renewing in serum+LIF. We added the following molecules individually, each at a saturating concentration: version of recombinant mouse FGF4 used in Fig. S21C (200 ng/mL), recombinant human FGF5 (200 ng/mL), recombinant mouse PDGFA (100 ng/mL), recombinant mouse VEGFB 186 (100 ng/mL), recombinant mouse VEGFA (100 ng/mL), recombinant human CYR61 (500 ng/mL), recombinant human CTGF (500 ng/mL), recombinant mouse CLU (200 ng/mL), recombinant human HSPA8 (500 ng/mL), recombinant human CYPA (PPIA) (1000 ng/mL), and recombinant mouse SCF (2000 ng/mL). After 6 days in a medium containing one of these molecules, we measured the fold-change in density (black bars) and differentiation efficiency (green bars) of the low-density population. n = 3; error bars are s.e.m. These results show that only the recombinant mouse FGF4 causes the fold-change in population density to be higher than one. All the other factors resulted in the low-density population either approaching extinction (fold change much less than 1) or becoming extinct (indicated with an asterisk). The black dashed line marks the maximum fold-change in population density achieved when the low-density population grows in the medium of a high-density population. The green dashed line marks the maximum differentiation efficiency achieved when the low-density population grows in the medium of a high-density population. The box beneath the plot shows which signaling factors were mixed together and then given to the low-density population in (B). **(B)** Results obtained by giving combinations of the 11 factors together to the low-density population, with the ingredients of the mixture indicated in the box below (A). Giving all 11 factors together at once yielded the highest growth (~4-fold increase in population density; black bar), which is almost equal to the maximum possible growth seen in our medium-transfer experiments (black dashed line indicates maximum fold-change achieved by incubating the low-density population in the medium of a high-density population). This suggests that FGF4's rescuing ability is enhanced by some of the ten other molecules. But, with the 11 molecules added together at once, the differentiation efficiency (green) remained rather low at ~20% compared to the ~40% (green dashed line) that we get from incubating the low-density population in the medium of a high-density population. As we progressively reduced the number of signaling factors in the mixture from 11 to 2, we observed only a modest decrease in population growth, down to about ~1 fold. Importantly, FGF4 was included in all these mixtures.

6

Cooperativity and habitat size determine collective survival

Parts of this chapter are also reported in Daneshpour et al. [2]

6.1. Introduction

To see how the various experimental findings merge into a coherent picture, we use quantitative models that take our key findings as their basic ingredients and aim to recapitulate all other experimental findings. First, we sought to confirm our hypothesis that diffusion of secreted factors with molecular weights as found in our experiments can occur on a millimeters-scale by using dimensional analysis to derive the necessary conditions. We then used the steady-state solution to the three-dimensional reaction-diffusion equation to confirm our hypothesis. Furthermore, we performed experiments to derive the diffusion constant of diffusible molecules of a known molecular weight in conditions similar to that of our cell-cultures (e.g., 37°C, 5% CO_2, same liquid culture-medium). By using the Stokes-Einstein relation we confirmed that millimeters-scale diffusion by ES-cell-secreted, survival-promoting factors (as suggested from our experiments) is possible. Lastly, we asked whether our mathematical model predicts any new behaviors that we could confirm experimentally.

6.2. Results

6.2.1. Secreted molecules are stable to explain their diffusion across macroscopic distances

Our experiments show that the cells secrete molecules that diffuse on the order of 1 mm. We first use calculations to show that physics of diffusion also allows for biomolecules to diffuse on the order of 1 mm.

At first, a millimeter-scale diffusion may seem counterintuitive. This is because one often does not think about two cells, 1 mm apart, signaling to each other with diffusible molecules. Aside from the traveling axion potentials among neurons, one often does not think of millimeter scale communication among mammalian cells that are relatively immobile like ES cells. But physics allows for this for the proteins with the sizes that we experimentally found. Consider the general form of **reaction-diffusion equation** for the concentration c of a secreted molecule at position $\vec{r}$ and time t:

$$\frac{\partial c}{\partial t} = D\nabla^2 c(\vec{r},t) - \gamma c(\vec{r},t) \tag{6.1}$$

where D and γ are the molecule's diffusion constant and degradation rate respectively. This equation lacks the molecule's source (i.e., secreting cell) for simplicity and because we are interested in how far the molecule diffuses, which is independent of the secretion rate. A molecule's diffusion length L is the characteristic (typical) distance that it travels before degrading. We can deduce L from dimensional analysis. Later on, we give the full, time-dependent solution to above equation

which yields the same conclusion as the one we give in this section. The only parameters in the above equation are D and γ. D has the dimension, length^2/time, and γ has the dimension, 1/time. Hence it follows that $L = \sqrt{D/\gamma}$, which is a well-known result. We can arrive at the same result through a more complicated way - by solving the reaction-diffusion equation above with a constantly secreting cell. But that is an overkill. We also have

$$\gamma = \frac{log(2)}{\tau} \tag{6.2}$$

where τ is the molecule's half-life. Next, as is common for biomolecules, we can estimate D by using the **Stokes-Einstein relation** for diffusing, spherical particles:

$$D = \frac{kT}{6\pi\eta r} \tag{6.3}$$

where k is the Boltzmann constant, T is temperature, η is the dynamic viscosity of the medium in which the molecule is diffusing, and r is the radius of the spherical particle that is diffusing. The ES cells grew at 37°C and in an aqueous medium. Thus, for an order of magnitude estimate, we can use the dynamic viscosity of water at 40°C: $\eta = 0.653x10^{-3}Ns/m^2$ [from: http://www.engineersedge.com]. This value nearly stays the same at 30°C and is thus insensitive to temperature for our purpose. Then, at 37°C, we have

$$D = \frac{3.5x10^{-19}m^3/s}{r} \tag{6.4}$$

Before estimating the r, we can estimate the maximum diffusion constant D_{max} for our molecules of interest. Our experiments with molecular filters showed that the secreted protein(s) must be in the neighborhood of ~100 kDa (specifically, between 50 to 300 kDa (Fig. 5.1); and more precisely, at least as low as ~25 kDa if we take the conservative estimate of ±50% error in the filter-pore sizes which we confirmed experimentally). Each amino acid has a mass of ~110 Da and end-to-end length of ~0.35 nm. Thus, our proteins of interest (of 100 kDa) would consist of ~1000 amino acids which, when joined stretched end-to-end, have a length of 350 nm (clearly a gross overestimate of the r for the secreted proteins). With this overestimate, we have $D_{max} = 1\mu m^2/s$, which is the conservative, lower bound given for the diffusion constant of large biomolecular machines such as ribosomes. In fact, the conventional values assigned to the diffusion constant of typical proteins inside a cytoplasm fall in the range of 5 - 50 $\mu m^2/s$ (from BioNumbers [195]). Since the cytoplasm is a highly crowded environment that limits diffusion, we can expect a higher value for the protein of our interest that diffuses in the liquid medium.

We now estimate the D. The typical value of r for proteins is ∼5 nm (from BioNumbers [195]). In contrast, $r \sim 30$ nm for eukaryotic ribosomes (from BioNumbers [195]), which are macromolecular complexes that are certainly heavier and larger than our proteins of interest as our experiments revealed. As a conservative estimate (i.e., to estimate a reasonable lower bound on the diffusion length), suppose that $r \sim 20$ nm for our proteins of interest, four times larger than the value of r for typical proteins (∼5 nm). Then according to above equation, we have

$$D \approx 20 \mu m^2/s \tag{6.5}$$

which is still reasonable in the ES cell's relatively non-viscous liquid medium (recall that 5 - 50 $\mu m^2/s$ for a crowded cytoplasm). Note that

$$\tau = \frac{L^2 log(2)}{D} \tag{6.6}$$

Hence, for a diffusion length L of 1 mm, we need $\tau \sim 12$ hours. Note that this is a conservative, overestimate of the secreted molecule's half-life since we underestimated the diffusion constant by assuming that the molecule is larger than half the radius of a ribosome (i.e., assumed r ∼ 20 nm). A more realistic estimate such as, for example, r ∼ 10 nm, would yield $\tau \sim 6$ hours. A more typical value that one assigns to r for proteins is $r \sim 5$ nm, which would yield $\tau \sim 3$ hours. In summary, both the conservative and more realistic estimates yield protein half-lives, which are required for a near millimeter-scale diffusion, that are well within the typically cited values of protein half-lives. Crucially, we measured the half-lives of the secreted molecules, including FGF4, in the supernatants of our cell cultures (Supp. Figs. 5.12-5.13) and found that they are longer than the calculated half-lives here, meaning that the secreted molecules can, in fact, reach further than the 1-mm diffusion length we used in our calculation here. Moreover, we confirmed this important notion with new experiments to measure the diffusion constant D of diffusive molecules with known size in conditions similar to those for our cell-cultures, and then to extrapolate these results for the cell-secreted, survival-promoting factors in order to obtain typical time-scales for millimeter-scale diffusion (Fig. 6.1).

Lastly, we use the steady-state solution to the three-dimensional reaction-diffusion equation to confirm our previous conclusions, which were based on dimensional analysis. Assuming the ES cell to be a spherical cell of radius R that secretes a molecule at a constant rate τ, equally in all directions, the three-dimensional reaction-diffusion equation is

$$\frac{\partial c}{\partial t} = \frac{1}{r^2}\frac{\partial}{\partial r}(Dr^2\frac{\partial c}{\partial r}) - \gamma c + \frac{\eta}{4\pi R^2}\delta(r-R) \tag{6.7}$$

where c is the concentration, r is radial distance from the center of the ES cell, and δ is the Dirac delta function. As one can verify by substituting into the reaction-diffusion equation, its steady-state solution is

$$c(r) = \frac{c_R R}{r} exp(-\frac{r-R}{\lambda}) \tag{6.8}$$

where $\lambda = \sqrt{D/\gamma}$ and

$$c_R = \frac{\eta}{4\pi R^2} \frac{\gamma}{\lambda} \frac{1}{1+\frac{\lambda}{R}} \tag{6.9}$$

Note that c_R is the steady-state concentration on the surface of the cell. The exponential term in the steady-state solution tells us that the characteristic length (i.e., diffusion length) is exactly $\sqrt{D/\gamma}$, which exactly matches the diffusion length that we derived from dimensional analysis. Thus, the conclusions based on the dimensional analysis holds true. Note that this was not guaranteed since there could have been a small, numerical factor that scaled the λ down by several orders of magnitude.

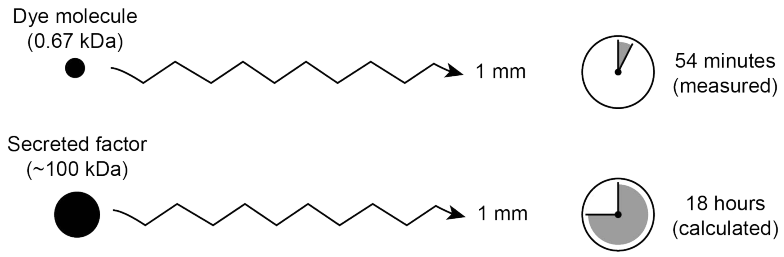

Figure 6.1: Calculations (Stokes-Einstein relation) and experiments (measuring diffusion constant) explain long-range diffusion of secreted molecules promoting collective survival. To further support the idea that diffusion alone spreads the cell-secreted factors in our experiments, we determined how fast a droplet of a dye molecule of a known weight spreads in a differentiation medium without any cells, under the same incubation conditions as our cell cultures. For this we used a gel loading dye of known molecular weight (0.67 kDa) and then used a wide-field microscope to observe how a single droplet of the dye in liquid culture medium at conditions equal to those used to culture ES cells at 37°C. From these observations we determined the dye's diffusion constant D and determined the time (~18 hours) a secreted, survival-promoting factor of ~100 kDa take to diffuse a distance of ~1 mm in liquid medium based on Stokes-Einstein relation. Hence the two days taken to observe appreciable amount of FGF4 and other survival-promoting factor(s) traveling millimeters and accumulating is consistent with the observed time. See detailed explanation in caption of Supp. Fig. 5.14.

6.2.2. Population's growth rate correlates with its initial density through a death-rate-independent mechanism

To build a simple mathematical model that recapitulates the ES-cell population's survival-vs-extinction fate, we first experimentally determined growth

and death rates from our time-lapse movies that we used to track and trace microcolonies (i.e., their areas) during the first four days of differentiation (see Chapter 3).

To obtain a death rate for each population as a function of its initial density, we analyzed when microcolonies die in the time-lapse movies (i.e., showing apoptotic bodies, lifting off from the plate bottom and often floating away) and then recorded all such cumulative "dead" areas over time to derive an equivalent "death rate" (Fig. 6.2A and Supp. Fig. 6.7). We found that the population's death rate (i.e., the rate at which microcolonies' areas are "lost" through death over time) is virtually independent of its initial density (i.e., for both extinction-bound and expanding populations the death rate is constant) (Fig. 6.2A). The growth rate (i.e., the rate at which microcolonies' area are "added" through expansion over time; see Chapter 3 and Supp. Fig. 6.8), however, correlates with the initial population density (Fig. 6.2B). Altogether, these results show that the net growth rate of differentiating populations is negative (i.e., below zero) for populations that eventually become extinct (i.e., for populations starting below ~1700 cells / cm^2) whereas it is positive (i.e., above zero) for populations that survive and expand (i.e., for populations starting above ~1700 cells / cm^2) (Fig. 6.2C) during differentiation.

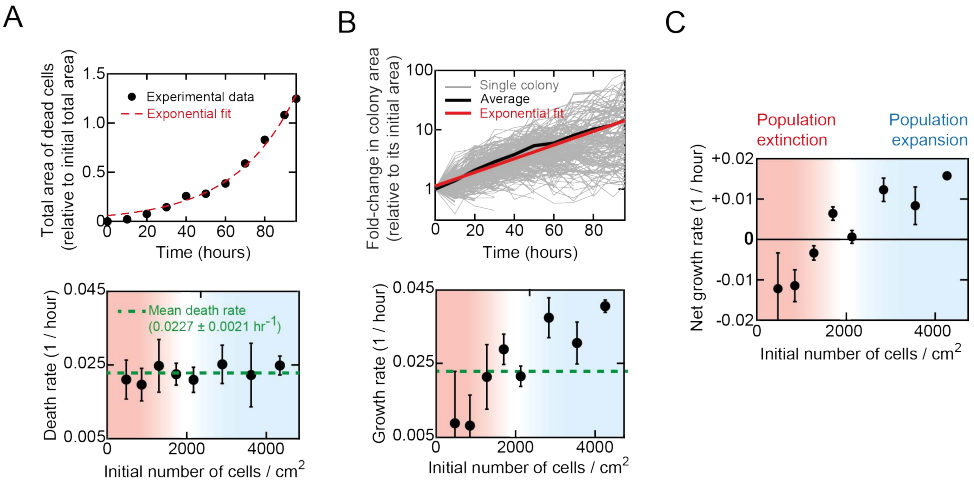

Figure 6.2: Differentiating population's net growth rate correlates with its initial density. (A) Death rates. (Top) We derived death rates from measuring cumulative areas of dead microcolonies over time for each initial population density. Detailed explanation is in the caption of Supp. Fig. 6.7. (Bottom) Death rates (= 0.0227 ± 0.0021 hr^{-1}) are virtually independent of initial population density. n = 3; Error bars are s.e.m. **(B)** Growth rates. (Top) We derived net growth rates from tracking and tracing areas of alive microcolonies over time. See detailed explanation in Chapter 3 and Supp. Fig. 3.8, 6.8. (Bottom) For each initial population density, we first obtained the net growth rate (C) as a function of the initial population density. We reconstructed a growth rate (shown here) by adding each replicate's (n = 3) net growth rate (C) to its death rate (A). n = 3; Error bars are s.e.m. **(C)** Net growth rates. Differentiating population's net growth correlates with its initial density. n = 3; Error bars are s.e.m.

6.2.3. Mathematical model with one fit parameter recapitulates main experimental observations

Our model has just one free parameter and is a modification of another model that we previously built to explain cooperative replications of yeasts at high temperatures [51]. In our stochastic model, a cell randomly chooses to either divide, die, or remain alive without dividing (Fig. 6.3A). Each of these choices occur with a certain probability which is determined by, for simplicity, just one molecule (FGF4) that every alive cell secretes at a constant rate. The probability of a cell replicating nonlinearly increases as the extracellular concentration of FGF4 increases (Fig 6.3B - blue). The probability of a cell dying is constant - it is independent of the FGF4 concentration (Fig. 6.3B - red) - which we experimentally verified in microscope-based time-lapse movies of cell growths and deaths (Figs. 6.2 and Supp. Figs. 6.7-6.8). Given that our experiments (e.g., see Chapter 3) and the Stokes-Einstein equation both show that FGF4 diffuses across a macroscopic distance (i.e., at least several millimeters), our model assumes, for simplicity, that FGF4 becomes well-mixed (uniformly mixed) throughout the liquid medium immediately after cells secrete it.

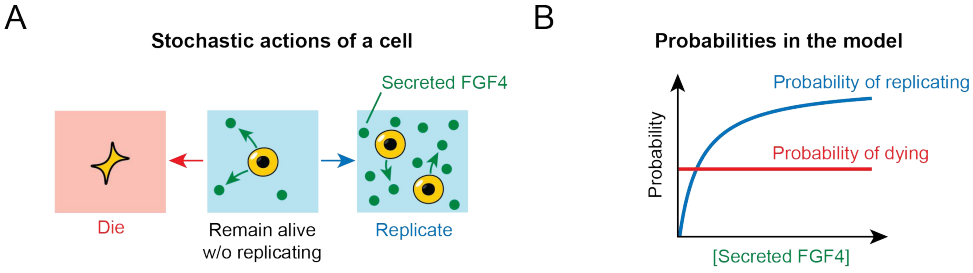

Figure 6.3: Stochastic actions of a cell and the basic parameter settings in our mathematical model. **(A)** Mathematical model with three possible, stochastic actions of a cell. **(B)** Probabilities used in the model: probability of a cell dying (red) and probability of cell replicating (blue), both as functions of extracellular concentration of FGF4. Probability of dying is constant (see Fig. 6.2A and Supp. Fig. 6.7 for experimental validation). The probability of replicating nonlinearly increases with the concentration of extracellular FGF4 and is based on growth rates of various populations that we measured (see Fig. 6.2B and Supp. Fig. 6.8).

Our model assumes differentiating ES cells constantly secrete a molecule. This molecule can be any molecule that promotes cell proliferation. For concreteness and based on our experiment, we will let the molecule be FGF4 but it can be any other molecule (note that our filter-based experiments (Figs. 5.1) established that a molecule that is heavier than FGF4 is also involved in determining the survival-versus-extinction fate). In our model, we assume for simplicity that cells secrete FGF4 at a constant rate. FGF4 extracellularly accumulates. To summarize, the probability of a cell replicating nonlinearly increases as the extracellular concentration of FGF4 increases (Fig. 6.3B - blue curve). For simplicity, we assume that

the probability of a cell dying is constant, as we experimentally verified (Fig. 6.3B).

Let N_t be a stochastic variable that represents the number of alive cells at time t. We take time in discrete integer steps. At each timestep, cells die with a constant probability P_γ and replicate with probability $P_\mu(t)$ which depends on the extracellular concentration of FGF4 (denoted M_t) at time t. The probability of replication $P_\mu(t)$, as a function of M_t, follows the Hill equation, with the Hill coefficient set to one for simplicity, and the maximum value μ. It is

$$P_\mu(t) = \mu \frac{M_t}{K + M_t} \tag{6.10}$$

where K is a constant.

FGF4 degrades with rate d. Our experiments establish a long half-life of FGF4 - it is at least 80 days (Supp. Fig. 5.12) - and a long, half-life for the mixture of all secreted molecules that determines the survival-versus-extinction fate (at least two days (Supp. Fig. 5.13)). At each time step t, the number of cells that replicate is sampled from a binomial distribution with $P_\mu(t)$ being the probability of one cell replicating. The number of cells that die at time t is sampled from a binomial distribution with P_γ being the probability of one cell dying. We assume that the molecule is well-mixed since our experiments established that the population effectively acts as a single entity that either dies or lives, due to the molecules that diffuse over several millimeters. Combining all the elements above, our model is completely described by the following set of stochastic equations:

$$N_{t+1} = N_t + \binom{N_t}{P_\mu(t)} - \binom{N_t}{P_\gamma} \tag{6.11}$$

$$P_\mu(t) = \mu \frac{M_t}{K + M_t} \tag{6.12}$$

$$P_\gamma = constant \tag{6.13}$$

$$M_{t+1} = \frac{N_t}{V} + dM_t \tag{6.14}$$

where V is the volume of liquid medium, and N_0 is the initial number of cells. Since cells start without any extracellular FGF4 (since the differentiation medium initially has no FGF4 or any molecules that determine the survival-versus-extinction fate), we must have $P_\mu(0) = 0$, which indeed follows from above equation. Note that we measure the FGF4 concentration (M_t and M_{t+1}) in units of secretion rate - the

additional concentration of FGF4 generated in one time step - as the secretion rate per cell is $1/V$ in the above equation.

The above set of equations has five parameters, four of which are directly fixed by our experimental data. Hence, we cannot freely tune the four parameters - μ, P_γ, V, and d - and hence our model is highly constrained. We measured the maximum possible growth rate μ in two ways: (1) time-lapse microscopy in which we tracked the area of each colony over time for four days (Supp. Figs. 3.8 and 6.8); and (2) by counting the number of cells over time in a population (Fig. 2.6, and Supp. Figs. 2.7 and 2.10). Both methods yielded a similar value: $\mu = 0.0519$. To directly read off the value of the death rate P_γ from the experiments, we used the fact that a population of a very low initial density never grows and thus its rate of decline in cell number is P_γ (green circle in Supp. Fig. 6.8C) which we found to be: $P_\gamma = 0.0256$. We determined V by directly measuring the volume of each liquid medium. Finally, we determined d by measuring the half-life of the mixture of all secreted molecules (Supp. Fig. 5.13) and the half-life of extracellular FGF4 alone (Supp. Fig. 5.12). We used the half-life of FGF4, which leads to $d = 0.99$ if we let each time step to represent 1 hour. With these constraints by the experiments, only one parameter, K, remains free for us to tune in the above set of equations. We chose the value for K such that the threshold density - at which the population can either survive or shrink towards extinction (Fig. 2.6A - middle row) - matches the experimentally determined threshold density. We thus let $K = 485{,}000$.

With the parameter values assigned as described above, our model recapitulates all the main features that we experimentally observed (Fig. 6.4). We ran stochastic simulations that are based on the equations of our model, with the above-mentioned parameter values, for a wide range of initial density N_0. For sufficiently low initial densities, we have $P_\mu(t) < P_\gamma$ for all times since cells are not able to accumulate enough FGF4 (cells continue to die and as this occurs, the cells' efforts to accumulate FGF4 is even further hindered). Thus, such a population goes extinct. For sufficiently high initial densities, we eventually have $P_\mu(t) > P_\gamma$ after some time. Here, M_t becomes sufficiently high - it goes above the necessary threshold concentration at which the probability of replicating equals the death rate - which results in the population expanding towards the carrying capacity. For a particular set of initial population densities, we eventually have $P_\mu(t) \approx P_\gamma$ for some stretch of time. This results in the population remaining nearly constant in cell numbers for some time. However, the population eventually gets pushed stochastically to either extinction or the carrying capacity (Fig. 6.4). This population-level stochasticity occurs due to the stochastic actions by just a few cells in the population - whether or not a few cells stochastically divide while $P_\mu(t) \approx P_\gamma$ and thus just slightly increases $P_\mu(t)$ above P_γ.

By running simulations for various initial densities at liquid volumes, we deter-

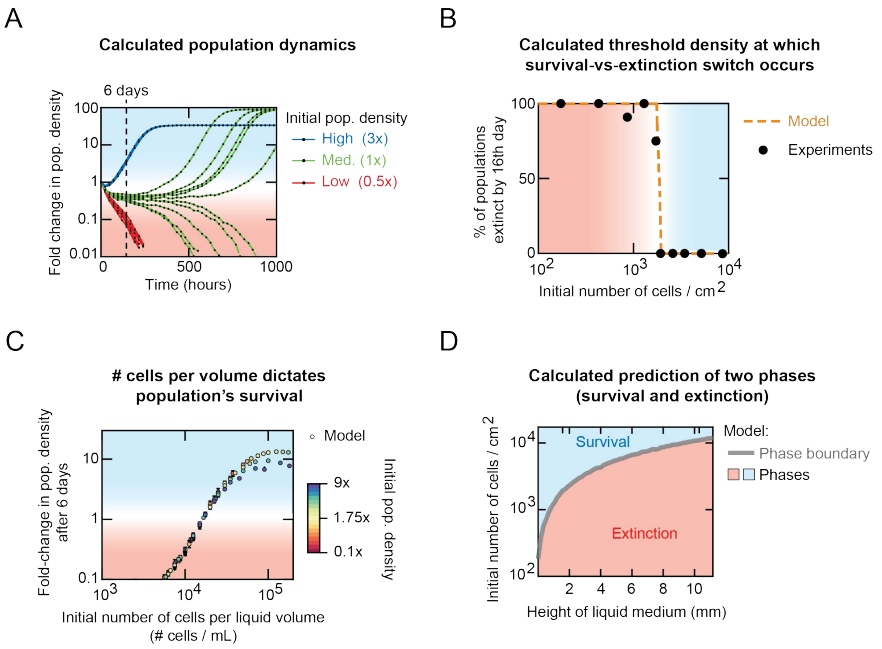

Figure 6.4: Mathematical model recapitulates key features of experiments and makes predictions about new behaviours. (A) Fold-change in population density, simulated by the model. Red: low-density population (862 cells / cm^2 initially). Green: near-threshold (medium) density population (1931 cells / cm^2 initially). Blue: high-density population (5172 cells / cm^2 initially). Vertical, dashed line marks 6 days after differentiation began (for comparison with Fig. 2.6). Blue and red shades indicate population expansion and extinction, respectively. **(B)** Percentage of populations, in an ensemble of populations that start with the same, near-threshold density (1931 cells / cm^2), that becomes extinct either before or on the 16th day of differentiation. Data for 46C cells differentiating in N2B27+RA after self-renewing in serum+LIF. Black data points are from measurements and orange curve is from running the stochastic model multiple times (one for each population in an ensemble). Subset of n = 86 populations shown as black points (see Supp. Fig. 2.9 for full data). Population was considered to have reached extinction if its fold change decreased to below 0.1, relative to initial density. Blue shade indicates population expansion and red shade indicates population extinction. **(C)** Data from model's prediction (small circles). Plotted here is the fold change in population density after 6 days as a function of the initial population density which is now measured as # cells per mL of liquid volume (instead of # cells / cm^2 that we used up to this point). Data from model predictions are from combining multiple volumes of liquid medium (in mL: 2, 5, 10, 18, 20, 30, 40 and 60) with initial cells / cm^2 (172, 431, 862, 1293, 1724, 1931, 2155, 2586, 3017, 3448, 4310, 5172, 6034, 8621, 9483, 12069 and 15517 – indicated by the color bar). To obtain # cells / mL, we multiplied the # cells / area by the total area of the cell-culture plate (same for all conditions) and then divided the resulting value by the liquid volume. Blue and red shades indicate population expansion and extinction, respectively. See Supp. Fig. 6.9 for full data set. Error bars are s.e.m.; n = 3. **(D)** Model-produced phase diagram (grey curve and blue-red shadings). Grey curve was constructed from the model by calculating, for each liquid medium height (volume), the threshold population density at which a population can either expand or become extinct (e.g., green curves in Fig. 6.4A). This, in turn, determines where the blue and red shades are in this plot.

mined the phase-boundary that separates the survival phase and extinction phase (boundary curve in Fig. 6.4D). To get the boundary curve, we ran the simulation

eight times for each pair of initial density and liquid volume. We then determined how many of these simulations, with the same initial condition, led to survival (and thus eventually reaching the carrying capacity) and how many of them led to a population extinction. In the extinction phase (red region in Fig. 6.4D), 100% of the simulations caused the population to become extinct. In the survival phase (blue region in Fig. 6.4D), 100% of the simulations caused the population to survive and eventually reach the carrying capacity. These determinations then allowed us to identify the boundary between the two phases - the phase boundary - which is shown as a curve in Fig. 6.4D. At this boundary, the probability of dying is equal to the probability of replicating, leading to equal numbers of cells replicating and dying, until stochastic fluctuations determine the population's fate (survival or extinction). We found that this boundary nearly linearly increases with the liquid volume in the regime of media volume that we could experimentally access given the dimensions of the cell-culture dish (10-cm diameter).

In summary, the model recapitulates the population dynamics as follows. As a population begins to differentiate, more cells die than replicate. This is because FGF4 is initially absent and thus the probability of replicating is initially zero while the probability of dying is non-zero. As the deaths occur, alive cells secrete and extracellularly accumulate FGF4 which, in turn, gradually increases the probability of replicating. If the population's initial density is below a threshold value, all cells would have died before the population had enough time to accumulate sufficient amount of FGF4 to save itself from extinction (Fig. 6.4A - red). If the population's initial density is above the threshold value, enough FGF4 accumulates and thus the probability of replicating eventually matches and then increases above the probability of dying (Fig. 6.4A - blue). The FGF4 concentration at which the probabilities of replicating and dying match is the model's sole fit parameter. If the population's initial density is near the threshold value, it either expands or becomes extinct (Fig. 6.4A - green) - which one of the two occurs is randomly determined - because the probabilities of replication and death nearly match for a prolonged time. This leads to the days-long, nearly static population density seen in our experiments (Supp. Fig. 2.9), until a few more cells stochastically replicating (dying) pushes the population towards expansion (extinction).

The model correctly recapitulates the threshold population density at which this stochastic population-level fate occurs (Fig. 6.4B). The model and analysis of the reaction-diffusion equation for secreted factor also explains why we see global effects but not local effects (i.e., larger colony is not more likely to survive because the far-away diffusing molecule does not locally linger around the secreting cells to create sharp concentration gradients around them; moreover, the factor concentration at which the probability of dying and probability of surviving match (Fig. 6.3B) contributes to why no local effect is seen).

6.2.4. Population density and liquid volume collectively determine survival-vs-extinction fate during differentiation

Aside from recapitulating the existing data, the model quantitatively predicted how populations would behave - whether it survives or becomes extinct - when one simultaneously changes the volume of liquid medium and the initial population density over wide ranges. We confirmed these predictions with additional experiments (Fig. 6.5 and Supp. Fig. 6.9).

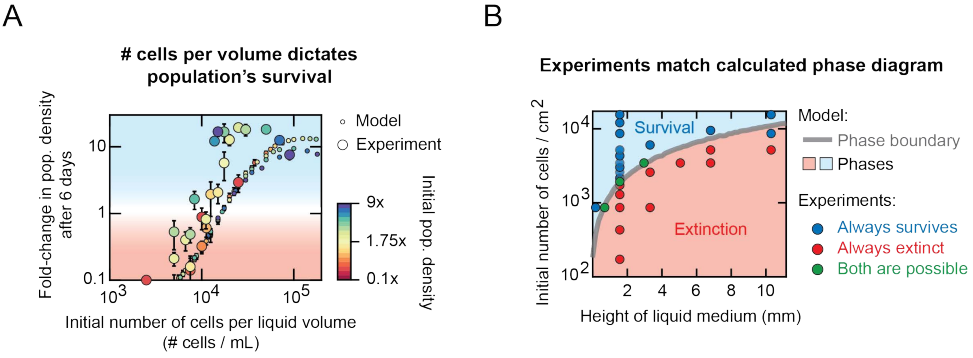

Figure 6.5: New experimental results confirm predictions from mathematical model. (A) Data from new experiments performed after building the model (large circles) and model's prediction (small circles). Data for 46C cells differentiating in N2B27+RA after self-renewing in serum+LIF. Plotted here is the fold change in population density after 6 days as a function of the initial population density which is now measured as # cells per mL of liquid volume (instead of # cells / cm^2 that we used up to this point). Data from experiments and model predictions are from combining multiple volumes of liquid medium (in mL: 2, 5, 10, 18, 20, 30, 40 and 60) with initial # cells / cm^2 (172, 431, 862, 1293, 1724, 1931, 2155, 2586, 3017, 3448, 4310, 5172, 6034, 8621, 9483, 12069 and 15517 – indicated by the color bar). To obtain # cells / mL, we multiplied the # cells / area by the total area of the cell-culture plate (same for all conditions) and then divided the resulting value by the liquid volume. Data for 46C cells differentiating towards NE lineage. Blue shade indicates population expansion and red shade indicates population extinction. See Supp. Fig. 6.9 for full data set. Error bars are s.e.m.; n = 3. **(B)** Model-produced phase diagram (grey curve and blue-red shadings) and experimental confirmation of the phase diagram (circles are from new experiments that were not used to build the model). Same experimental data as in Supp. Fig. 6.9 (n = 3; error bars are s.e.m.). Grey curve was constructed from the model by calculating, for each liquid medium height (volume), the threshold population density at which a population can either expand or become extinct (e.g., green curves in Fig. 6.4A). This, in turn, determines where the blue and red shades are in this plot. Circles are from experiments. Blue circles ("always survives") are for initial conditions - defined by liquid medium's height and initial number of cells / cm^2 - for which all replicate populations expanded. Red circles ("always extinct") are for initial conditions for which all replicate populations decreased in their density after 6 days (average of their fold change was below 0.6). Green circles ("both are possible") are for initial conditions for which some replicate populations expanded after 6 days while some did not (average of their fold change was between 0.6 and 1).

In particular, the model predicted the precise shape of a phase boundary - precise combinations of volume (height) of liquid medium and initial population density for which a population's survival-versus-extinction fate is random (Fig. 6.5B - grey curve) - which we have not yet investigated (we investigated the liquid volume for

only two initial population densities thus far (Fig. 3.6)). We performed additional experiments in which we simultaneously varied the initial population density and the liquid volume (i.e., the height of the liquid on top of the adherent cells) over wide ranges. The results of these experiments closely matched the model's quantitative prediction of the phase boundary shape (Fig. 6.5B - circles; and Supp. Fig. 6.9). By accurately and comprehensively summarizing the experimental findings into a coherent picture, our simple model supports the conclusions that we have drawn from the experiments.

6.3. Conclusions

We showed that a simple mathematical model - that uses key findings from our previous experiments as its basic ingredients - recapitulates the main phenomena we discovered, starting in Chapter 2: ES-cell populations secrete far-away (well-mixed) diffusing factors (such as FGF4) that control the population's survival-vs-extinction fate based on its initial density during differentiation, including the threshold-density where fates are determined stochastically. Moreover, our model also predicted new behaviors which we confirmed with new experiments: population's initial density and volume of liquid medium together determine the survival-vs-extinction fate. Our experiments and model tell us the following story (Fig. 6.6). ES-cell populations require sensing sufficient concentrations of diffusive, survival-promoting factors during the first few days of differentiation which the cells themselves produce. The more cells there are, the more factors are produced. And thus, the higher the concentration of the factors to surpass everyone's threshold needed to survive and avoid extinction (we prove this mathematically and experimentally in Chapter 8). This concentration is set by the initial population density (cooperation) and the volume of the liquid medium (habitat) that collectively decide the population's survival-vs-extinction fate.

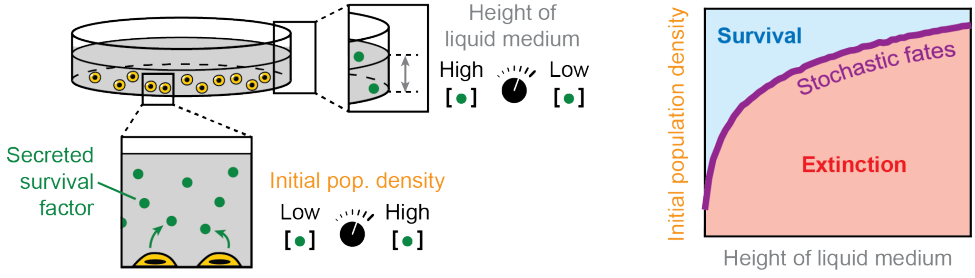

Figure 6.6: Cooperativity and habitat size collectively determine survival during differentiation. ES cells (yellow) depend on self-produced survival factors (such as FGF4 - green circles) during differentiation to decide whether the entire population either survives or becomes extinct. By cooperatively amassing sufficient concentrations of the factors within the first few days and by setting the height of the liquid medium (grey), the population's survival-vs-extinction fate (phase diagram) depends on the tuning of the initial population density and the confines of the liquid environment.

6.4. Supplementary Information

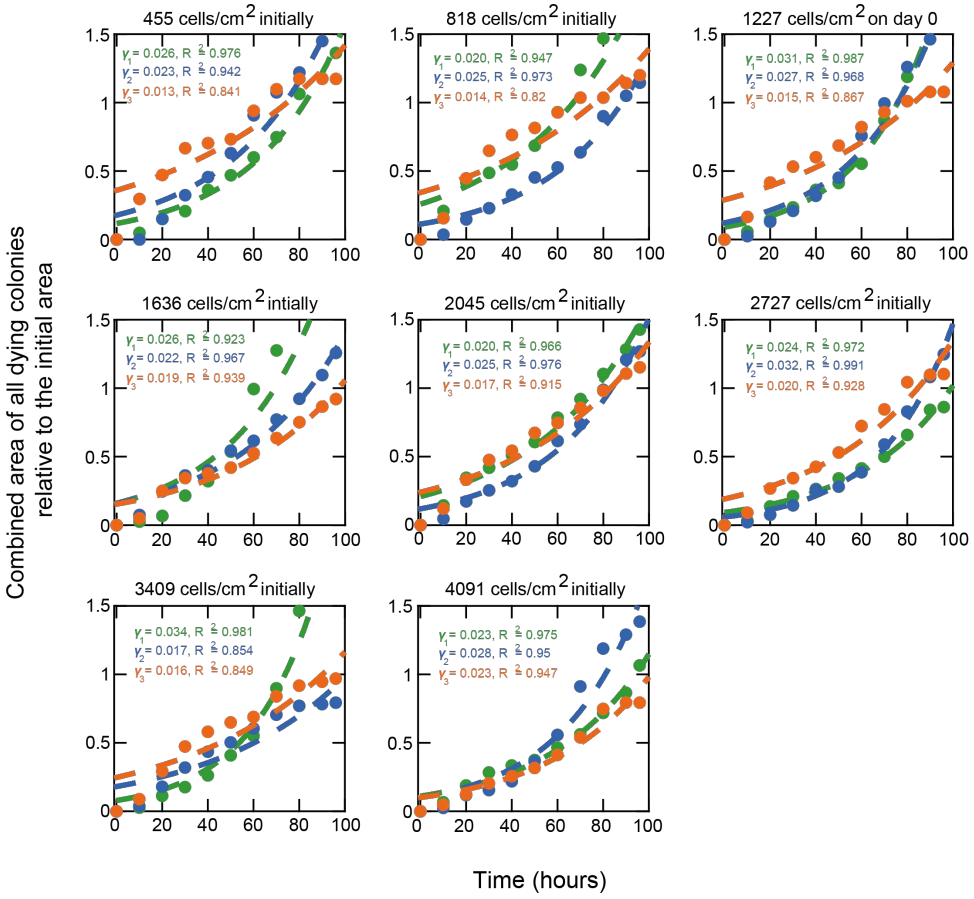

Figure 6.7: Determining the rate of cell death with time-lapse microscopy. We sought to verify that the rate of cell death is independent of the initial population density. This is an ingredient of our mathematical model. With time-lapse microscopy, we measured the growth of individual microcolonies over four days for a wide range of initial population densities. We used E14 cells undergoing unguided differentiation in N2B27 after self-renewing in serum+LIF. Each box shows a population of a different starting density (indicated above each box). For each population density, we tracked microcolonies in 17 fields of view. Each field of view has a dimension of 1.40 mm x 0.99 mm. We examined all densities in triplicates (each color represents an independent replicate). Dying colonies typically lifted off the plate (and thus disappeared from the field of view) or started to display clearly visible apoptotic bodies. From these movies, we inferred the death rate of cells by taking the cumulative sum of the last recorded areas of each colony just before it died, as a way to measure how much colony area is "lost" (i.e., deaths) in time. We then divided this combined area of all dead cells by the combined initial area. We determined the death rate by fitting a single exponential function - with the death rate γ (in 1/hours) - to the data points (dashed curves represent the fits to data points of corresponding color; each color is a single replicate; n = 3 for each initial density) (see Fig. 6.2 and Supp. Fig. 6.8 for a demonstration of this procedure). The values of γ and corresponding R^2 are indicated in each plot. Error bars are s.e.m. This figure complements Supp. Fig. 6.8.

A

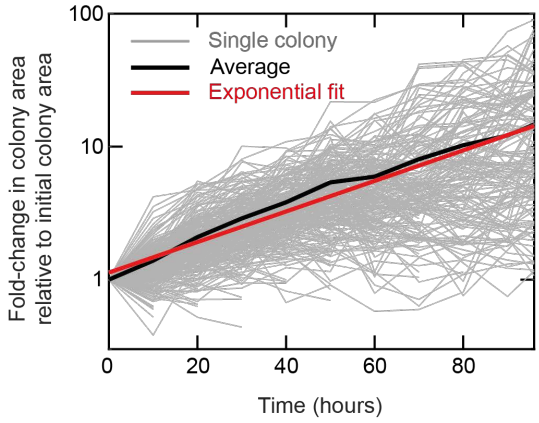
Single colony
Average
Exponential fit
Fold-change in colony area relative to initial colony area
100
10
1
0
20
40
60
80
Time (hours)

B

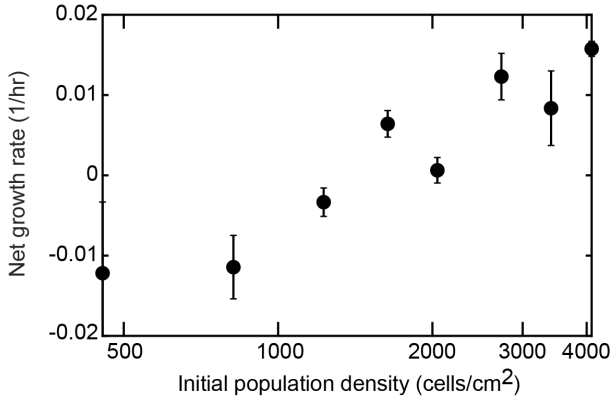
Net growth rate (1/hr)
0.02
0.01
0
-0.01
-0.02
500
1000
2000
3000
4000
Initial population density (cells/cm2)

C

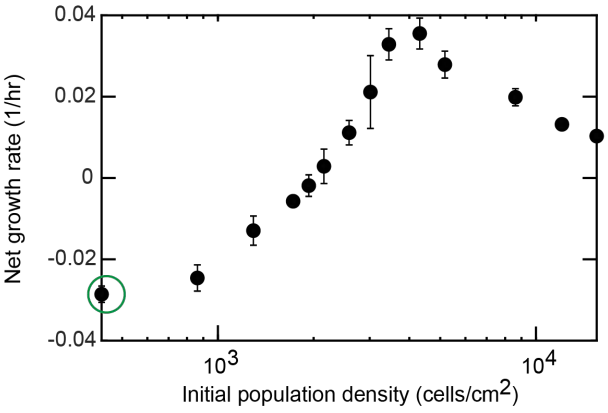
Net growth rate (1/hr)
0.04
0.02
0
-0.02
-0.04
10^3
10^4
Initial population density (cells/cm2)

Figure 6.8 ***(preceding page)*****: Density-dependent net growth rate (= growth rate - death rate) measured in two ways.** Net growth rate is negative if the death rate is higher than the growth rate (i.e., for a population that becomes extinct). It is positive if the growth rate is larger than the death rate (i.e., for a population that grows). We measured the cells' net growth rates in two different ways. In one, we used time-lapse microscopy data to measure colony growths. In the other, we manually counted cells -and thus the population density over time as in Fig. 2.6. **(A)** Example showing the microscope-based method of determining the net growth rate for a given initial population density. As shown in Fig. 2.14 and described in the caption there, we measured the area of each colony over time for four days, imaging 17 fields of view for each starting population density. Shown here is an example for E14 cells. Each grey curve shows the area of a single microcolony over time. Each colony's area is normalized to its initial area (thus all curves here start at a value of one on the vertical axis). Black curve is the average of all the grey curves. Red line is an exponential curve (line in this semi-log plot) that we fitted to the black curve (i.e., fitted to the population average). The slope of the red line is the net growth rate for this population. **(B)** Using the microscope-based method outlined in (A) for every initial population density, we obtained the growth rate (black dots) as a function of the initial population density. n = 3; Error bars are s.e.m. **(C)** Net growth rates determined by manual counting of cells (i.e., data in Supp. Fig. 2.10) rather than from the microscopy data. n = 3; Error bars are s.e.m. To determine the (not net) growth rate for each initial population density, we added the constant death rate (determined in Supp. Fig. 6.7) to the net growth rate. We found that the maximum possible growth rate is 0.05219 hr^{-1}, which we used as one of the parameter values in our mathematical model. From (C), we found that the lowest possible net growth rate is -0.026 hr^{-1} (indicated with green arrow in (C)). This value nearly matches the death rate (0.023 ± 0.002 hr^{-1}; found in Supp. Fig. 6.7), a consequence that we explore in our mathematical model.

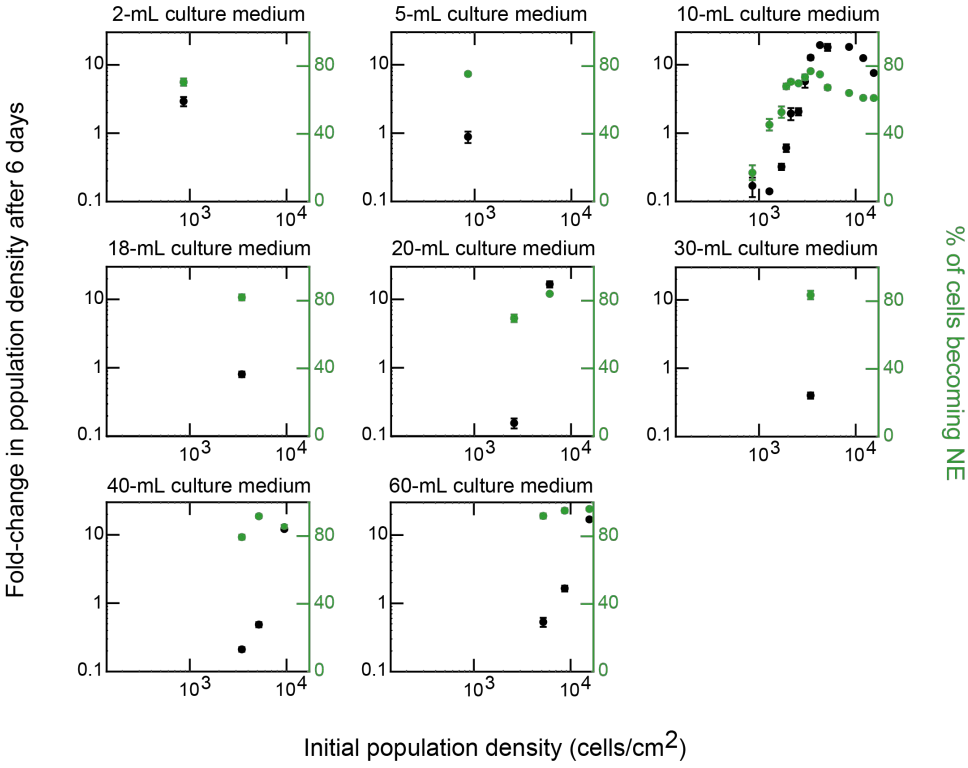

Figure 6.9: Volume of liquid medium at the start of differentiation determines survival-vs-extinction fate of differentiating populations. To experimentally test the model's prediction (i.e., to verify that the model-produced phase diagram in Fig. 6.4D is correct as is the model's prediction in Fig. 6.4C), we incubated 46C populations of different starting densities in different volumes of liquid medium (and thus in different heights of liquid medium). We induced the cells to differentiate in N2B27+RA toward the Neural Ectoderm (NE) lineage with Retinoic Acid (RA) after self-renewing in serum+LIF. Each box shows a different volume of liquid medium. Horizontal axis of each box is the initial population density. Black points are the fold changes in the population density (relative to the initial density) after six days. Green points are the percentages of cells that entered the NE lineage (*Sox1*-GFP positive cells measured with flow cytometer). n = 3; Error bars are s.e.m.; n = 3. As seen in Fig. 6.5, these results match the phase diagram produced by the model (i.e., data points of the right type fall on the right side (above or below) the model-produced phase boundary in Fig. 6.4D).

7

Materials and methods

7.1. Cell lines and cell-culture media

7.1.1. Short description of methods

We used three murine ES cell lines: E14Tg2A.IV (129/Ola), 46C, *Brachyury*-eGFP and *Oct4*-GFP. The 46C cell line (*Sox1* promoter driving GFP) was previously described by Ying et al. [126] and was a kind gift from Austin Smith whose lab constructed it by targeting GFP to the endogenous *Sox1* locus. Thus, the 46C cells had the *Sox1* promoter controlling a GFP expression. The *Brachyury*-eGFP cell line was previously described by Fehling et al. [172] and Pearson et al. [173] and was a kind gift from Valery Kouskoff whose lab constructed it by targeting eGFP to the endogenous *Brachyury* (*T*) locus. Thus, this cell line had the *Brachyury* (*T*) promoter controlling an eGFP expression. The *Oct4*-GFP cell line (*Oct4* promoter driving GFP) was previously described by Nichols et al. [174] and Silva et al. [116] and was a kind gift from Austin Smith whose lab constructed it by targeting GFP to the endogenous *Oct4 (Pou5f1)* locus.

To keep ES cells pluripotent, we routinely (every 2 days, with 1/10 dilution) passaged (propagated) them in either a serum-based (FBS) or a serum-free (2*i*) pluripotency medium. The serum-based medium (denoted serum+LIF) consisted of high-glucose DMEM (Gibco) supplemented with 15% fetal bovine serum (Gibco, ES qualified), 1X MEM non-essential amino acids (Gibco), 1 mM sodium pyruvate (Gibco), 1X glutaMAX (Gibco), 0.1 mM 2-mercaptoethanol (Gibco), 1000 U/mL penicillin-streptomycin (Gibco) and 1000 U/mL Leukemia Inhibitory Factor (LIF, Polygene). The serum-free medium (denoted 2*i*+LIF) consisted of approximately half-and-half mixture of Neurobasal (Gibco) and DMEM/F12 (Gibco) abd was supplemented with 1X MEM non-essential amino acids (Gibco), 1 mM sodium pyruvate (Gibco), 1X glutaMAX (Gibco), 1X N-2 (Gibco), 1X B-27 minus vitamin A (Gibco), 0.1 mM 2-mercaptoethanol (Gibco), 50 μg/mL BSA (Sigma, fraction V), 1000 U/mL penicillin-streptomycin (Gibco), 1000 U/mL Leukemia Inhibitory Factor (LIF, Polygene), 3 μM CHIR99021 and 1 μM PD0325901. We performed sterile filtration of all cell culture media with a 0.2-μm bottle top filter. Cells were maintained in the pluripotency medium on 10-cm diameter tissue-culture dishes (Sarstedt, TC Dish 100 standard) that were coated with 0.1% gelatin in water (Sigma, from bovine skin Type B) at 37°C for at least 20 minutes prior to seeding cells.

7.1.2. Protocol for preparing cell-culture media

Serum+LIF medium is a 15% serum-containing medium, suitable for monolayer growth of mESC on 0.1%-gelatin coated TC dishes. Note: use ES-qualified serum if available (specifically tested for maintaining pluripotent morphologies by manufacturer).

Content (250 mL)

- 205 mL: DMEM (High Glucose)
- 37.5 mL: FBS (15% in final volume)
- 1.25 mL: NEAA, Non-Essential Amino Acids (100X)
- 1.25 mL: Sodium Pyruvate (100X)
- 1.25 mL: GlutaMAX-I (100X)
- 454 μL: 2-Mercaptoethanol (55 mM in PBS, 0.1 mM in final volume)
- 2.5 mL: Penicillin-Streptomycin (10,000 U/ml; 100X)
- 25 μL: LIF (10^7 U/mL; 10,000X))

N2B27 medium (N2B27) is a serum-free, defined medium as a basis for keeping ES cells pluripotent or for differentiation ES cells. Adding Leukemia Inhibitory Factor (LIF), CHIR99021 (CHIR) and PD0325901 (PD0) to N2B27 is often used to maintain (ground-state "naive"; see [196, 197]) pluripotency under serum-free conditions. LIF acts to inhibit differentiation. CHIR indirectly activates the Wnt pathway by directly inhibiting the downstream GSK3 and promoting transcription of pluripotency factors. PD0 inhibits MEK1 and MEK2, stopping the activation of MAPK and inhibiting differentiation while promoting proliferation.

Content (250 mL)

- 120 mL: Neurobasal
- 118 mL: DMEM/F-12 + GlutaMAX-I (2.5 mM) + Sodium Pyruvate (0.5 mM)
- 1.25 mL: NEAA, Non-Essential Amino Acids (100X)
- 1.25 mL: Sodium Pyruvate (100X)
- 1.25 mL: GlutaMAX-I (100X)
- 1.25 mL: N2 (100X)
- 2.5 mL: B27 minus Vitamin A (50X)
- 166 μL: BSA (7.5% stock (75 mg/ml), 1,500X; 50 μg/ml in final volume)
- 454 μL: 2-Mercaptoethanol (55 mM in PBS, 0.1 mM in final volume)
- 2.5 mL: Penicillin-Streptomycin (10,000 U/ml; 100X)
- (*optionally*: 25 μL: LIF (10^7 U/mL; 10,000X))
- (*optionally*: 80 μL: CHIR (10 mM 3,333X stock in DMSO))
- (*optionally*: 25 μL: PD0 (10 mM 10,000X stock in DMSO))

7.1.3. Key ingredients of N2B27 and their molecular weights

We obtained this information from ATCC, Ying et al. [126], Mittal and Voldman [191], and Brewer et al. [198]. Most components of differentiation medium (N2B27) are smaller than the smallest filter pore size that we used (3 kDa), and if larger then not vital for the survival/growth of ES cells (see Supp. Fig. 5.6 and Mittal and Voldman [191]).

Abbreviations: MW = molecular weight, Da = Daltons, N/A = not applicable (i.e., not included in mixture), CONF = confidential, propriety information (Invitrogen).

Compound Name	MW (Da)	Conc. in DMEM/F-12 (µM)	Conc. in Neurobasal (µM)	Conc. In N2 supplement (µM)	Conc. In B-27 minus vitamin-A supplement (µM)
Inorganic salts					
CaCl2 (anhydrous)	111	1000	1800	N/A	N/A
CuSO4 (anhydrous)	160	0.01	N/A	N/A	N/A
Fe(NO3)3·9H2O	404	0.13	0.25	N/A	N/A
FeSO4·7H2O	278	1.5	N/A	N/A	N/A
MgSO4 (anhydrous)	120	700	812	N/A	N/A
KCl	75	4000	5333	N/A	N/A
NaHCO3	84	14,300	26,000	N/A	N/A
NaCl	58	120,000	51,300	N/A	N/A
Na2HPO4 (anhydrous)	142	500	N/A	N/A	N/A
NaH2PO4 ·H2O	120	500	1,000	N/A	N/A
ZnSO4·7H2O	288	1.5	N/A	N/A	N/A
Amino Acids					
L-Alanine	89	50	22.5	N/A	N/A
L-Arginine·HCl	210	700	400	N/A	N/A
L-Asparagine·H2O	150	50	5	N/A	N/A
L-Aspartic Acid	133	50	N/A	N/A	N/A
L-Cystine·HCl·H2O	294	60	N/A	N/A	N/A
L-Cystine·2HCl	312	100	10	N/A	N/A
L-Glutamic Acid	147	50	N/A	N/A	N/A
L-Glutamine	146	2,500	500	N/A	N/A
Glycine	75	250	400	N/A	N/A
L-Histidine·HCl·H2O	209	150	200	N/A	N/A
L-Isoleucine	131	415	800	N/A	N/A
L-Leucine	131	450	800	N/A	N/A
L-Lysine·HCl	146	625	1,000	N/A	N/A
L-Methionine	149	115	200	N/A	N/A
L-Phenylalanine	165	215	400	N/A	N/A
L-Proline	115	150	67	N/A	N/A
L-Serine	105	250	400	N/A	N/A
L-Threonine	119	450	800	N/A	N/A

Figure 7.1

L-Tryptophan	204	45	80	N/A	N/A
Vitamins					
D-Biotin (B7)	244	0.01	CONF	N/A	N/A
Choline Chloride	140	64	28	N/A	N/A
Folic Acid (B9)	441	6	9	N/A	N/A
myo-Inositol (B8)	180	70	40	N/A	N/A
Niacinamide (B3)	122	16.5	33	N/A	N/A
D-Pantothenic Acid (B5)	219	10	8	N/A	N/A
Pyridoxine·HCl (B6)	202	10	20	N/A	N/A
Riboflavin (B2)	376	0.6	1	N/A	N/A
Thiamine·HCl (B1)	373.5	6	10	N/A	N/A
Vitamin B-12	1,355	0.5	0.25	N/A	N/A
Proteins					
Insulin	5,800	N/A	N/A	4.3	CONF
Serotransferrin	77,000	N/A	N/A	1.33	CONF
BSA	66,000	N/A	N/A	0.75	CONF
SOD-1 (Dimer)	32,000	N/A	N/A	N/A	CONF
Catalase (Tetramer)	240,000	N/A	N/A	N/A	CONF
Other					
D-Glucose	180	17,500	25,000	N/A	N/A
HEPES	238	15,000	10,000	N/A	N/A
Hypoxanthine	136	17.5	N/A	N/A	N/A
Linoleic Acid	280	0.16	N/A	N/A	N/A
Phenol Red, Sodium Salt	354	23	23	N/A	N/A
Putrescine·2HCl	161	0.5	N/A	N/A	N/A
Pyruvic Acid·Na	111	500	225	N/A	N/A
DL-Thioctic Acid	206	0.5	N/A	N/A	N/A
Thymidine	242	1.5	N/A	N/A	N/A
Progesterone	314	N/A	N/A	0.02	CONF
Sodium Selenite	173	N/A	N/A	0.02	CONF
Putrescine	88	N/A	N/A	180	CONF
Lecithin	770	N/A	N/A	N/A	CONF
Linolenic Acid	278	N/A	N/A	N/A	CONF
Phosphatidylcholine	776	N/A	N/A	N/A	CONF
Retinol	286	N/A	N/A	N/A	CONF
Retinyl Acetate	328	N/A	N/A	N/A	CONF
Sodium Selenite	173	N/A	N/A	N/A	CONF
T3 (Triodo-I-Thyronine)	650	N/A	N/A	N/A	CONF
DL-α-Trocopherol (Vitamin E)	431	N/A	N/A	N/A	CONF
DL-α-Trocopherol Acetate	473	N/A	N/A	N/A	CONF
L-Tyrosine·2Na·2H2O	263	200	400	N/A	N/A
L-Valine	117	450	800	N/A	N/A

Figure 7.2

7.1.4. Heat inactivation of Fetal Bovine Serum (FBS)

Fetal Bovine Serum (FBS) needs to be heat inactivated ('decomplemented') in a 56°C water bath to destroy heat-labile complement proteins prior to use in cell growth medium. To do this, the following protocol can be used.

1. Remove 500-mL bottle of FBS (Gibco) from –20°C freezer and place in refrigerator to thaw overnight. Complete thawing of serum the following day by placing serum in a 37°C water bath with a water level higher than the serum level in the bottle. Mix by inversion.

2. Once serum is completely thawed, incubate for an additional 15 min to allow serum to equilibrate with the 37°C bath.

3. Raise the temperature setting of the bath to 56°C. Use a timer to measure the 35 min needed for the temperature of the bath and serum to come to 56°C. During this incubation, invert the bottle to mix the serum every 10 min. If necessary, allow an additional 5 min for bath to reach 56°C.

4. Once bath reaches 56°C, incubate serum for 30 min. Invert bottle every 10 min.

5. Remove serum from water bath and allow to cool at room temperature for 30 min. Reset water bath to the 37°C mark.

6. Aliquot 50 mL of treated serum into conical tubes and store at 4°C or freeze at –20°C.

7.1.5. Gelatin-coating of tissue-culture dishes

In order to grow mouse Embryonic Stem (ES) cells on tissue-culture dishes, the surface of the dishes must be coated with gelatin for the cells to attach. Mouse ES cells can also attach to non-gelatinized surfaces but can detach easily due to shaking or movement of medium (e.g., during passaging).

To make 0.1% gelatin solution in water from gelatin powder.

1. To prepare n mL of 0.1% gelatin in water from powder, weigh $(n * \frac{0.1}{100})$ grams of gelatin powder, and add this to a clean, autoclaved bottle of appropriate size.

2. Add n mL of Milli-Q water to the bottle.

3. Swirl to mix. At this point, the powder is not soluble yet.

4. Autoclave the bottle for 30 minutes within 2 hours after mixing water and gelatin powder (Choose "program 4" for the autoclave machine).

5. After autoclaving, allow 0.1% gelatin solution to cool down to room temperature on the bench. Check if the solution is clear.

6. Store the labeled bottle with 0.1% gelatin solution at 4°C. Use the solution within 2 months, and check frequently if the solution in the bottle remains clear.

7. **For coating.** Take out the 0.1% solution from the fridge, and add 10 mL to a 10-cm TC dish inside a laminar flow hood.

8. Shake the plate back and forth, then left to right, to spread the gelatin solution on the dish surface.

9. Incubate the plate at 37°C for >30 minutes. Dishes with excess gelatin solution can be stored in the 37°C incubator for up to a week.

10. After ≥30 minutes, aspirate off excess gelatin solution. Allow gelatin on dish surface to dry for a few minutes, by removing the dish lid inside the laminar flow hood. Add pre-warmed culture medium to proceed with culturing.

7.1.6. Freezing of cell lines

Cells should be frozen at a 1:1 or lower concentration. E.g. one 10-cm TC dish into a vial to be thawed into one 10-cm diameter TC dish (1:1) or three wells of a 6-well plate (2:1).

1. Change (i.e. Refresh) the media 2-4 hours prior to freezing. Cells must be 80% confluent and healthy prior to freezing.

2. Prepare 2X freezing media (80% FBS + 20% DMSO) and label cryovials with date/name/number of cells, and pre-chill the vials on ice.

3. When cells are ready to be frozen, aspirate off old media and wash with 5 mL pre-warmed 1X PBS. When doing this, add the PBS gently to the side of the plate to avoid disrupting the cells.

4. Aspirate off PBS.

5. Add 1 mL of pre-warmed trypsin. Be sure to cover the entire plate by carefully swirling the plate.

6. Incubate the plate at 37°C for 5 minutes. (Check under microscope. If you see big clumps of cells, incubate additional 2-5 minutes.) Do not overtrypsinize.

7. While cells are incubating, add 5 mL of pre-warmed Medium into 15-mL Falcon tube.

8. Once majority of the cells are uniformly dispersed into small clumps or single cells, tilt the plate to gather most of the trypsin at one side of the plate (you see some clumps sliding). Pipette about 10 times the trypsin/cell mixture, against the tilted surface of the 10-cm TC dish (to make sure you gathered most of the cells). Avoid making bubbles.
9. Transfer the trypsin/cell mixture into the 15-mL Falcon tube, and pipette the entire mixture for 2-5 times.
10. Spin down the cells by centrifuging the Falcon tube at 200 x g for 5 minutes at RT.
11. Aspirate off the supernatant (containing Media and trypsin) down to about a small amount of a left-over.
12. Resuspend the cell pellet into 10 mL 1X PBS. Pipette and mix the mixture with a ≥5-mL pipette.
13. Spin down the cells by centrifuging the Falcon tube at 200 x g for 5 minutes at RT.
14. Aspirate off the supernatant down to about a small amount of a left-over.
15. Resuspend the cell pellet into 3 mL (or other volume) pre-chilled Medium. Pipette and mix the mixture with a ≥5-mL pipette.
16. For 1 cryovial, add 500 μL 2X freezing media together with 500 μL cell mixture.
17. Put the cryovial inside the "Mr. Frosty Freezing Container", and store the container at –80°C for 1-2 days. After that, store the cryovials (not with the container!) at –150°C.

7.1.7. Thawing and plating of cell lines

Note: when taking the cryovials out of Liquid Nitrogen vapor phase for thawing, one needs to work quickly (and carefully) to avoid cells from dying as much as possible, since DMSO is toxic for the cells when thawed.

1. Take a 10-cm TC dish (with red label) and label with name/date/number of cells.
2. Add 10 mL 0.1% gelatin in H_2O to the center of the dish surface.
3. Shake the plate back and forth in order to evenly spread the gelatin over the surface.
4. Incubate the plate at 37°C, for at least 30 minutes before use.
5. Add 10 mL of pre-warmed serum+LIF medium into a 15-mL Falcon tube.

6. Remove the 10-cm TC dish from the 37°C incubator, and remove the 10-mL gelatin.
7. Add 5 mL of pre-warmed serum+LIF medium in the gelatin-coated dish, and gently swirl to spread the medium over the plate surface.
8. Take 1 cryovial from the Liquid nitrogen vapor phase (–150°C), and partially thaw it in a water bath at 37°C until a pea-size frozen portion remains (~30-60 secs).
9. Transfer the cell/DMSO mixture (~1 mL) into the 15-mL Falcon tube with 5 mL of pre-warmed serum+LIF. An additional 1 mL of pre-warmed serum+LIF can be added to the empty cryovial, in order to dissolve and transfer the left-over cells.
10. Spin down the cells by centrifuging the Falcon tube at 200 x g for 5 minutes at RT.
11. Aspirate off the supernatant (containing medium and DMSO) down to about a small amount of a left-over.
12. Resuspend the cell pellet into 10 mL 1X PBS. Pipette and mix the mixture with a ≥5-mL pipette.
13. Spin down the cells by centrifuging the Falcon tube at 200 x g for 5 minutes at RT.
14. Resuspend the cell pellet into 5 mL pre-warmed medium. Pipette and mix the mixture with a ≥5-mL pipette.
15. Transfer this amount (5 mL) into the 10-cm TC dish (containing 5 mL of pre-warmed medium).
16. Shake (gently) the plate back and forth then left to right, allowing time for the cells to settle between shakes.
17. Incubate the plate at 37°C, and do not disturb the plates for 16 hours after shaking.

7.1.8. Maintaining or passaging of cell lines

Maintaining ES cells in healthy cultures, requires active care. Ideally, the culture medium should be changed and therefore refreshed before the cells run out of chemicals required for growth, and/or maintenance of pluripotency, and/or (guided) further differentiation. Replacing old with new medium may (still) cause disruptions to adherent cells.

Maintaining cell cultures

1. Take the 10-cm TC dish with adherent cells from the 37°C incubator.
2. Aspirate off the old medium.
3. Add 10 mL pre-warmed medium to the plate. When doing this, add the fresh medium gently at the sides of the plate to avoid disrupting the cells.
4. Gently shake the plate back and forth, and then left to right, allowing the medium to settle between shakes.
5. Incubate the plate at 37°C, and do not disturb the plates for 16 hours after shaking.

Passaging cell cultures

1. About two hours before passaging, refresh the medium of the cells.
2. Coat 10-cm TC dish with 10 mL of 0.1% gelatin solution at 37°C for geq30 minutes.
3. Pre-warm new medium, PBS and accutase (or Trypsin-EDTA) at 37^{circ}C.
4. Take the 10-cm TC dish with adherent cells from the 37°C incubator.
5. Aspirate off the old medium.
6. Rinse cells with 10 mL of 1X PBS (pre-warmed).
7. Aspirate off PBS.
8. Add 1 mL of accutase to cells, from the center of the dish. Cover entire dish by tilting the dish in different directions.
9. Incubate dish at 37°C for 5-10 minutes. Check with microscope, if colonies got "loose", and if cells have lifted off from the surface, appearing round while floating in the medium. Use a microscope for this.
10. Add 4 mL of PBS to plate, to deactivate accutase. Mix, to create a single-cell suspension, while avoiding bubble formation.
11. Transfer 5 mL mixture to 15-mL tube, already containing 5 mL of PBS.
12. Spin down cells at 200 x g for 5 minutes.
13. Aim to observe a (small) cell pellet. Aspirate off supernatant, down to the cell pellet (a left-over liquid is OK).
14. Resuspend cell pellet in 10 mL of PBS (2nd time).
15. Spin down cells at 200 x g for 5 minutes.
16. Aspirate off supernatant, down to the cell pellet (a left-over liquid is OK).

17. Resuspend cell pellet in 10 mL of new medium.
18. Take out 10-cm TC dish with gelatin from the 37°C incubator, and aspirate off excess gelatin.
19. Leave the dish lid open for a few minutes inside the laminar flow hood, to allow the gelatin on the dish surface to dry.
20. Gently add the cell mixture to the dish. Gently shake the plate back and forth, and then left to right, allowing the medium to settle between shakes.
21. Incubate the plate at 37°C, and do not disturb the plates for 16 hours after shaking.

7.1.9. Collecting and counting of cell lines

Note: if cells are 80-90% confluent (i.e., there is still about of 10-20% visible surface area not covered with cells), then cell must be passaged.

To obtain cell counts:

1. Follow steps 4-16 of "Passaging cell cultures" in 7.1.8.
2. Resuspend cell pellet in x mL of PBS to make a cell suspension, depending on how confluent the cell culture is. For 80-90% confluent population, then use x = 5-10 mL. For very few (if any) cell colonies, then use x =~1 mL.
3. Prepare an autoclaved 2-mL tube and combine y μL of cell suspension and z μL Trypan Blue solution (0.4%, Thermo Fisher). Trypan Blue solution is used to visually exclude dead, stained cells from alive, non-stained cells during cell counting. For 80-90% confluent population, then use y = 10 μL and z = 190 μL (1:20, dilution factor = 20). For very few (if any) cell colonies, then use y = 20 μL and z = 20 μL (1:2, dilution factor = 2).
4. Take 20 μL of stained-cell solution (irrespective of dilution factor) and insert in the cell count chamber (Marienfeld Buerker, no. 631-0921).
5. For each of the 5 large squares* (each containing 16 smaller squares) count the number of alive, non-stained cells. Stained cells are dead cells and should be excluded from the total counts.
6. Concentration of cells (number cells per mL solution) = (counts/5*) x dilution factor x 10,000

7.1.10. Differentiation experiments

To initiate differentiation, we detached and collected ES cells from dishes by incubating them with 1 mL of accutase (Gibco, StemPro Accutase Cell Dissociation Reagent) in 37°C for 5 minutes. After collecting the cells, we washed them twice

with 1X PBS and then centrifuged them to remove any remaining accutase from the resulting cell pellet. We then resuspended the cell pellet in N2B27 which was prepared according to established protocols [126, 171]. We then counted the number of cells per mL in this resuspension, as described in the "Cell counting" section below. Afterwards, we calculated the volume of this resuspension required to achieve a desired number of cells per cm^2 on a dish and then pipetted this volume into a tube containing 10 mL of N2B27 that was pre-warmed N2B27 to 37°C. We then transferred this onto a 10-cm diameter dish whose bottom was coated with a 0.1%-gelatin. We distributed the cells across the surface area of the dish by gently shaking the dish and then incubated the cells at 37°C with 5% CO_2. Importantly, we did not disturb the plate for at least 6 hours after the plating to allow the cells to sediment and attach to the gelatinized plate bottom. We defined this moment to be the start of differentiation time-course (day 0). Cells were left for 2 days in N2B27 and then the spent medium was replaced with either fresh, pre-warmed N2B27 (for unguided differentiation), or N2B27 supplemented with 500 nM of Retinoic Acid (for Neural Ectodermal differentiation), or N2B27 supplemented with 3 μM of CHIR99021 (for Mesendodermal differentiation). We then left the plate for further incubation at 37°C with 5% CO_2. Subsequently, we collected the cells from dishes for counting and flow cytometry. Importantly, we confirmed that large majority of ES cells ($\geq$80%) differentiates into the Neural Ectoderm lineage without any inducer (such as RA; denoted "unguided differentiation") and regardless of which medium (2*i*+LIF or serum+LIF) the ES cells were previously self-renewing in.

7.2. Single-cell measurements with flow cytometry

The following description is adapted from BD's instruction manual for FACSCelesta Flow Cytometer.

BD's FACSCelesta Flow Cytometer enables quantitative sorting a heterogeneous mixture of biological cells through cell-specific light scattering and fluorescent characteristics. The cell suspension is forced up and injected into a lower chamber of conical shape. The created laminar sheath flow carries the cells or particles to be measured individually through the center of the flow cell where they are intercepted by the laser beam. The optics system consists of lasers, optical filters and detectors. Lasers illuminate the cells or particles in the sample and optical filters direct the resulting light scatter and fluorescence signals to the appropriate detectors. When a cell or particle passes through a focused laser beam, laser light is scattered in all directions. Light that scatters axial to the laser beam is called forward scatter (FSC) and light that scatters perpendicular to the laser beam is called side scatter (SSC). FSC and SSC are related to certain physical properties of cells. FSC indicates relative differences in the size of the cells or particles. Larger cells scatter more light and therefore they are higher in FSC. SSC indicates relative dif-

ferences in the internal complexity or granularity of the cells or particles. More granular cells deflect more light than less granular cells, and therefore are higher in SSC. When cells or particles stained with fluorochrome-conjugated antibodies or other dyes pass through a laser beam, the dyes can absorb photons (energy) and be promoted to an excited electronic state. In returning to their ground state, the dyes release energy, most of which is emitted as light. This light emission is known as fluorescence. The instrument should be primed, calibrated with beads and cleaned in a proper way.

Specifically for our experiments we collected cells using accutase, washed them with PBS, resuspended them in PBS + 4% FBS and kept them on ice before measurements with a flow cytometer. We used a BD FACSCelesta system with a High-Throughput Sampler (HTS) and lasers with the following wavelengths: 405 nm (violet), 488 nm (blue) and 561 nm (yellow/green). We calibrated the FSC and SSC gates to detect only mouse ES cells (FSC-PMT = 231 V, SSC-PMT = 225 V, GFP-PMT = 476 V; as a control, flowing plain PBS yielded no detected events). We measured the GFP fluorescence using the FIT-C channel. We analysed the flow-cytometry data using FlowJo and custom MATLAB script (MathWorks).

7.3. Time-lapse microscopy

We used a wide-field microscope (Nikon SMZ25) to track the growth of microcolonies as a function of the initial population density (E14Tg2A cell line). Cells were cultured on a 6-cm diameter tissue-culture dishes (Sarstedt, TC Dish 60, Standard) coated with 0.1% gelatin (Sigma, from bovine skin Type B) in water, fed with 5-mL differentiation medium (N2B27) and incubated inside a temperature-, CO_2- and humidity-controlled microscope chamber (Okolab) with steady conditions of 37°C with 5% CO_2. We imaged microcolonies with the following initial population densities (in number of cells / cm^2): 476, 857, 1285, 1714, 2142, 2857, 3571 and 4285 cells per cm^2 dish area. Previously, we kept cells in pluripotency medium on 10-cm diameter dishes and routinely passaged (every 2 days). Importantly, cells were allowed for approximately 6 hours to settle and attach to the gelatinized bottom of the plate before the image acquisition.

The microscope's mono acquisition settings included a 1X microscope objective, 90.0X magnification, 28.5 (arbitrary units) of DIA intensity, 300-ms exposure time and 2.2X analog gain. Before image acquisition we picked a total of 17 fields-of-view that were evenly spread across the entire 6-cm diameter plate with each field-of-view being 1399.16 μm x 994.95 μm. Images were acquired with 1-hour intervals in a total of 96-hour duration (i.e., 4 days of imaging) during which cells were maintained in N2B27 without refreshing and thus disturbing cells. We analyzed the microscope images using custom MATLAB script (MathWorks). We found at most ~10 colonies per field-of-view for the lowest population densities and at most

~50 colonies per field-of-view for the highest population densities. For each population density, we analyzed three separate dishes, each in a different week (three biological replicates).

7.4. Characterization of conditioned media

7.4.1. Medium-transfer experiments

We collected liquid medium of a high-density population (5172 cells / cm^2), centrifuged it at 200 x g for 5 minutes to pellet and eliminate any remaining cells or other debris from the medium, and then transferred the medium to a low-density population (862 cells / cm^2) after first removing the liquid medium of the low-density population. Specifically, we did this medium transfer in two ways. In one scenario (Fig. 3.2 – labelled as "1"), we collected the medium of a high-density population as described above on day X – the X here means X days after we initiated differentiation– and then incubated a low-density population in this medium to initiate its differentiation (i.e., the low-density population was in a self-renewing state before this medium transfer). In the second scenario (Fig. 3.2 – labelled as "2"), we collected the medium of a high-density population as described above on day X, and then incubated in it a low-density population that was differentiating for X days in its own medium. In this method, we measured the population density of the low-density population four days after the medium transfer (i.e., X+4 days) rather than on the same day for all values of X. This ensured that we could fairly compare the different low-density populations (i.e., same number of days (4) spent in the medium of the high-density population).

7.4.2. Medium-filtration experiments

We collected the liquid medium of a high-density population (5172 cells / cm^2) 2 days after we initiated its differentiation, centrifuged the medium at 200 x g for 5 minutes to eliminate any cells and other debris from the medium, and then transferred the medium to a second centrifugal tube for ultrafiltration. The filter unit consisted of two compartments that were physically separated by a regenerated cellulose membrane which separates soluble molecules, depending on their molecular size and shape. Specifically, the membrane has pores that either pass or hold soluble molecules based on their molecular weight (in kDa) during a high-speed centrifugation. We used filter sizes of 3 kDa (Merck, Amicon Ultra-15 Centrifugal Filter Unit, UFC900324), 30 kDa (idem, UFC903024), 50 kDa (idem, UFC905024), 100 kDa (idem, UFC910024) and 300 kDa (Merck, Vivaspin 20 centrifugal concentrator, Z629472). We centrifuged the medium of the high-density population with spin times specified by the manufacturer. After the filtration, the centrifugal tube with the membrane filter contained two supernatants, each in separate compartments: one that contained all molecules that were larger than the filter

size - this portion was much less than 1 mL and stayed on top of the membrane filter - and one that contained all molecules that were smaller than the filter size. We added the supernatant containing larger-than-filter-size molecules to a 10-mL N2B27 with 500 nM of retinoic acid (for Neural Ectoderm differentiation). In this mixed medium, we incubated a low-density population that had been differentiating for 2 days in its own N2B27. The results of this experiment are in the bottom graph of Fig. 5.1.

For a second experiment, we added 500 nM of retinoic acid to the ∼9 mL of the supernatant that contained all the molecules that were smaller than the filter size. We then incubated in it a low-density population that had been differentiating for 2 days in its own N2B27. The results of this experiment are in the top graph of Fig. 5.1. According to the manufacturer, in order to ensure that one captures proteins of a desired molecular weight, one needs to use a filter size that is at least two times smaller than the desired molecular weight. This sets a conservative safety/error margin that we took into account in the conclusions that we drew from the results in Fig. 5.1, as explained in the main text. Finally, the few large molecules (> 3 kDa) that are ingredients of N2B27 were previously shown to have either no effect or a small growth-promoting effect on ES cells (i.e., they do not inhibit ES cell growth) [191].

7.5. RNA-based measurements

7.5.1. Transcriptome analysis with RNA Sequencing (RNA-Seq)

We performed RNA-Seq on 46C populations of three different initial densities which were (in number of cells / cm^2): 862, 1724 and 5172. These populations were undergoing an unguided differentiation (i.e., in N2B27 without any inducers) and we examined their transcriptome 1 day after and 2 days after initiating their differentiations (Fig. 4.1). We also performed RNA-Seq on a pluripotent 46C population, which would show the initial transcriptome of the three differentiating populations (Fig. 4.1 - first column). To perform RNA-Seq, we collected cells from each population and then centrifuged them using a pre-cooled centrifuge. We then extracted RNA from each cell pellet using the PureLink RNA Mini Kit (Ambion, Life Technologies) according to the manufacturer's protocol. We next prepared the cDNA library with the 3 mRNASeq library preparation kit (Quant-Seq, Lexogen) according to the manufacturer's protocol. We then loaded the cDNA library onto an Illumina MiSeq system using the MiSeq Reagent Kit v3 (Illumina). We analyzed the resulting RNA-seq data as previously described in Trapnell et al. [199]. We performed the read alignment with TopHat, read assembly with Cufflinks, and analyses of differential gene expression with Cuffdiff. As a reference genome, we used the genome sequence of *Mus musculus* from UCSC (mm10). We performed enrichment analysis of genes based on their FPKM values (i.e., more than 2-fold

expressed when two initial population densities are compared) by using GO-terms from PANTHER ([200–202]) and a custom MATLAB script (MathWorks). We visualized the results of pre-sorted, YAP1-related genes [177–184] as heat maps which displayed the normalized expression value (row Z-score) for each gene and each condition.

7.5.2. Reverse transcription quantitative real-time PCR (RT-qPCR)

We performed RT-qPCR on 46C populations of two different initial densities which were (in number of cells / cm^2): 862 and 5172. We observed them on each of four days of differentiation in N2B27 that was supplemented with 500 nM of Retinoic Acid (for Neural Ectodermal differentiation). We collected the cells and extracted their RNA with PureLink RNA Mini Kit (Ambion, Life Technologies) according to the manufacturer's protocol. Then, we reverse transcribed RNA into cDNA using iScript Reverse Transcription Supermix for RT-qPCR (Bio-Rad). Next, we performed qPCR in 10-μL reactions with iTaq Universal SYBR Green Supermix (Bio-Rad) and 100 nM of forward and reverse primers. We verified the primer specificity and primer-dimer formation by using the melt curve analysis which showed one peak. See the list of primers that we used in section 7.6.3. We normalized all expression levels for a population by that population's *Gapdh* expression level. We then further normalized the resulting value for a gene by dividing it by that gene's normalized (by *Gapdh*) expression level in one-day-old low-density population. We performed all reaction in triplicates on a QuantStudio 5 Real-Time PCR System (Thermo Fisher).

7.5.3. List of primers used for RT-qPCR

Amotl2_FWD	CAGAGGGACAATGAGCGATTGC
Amotl2_REV	TCACGCTTGGAAGAGGTCCTCA
Bcl2_FWD	TGTGGATGACTGAGTACCTGAAC
Bcl2_REV	GAGAAATCAAACAGAGGTCGCATG
Cyr61_FWD	GGATGAATGGTGCCTTGC
Cyr61_REV	GTCCACATCAGCCCCTTG
Bax_FWD	GGGGCCTTTTTGCTACAGGG
Bax_Rev	AAAGATGGTCACTGTCTGCC
Bbc3_FWD	GTGTGGAGGAGGAGGAGTG
Bbc3_REV	TCGATGCTGCTCTTCTTGTC
Mdm2_FWD	GAAGGAGGAAACGCAGGACA
Mdm2_REV	CCTGGCAGATCACACATGGT
Gapdh_FWD	TGACCTCAACTACATGGTCTACA
Gapdh_REV	CTTCCCATTCTCGGCCTTG
FGF4_Fwd	AAGGCACCTGCCCTGTTCTG
FGF4_Rev	GGGAGCTAGCTGGCTGAAGAAA
FGF5_Fwd	AACTCCATGCAAGTGCCAAAT
FGF5_Rev	CGGACGCATAGGTATTATAGCTG
FGFR1_Fwd	TGGACCGCATTGTGGCCTTGAC
FGFR1_Rev	TCAGCGCCGTTTGAGTCCACTG
FGFR2_Fwd	TGCACGCAGGATGGACCTCTCT
FGFR2_Rev	TGCTCCTCGGGGACACGGTTAA
FGFR3_Fwd	AAGCCAGCCAGCTGCACACA
FGFR3_Rev	TCAAACGGCACGGAGAGGTCCA
FGFR4_Fwd	TAATGAGGGAGTGCTGGCACGC
FGFR4_Rev	AGGGTCGTGGCTGAAAACCGAG

Figure 7.3

7.6. Quantitative biochemistry assays

7.6.1. ELISA for Fibroblast Growth Factor 4 (FGF4)

We measured concentrations of extracellular FGF4 in 10-mL liquid media (N2B27) as follows. We used Mouse FGF4 ELISA Kit (ELISAGenie / Westburg, no. MOES00755) and followed the manufacturer's protocol. The assayed involved measuring the absorbance at 450 nm for various samples as a direct measure of the FGF4 concentration in the sample. We verified the absorbance signals are real and sufficiently high relative to the lower detection-limit of the ELISA kit by constructing a standard curve (Supp. Fig. 5.9). We measured the absorbances on a Synergy HTX Multi-Mode Reader (BioTek). We measured the concentration of extracellular FGF4 relative to that of a highly confluent population of pluripotent cells for comparison. It makes sense to normalize all our ELISA measurements of FGF4 concentration by that of the pluripotent population because the antibodies used in the ELISA kit may not detect 100% of all FGF4s that are secreted (e.g., due to antibodies being designed for specific, recombinant forms of the mouse FGF4). By using three different forms of FGF4 - one from the ELISA kit, FGF4 secreted by the cells in our experiments, and a recombinant form of FGF4 from a different company - we found that indeed the ELISA kit does not detect all forms of mouse FGF4 but that it does detect the form secreted by the cells in our experiments, though less efficiently than it detects the recombinant FGF4 that accompanied the ELISA kit (Supp. Fig. 5.9).

7.6.2. ELISA for phosphorylated YAP1 protein (p-YAP1)

We examined the endogenous levels of phosphorylated YAP1 protein in four different conditions (Fig. 4.3A and Supp. Figs. 4.8 and 5.10). For each measurement, we collected cells in 10-mL tubes, counted the total number of collected cells with the counting method described in "Cell counting" section, and then centrifuged them to form a pellet. We then lysed the cells with a lysis buffer (Cell Signaling Technology, no. 9803) and 1 mM of PMSF (Sigma-Alderich, no. P7626). We incubated the cell lysates with Phospho-YAP (Ser397) rabbit antibody and performed a sandwich-ELISA assay by using PathScan Phospho-YAP (Ser397) Sandwich ELISA Kit (Cell Signaling Technology, no. 57046). We then used a Synergy HTX Multi-Mode Reader (BioTek) to measure each sample's absorbance at 450 nm. The absorbance is a direct measure of the abundance of phosphorylated YAP1. To compare the different absorbances, we constructed a standard curve by serially diluting a lysate of pluripotent cells (Supp. Fig. 4.8). We used the standard curve to report the levels of phosphorylated YAP1 in all differentiating populations.

7.6.3. Real-time apoptosis detection assay for caspase-3

We measured the protein-level activity of Caspase-3 (well-known apoptosis executioner inside cells) in E14 cells that were maintained in a pluripotency medium (serum+LIF) or were differentiating in N2B27 with 500 nM of Retinoic Acid. We examined three differentiating populations: high-density population (6896 cells / cm^2 initially), a low-density population (517 cells / cm^2 initially), and a low-density population that was rescued by the medium of the high-density population after two days of differentiating. We collected the cells of each of these populations and then performed a membrane-permeable DNA-dye-based assay that measures the amounts of active Caspase 3/7 in intact, alive cells (NucView 488 Caspase-3 Assay Kit for Live Cells). We followed all steps according to the manufacturer's protocol. We used a flow cytometer to measure the amounts of active Caspase-3 in single cells. We normalized the Caspase-3 level per cell by the average Caspase-3 level of an ES cell (i.e., mean level per cell of the pluripotent population.) Results of these experiments are in Fig. 4.4 and Supp. Fig. 4.10.

7.7. Small-molecule experiments

7.7.1. Inhibiting FGF receptors (FGFR) with PD173074

We examined the fold changes in population densities after several days of inhibiting FGF receptors (FGFRs) with a small-molecule inhibitor, PD173074 (PD17, Tocris, no. 3044) (previous studies characterized this inhibitor: see [133, 192]). We used 46C cells differentiating into the NE lineage. We examined the following initial population densities (in number of cells / cm^2): 172, 431, 862, 1931, 5172, 8620 and 15517. To inhibit the FGFRs, we added 2 μL of 10-mM PD173074 (PD17) to a 10-mL N2B27 medium. We dissolved the stock of PD17 in DMSO to a final concentration of 2 μM (1056 ng/mL). After 6 days, we measured each population's density and differentiation efficiency. As a control, we examined the effect of adding 2 μL of DMSO to cell-culture medium without any PD17. This ensured that our results were not due to any side effects of having DMSO that was carried over with the PD17 that we added to each medium. Results of these experiments are in Fig. 5.2.

7.7.2. Inhibiting YAP1 function with Verteporfin

We examined the fold changes in population densities after several days of incubation verteporfin (R&D Systems, no. 5305), which prevents active YAP1 from entering the nucleus to control expression of its myriad target genes. We used 46C cells that were differentiating into the Neural Ectoderm lineage. We supplemented the N2B27 with 1 μM of verteporfin that was dissolved in DMSO (based on LeBlanc et al., [177]). After 6 days, we measured each population's density and differentiation efficiency. As a control, we examined the effect of adding only DMSO to cell-

culture medium without any verteporfin. This ensured that our results were not due to any side effects of having DMSO that was carried over with the verteporfin that we added to each medium. Results of these experiments are in Fig. 4.2.

7.7.3. Growth kinetics with recombinant proteins

We examined whether we could rescue a low-density population from extinction by adding one or a combination of 11 different autocrine-signaling molecules (all recombinant versions from mouse/human). We considered 46C cells in a low-density population (862 cells / cm^2 initially) After 2 days of culturing in N2B27, we added one or combinations of the following recombinant proteins to the medium: 200 ng/mL of recombinant mouse FGF4 (RD Systems, no. 7486-F4), 200 ng/mL of recombinant human FGF5 (RD Systems, no. 237-F5), 100 ng/mL of recombinant mouse PDGFA (Novus, no. NBP1-43148), 100 ng/mL of recombinant mouse VEGFB 186 (Novus, no. 767-VE), 100 ng/mL of recombinant mouse VEGFA (Novus, no. 493-MV), 500 ng/mL of recombinant human CYR61/CCN1 (Novus, no. 4055-CR), 500 ng/mL of recombinant human CTGF/CCN2 (Novus, no. 9190-CC), 200 ng/mL of recombinant mouse CLU (Novus, no. 2747-HS), 500 ng/mL of recombinant human HSPA8/HSC70 (Novus, no. NBP1-30278), 1000 ng/mL of recombinant human PPIA (Novus, no. NBC1-18425), or 2000 ng/mL of mouse recombinant SCF (STEMCELL, no. 78064). After incubating in a medium containing one or a combination of these molecules for four days, we collected the cells for counting and flow cytometry to determine whether the population survived or not and its differentiation efficiency. Results of these experiments are in Supp. Fig. 5.16.

7.8. Procedure for seeding a macroscopic colony

Our standard cell-seeding method involves spreading a desired number of cells across the gelatin-coated surface of a centimeters-sized dish. Unlike this method, we clustered a relatively low number of cells (~5000 46C cells per mL of N2B27) by injecting a few-microliter droplet of N2B27 containing the amount of cells at the center of a 10-cm or 6-cm diameter dish that was coated with 0.1% gelatin and contained the same volume of N2B27 as in the case of the standard cell-seeding method (e.g., 10-mL for 10-cm diameter dish and 4-mL for 6-cm diameter dish). The cells that were initially confined by a droplet were then allowed to sediment and attach to the gelatinized dish bottom, which resulted in a ~mm^2 area occupied by microcolonies. We observed localized, individual microcolonies that were not touching each other within a small area (~28 mm^2) with a brightfield microscope ~24 hours after clustering of cells (Fig. 8.6B) as opposed to sparsely spread microcolonies (each ~400 μm^2) when applying the standard seeding method (Fig. 8.6A).

8

Epilogue: A look ahead with reflections and new studies

8.1. Reflections

We sought to quantitatively understand how living cells navigate themselves in their habitat by communicating with each other. Embryonic Stem (ES) cells are an *ex vivo* model system derived from preimplantation mouse embryos and known to depend on myriad communication signals, many of which the cells themselves produce. As a case study, we systematically explored how ES cells may cooperate with each other in a synthetic habitat - i.e., typically grown at clonal densities (monolayer) and exposed to a bulk liquid culture through which molecules freely diffuse - across relevant length-scales and time-scales.

In this final chapter we reflect on our findings and present key lessons learned from integrating quantitative experiments and modelling to address the seemingly simple question, "*Who is talking to whom?*", for cells in a large population. We put these lessons into perspective and further discuss other "community effects" (originally coined by Nobel laureate John Gurdon) and design principles of cell death and differentiation. Lastly, we also discuss new studies as possible directions for future research.

8.1.1. Key lessons learned

Addressing how communication signals spatiotemporally control collective behaviours of cells often remains challenging. Conventional methods – for example, transferring of conditioned media or microfluidic approaches – destroy the necessary, spatial information such as how far each signaling factor travels when undisturbed. A quantitative, comprehensive picture may reveal how to better intercept and improve the lines of communication between cells for *ex vivo* engineering (e.g., designing synthetic cells) or therapeutic purposes (e.g., regenerative medicine). Communicative cells - as we show for ES cells - may require to cooperate beyond the confines of their local environment. To put it broadly, a technical and conceptual challenge is to determine a cell's degree of autonomy for making decisions and performing biological functions.

Our approach lead to novel insights despite its simplicity. We systematically examined an emergent behaviour at the cell-population level (**Chapter 2**) and then progressively focused on the underlying mechanisms at the level of cell colonies (**Chapter 3**), the intra-cellular factors (**Chapter 4**) and the extra-cellular (signalling) factor (**Chapter 5**). We built simple quantitative models (including those in **Chapter 6**) along the way to make new predictions and recapitulate key experimental findings.

Having more communicative ES cells on a dish (which sense and secrete myriad growth factors including Fibroblast Growth Factor 4 (FGF4)) could mean a "better" growth. But our quantitative approach revealed a phenomenon that is qualitatively

different from this view. It is not that having more cells simply means increased or faster growth but that, as we uncovered here, the entire population either becomes extinct or survives and expands to the carrying capacity based on the initial population density: a population-level fate is decided in a switch-like manner (a less than a two-fold difference in the initial number of cells that are scattered across multiple centimeters). The conventional view (e.g., based on autonomous cell growth or collective cell growth without a threshold) would potentially allow for even a lowest starting population density to expand towards the carrying capacity, albeit more slowly than a high-density population).

Even when one knows that secreted growth factors can accumulate at higher cell densities, there is an ambiguity:

1. Does a cell survive because there are sufficiently many cells **nearby** that are all helping each other by secreting growth factors (as can be the case in a high density population in which the distances between cells may be small and only local communication exists)?

2. Or does a cell survive because distant cells that are **centimeters away** help one another grow and survive (as can be the case in high density population in which a global communication exists but insufficient local communication exists due to a fast, far-away diffusing molecule that does not linger locally)?

Ambiguity arises here because both scenarios can result in the same abundance of growth factors in the pooled medium. In developing an approach to address this ambiguity, we discovered that when mouse ES cells begin to differentiate, they also begin to cooperate on a macroscopic scale to help each other survive the differentiation process.

We found that an insufficient cooperation drives a population to extinction and that the "amount" of cooperation is proxied by the population density that is measured over a centimeter-scale. A nonlocal communication, tunable up to many millimeters, mediates the large-scale cooperation and involves multiple secreted molecules – a crucial one of which is FGF4 – that dephosphorylate and thus activate the transcriptional regulator YAP1 which in turn activates anti-apoptotic genes such as *Bcl2*. The same long-range communication then connects initially scattered cells to form a global community that spans the entire cell-culture plate. Hence, differentiating ES cells form one macroscopic entity that either lives or dies as one body during pluripotency exit and whose constituents (cells) are distributed across many centimeters yet whose livelihoods depend on one another.

We found that this phenomenon occurs in the first 2-3 days after removing Leukemia Inhibitory Factor (LIF) (i.e., during pluripotency loss and before adding any inducers such as Retinoic Acid), meaning that the phenomenon that we observed is not

for pluripotency but for pluripotency loss - which is relevant for differentiation into any lineage - rather than for differentiation into a specific lineage (e.g., Neural Ectoderm). In light of the early time window for which the survival-vs-extinction fate is determined upon LIF withdrawal and the time it takes for secreted factors to globally accumulate, it is sensible why the *initial*, rather than *instantaneous*, population density matters most.

Cooperative behaviours allow artificial environments of microscopic cells, such as those of *ex vivo* culture models like ES cells, to be habitable and may span vast length-scales (centimeters). We learned that cooperative interactions between ES cells in their habitat tunably and globally dictate the cells' survival-vs-extinction fate during differentiation (not during pluripotency). Why death seems to take such prominent role in differentiation, what advantageous long-range communication brings to cells and how another "knob" besides population density and liquid medium (volume of habitat) tunes ES cells' lives, are subjects for discussion in the following sections.

8.1.2. Extension of community effects

Over six decades ago the work of a then-aspiring[1] developmental biologist captured the attention of the scientific community as his experiments changed the conventional notion of development being a script set in stone. In 2012, John Gurdon was awarded the Nobel Prize in Physiology or Medicine together with Shinya Yamanaka for the discovery that "mature cells can be reprogrammed to become pluripotent" (i.e., the possibility of converting any somatic cell (say, a skin cell) into a completely different somatic cell (a heart cell) by first transforming it into a pluripotent cell). Gurdon's approach took the somatic cell nucleus of *Xenopus laevis* (i.e., a frog) and injected this into an unfertilized frog egg which then developed into an adult frog [203–205]. This cut-and-paste technique also allowed Gurdon to change cells' course of differentiation – for example, from epidermis to mesoderm – and in doing so, he made yet another remarkable discovery. All cells adopted a redirected fate only if they were in a community of sufficiently many (hundreds) of them. Gurdon coined the term "community effect" to describe, in his own words, that "it therefore appears that cells pass through a phase in their adolescence when they require proximity to, and perhaps signals from, like neighbours to proceed to their normal differentiation fate" [45, 46].

Community effect: A conventional view

This community effect differs from cells simply influencing each other's behaviours as it involves large numbers of cells cooperating by emitting a so-called "commu-

[1] John Gurdon's former schoolmaster once stated, "I believe he has ideas about becoming a scientist, on his present showing this is quite ridiculous"

nity signal" (either a diffusible one that is secreted and sensed in the environment, or one that is mediated through direct contact between cells). In an attempt to identify potential community factors, Gurdon and colleagues reported that FGF signalling is essential and eFGF protein is expressed in the *Xenopus* muscle progenitor cells at the right time to mediate a community effect during myogenesis [206]. Gurdon reasoned and predicted that if it were a diffusible community factor, then its concentration would be greater when many secreting cells are closer together than when only one or a few are present [46]. Therefore a community effect may arise if the cell density exceeds a certain threshold while the cells themselves require sensing concentrations of the community factor that exceed a certain threshold to generate a collective response.

The identity and spatiotemporal effects of such community factors – and thus, how exactly the community effect works – largely remains enigmatic. Nevertheless, researchers frequently reported on the apparent dependence of preimplantation embryos (blastocysts) on survival-promoting factors released by the embryos themselves. Paria & Dey discovered a cooperative interaction among *in vitro* mouse blastocysts that are co-cultured in single droplets and that release specific growth factors – such as TGF-β1, TGF-α and PDGF-A – to stimulate each other's growth and subsequent development [207]. The researchers noticed weakened interactions when a same number of blastocysts was cultured in larger volumes of droplets indicating that these factors must be secreted and diffusing within the droplets.

Others reported on a similar phenomenon: both the density of co-cultured embryos as well as the incubation volume determine the embryo's *in vitro* development and viability [208–215]. Predicting the viability and development of embryonic cells and manipulating the culture habitat and "cross-talk" of embryos remain subjects of great interest and importance [170, 216–221] which led to the discovery of simple, defined media for *ex vivo* culturing of ES cells without the need of feeder cells or serum [126].

Our work shows that some colonies can still survive in the low-density populations that approach extinction, but the probability of a colony surviving is low (Fig. 2.6A - bottom: ∼5% of cells remain alive after six days of differentiation). It may be possible that some cells are further along the differentiation process (e.g., towards NE lineage) than other cells in the population. Perhaps these faster differentiators are the ones that survive in these extinction-bound populations. Indeed, we found that the nonlocal communication is only necessary in the early days (first 2-3 days) of differentiation. Hence, it is plausible that cells that enter NE or ME lineage faster than others survive the extinction fate (i.e., reason that the population size does not become exactly zero after six days). Future work may verify this hypothesis.

Global community effect: An extended view

We can cast our observations as an extension of Gurdon's community effect (Fig. 8.1). Since Gurdon's discovery, most studies of community effects have focused on aggregates or colonies differentiating by locally cooperating with each other as recently demonstrated, for example, in mouse T-cells that locally interact with each other in microwells by secreting and sensing the cytokines, IL-2 and IL-6, inducing differentiation into memory T-cells [47]. Our work extends this classic framework for cooperative differentiation by showing that ES cells exhibit a "global community effect", in which isolated single cells cooperate across macroscopic distances to determine their fate - dying or living and differentiating - through a long-range communication.

The global community effect for ES cells is reminiscent of quorum sensing [48]. Indeed, autocrine signaling with negligible self-communication - meaning that each cell captures very few copies of its own secreted molecule - can lead to quorum sensing in some contexts [19, 20, 22, 164]. Despite the fact that we know of many autocrine-signaling molecules that promote growth of ES cells, including FGF4 [158, 165–168], it has generally remained unclear to what degree a cell stimulates its own growth (self-communication) versus being stimulated by the other cells (neighbor-communication) and, if neighbor-communication occurs, then which pairs of cells stimulate one another (either nearby or distant cells) and by how much (and how far apart two cells can be to stimulate one another through the autocrine growth factors).

In other words, every cell can be secreting the same autocrine-signaling molecule that promotes the growth a cell that senses it, but that does not necessarily mean that every cell is helping each other grow. For example, EGF receptors have such a high binding affinity for EGF that an EGF-secreting cell can capture most of its own copies of secreted EGF [222], which would result in negligible or highly reduced neighbor-communication [19, 20, 22, 164].

Resolving the issues mentioned above regarding self- versus neighbor-communication requires systematically and quantitatively decoupling communication at different length-scales, which we have done here. Consequently, we found that a long-range communication (neighbor-communication) occurs for differentiating ES cells through at least two secreted-and-sensed molecules, a crucial one of which is FGF4. Interestingly, researchers recently showed that cells in the inner cell mass collectively control the relative abundances of the three cell types that form in a mouse blastocyst, by communicating through FGF4 at length scales of up to ~100 microns [158].

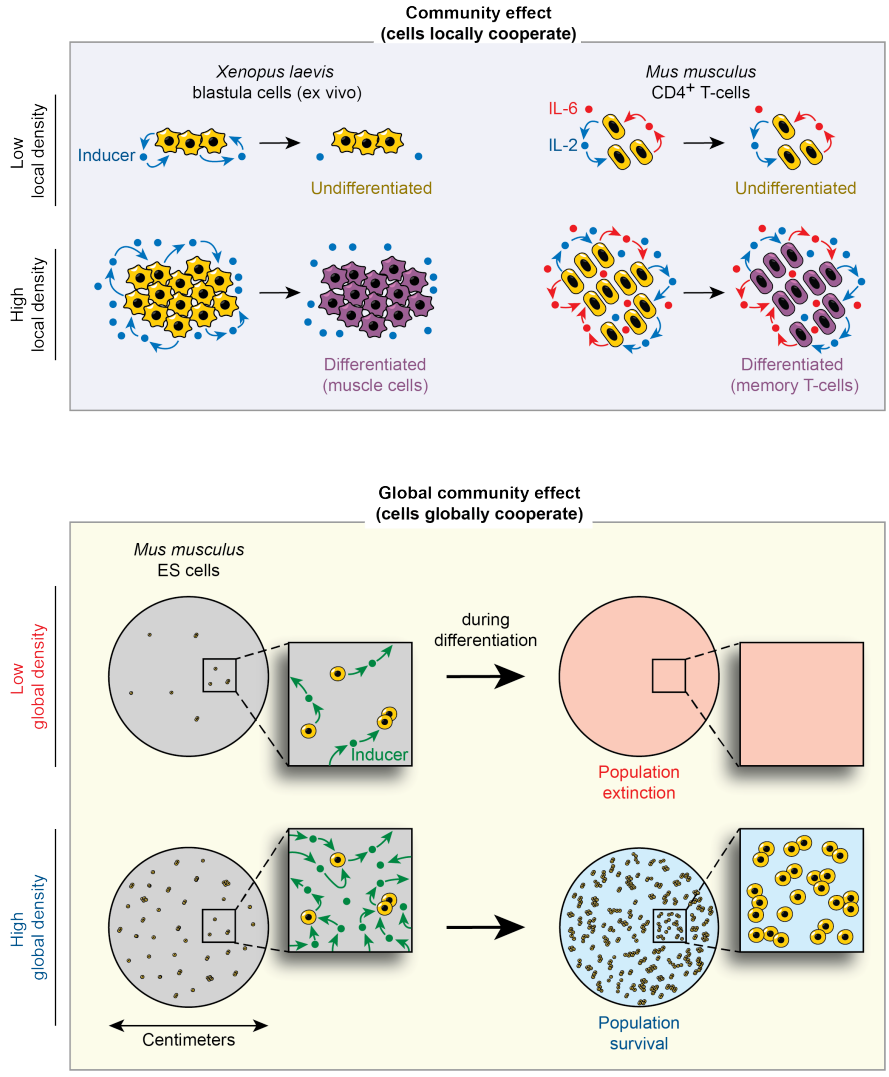

Figure 8.1: Global community effect. Upper panel: conventional community effect, as originally described by John Gurdon in frog embryonic cells [45, 46] (left column) and recently also discovered for microwells of mouse T-cells that cooperatively differentiate into memory T-cells through local cooperation (within microwell) [47] (right column). In both examples, upper row shows differentiation failing to occur when the local population density (# of cells in a microwell or cell aggregate) is too low while bottom row shows differentiation occurring when the local density is sufficiently high (due to local cell-cell cooperation, mediated by secreting and sensing autocrine inducer). Lower panel: summarizes our work. Upper row shows differentiation failing (population becoming extinct) when the global density (# of cells measured over a macroscopic scale (over several centimeters)) is below a threshold value while the bottom row shows a successful differentiation occurring when the global density is higher than the threshold value (due to global cell-cell cooperation, mediated by secreting and sensing a long-range, autocrine inducer (green circle)).

Applications of community effects

Cell cultures, despite their limitations of not faithfully capturing numerous *in vivo* processes, are still important testbeds in synthetic biology for revealing principles of cell-cell communication and for engineering synthetic, multicellular systems. While ES cells are derived from the inner cell mass and the global community effect occurs just after removing LIF, one must be careful in translating any results from ES cell cultures to *in vivo* embryos because *ex vivo* growth conditions clearly differ from the *in vivo* conditions (i.e., inside the blastocyst). But our discovery of the long-range communication still reveals an important design principle that is relevant for tightly packed, differentiating ES cells inside *ex vivo* colonies or an *in vivo* blastocyst. Namely, the extremely long-distance nature of autocrine-signaling molecules (such as FGF4) tells us the following scenario.

Suppose that a cell must detect some minimum concentration of a molecule to live and that its nearby cell must supply this molecule by secretion. If the molecule has a long diffusion length, then the nearby cell would need to secrete it at a higher rate than if the molecule had a shorter diffusion length because the more diffusive molecule spreads out more and thus concentrates less in a region than the less diffusive molecule. Alternatively, there would need to be more of the molecule-secreting cells surrounding the molecule-receiving cell (receiver) in order to elicit the receiver's response - to create more than the threshold concentration required for response - which creates an ideal setting for engineering or naturally developing a switch-like response to a local population density (i.e., create locally collective behaviors). Trade-offs seen in these two examples, derived from studying macroscopic distances, are important to consider to better understand design principles of local communication among cells in compact aggregates. In addition to revealing such design principles, we expect that using our approach to study cell-cell communication in cell cultures will aid in rigorously investigating how communication among cells - over distances not yet specified - may influence the success rate of reprogramming adult cells into induced Pluripotent Stem Cells (iPSCs) on a plate, which has been hypothesized but difficult to rigorously evaluate [169].

Given that ES cells are important, *ex vivo* tools for synthetic biology, it would be useful to examine whether global community effects also exist among *ex-vivo*, multicellular structures on plates such as synthetic blastocysts [155, 223–226]. Indeed, there are long-standing hints, but not yet quantitative proofs, of community effects occurring among *ex vivo* structures - these structures may be sharing their secreted mitogens to help each other develop [227, 228]. This, combined with our study, suggests that one may find global community effects among *ex vivo* multicellular structures, in which large numbers of multicellular structures communicate amongst them on a plate. Using our type of systematic approach, one may uncover such global community effects which may involve both secreted molecules

[21, 47, 58, 64, 67, 138, 229] and cell-cell contact-mediated communication [147, 230–232]. The latter did not enter our analysis as we sparsely seeded near-single cells. If there are global community effects among synthetic multicellular structures, then one may engineer cooperative decision-making circuits by dynamically (temporally) tuning the secretion and sensing of autocrine-signaling molecules and controlling cells' temporally changing response to the molecules.

Our work shows that manipulating the macroscopic environment - changing the liquid medium as in our study and, equivalently, changing the macroscopic shape of the cellular habitat - which may be more accessible than genetic manipulations, can tune the global community effects. Such environmental manipulations may be promising yet underexplored routes for building *ex vivo* synthetic structures [161, 233]. Moreover, by revealing a large-scale cooperation during differentiation, our work provides a basis for and shows that it would be possible to tune long-range communication and cooperation [234] to build a completely synthetic, macroscopic structure - one without an *in vivo* analogue - that consists of spatially disconnected cells spanning many centimeters and coherently functioning as a single entity. Such structures, together with our systematic approach for determining spatial range of cell-cell communication, may provide new testing grounds in synthetic biology for quantitatively understanding how microscopic cells can bridge vast length-scales to perform a coherent, biological function as well as help in elucidating physical principles that underlie multicellular systems [127, 150, 233, 235–239].

What advantageous may a community effect bring to cells from mammalian embryos?

A community effect may make sense in light of the seeming autonomy of preimplantation embryos from external signals required for growth and subsequent development. A possible explanation is the cells' need to combat stochasticity in gene expression and to perhaps create homogeneity in a heterogeneous cell population or to mark out various communities of alike cells (such as a mesoderm, ectoderm and endoderm in a developing embryo). This would enable the successive developmental stages directly following the fertilization of the egg by the sperm.

Another explanation links apoptosis to differentiation for functional and evolutionary reasons which is the topic of the next section.

8.1.3. Design principles of death and differentiation

In 1959, Conrad Waddington – one of the first systems biologists – spoke of a "Constancy of the Wild Type" [240, 241] when referring to the developmental process and its remarkable ability to buffer most of the environmental and genetic disturbances to make development appear as the execution of a script or that static picture in all high-school biology books. At the same time, why directed differen-

tiation of ES cells in a dish is often difficult to control and therefore unpredictable (such as variable plating and differentiation efficiencies) remains poorly understood. If development is about cells making decisions on proliferating and differentiating in the right place at the right time, then what if cells make mistakes? Or what if they don't keep up with their neighbours? Could cell death perhaps create order in development?

It turns out that death and differentiation are tightly linked. Programmed cell death, or apoptosis, has an essential role in many abnormalities in development and human diseases, and oftentimes the tuning of apoptosis is the cause and the cure of the resulting pathology [148, 242, 243]. Excessive apoptosis is involved in many diseases such as neurodegenerative disorders (Alzheimer's and Parkinson's), stroke and AIDS whereas insufficient apoptosis often leads to cancer and autoimmunity. The formation of the preamniotic cavity – which is the inner part of a 4-day-old preimplantation embryo where ES cells are derived from – is the result of an interplay between contact-dependent survival signals and short-range death signals from the outer (endoderm) to the inner (ectoderm) layer that ultimately carve out a "hole" for the developing fetus [244].

The molecular machinery that regulates apoptosis inside cells is evolutionarily conserved among diverse species such as the fruit fly (*D. melanogaster*), the nematode (*C. elegans*) and the mouse (*M. musculus*) and therefore it is thought that the function of apoptosis is to remove excess, misplaced or damaged cells with high precision and efficiency and to provide cells with a repair and quality-control mechanism [112, 113, 148, 242, 243, 245]. In simple terms, development first produces cells in high numbers and then uses apoptosis to sculpt form, function and quality into the excess of cells to realize organ function [245]. Apoptosis and survival are controlled by major intracellular signalling pathways, such as PI3K/AKT, MAPK/ERK and JAK/STAT [111, 246], and myriad (secreted) signalling factors such as FGFs, VEGFs and interleukins that also stimulate the formation of colonies [112, 113, 247].

Specifically, caspases are known to play a major role in differentiation [248]. This is remarkable because caspase activation often occurs together with p53 activation, release of cytochrome c from mitochondria, cytoskeletal degradation, and DNA fragmentation occur during apoptosis [249] – and yet it seems to have a dual role in development [151, 248, 250]. Caspases are a conserved family of proteases found in many multicellular and unicellular eukaryotes and even some prokaryotes, and they are thought to have assumed a suicidal function for the cell after it already had a major role in cellular differentiation, hinting that apoptosis may be the extreme result of "hyperactive differentiation" [248, 250]. Initially synthesized as inactive procaspases, caspases are activated by cells that commit suicide either by sensing stress in their environment (intrinsic pathway – through release

of cytochrome c from mitochondria) or from signals (extrinsic pathway – either apoptosis-preventing or apoptosis-promoting signals, such as Fas ligands binding to Fas receptors) both of which lead to the activation of a group of initiator caspases (caspases 8 and 9 for the extrinsic and intrinsic pathways, respectively), followed by the activation of executioner caspases (caspases 3, 6 and 7), before cells enter an irreversible series of events leading to their death [249, 251]. Importantly, the major death executioner, caspase 3, was found to cleave the pluripotency factor NANOG to help cells exiting pluripotency during differentiation [252], and its cleavage precedes and coincides with neuronal commitment [253]. Moreover, the formation of the apoptosome, which recruits and activates procaspases, is delayed in differentiating cells compared to apoptotic cells, possibly explaining how differentiating cells ultimately avoid death despite high caspase activity [251, 254].

The apparent expression of death factors during differentiation comes at a cost for ES cells and soon after withdrawal of Leukemia Inhibitory Factor (LIF) it results in a cell-culture phenomenon colloquially known as "apoptotic crisis". In the presence of LIF, activation of STAT3, ERK1/2 and JNK1 stimulate survival, but upon LIF's withdrawal ES cells loose the expression of major anti-apoptotic genes (such as *Bcl2*) only to be restored again during 3-4 days while the expression of major pro-apoptotic genes (such as *Bax1* and *Bcl2l1*) are highly and invariably expressed [255, 256]. The imbalance between pro- and anti-apoptotic genes, with pro-apoptotic genes being highly over-expressed, can cause cells to release cytochrome c and it is thought that a threshold level of these apoptotic signals might commit some cells towards irreversible apoptosis [256, 257].

Researchers have observed that a balance in the expression of SOCS proteins (notably, SOCS1 and SOCS3) and p38 activation are crucial for survival [253, 255–257], and that BCL2 itself (a transcriptional target of p38) is critical for neuronal commitment [258]. On how cells avoid "hyperactivation" of the apoptotic cascade during differentiation, it was recently shown that YAP1 prevents excess cell deaths by strongly activating anti-apoptotic genes [177]. While apoptosis irreversibly culls cells that may fail to differentiate [259], ES cells can also enter a state of dormancy during which they show no appreciable apoptosis nor deviations in their cell cycle distribution or pluripotency state [153]. Upon (re-)activation of mTOR or depletion of the apoptotic/oncogene c-MYC [122], dormant ES cells can resume proliferation and differentiation which is reminiscent of embryonic diapause where a blastocyst delays its own implantation in the uterus due to unfavourable environmental or metabolic conditions [152].

During development, cells must irreversibly commit to fates in the right place at the right time, and for this, they rely on spatiotemporal signals from their environment [112, 113, 149]. Diffusible signals – such as FGF4 promoting survival or Retinoic Acid inducing Neural Ectoderm (NE) differentiation – are either transient

or non-transient depending on their concentration, diffusivity and exposure time to cells. A fundamental question is how cells make firm decisions about their fates based on real, non-transient signals (Fig. 8.2 - top). We hypothesize that collective decision-making through long-range communication and quorum-sensing (similar to the phenomenon we discovered here) might be a useful strategy for ES cells to achieve this goal (Fig. 8.2 - bottom). It is the balance between variably expressed survival factors (in turn controlling anti-apoptotic genes) and invariably expressed death factors (pro-apoptotic genes) that determines whether an ES cell survives or dies. We might expect various possible scenarios based on the underlying mechanism. For one, each cell autonomously decides whether it survives or dies as none of the survival factors are secreted and therefore the outcome – a cell surviving or not – solely depends on the intracellular balance between survival and death factors (Fig. 8.2B – Scenario 1). A cell may also secrete its survival factors and in turn sense these factors with its own cognate receptors (self-communication), or at most share these factors with its local neighbours to achieve a short-range communication, but the outcome – a cell surviving or not – would mostly depend on its variable, local levels of survival factors (Fig. 8.2 – Scenario 2). Lastly, cells that collectively amass their secreted survival factors with most or all neighbours and then let the outcome – surviving or not – depend on a threshold level of survival factors, allows them to coordinate their response and to respond to real, non-transient signals most cells have also seen (Fig. 8.2 – Scenario 3).

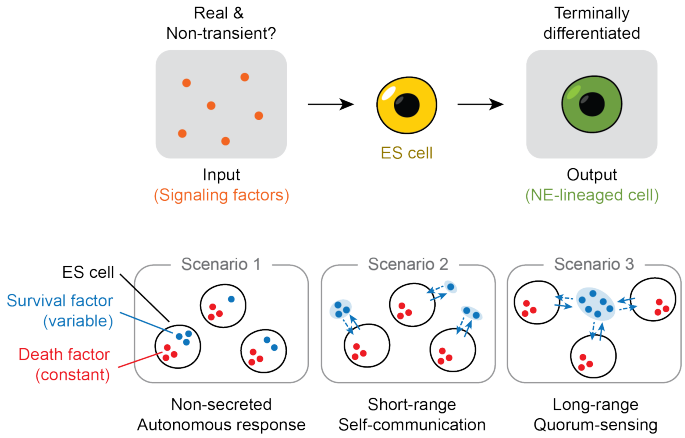

Figure 8.2: Long-range communication and quorum-sensing may be useful strategies for ES cells when committing to a fate. (Top) An ES cell must irreversibly commit to a fate (e.g., Neural Ectoderm (NE) lineage) based on real, non-transient signals next to other, transient signals in its environment. (Bottom) Scenario 1: a cell surviving or not depends on the balance between non-secreted, variably expressed survival factors and invariably expressed death factors (i.e., cell-autonomous survival response). Scenario 2: a cell secretes its survival factors but its survival mostly depends on its (local) levels of survival factors which it senses. Scenario 3: All cells collectively amass secreted survival factors and then respond to a threshold level of factors which allows for a collective strategy for survival based on real, non-transient signals.

8.2. Directions for future research

8.2.1. Scale of communities of interacting cells

We found that differentiating ES cells use long-range communication via diffusible factors (including FGF4) to determine collective survival at a near-centimeter scale. This raises a general question of how large a system, or a community, of interacting cells can be for its parts (the cells) to show a coordinated behavior and before interactions across space and time are no longer possible. What may set the size of a community of interacting cells are the functional and ultimately evolutionary advantages a smaller or larger community does not (yet) benefit from such as growth control, specialisation, organ size determination, pattern formation and robustness against genetic and environmental perturbation [260]. Why a biological system shows a *particular* "design", in general, remains a fundamental and often open question – in part because any biological system is continuously subject to the laws of evolution. Nevertheless, how a biological system benefits from its current "design" to achieve a desired goal is addressable with quantitative experiments and modelling. Communal systems of cells are ubiquitous in prokaryotes (such as bacteria) and eukaryotes (such as mammalian cells).

Bacteria are known to live in communities and the formation of these communities is often fuelled by competition for space, food and thus survival [261, 262]. Bacterial communities have evolved to range in scale (from individual cells to multicellular aggregates and colonies with billions-to-trillions of cells) and complexity (from multiple interacting subspecies within one community to multiple interacting communities). In this way, bacteria may coordinate their gene expression by responding to a minimal threshold concentration of a secreted, diffusible factor (auto-inducer) which in turn is a proxy for the population density; this phenomenon is known as quorum sensing [48].

As an example of positive interaction, the marine bacterium, *V. fischeri*, colonizes the light organ of the Hawaiian bobtail squid, *E. scolopes*, to provide the squid with a source of light (by producing luminescence at high-enough population densities) for camouflage at night, and in return, the squid provides space and food for the bacteria to survive and grow to high population densities, enabling the existence of a symbiotic bacterial community spanning many hundreds of microns in size (up to ~1 mm) [263]. Communities of negatively interacting bacteria can also change their environment at high population densities in detrimental ways – by depleting resources or producing toxic factors – leading to suicide and thus extinction of the whole community [264].

Signalling in bacterial communities often shows diverse spatiotemporal features. As an example, *B. subtilis* actively pumps potassium ions across its cell membrane to induce synchronized oscillations in membrane potential, and thus, allowing for

a long-range, electrical signalling in biofilm communities, with typical propagation distances of ∼1 mm in ∼20 minutes [9, 10]. Short-range signalling, on the other hand, can also be used to maintain and limit the coupling between different communal species, as in the case of synthetic communities of *E. coli*, which were found to exchange self-produced metabolites only with their local neighbours (up to ∼10 microns away) that also contribute to the production while excluding non-local, possibly non-producing ("cheating") neighbours [52].

Mammalian cellular communities often show myriad complex interactions that involve multiple length-scales and time-scales [1]. Immune cells can locally interact with their immediate neighbours, to create a local concentration of secreted factors such as IL-2 as in the case of mouse CD4+ memory T-cells [47], to control their proliferation and differentiation through short-range communication.

In another example, researchers examined the beginnings of tumor formation after mutations and damages to certain sites in DNA of healthy cells [54]. They showed that turning on oncogenes in individual or a few isolated cells in the mammary acini (part of the mammary gland in the mouse breast) do not result in cells dividing uncontrollably and thus forming tumors. This is because surrounding, healthy tissue produces inhibitory signals, and therefore only a sufficiently large community of oncogene-driven cells begin to communicate at such amplitude which is sufficient to overcome these inhibitory signals, leading to the formation of tumors. The mechanism of healthy tissue inhibiting tumor formation only in smaller communities of oncogene-driven cells remains unclear.

Community-level behaviour also occurs at the organ level through long-range communication (the order of ∼1 mm) as in the case of regeneration of plucked hair only occurring if the density of plucked hair follicles exceeds a certain threshold [67]. Researchers showed that this mechanism likely allows the skin to disregard milder injuries while being fully involved in meeting more severe injuries with the required (involved) activation of stem cells.

In our experiments, we examined a coordinated behaviour of a community of ES cells – the survival-vs-extinction fate during differentiation – which spans the entire centimeters-sized dish (10-cm diameter in Chapter 2, and also 6-cm diameter in Chapter 3) and involves long-range communication with secreted factors such as FGF4 that diffuse over at least several millimetres. We found that initial population density and volume of culture medium together dictate the switch-like behaviour of the community.

Building upon our findings, we suggest future studies to further examine the community behaviour as a function of the dimensions of the dish, which in turn sets the population density and the height of the culture medium on top of the monolayer cell population, to address what community size and culture conditions make

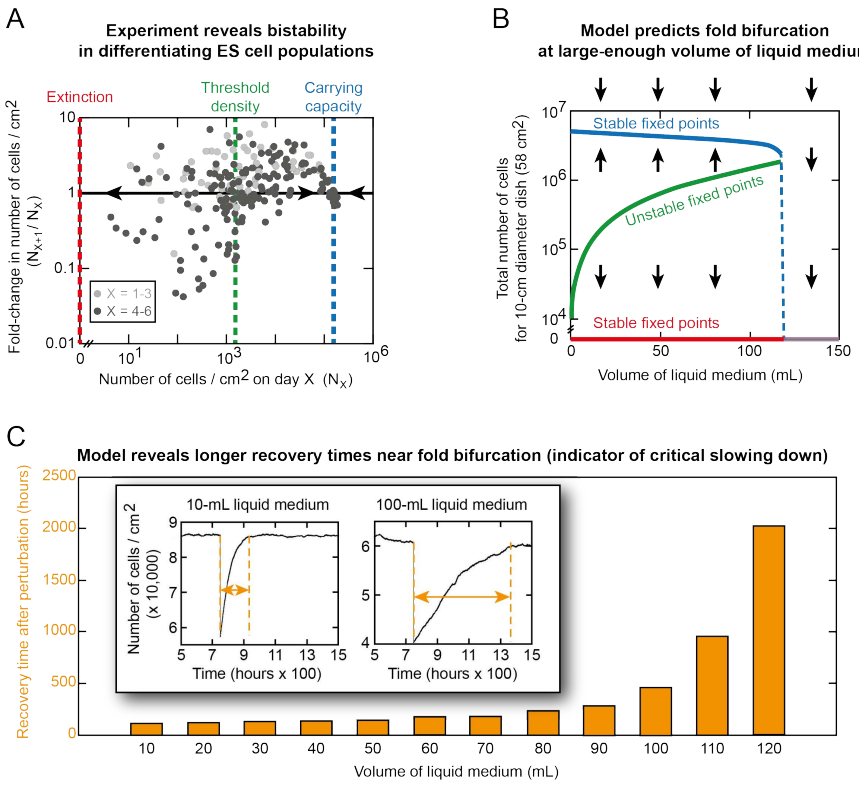

Figure 8.3: Model predicts slower recovery from small perturbations in populations of differentiating ES cells incubated in larger volumes of liquid medium (signature of critical slowing down). **(A)** Experimental results. Dots represent individual populations that started at different initial densities during a 6-day Neural Ectoderm (NE)-induced differentiation (same data as described in Chapter 2). Light grey dots are populations between days 1-3 and dark grey dots are populations between days 4-6. Plotted is each population's density on day X (horizontal axis) versus the fold-change in density with respect to that on the following day (vertical axis). Populations (dots) that are above fold-change = 1 grew on the next day whereas those below fold-change = 1 shrank. Green dashed line indicates threshold (an unstable fixed point) of initial population density (~1700 cells / cm^2 on day 0) above which populations generally expand to the carrying capacity (indicated with blue dashed line; as a stable fixed point) and below which populations generally become extinct (indicated with red dashed line; as a stable fixed point). **(B)** Stochastic model. See details of model in Chapter 6. Same result as shown in Fig. 6.4D. Now, we ran simulations beyond ~10-mm in height of liquid medium (corresponds to ~58-mL in volume). We observed that the unstable fixed points (green curve; similar to phase boundary shown in Fig. 6.4D) meet the stable fixed points representing the carrying capacity (blue curve). As a result, any alive population starting differentiation with more than ~120-mL of liquid medium (~21-mm in height of liquid medium) always "collapses" and thus becomes extinct. Arrows indicate how populations expand/shrink over time. Note that ~100-mL volume of liquid medium corresponds to ~17-mm in height of the liquid medium (not practical to fit in a standard 10-cm diameter dish (Sarstedt, #83.3902) that we used for our experiments). **(C)** Stochastic model as described in (B). By using simulations, we let two populations, one starting with 10-mL and the other with 100-mL volume of liquid medium, expand until they reached the carrying capacity (blue curve in (B)).
(*Caption continued on next page.*)

Figure 8.3 ***(previous page)*:** Once at the carrying capacity, we perturbed each of the two populations by setting back their density by a factor of 2 (i.e., half of the density at the carrying capacity) and recorded how the populations "recovered" from this perturbation to (again) reach the carrying capacity. The population starting with 10-mL volume of liquid medium recovered in ~150 hours whereas the one starting with 100-mL volume of liquid medium recovered in ~500 hours. A simple explanation is the closer proximity to the unstable fixed points (green curve in (B)) for a 100-mL population compared to a 10-mL population. The slower recovery rates upon small perturbations for populations that are closer to the fold bifurcation (~120-mL volume of liquid medium; see (B)) is a signature of "critical slowing down", which occurs in diverse systems with a "tipping point". Such system of interacting units (e.g., communicating ES cells) is often characterized by its homogeneity among the units and the strong connectivity between its units [265, 266].

community-level behaviour no longer possible, and perhaps, as a result, sub-communities begin to exist (community "patches" that may display a survival-vs-extinction behaviour on their own) or otherwise. As a first experiment, one can use tissue-culture dishes or flasks that have smaller or larger growth areas than used in our experiments (we used 58 cm^2 for a 10-cm diameter dish and 21 cm^2 for a 6-cm diameter dish) and then test whether the initial population densities as reported in our study give rise to the same switch-like phenomenon (i.e., above ~1700 cells / cm^2 population expansion occurs, whereas below ~1700 cells / cm^2 population extinction occurs). One should carefully perform and interpret the results of such exploratory studies because – as we have noticed from our experiments – populations may exhibit stochastic behaviors near the threshold densities as it is experimentally challenging to uniformly distribute isolated microcolonies across the surface of the dish.

Moreover, a closer examination of the population-level behaviour near the critical threshold-density (~1700 cells / cm^2) where either population expansion or population extinction occurs may reveal additional properties that are reminiscent of "*critical slowing down*" in systems with critical transitions [265, 266] (Fig. 8.3). Such systems have a "tipping point" (or fold bifurcation) near which the system may change abruptly from one state to another, oftentimes exhibiting "early warning signals" that the system is approaching a large-scale collapse. A generic indicator of such collapse is a loss of resilience as the system would show slower recovery when subject to small perturbations near the threshold. Interestingly, critical slowing down is found in many, unrelated systems that have tipping points, such as the collapse of the global financial market in 2008 [267], the sharp shift following a period of flickering from Pleistocene (Ice Age) to the current relatively warm and stable geological epoch (Holocene) [268], the large-scale collapse of the Caribbean coral systems during the 1980s [269], the collapse of *S. cerevisiae* (yeast) populations subject to salt shocks [270], the differentiation of mouse blood progenitor cells [239], and the differentiation of human induced pluripotent stem cells [271]. Such systems of interacting units are often characterized by the strong connectivity

between the units and the homogeneity among units.

Although experimentally challenging, one could test whether critical slowing down occurs in ES cells by comparing the population behaviour of two initial densities (Fig. 8.3). For one, ES cells are plated near but not too close to the density-threshold (for example: ∼2000 cells / cm^2, a 10-cm diameter dish requires 10-mL culture-medium), allowed to grow for 1-2 days in differentiation medium, and then perturbed, either physically (scraping off colonies from the dish bottom) or chemically (e.g., using DMSO) by killing a few cells, or by setting back the density (collecting all cells from the dish, and then putting them back on a new dish at a lower-than-before density), and then one should observe how fast the population recovers from the perturbation by growing towards the carrying capacity. As a control, the same protocol should be followed, but then for higher initial population densities (e.g., ∼6000 cells / cm^2). Examining various perturbation strengths (killing or setting back more/less cells), the population density that is closer to the density-threshold is expected – as a sign of critical slowing down – to recover slower (longer recovery times) with larger perturbations.

8.2.2. Dynamics of long-range and short-range communication

Our experiments show that the dynamics and the tuning of signalling across space and time is essential for ES cells during differentiation. When and for how long cells see signalling factors to elicit a proper response determines the functional capacity of differentiating cells [272]. We also observed that extinction-bound cells must see survival-promoting factors within the first ∼3 days, or else they would still head for extinction despite the diffusible factors being either secreted or at least stable for up to ∼5 days (Fig. 3.2). As a natural extension of our work, it was shown that ES cells make use of long-range, diffusible factors (a crucial one being Sonic Hedgehog (SHH)) to inhibit apoptosis and promote proliferation at day ∼10 of differentiation, much after cells have entered the Neural Ectoderm (NE) lineage as evidenced by the expression of *Sox1* [145]. Long-range communication can also occur through so-called "tunnelling nanotubes" (TNTs) which are membrane-bound extensions connecting cells and colonies that can be as far apart as ∼100 microns, through which exchange of important signals and cargoes is made possible [273]. Recent work also showed the importance of short-range communication mediated by cadherins – that work to bind direct neighbours with each other – to stabilize newly adopted fates of ES cells, such as a neural identity, while reducing the effects of non-neural factors [230, 274, 275]. These and our results combine long-range and short-range communication into a coherent picture that may describe the full behaviour of ES cells during differentiation. We hypothesize that ES cells employ a two-step strategy for survival and differentiation (Fig. 8.4).

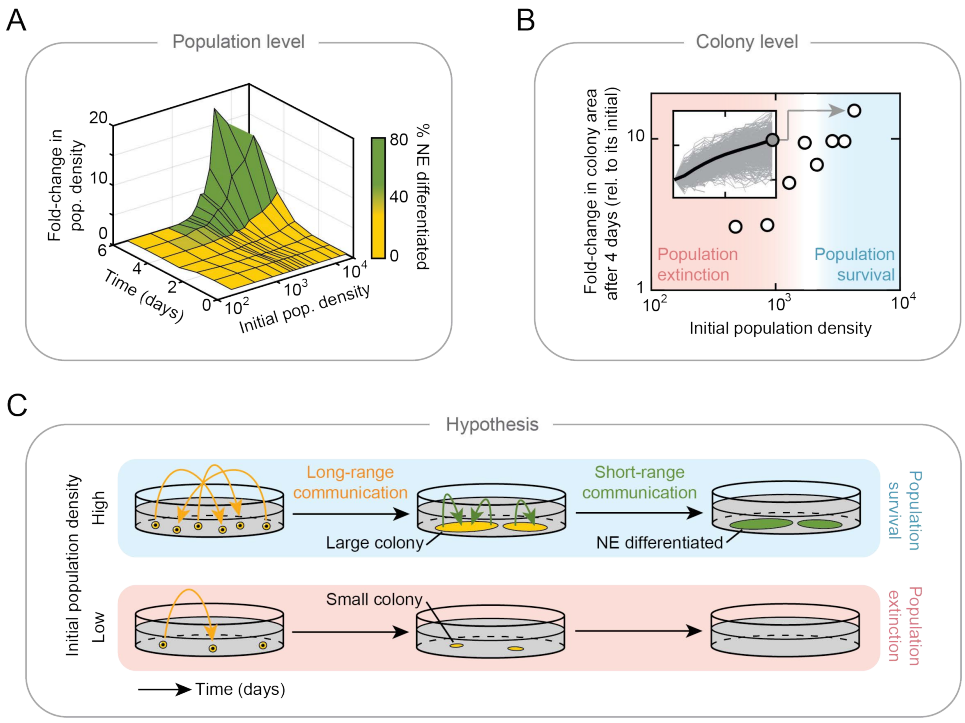

Figure 8.4: Hypothesis: ES cells use long-range communication for replication (survival) and short-range communication for differentiation. **(A)** Differentiating populations starting at high densities (above ~1700 cells / cm^2) avoid extinction, and instead survive, expand and then more efficiently differentiate into the Neural Ectoderm (NE) lineage. **(B)** Surviving populations generally consist of larger colonies than those from extinction-bound populations. Smaller subplot is derived from Fig. 3.8 and shows time in hours (from 0 to 96 hours) versus the fold-change in colony area relative to the initial colony area. **(C)** Our hypothesis. ES cells first use long-range communication to promote everyone's survival and colony growth only at high-enough population densities, and then use short-range communication within large-enough colonies for more efficient differentiation into a (e.g., NE) lineage.

8

As the first step, ES cells make use of long-range communication by secreting and sensing diffusible factors to help each other to survive, grow, and to determine the global population density on the dish during the first few days of differentiation. Initially when microcolonies are scattered as near-single ES cells across the bottom surface of a 10-cm diameter dish, the typical distances between microcolonies (~450 microns, see Fig. 2.13) only allow for far-diffusing factors to be the mediators of survival-promoting communication. We found that populations starting at densities above a critical threshold (~1700 cells / cm^2) not only survive and achieve a ~10-fold change in population density over 6 days (Fig. 8.4A), at the colony level, they also achieve higher fold-changes in colony area after 4 days whereas populations that become extinct – because they start at densities lower

than the critical threshold – have microcolonies that are generally smaller in size (Fig. 8.4B). The apparent correlation between colony size and (the ability to reach higher) differentiation efficiency (Fig. 8.4A) may suggest that ES-cell colonies need to reach a certain size (measured as their 2-dimensional area on the dish) before they can survive in general, and then to reach high differentiation efficiencies.

Why low-density populations - those starting differentiation below the critical threshold (~1700 cells / cm^2) - become extinct instead of growing, albeit at a slower rate than higher density populations, towards the carrying capacity (as pluripotent populations do) remains unclear. Speculatively, it may be worthwhile to let populations of sufficiently high densities to survive and thus differentiate, as these have a higher chance of giving rise to large enough colonies that in turn may be beneficial for differentiation. Apparently, timing is of great importance for survival and growth, so if populations and thus the colonies have not expanded to a certain extent (approximately ~10 fold after ~4 days), then populations become extinct instead of continuing to grow, and differentiate yet later in time (i.e., entry into Neural Ectoderm lineage must happen around day 4 (Fig. 8.4A)). In other words, quorum sensing lets everyone's fate (surviving or not) depend on the size of the community, to inform everyone of the likeliness to reach sizeable colonies at the right time.

As the second step, sizeable colonies that consist of more, packed cells benefit from short-range communication through the binding of neighbours, with e.g. cadherins, to stabilize newly adopted fates. Our data suggests a positive correlation between colony size (measured in area) and differentiation efficiency (percentage of cells differentiated into a Neural Ectoderm lineage).

To test our hypothesis, we expect to find (if our hypothesis were to be true) a positive correlation between the size of a differentiating ES-cell colony and how "well" that colony has differentiated into a certain lineage. This may be examined by using microscopy to determine for several ES-cell colonies during differentiation – ideally those that are part of a population that started differentiation near the critical threshold of ~1700 cells / cm^2 as some populations expand and differentiate whereas some become extinct - if there is a positive correlation between the size of a (e.g. 4-day-old) ES-cell colony and the colony-level differentiation efficiency (percentage of *Sox1*-GFP positive cells, or the total *Sox1*-GFP fluorescence level).

Given our hypothesis and observations, one may ask:

When does having more cells in an initial colony enhance survival of the colony?

In other words, when is an initial colony large enough to survive during differentiation? In Chapter 3 we found that the areas (i.e., sizes) of sparsely distributed initial colonies (typically ~400 μm^2) show no correlation with how well the colonies grow

and whether or not the colonies survive after 4 days of differentiation (Fig. 3.5). We sought to find a criterion based on a model that determines when an intra-colony communication is sufficient for survival by using the theory and assumptions from Chapter 6.

To do this, we use the steady-state concentration of a secreted molecule (factor), given as:

$$c(r) = \frac{c_R R}{r} exp(-\frac{r-R}{\lambda}) \tag{8.1}$$

where $\lambda = \sqrt{D/\gamma}$ is the diffusion length and c_R is the concentration on the cell surface (i.e., $r = R$). Let us consider c in units of c_R. This normalized concentration is simply

$$\frac{c(r)}{c_R} = \frac{R}{r} exp(-\frac{r-R}{\lambda}) \tag{8.2}$$

Consider a line of identical, spherical cells without any gap between them. Let us call the cell at the leftmost end of the line as a "receiver cell". The cell to its immediate right is called the "1st cell". The cell to the immediate right of this cell is "2nd cell", and so on. We want to calculate the normalized signal (secreted molecule) concentration created by all the other cells on the receiver cell. The distance r_m between the receiver cell's surface and the center of the m-th cell is

$$r_m = (2m-1)R \tag{8.3}$$

where $m \geq 1$. Then the normalized concentration created by the m-th cell on the receiver cell's surface is

$$\frac{c(r_m)}{c_R} = \frac{1}{2m-1} exp(-\frac{2(m-1)R}{\lambda}) \tag{8.4}$$

Now, imagine a 2-dimensional, circular colony formed by adherent cells. For simplicity, we can imagine that this colony is formed by a series of concentric circles, with spherical cells positioned circularly around each concentric circle. At the center of this circle is our receiver cell. It is surrounded by rings (concentric circles) of radii $R + r_1$, $R + r_2$, $R + r_3$, and so on. Let N_m be the total number of spherical cells that are circularly arranged on the ring of radius r_m. We can estimate N_m as the total number of cell diameters ($2R$) that can fit on the circumference of the ring:

$$N_m = \frac{2\pi(R + r_m)}{2R} = 2m\pi \tag{8.5}$$

This is an overestimate of N_m because this ignores parts of the ring that cannot be accessed by another cell due to the curvature of an occupying cell (i.e., it assumes that one can bend a diameter). One can quickly see that this is a good estimate by noting that $N_1 \sim 6$, which is also the number that one gets from hexagonally packing spheres (cells) in a ring whose center has the receiver cell. Note that hexagonal packing yields the maximum possible number of spheres packed in a given space, both in 2D and 3D. Then the total concentration c_{tot} of signaling molecule created by all the other cells in a colony on the receiving cell at the colony center is

$$\frac{c_{tot}}{c_R} = \sum_{m \geq 1} N_m \frac{c(r_m)}{c_R} \tag{8.6}$$

which simplifies to

$$\frac{c_{tot}}{c_R} = \sum_{m \geq 1} \frac{2m\pi}{2m-1} exp(-\frac{2(m-1)R}{\lambda}) \tag{8.7}$$

We can see that when m is large, the cells on the ring of radius $R + r_m$ contributes negligible concentration to the center cell because the summand in the above equation approaches zero as m increases. Specifically, we have

$$\frac{2m\pi}{2m-1} exp(-\frac{2(m-1)R}{\lambda}) \sim exp(-\frac{2mR}{\lambda}) \qquad \text{(for large } m\text{)} \tag{8.8}$$

Hence, in our circular colony, cells that are much further away from the diffusion length λ contribute negligible concentration of signal to the colony center. This makes intuitive sense.

The above analysis also shows that dispersed cells (or other colonies) can contribute a non-negligible concentration on a receiving cell only if the diffusion length λ is sufficiently large. Only then, we have $2mR/\lambda < 1$, meaning that the contributed concentration (i.e., $exp(-2mR/\lambda)$) is non-negligible. This is consistent with our finding that the diffusion length is near-centimeter scale.

But total concentration c_{tot} alone is insufficient to determine when a survival of a colony can be determined by an intra-colony communication with the same signaling molecule. To determine that, we need to compare the threshold concentration c_{thresh} to c_{tot}. Basically, if c_{thresh} is sufficiently low, then a small colony can generate enough concentration at the receiver cells so that c_{tot} is above the threshold. In

this case, according to our stochastic model (Fig. 6.4), we should observe a positive correlation between a colony's initial size and its probability of surviving (equivalently, its growth rate since the net growth rate is proportional to the difference between a cell's growth rate and its death rate). Having no correlation between the two quantities means that c_{thresh} is sufficiently high, meaning that it is higher than the c_{tot} realized by any of the colonies. Since c_{tot} is larger for larger colonies, a sufficiently high c_{thresh} means that no colony is sufficiently large to begin with. Our data is consistent with this latter scenario: we do not observe any correlation between colony size and its survivability (Fig. 3.5).

If we had a collective behaviour without a threshold (Fig. 2.1), above argument would not hold because in this case, a larger colony should grow faster. Having a threshold concentration binarizes the outcome so that a larger colony does not survive better than a smaller colony because both colonies can be too small to realize c_{tot} that is larger than c_{thresh}.

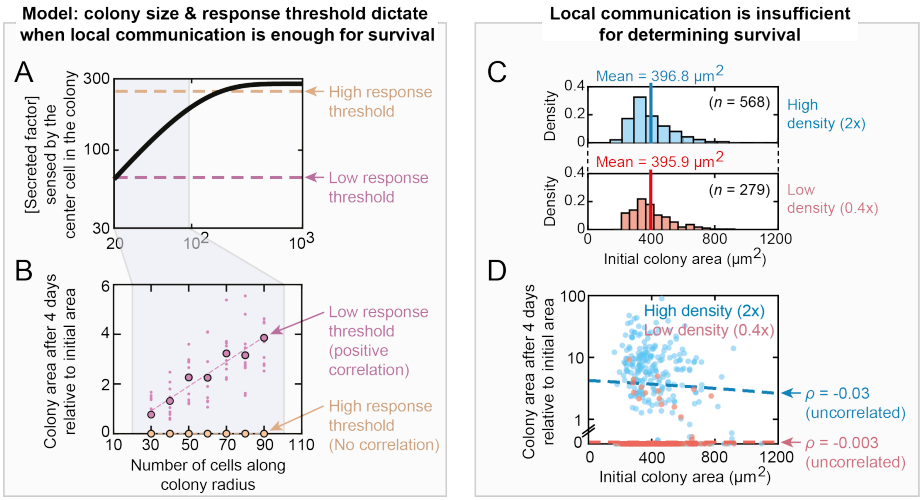

Figure 8.5: Modelling and experiments explain how initial colony size, diffusion length of secreted survival factors and cells' survival threshold collectively determine survival of ES cell colonies during differentiation. (A) Our model (see text for detailed explanation) shows that the initial colony area (for simplicity, colony's circular size formed by a series of concentric circles (cells)) sets the [secreted molecules] sensed by the center cell in the colony. As shown in the text, the sensed [secreted molecules] $\sim exp(\frac{2mR}{\lambda})$ with m = initial colony size as the # of cell diameters from center cell, R = radius of cell and λ = diffusion length of secreted molecule. Hence, the sensed [secreted molecules] $\sim exp(\frac{\sqrt{A_i/\pi}}{\lambda})$ by using the (circular) area of an initial colony ($A_i = \pi(2mR)^2$). The model shows that larger initial colonies result in higher sensed [secreted molecules] (this makes intuitive sense), but for survival (response to sensing of secreted molecules) the total [secreted molecules] needs to surpass a threshold concentration. A low threshold allows initial colonies within a range of sizes to achieve this, but a high threshold does not (unless the initial colony areas are larger).
(*Caption continued on next page.*)

Figure 8.5 ***(previous page)*****: (B)** Our stochastic model (see text Chapter 6 for detailed explanation) shows that a low threshold results in a positive correlation (Pearson correlation coefficient $\rho = 0.98$) between initial colony area and the growth of the areas after 4 days. A high threshold, however, results in no correlation ($\rho = 0$). These two distinct scenarios (positive correlation versus no correlation) allow us to verify whether the experimentally observed initial colony sizes correlate with the colony's growth (and thus, survival) during differentiation. The parameter values of the stochastic model are the same as those used in Chapter 6, except for the (only) free parameter K. The low-threshold scenario uses $K = 4000$ and the high-threshold scenario uses $K = 10^6$. **(C)** Histograms of initial colony areas shown for two initial population densities. Top histogram (blue) shows a high initial density that expands during unguided differentiation (2727 cells / cm^2) with mean = 396.8 μm^2 and bottom histogram shows a low initial density that goes extinct during unguided differentiation (818 cells / cm^2) with mean = 395.9 μm^2. Also see captions of Supp. Fig. 3.8 and 3.9. **(D)** Scatter plots of initial colony areas versus the corresponding colony area after 4 days of unguided differentiation relative to the initial area. Shown are the same initial population densities as in (C). Also see Fig. 3.5 and Supp. Fig. 3.9. For both initial population densities, we observe no correlation (i.e., Pearson correlation coefficient $\rho \sim 0$) suggesting that the experimentally observed initial colony areas are not large enough to generate [secreted molecules] > cells' survival threshold.

According to the above analysis, a sufficiently large colony should survive based solely on the intra-colony communication (i.e., even when the colony is by itself on a plate) (Fig. 8.5A and B). Evidently, the colony sizes in our experiments are not sufficiently large (Fig. 8.5C and D). The condition that very large colonies survive on their own accompanies the condition that the diffusion length must be at least as large as such colonies. Otherwise, due to the exponential decay term, $exp(\frac{-2mR}{\lambda})$, having a larger colony would make no difference to the concentration of the receiving cell. This reasoning is consistent with our finding that the diffusion length λ is near centimeter (every colony we observed is much smaller than a millimeter in diameter).

Our cell-seeding method involved counting cells that were suspended in liquid (N2B27), and then spreading them out onto 10-cm diameter dish. Spreading a low concentration of cells (5000 cells / mL) led to a low-density population consisting of many individual colonies, each with an average area of ~400 μm^2, that eventually went extinct (Fig. 8.6A). As a different seeding method, we seeded the same, low concentration of cells (5000 cells / mL) but confined within a small area of the 10-cm diameter dish at the center (Fig. 8.6B - schematic; see Materials and methods). This seeding method produced a single region of ~28 mm^2 that contained and started with many individual colonies that did not touch each other yet, which we confirmed with a microscope image taken ~24 hours after the seeding (Fig. 8.6B - middle). This population survived whereas it would become extinct if it were spread out over the dish. Over the next five days, these colonies grew and merged to form a macroscopic colony, whose characteristic length (diameter) was 3-4 mm (Fig. 8.6B - right). This population was visible by eye as single, three-dimensional colony in other biological replicates (Fig. 8.6C-D - for other biological replicates).

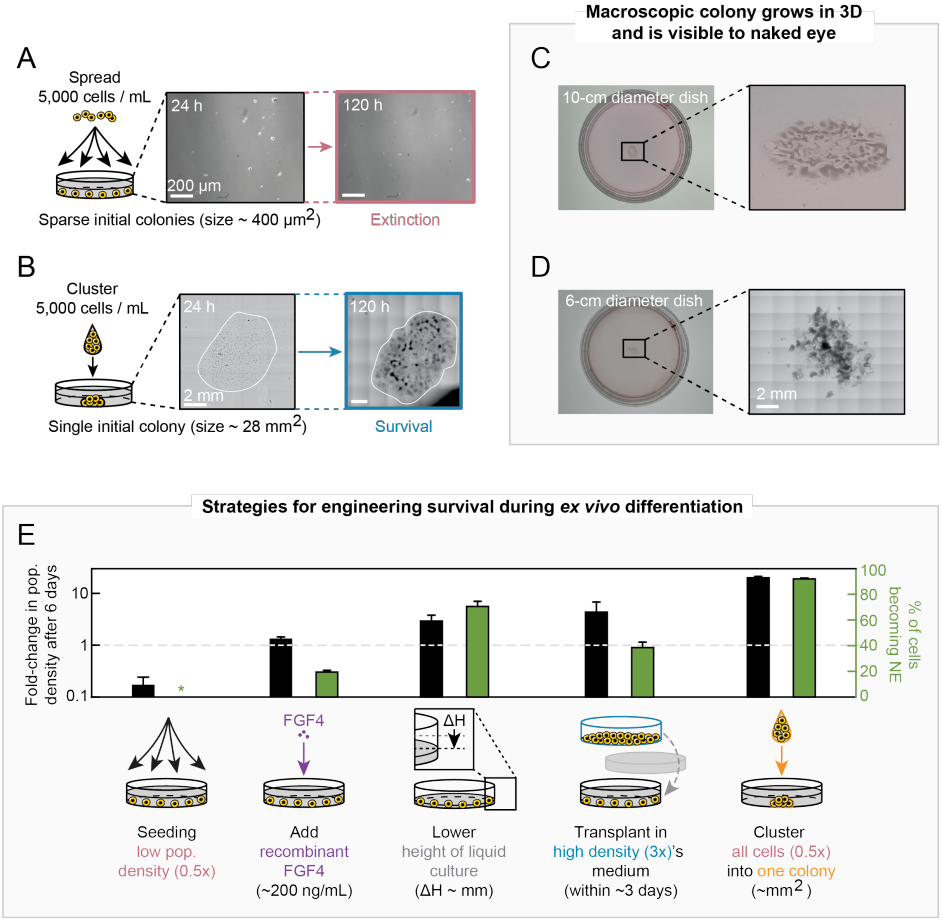

Figure 8.6: Quantitative experiments and modelling reveal strategies for engineering survival during *ex vivo* differentiation. **(A)** Small ES cell colonies (~400 μm^2 per colony) that are seeded by (sparsely) spreading them across the surface of a dish (shown here: 50,000 cells across 58 cm^2 surface area of a 10-cm diameter dish with 10-mL culture medium) results in population-level extinction during differentiation. Scale bars are 200 μm. Microscopy images are taken 24 hours and 120 hours during unguided differentiation. **(B)** A low number of ES cells (shown here: 5,000 cells / mL), similar to (B), that are initially clustered into single large colony (shown here: ~28 mm^2) result in survival of the colony during differentiation (also see E). Scale bars are 2 mm. Microscopy images are taken 24 hours and 120 hours during unguided differentiation (N2B27 medium). **(C, D)** A millimeter-sized colony, that survives after clustering and seeding a low number of cells (see D) at the center of a dish, is visible to the naked eye (see top images) and further expands in lateral (at the edge of the colony) and nonlateral (cells on top of each other (darker spots in the colony)) directions (see bottom images). The top images are based on 50,000 initially clustered cells on a 10-cm diameter dish (58 cm^2 surface area) and the bottom images are based on 18,000 initially clustered cells on a 6-cm diameter dish (21 cm^2 surface area), because the same cell numbers but sparsely distributed across the surface area results in extinction. Image taken after 5 days during unguided differentiation (N2B27). Scale bar is 2 mm.
(*Caption continued on next page.*)

Figure 8.6 ***(previous page)*****: (E)** A "standard" procedure of seeding a too low-density population (818 cells / cm^2) by spreading initial colonies across the dish results in population-level extinction during differentiation. Shown here are 46C cells when differentiating in N2B27 supplemented with RA to promote differentiation into Neural Ectoderm lineage, but the same phenomenon occurs for different cell types, different media conditions and all differentiations (see Supp. Fig. 2.13). All data shown have n > 3 and error bars are s.e.m. Incubation in medium conditioned by a high-density population (5172 cells / cm^2 initially) that survives and expands to the carrying capacity, rescues a low-density population from extinction (~4.3 fold growth and ~38.5% becoming NE progenitors). Also see Fig. 3.1 and 3.2. Differentiation medium supplemented with ~200 ng/mL recombinant human FGF4 rescues a low-density population from extinction (~1.3 fold growth and ~19.4% becoming NE progenitors). Also see Fig. 5.3. Lowering the height (and therefore the volume) of liquid culture by millimeters (here: from 10 to 2 mL liquid culture which is equivalent to lowering the height of the liquid culture in the dish from 1.7 to 0.3 mm) rescues a low-density population from extinction (~2.9 fold growth and ~70.5% becoming NE progenitors). Also see Fig. 3.6 and Supp. Fig. 3.12. Clustering cells into a large-enough colony (~mm^2) at the start of differentiation, rescues a low-density population from extinction (~20 fold growth and ~92% becoming NE progenitors).

This result matches our model's prediction, mentioned earlier (Fig. 8.5A - top), which was that a colony that is sufficiently large survives purely due to intra-colony communication. Specifically, this discovery is another confirmation that the cells communicate over many millimeters: if they did not, then having a larger colony should not make a difference in the cells' survival because many cells in the colony would be unable to communicate with each other because they are further apart then the diffusion length. If the macroscopic colony did not survive, then our models of cell-cell communication would be incorrect.

8.2.3. Differentiation under various habitat temperatures

What determines the timing and robustness of development is yet another fundamental question in biology. We learned that ES cells – as *ex vivo* models for studying development – cooperatively interact with each other in their habitat to survive and differentiate successfully at various culture settings; yet within limits, as some combinations of initial settings (initial population density and volume of liquid culture) result in population extinction. If development is like the playing of a movie, based on a script, understanding the timing and robustness – and thus, tunability – of the series of events from a single cell to a complex multicellular organism may provide insights for engineering *ex vivo* synthetic structures and regenerative medicine [103].

We do know how the "script" reads (Fig. 8.7). Specific genes must be turned on and off only at certain times. Upon withdrawal of LIF (day 0), ES cells exit the state of pluripotency before they can commit to a specific lineage [276, 277]. First, the expression of pluripotency genes (such as *Oct4*, *Nanog*, *Sox2*, *RexX1*) is downregulated, which is followed by the expression of genes (such as *Dnmt3b*) that mark the ES cells' exit from pluripotency (day 2). After that, lineage markers show up

(such as *Sox1* and *Nes* for Neural Ectoderm (NE) lineage at day 4) before cells terminally differentiate (*Tubb3* being a marker for neurons at day 8). The expression of specific markers at specific time points suggests that the "playing of the developmental movie" happens at a defined rate. In our experiments, we observed that populations that start differentiation below ~1700 cells / cm^2 (critical threshold) not only become extinct (Fig. 2.10), and thus excluded from the "movie", they also seem to lag behind in exiting pluripotency (Fig. 2.8) and differentiating, as they consist of at most or else less than ~40% cells differentiated into the NE lineage before mass extinction occurs (Fig. 2.11 and Fig. 8.4A).

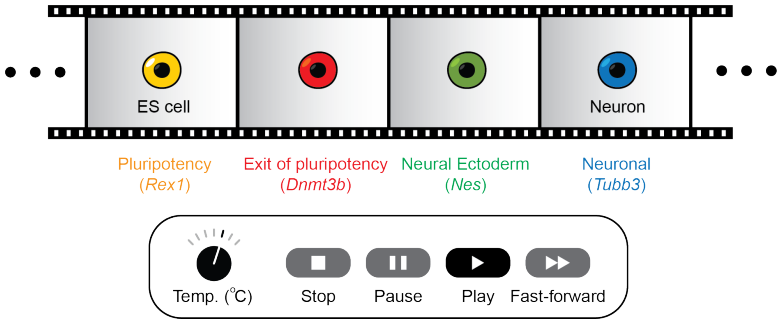

Figure 8.7: Editing the developmental "script" by varying habitat temperature of ES cells. Development comprises of a series of ordered cell-fate decisions. For ES cells, each stage (cell state) is characterized by markers: pluripotency (*Rex1*), exit of pluripotency (*Dnmt3b*), entry into Neural Ectoderm lineage (*Nes*) and neuronal fate (*Tubb3*). Just as temperature affects rates of biochemical reactions, it may also affect the rate of development from a pluripotent ES cell to a terminally differentiated cell, such as a neuron.

Temperature is often used to control the rates of biochemical reactions [278, 279], and thus to speed up or slow down (preserve) key processes of biological systems [280]. For the nematode, *C. elegans*, the temperature range of 16-25°C has been reported to be resulting in a normal developmental process; although a reduced egg yield, altered egg laying and greater population spread were reported for development near 25°C [281]. Similarly, also for the zebrafish, *D. rerio* [282], and the fruitfly, *D. melanogaster* [283], a normal development takes place within the temperature ranges of 17.5-32.5°C and 25-33°C, respectively. Interestingly, in all cases there is an almost linear relation between temperature and speed of embryogenesis, yet relative time between key developmental events is exactly the same for temperatures within the acceptable range [283]. Although mammalian development (for example, of humans or mice) takes place at a nearly constant temperature (generally around 37°C), variations in temperature are not uncommon, and in fact, can have a functional purpose [284]. Body temperature can vary due to physical activity, menstrual cycle, pregnancy, hibernation or in specific tissue that requires a different temperature (the production of viable sperm in humans requires a lower temperature than the normal body temperature) [284].

How temperature affects development – whether it is really as simple as higher temperature leading to faster chemical rates and thus development – is largely unknown. To understand what temperature *does*, as a case study, we[2] examined how temperature affects differentiation of mouse ES cells toward the Neural Ectoderm (NE) lineage (same protocol as described in Chapter 2). Given the above reasons, we may think of this differentiation as a movie of which we know the "script" (how cells grow and when certain genes are active), and thus we want to understand how temperature affects the playing of the developmental movie.

Living cells are subject to their habitat (artifial or natural), which the cells themselves can influence (by secreting and sensing factors to cooperate) or which can be imposed upon the cells. Here, we sought to understand how the temperature of the habitat may influence the behaviours of ES cells. More specifically, we want to understand how different incubation temperatures affect proliferation, loss of pluripotency, NE lineage commitment, and the expression of early and late markers during NE differentiation of ES cells.

We triggered the differentiation of pluripotent ES cells at an initial density of 5172 cells / cm^2 (considered a "high" density because the population survives and expands to the carrying capacity at standard 37°C – see Chapter 2) toward the Neural Ectoderm (NE) lineage at incubation temperatures of 26, 33, 35 and 39°C. At specific time points during an 8-day differentiation, we detached cells from the dish, counted their numbers in suspension to derive the "fold-change in population density" as a measure for proliferation (Fig. 8.8A) and quantitatively determined the median levels of *Oct4*-GFP in a population (as a measure for the loss of the pluripotency marker – Fig. 8.8B) and percentage of cells expressing *Sox1*-GFP in a population (as a measure for how many cells express the NE-lineage marker *Sox1* and thus have differentiated into the NE lineage – Fig. 8.8C) with a flow cytometer. Full details of the cell counting procedure and flow cytometry are in Chapter 2 and Materials and methods. Populations that began differentiation at standard 37°C or at a higher temperature (39°C) expanded about ~40 times by day 8 relative to their initial density on day 0, whereas slower population expansion occurred for lower temperatures of 35°C (fold change of ~20) and 33°C (fold change of ~3). At 26°C, populations did not expand beyond a fold-change of 1, nor showed any appreciable cell death during 8 days of differentiation (visually and also confirmed with a cell viability assay (Trypan Blue solution) to exclude dead cells from live-cell counting). We also confirmed cell viability at these lower-than-usual incubation temperatures (including 26°C) by first pre-incubating pluripotent ES cells in serum+LIF for 2 days, and then transferring the cells from a lower-temperature pre-culture to a differentiation medium at 37°C to trigger differentiation at standard temperature

[2]The work presented here has been in collaboration with **Lars-Eric Fielmich**, **Marloes Arts** and **Pim van den Bersselaar**

again. These populations did expand appreciably over time (data not shown).

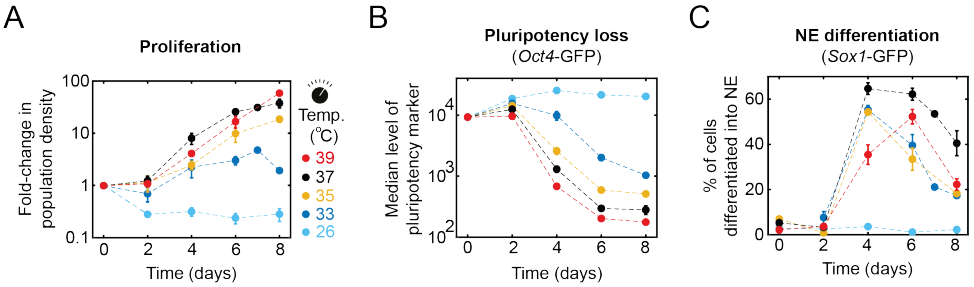

Figure 8.8: Incubation temperatures lower than standard 37°C hamper proliferation, loss of pluripotency (*Oct4*) and commitment to Neural Ectoderm (NE) lineage (*Sox1*) of ES cells. We used the same differentiation protocol as described in Chapter 2. In short, we seeded 5172 cells / cm^2 (considered a "high population density", i.e. one that always survives and expands under standard conditions) ES cells on a 10-cm diameter dish with 10-mL of N2B27 medium on day 0 and Retinoic Acid (RA) was added on day 2 to induce differentiation into Neural Ectoderm (NE) lineage (i.e., differentiation in N2B27+RA). We cultured cells at various incubation temperatures (26°C, 33°C, 35°C, 37°C and 39°C). We then collected cells at various time points and determined **(A)** alive cell counts (using Trypan Blue staining) to obtain the fold-change in population density as a measure for proliferation, **(B)** population's median levels of *Oct4*-GFP as a measure for loss of pluripotency, and **(C)** percentage of cells differentiated into NE lineage (*Sox1* is a marker of NE lineage). Cell lines used: *Oct4*-GFP for (A) and (B), 46C for (C); similar proliferation was observed for E14 and 46C, and RT-qPCR confirmed gene expression trends (data not shown). n ≥ 2 (but mostly, n > 3). Error bars are s.e.m.

Moreover, differentiating populations at colder temperatures loose the expression of pluripotency marker *Oct4* at a slower rate, eventually showing no appreciable loss of the pluripotency marker over an 8-day period despite culture conditions that trigger the cells exit from pluripotency (Fig. 8.8B). We used a flow cytometer to determine the median values of a population's GFP levels as a measure for the cell population's pluripotency state). As these median-level trends are based on *Oct4*-GFP (i.e., they depend on how fast GFP is degraded and produced, albeit driven by the *Oct4* promoter), we observed a similar, slower loss of pluripotency through Oct4 at colder temperatures at the RNA level by using a different method (RT-qPCR; data not shown). Additionally, differentiating populations reach lower differentiation efficiencies (peak of ~55% differentiated toward NE lineage) at lower temperatures relative to a standard temperature (peak of ~65%), with a higher temperature (39°C) resulting in a 2-day delay of the peak and a very low temperature (26°C) resulting in no peak (no entry into NE lineage) at all during 8 days of differentiation (Fig. 8.8C). Together, these results tell us that incubation temperature affects the rate of pluripotency loss and differentiation efficiency; with a temperature at the lowest end (26°C) resulting in no appreciable population expansion/decline, loss of pluripotency or lineage commitment during 8 days of differentiation.

To understand how a different incubation temperature affects the appearance of

key early and late markers of pluripotency and differentiation, as a first step, we measured the expression of key genes that mark the state of pluripotency (*Rex1*), exit of pluripotency (*Dnmt3b*), commitment to NE lineage (*Nes*) and neuronal differentiation (*Tubb3*) at the standard temperature of 37°C (for comparison) and at a lower temperature of 33°C (Fig. 8.9). For illustrative purposes and easy comparison, we further normalized the *Gapdh*-normalized (housekeeping gene) to each gene's minimum (= 0) or maximum (= 1) value during the 8 days to closely examine each gene's expression level over time. At standard 37°C (Fig. 8.9 – upper figure), we expect and observe differentiating populations to losing (*Rex1*) and exiting (*Dnmt3b*) pluripotency (*Rex1*) in 2 days. Yet, at a lower temperature (Fig. 8.9 – lower figure), we observe that populations exhibit a slower loss and exit of pluripotency during 8 days of differentiation, with the key pluripotency marker *Rex1* showing no decrease during a period of 6 days. On the other hand, expression of late markers during differentiation (lineage commitment and terminal differentiation) increases over time, albeit peaking 2 days earlier at 33°C relative to 37°C. We expected to observe populations first exiting pluripotency and then differentiating towards a lineage. Yet, there appears to be a time period of overlap between early (pluripotency) and late (differentiation) markers between days 4 and 6. Although the expression level of single genes does not provide a full picture, future studies should focus on confirming these trends with other but similar early and late markers. The results suggest that ES cells do not need to fully downregulate pluripotency markers to upregulate differentiation markers, thus exhibiting plasticity in the consecutive expression of key genes during differentiation.

Ultimately, the expression of key genes for pluripotency and differentiation depends the activity of transcription factors that make those genes expressed in the first place. It is the structure of the chromatin (compacted DNA as a result of DNA being wrapped around core histones like a string with beads [285]) – particularly the role of histone-modifying proteins, chromatin-remodelling proteins and chromatin-associated proteins – and therefore the global organization of the genome which determines the accessibility and activity (the transcriptional status) of key ES-cell genes such as *Oct4* and *Nanog* [286]. Pluripotent ES cells are generally characterized by their globally "decondensed" chromatin, which often shows itself through the absence of heterochromatin foci (densely packed (folded) regions in the chromatin, with generally low transcriptional activity) [286, 287]. The formation of heterochromatin foci usually coincides with differentiation, as cells begin to possess a more restricted pool of genes to transcribe (activate) and therefore lineages to commit to [288, 289]. As a first step toward a mechanism behind a temperature-dependent control of proliferation and differentiation in ES cells, we hypothesize that temperature affects chromatin folding and thus the accessibility of key ES-cell genes during differentiation.

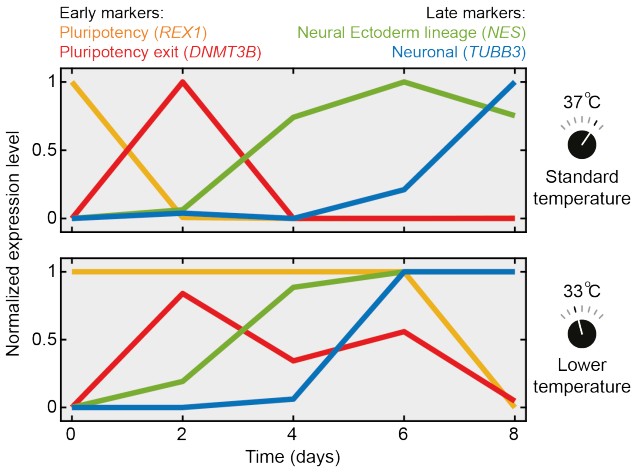

Figure 8.9: Incubation temperature affects the appearance and expression duration of key markers of pluripotency and differentiation. Normalized expression level over time after initiating differentiation toward Neural Ectoderm (NE) lineage with Retinoic Acid (RA) at 33°C and 37°C. We used the same differentiation protocol as described in Chapter 2 and Materials and methods. Data obtained from E14 cells seeded at 5172 cells / cm^2 with RT-qPCR. Different colors represent important markers of pluripotency and differentiation: *Rex1* (pluripotency), *Dnmt3b* (exit from pluripotency), *Nes* (NE lineage) and *Tubb3* (neuronal). On each day, we first normalized a population's gene expression level by that population's *Gapdh* level. Afterwards, we divided each population's *Gapdh*-normalized gene expression level on a given day by the *Gapdh*-normalized value of day-0 population. For illustrative purposes, plotted on the vertical axis, we set *Rex1*'s day-0 level to be equal to 1, all other genes' day-0 levels to be equal to 0 and the minimum or maximum values (i.e., 0 or 1, respectively) are based on 37°C. n = 3. Pluripotency marker *Rex1* displays a 6-day delay to show a decrease over time during differentiation while *Dnmt3b* (marks the exit of pluripotency) shows a prolonged expression until day 8 (*Dnmt3b* usually peaks around day 2 of differentiation at standard 37°C) when comparing 33°C with 37°C. Moreover, for the same comparison of temperatures, expression of differentiation markers (*Nes* and *Tubb3*) is pushed up by 2 days.

To test whether there are significant differences in chromatin structure as a function of incubation temperature, we quantitatively determined the number of heterochromatin foci (condensed regions, or spots, in the overall structure of chromatin) as a first measure of transcriptionally active chromatin regions (i.e., more foci means fewer active genes) [287, 288]. For this, we stained the DNA of fixed ES cells with a common staining solution (DAPI) on day 0 (pluripotent) and day 6 of differentiation toward the NE lineage (Fig. 8.10). As heterochromatin foci are more densely packed chromatin regions, a local increase in blue fluorescence (DAPI) marks the foci as condensed DNA "spots" (Fig. 8.10 – indicated by white arrow). We then counted the number of condensed DNA spots per cell (a single cell is represented by a single DNA structure (Fig. 8.10 – indicated by grey arrow) by applying a threshold to distinguish the condensed DNA spots from the background (i.e., to separate individual, white spots from the grey background). After applying a single threshold, we determined the geometric mean of the number of spots per

cell for all cells from a certain incubation temperature (orange and green colour for day 0 and day 6, respectively); these average numbers of condensed DNA spots (i.e., heterochromatin foci) per cell are then plotted against the incubation temperatures of 26°C, 30°C, 37°C and 40°C (Fig. 8.10). Although differentiation is generally characterized by an increase in the number of heterochromatin foci as a result of DNA methylation [286], the transition from pluripotency to terminally differentiated cells first shows a general decrease in the number of heterochromatin foci [287]. In line with the latter notion, we confirmed that at a standard incubation temperature of 37°C pluripotent ES cells (day 0) have a higher number of condensed DNA spots per cell (average of ~12) relative to those of differentiated cells on day 6 (average of ~8). Importantly, pluripotent ES cells at lower-than-standard incubation temperatures – those of which their population shows a slower proliferation, slower loss of expansion, and lower efficiency in NE commitment – generally have higher number of condensed DNA spots, up to an average of ~19 spots per cell.

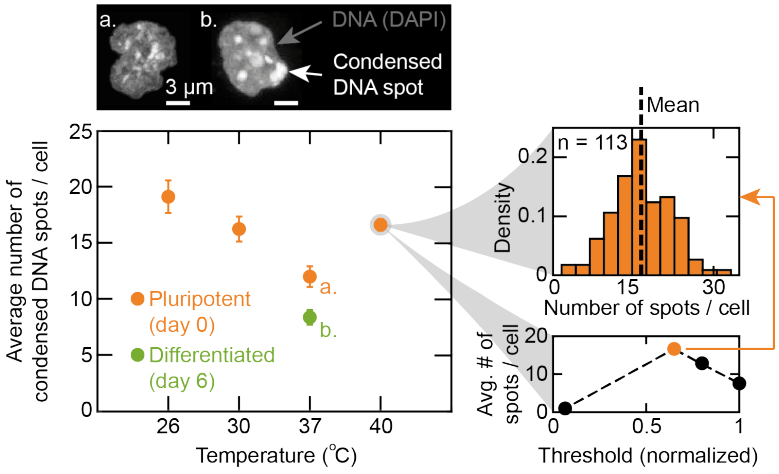

Figure 8.10: Hypothesis: Incubation temperature controls chromatin structure and thus the transcriptional status of ES-cell genes important for proliferation, pluripotency and differentiation. Average number of condensed DNA spots per ES cell as a function of different incubation temperatures. Data obtained for E14 cells that were kept pluripotent in serum+LIF medium (orange), or differentiated into Neural Ectoderm (NE) lineage with Retinoic Acid (RA) and imaged on day 6 (green). We hypothesize that temperature may effect DNA folding into euchromatin (i.e., with genes that are accessible for active transcription) and heterochromatin (i.e., condensed DNA) that in turn affects regulation of genes required for pluripotency and differentiation. As a first step, we tested whether DNA condensation is affected by temperature. We fixed cells by treating them with 4% formaldehyde and then permeabilized their membrane for DNA-staining agents with 0.01% Tween/Triton. Afterwards we stained DNA by treating fixed, permeabilized cells with ~10 μg/mL DAPI and then imaged DNA-stained, fixed cells on cover glass with a confocal microscope (see microscopy images at the top; scale bar is 3 μm). We observed fluorescently stained DNA (see microscopy images, shown in grey) and spots indicating densely packed chromatin regions, i.e. more condensed DNA (see microscopy images, shown in white).
(*Caption continued on next page.*)

Figure 8.10 ***(previous page)*****:** We analyzed the condensed DNA spots with custom ImageJ and MATLAB scripts as a function of a threshold value to distinguish the spots from the background fluorescence. Applying a single value of threshold (indicated with orange arrow) to all images we determined the average number of spatially distinct spots per cell (geometric mean from histograms) as a function of temperature (26°C, 30°C, 37°C, 40°C) and culture condition (pluripotent (day 0) or differentiated (day 6)). Error bars are s.e.m.; n = 52 cells (26°C), n = 40 cells (30°C), n = 34 (37°C, pluripotent), n = 30 (37°C, differentiated), n = 113 (40°C). We observed significantly fewer number of condensed DNA spots per pluripotent ES cell for incubation temperatures that are higher and lower than standard 37°C.

Future work may verify these observations with more, complementary methods (RT-qPCR at RNA level; western blot or ELISA at protein level; ATAC-seq and Hi-C at chromatin-organization level). Also, we hypothesize that the observed effects of incubation temperature are reversible, that is, a transfer of ES cells back to a standard incubation temperature (37°C) may allow ES cells to proceed with (faster) proliferation and differentiation. Additionally, chromatin structure is known to be organized and remodelled by polycomb-group proteins (such as Ring1 and Suz12 making up the PRC1 and PRC2 complex, respectively) [290]; the expression of some of these key PRC1/PRC2 complex proteins as a function of incubation temperature may also provide insights complementary to those we observed so far in Fig. 8.9 and 8.10.

In summary, the results of these experiments suggest a following picture. The global chromatin structure controls the regulation of key genes, and thus the state of ES cells during differentiation (surviving, apoptotic, committing to lineage, terminally differentiated), and both "internal" factors (such as cooperativity by secreting and sensing molecules) and "external" factors (such as the habitat size and temperature) may together set these states, and thus critically tune the overall process of differentiation.

There is nothing over which a free man ponders less than death;
his wisdom is, to meditate not on death, but on life.

Baruch Spinoza

Acknowledgements

One can make discoveries that may challenge present knowledge, but my biggest (and fortunate) discovery has been the people I was surrounded by and working with – and who made it possible to (even try to) summit an academic peak. These people helped me to become a brave, critical, independent, and caring human being. Here is to those who walked along with me.

First and foremost, I want to thank my daily supervisor, **Hyun Youk**. Our interactions lifted me - both professionally and personally - to such great altitudes, too blurry for me before I joined the lab. I learned not only how to do science, but also the sometimes embarrassingly "little" yet equally (if not more) important things such as presenting engagingly, summarizing succinctly, distinguishing good from bad failures, writing emails, being patient, taking responsibility, doing one thing at a time, and truly believing that things will work out in the end but only if one works hard. Your high aspirations are contagious, and infected me to continue aspiring in bold ways for my future. I sincerely wish you the best of luck in your career, now at the University of Massachusetts, and in your personal life as well.

On to my partner in crime along this journey, **Pim van den Bersselaar**. I don't think I would have reached these altitudes in such fun, productive and relatively smooth way myself, if we didn't meet and work together. It's impossible to count all the moments we laughed together; the pellets of plates we used and the hours and weekends we somehow happily sacrificed in a cave-like room to watch and grow these cells with Dua Lipa playing in the background (on repeat); and the times you gave us courage to continue despite failure or resistance. From a quiet masters student, to a technician, to a friend, and now to an aspiring Doctor of Philosophy at TU Eindhoven. I wish you a healthy, bright and fun future and we keep in touch.

Then our lab's oracle ánd a friend, **Théo Maire**. I really admire your sense of humour, down-to-earthness, casualness, discipline, and willingness to have a scientific, random or uplifting chat at any moment of the day. These traits make you a very reliable person. Our trip to Banff (Canada) and San Francisco (including the road trips) are still highly memorable to me. We keep in touch and I know that you'll have a bright (academic) future ahead of you.

An important person who taught me to always aim for the highest while keeping both feet on the ground is my friend, **Eduardo Olimpio**. I've rarely seen anyone so knowledgeable, friendly, dedicated and full of energy as you are. You were an

important reason for me to obtain a doctoral degree, because, to me, that meant curiously getting to the root of challenging problems in question. I'll never forget our nice conversations, our trip to Chicago and Michigan ("Ya sure ya wanna walk?"), your cooking skills, your contagious positivity, and your lovely wife Gabriela. I wish you, your wife and your kids a happy and healthy future in Brazil. I hope we get to see each other soon.

Another person I met and worked with was our lab's family man, **Lars-Eric Fielmich**. Thanks for our short but sweet collaboration on a new project and for teaching me things about development, worms (I mean, *Caenorhabditis elegans*), avocado plants, and how to eat kiwis with the skin even if one hates kiwis in the first place. But most importantly, thanks for reminding me and everyone else in our lab the importance of having and running a family besides a demanding job. I wish you and your family a healthy future.

Mehran Mohebbi, you were one of the lab's first PhDs, a co-Iranian (though I dislike labels) and a former roommate. Thanks for the good moments we shared and that you organized in our department (Whiskey Club and Movember). I know for a fact how important your friendship and contributions were to many around you which makes you a true beacon of trust. I wish you the best of luck in your life and career in Groningen.

A big thanks to **Diederik Laman Trip** for the many nice moments together, silly talks, drinks and food that we shared. It was much fun to spend time with you during our lab's outings, group meetings and conference visits.

Another big thanks to **Diego Gomez Alvarez** (also a former roommate). It was always fun to talk to you, whether that was accompanied by quirky jokes or shots of imported tequila. **Yiteng Dang**, in your own way you are a special person with a soft outside (your personality) and a dedicated inside (your technical skills). And **Milan Lacassin**, who joined the lab half-way through my PhD, but brought with him lots of humour and energy; thanks for the many uplifting talks we had and the good food and drinks we shared. **Eve Helguero**, thanks for your lively enthusiasm, your distinctive but catchy laugh, and the lab skills you taught me.

Also thanks to **Berkalp Doğaner** (for the love of the amazing Fazil Say, which got us to go to Antwerp for an evening concert), **Arie Ravensbergen** ("Moahhh"), **Max Betjes** (a fun, facts enthusiast), **Jasper Veerman** (one of the best presenters I've seen), **Tim Allertz** (a devoted chess player), **Yuliia Didan** (I'm still hearing your dedicated mouse clicks), **Jacinta van de Grint**, and still many others.

My very first student was **Javier Tejeda Mora**. I appreciate how honest, interested and committed you were from the very beginning which got you to fly over from México to do an internship in our lab with me. I'm sure you'll have a bright future

ahead of you.

Stefan Hagedoorn, it was never boring around you. You worked hard during your time with me and yet you brought with you positive vibes and energizing laughter. And this makes you a great-to-have team member. (Un)fortunately I won't easily forget your "Hello hello" video.

Another great person I worked with was **Marloes Arts**. You not only spent countless hours with me in the lab, you were always in for a fun and uplifting conversation. Thanks for your time here and I wish you the very best at the University of Copenhagen.

Brian Analikwu and **William Verstraeten**, you both started at the same time, hoping to do some lab work with me, but soon our world changed and forced all of us to work from home instead. Yet the two of you kept your momentum going and started to work on something much more complicated. And you were successful, way beyond any supervisor could wish for. Brian, all the best for your studies at TU Delft & Erasmus University, career and life. And the same to you, William, now at EPFL in Lausanne.

Also thanks to **Claudia Tugui** and **Martin Pabst** (Department of Biotechnology) for teaching me the basic principles of mass spectrometry.

The Department of Bionanoscience (Kavli Institute of Nanoscience) was a vibrant and engaging environment to be part of while walking the path toward obtaining a doctoral degree. Kavli Days in Amsterdam and The Hague, Quo Vadis, pizza poster sessions, Winter School in Courchevel (France), Spring School in Heeg (Friesland) – I treasure these fun (learning) experiences.

Particularly, I want to acknowledge the principal investigators who expressed their support or provided feedback to me during my time in the department. To begin with, thank you **Greg Bokinsky** and **Yaroslav Blanter** (Department of Quantum Nanoscience), as my (co)promotors, for being supportive and responsive in order to make progress whenever this was (or wasn't yet) necessary. Thank you, **Marileen Dogterom**, for being the Chair of our department, but above all else, for always being approachably friendly and supportive to me. Also thank you, **Bertus Beaumont** and **Christophe Danelon** for providing critical feedback on my presentations in the department; **Martin Depken**, now as the new Chair of our department, for generally being a great and open-minded person to talk to; and **Stan Brouns**, for hosting me as a supervisor of TU Delft's amazing 2017 iGEM team. My gratitude goes to the department's secretaries, **Dijana Boric**, **Amanda van der Vlist** and **Nadine Kuijvenhoven**, for co-organizing the many events and for helping me with daily practicalities.

Importantly, my gratitude also extends to the many PhD candidates and postdocs

who enriched the life in our department. It'd be impossible to list each and everyone of you, or even those who I had some form of interaction with. Even though I'm forgetting many others, let me (at least) thank the following few. **Enzo Kingma**, we know each other since 2011 (!), both enrolled in the Applied Physics bachelor's programme, and ultimately both pursuing a PhD in the same department. It was always much fun to have a chat with you. **Fabai Wu**, for being so nice and welcoming to me during my first months in the department. You are by far my band's biggest fan. Thanks for sharing great musical moments. I hope that all is well with you. **Helena Shomar** ("Suuuup"), it was always fun to be around you as a vibrant member of our department. I hope we can do some songs together again in the future. BN's one and only jazz band; thanks a lot **Da Wei** (for the positivity and energy you contagiously radiate in every single conversation we had), **Maurits Kok** (for teaching me so many interesting new facts about music theory and jazz), **Vladimir Volkov** and **Louis Reese**; I have fond memories of us practicing and playing together. **Anthony Birnie** and **Kevin Felter** (Department of Chemical Engineering), I'm still very proud of us organizing our faculty's first large career event (now happening annually) to help PhD candidates prepare for their next career step. Lastly, I also do want to mention and thank the following members: **Benjamin Lehner** (you're just great to talk to), **Alicia Soler Canton** (my energetic and awesome companion in the cell-culture room), **Mohamed Fareh** (for teaching me how to work with mammalian cells), **Mathia Arens** (for teaching me the basics of RNA Seq; I'm still very deeply saddened by the news of your loss...), **Esengul Yildirim** (always fun and uplifting to have a chat with), **Nicole Imholz** ("Suuuup", and a great lab neighbour) and **David Foschepoth**.

I also want to thank all members of the doctoral committee - my (co)promotors, **Martin Depken** (again), **Tom de Greef** (TU Eindhoven), **Allyson Sgro** (Boston University), **Amir Mitchell** (University of Massachusetts Medical School), and **Nynke Dekker** (TU Delft) - for their time to evaluate my dissertation and participating in the doctoral defence ceremony.

Much of my happiness and courage through this journey - despite failures and struggles - stemmed from the following group I'd like to thank as well: **Cristina**, **Larissa**, **Jennifer**, **Stefan**, **Koen**, **Alex**, **Dimitris**, **Shubhankar**, **Apurva**, **Leoncio**, **Sid**, **Kostas**, **Manuel**, **Nick**, **Thomas**, **Michael**, and others.

But by far, the two most important persons, **my parents**: your love and support remains unconditional and critical for any success in my life.

References

1. Daneshpour, H. & Youk, H. Modeling cell–cell communication for immune systems across space and time. *Current Opinion in Systems Biology* **18,** 44–52. ISSN: 24523100. https://doi.org/10.1016/j.coisb.2019.10.008 (2019).
2. Daneshpour, H., van den Bersselaar, P. & Youk, H. Global community effect: Large-scale cooperation yields collective survival of differentiating embryonic stem cells. *bioRxiv*. ISSN: 26928205 (2020).
3. Lieverse, A. R., Temple, D. H. & Bazaliiskii, V. I. Paleopathological Description and Diagnosis of Metastatic Carcinoma in an Early Bronze Age (4588+34 Cal. BP) Forager from the Cis-Baikal Region of Eastern Siberia. *PLoS ONE* **9** (ed Caramelli, D.) e113919. ISSN: 1932-6203. https://dx.plos.org/10.1371/journal.pone.0113919 (2014).
4. Krugman, P. *The Self Organizing Economy* (ed Wiley-Blackwell) ISBN: 978-1-557-86698-1 (1996).
5. Lima, S. L. & Dill, L. M. Behavioral decisions made under the risk of predation: a review and prospectus. *Canadian Journal of Zoology* **68,** 619–640. ISSN: 0008-4301. http://www.nrcresearchpress.com/doi/10.1139/z90-092 (1990).
6. Foster, W. A. & Treherne, J. E. Evidence for the dilution effect in the selfish herd from fish predation on a marine insect. *Nature* **293,** 466–467. ISSN: 0028-0836. http://www.nature.com/articles/293466a0 (1981).
7. Graham, J. M., Kao, A. B., Wilhelm, D. A. & Garnier, S. Optimal construction of army ant living bridges. *Journal of Theoretical Biology* **435,** 184–198. ISSN: 00225193. https://linkinghub.elsevier.com/retrieve/pii/S0022519317304356 (2017).
8. Ben-Jacob, E., S. Coffey, D. & Levine, H. Bacterial survival strategies suggest rethinking cancer cooperativity. *Trends in Microbiology* **20,** 403–410. ISSN: 0966842X. https://linkinghub.elsevier.com/retrieve/pii/S0966842X12001011 (2012).
9. Prindle, A. *et al.* Ion channels enable electrical communication in bacterial communities. *Nature* **527,** 59–63. ISSN: 0028-0836. http://www.nature.com/articles/nature15709 (2015).
10. Larkin, J. W. *et al.* Signal Percolation within a Bacterial Community. *Cell Systems* **7,** 137–145.e3. ISSN: 24054712. https://linkinghub.elsevier.com/retrieve/pii/S240547121830245X (2018).

11. Steinberg, N., Rosenberg, G., Keren-Paz, A. & Kolodkin-Gal, I. Collective Vortex-Like Movement of Bacillus subtilis Facilitates the Generation of Floating Biofilms. *Frontiers in Microbiology* **9.** ISSN: 1664-302X. http://journal.frontiersin.org/article/10.3389/fmicb.2018.00590/full (2018).
12. Borges, A. L. *et al.* Bacteriophage Cooperation Suppresses CRISPR-Cas3 and Cas9 Immunity. *Cell* **174,** 917–925.e10. ISSN: 00928674. https://linkinghub.elsevier.com/retrieve/pii/S0092867418307384 (2018).
13. Bernheim, A. & Sorek, R. Viruses cooperate to defeat bacteria. *Nature* **559,** 482–484. ISSN: 0028-0836. http://www.nature.com/articles/d41586-018-05762-1 (2018).
14. Wilson, K. G. The renormalization group: Critical phenomena and the Kondo problem. *Reviews of Modern Physics* **47,** 773–840. ISSN: 0034-6861. https://link.aps.org/doi/10.1103/RevModPhys.47.773 (1975).
15. Altan-Bonnet, G. & Mukherjee, R. *Cytokine-mediated communication: a quantitative appraisal of immune complexity* 2019.
16. Antonioli, L., Blandizzi, C., Pacher, P., Guilliams, M. & Haskó, G. *Rethinking Communication in the Immune System: The Quorum Sensing Concept* 2019.
17. Francis, K. & Palsson, B. O. Effective intercellular communication distances are determined by the relative time constants for cyto/chemokine secretion and diffusion. *Proceedings of the National Academy of Sciences* **94,** 12258–12262. ISSN: 0027-8424. http://www.pnas.org/cgi/doi/10.1073/pnas.94.23.12258 (1997).
18. Alberts, Johnson, Lewis, Raff, Roberts, W. *Molecular Biology of the Cell* 5th editio, 1503. ISBN: 1136844422, 9781136844423 (Taylor Francis Group, 2007).
19. Youk, H. & Lim, W. A. Secreting and Sensing the Same Molecule Allows Cells to Achieve Versatile Social Behaviors. *Science* **343.** ISSN: 0036-8075 (2014).
20. Doğaner, B. A., Yan, L. K. & Youk, H. Autocrine Signaling and Quorum Sensing: Extreme Ends of a Common Spectrum. *Trends in Cell Biology* **26.** ISSN: 09628924 (2016).
21. Shvartsman, S. Y., Wiley, H. S., Deen, W. M. & Lauffenburger, D. A. Spatial Range of Autocrine Signaling: Modeling and Computational Analysis. *Biophysical Journal* **81,** 1854–1867. ISSN: 00063495. https://linkinghub.elsevier.com/retrieve/pii/S0006349501758377 (2001).
22. Coppey, M., Berezhkovskii, A. M., Sealfon, S. C. & Shvartsman, S. Y. Time and Length Scales of Autocrine Signals in Three Dimensions. *Biophysical Journal* **93.** ISSN: 00063495 (2007).
23. Cantrell, D. & Smith, K. The interleukin-2 T-cell system: a new cell growth model. *Science* **224,** 1312–1316. ISSN: 0036-8075. https://www.sciencemag.org/lookup/doi/10.1126/science.6427923 (1984).

24. Malek, T. R. The Biology of Interleukin-2. *Annual Review of Immunology* **26,** 453–479. ISSN: 0732-0582. http://www.annualreviews.org/doi/10.1146/annurev.immunol.26.021607.090357 (2008).
25. Schroder, K., Hertzog, P. J., Ravasi, T. & Hume, D. A. Interferon-γ: an overview of signals, mechanisms and functions. *Journal of Leukocyte Biology* **75,** 163–189. ISSN: 07415400. http://doi.wiley.com/10.1189/jlb.0603252 (2004).
26. Sporn, M. B. & Todaro, G. J. Autocrine Secretion and Malignant Transformation of Cells. *New England Journal of Medicine* **303,** 878–880. ISSN: 0028-4793. http://www.nejm.org/doi/abs/10.1056/NEJM198010093031511 (1980).
27. Chitu, V. & Stanley, E. R. Colony-stimulating factor-1 in immunity and inflammation. *Current Opinion in Immunology* **18,** 39–48. ISSN: 09527915. https://linkinghub.elsevier.com/retrieve/pii/S0952791505001974 (2006).
28. Heldin, C.-H. & Westermark, B. Mechanism of Action and In Vivo Role of Platelet-Derived Growth Factor. *Physiological Reviews* **79,** 1283–1316. ISSN: 0031-9333. https://www.physiology.org/doi/10.1152/physrev.1999.79.4.1283 (1999).
29. Holz, R. W. & Fisher, S. K. in *Basic Neurochemistry* 235–257 (Elsevier, 2012). https://linkinghub.elsevier.com/retrieve/pii/B9780123749475000122.
30. Courtney, A. H., Lo, W.-L. & Weiss, A. TCR Signaling: Mechanisms of Initiation and Propagation. *Trends in biochemical sciences* **43,** 108–123. ISSN: 0968-0004. http://www.ncbi.nlm.nih.gov/pubmed/29269020http://www.pubmedcentral.nih.gov/articlerender.fcgi?artid=PMC5801066 (2018).
31. Artavanis-Tsakonas, S. Notch Signaling: Cell Fate Control and Signal Integration in Development. *Science* **284,** 770–776. ISSN: 00368075. https://www.sciencemag.org/lookup/doi/10.1126/science.284.5415.770 (1999).
32. Mattes, B. & Scholpp, S. Emerging role of contact-mediated cell communication in tissue development and diseases. *Histochemistry and Cell Biology* **150,** 431–442. ISSN: 0948-6143. http://link.springer.com/10.1007/s00418-018-1732-3 (2018).
33. Yang, W.-H. *et al.* Juxtacrine Signaling Inhibits Antitumor Immunity by Upregulating PD-L1 Expression. *Cancer Research* **78,** 3761–3768. ISSN: 0008-5472. http://cancerres.aacrjournals.org/lookup/doi/10.1158/0008-5472.CAN-18-0040 (2018).
34. Eyckmans, J., Boudou, T., Yu, X. & Chen, C. S. A Hitchhiker's Guide to Mechanobiology. *Developmental Cell* **21,** 35–47. ISSN: 15345807. https://linkinghub.elsevier.com/retrieve/pii/S1534580711002498 (2011).

35. Pinto, G., Brou, C. & Zurzolo, C. Tunneling Nanotubes: The Fuel of Tumor Progression? *Trends in Cancer* **6,** 874–888. ISSN: 24058033. https://linkinghub.elsevier.com/retrieve/pii/S2405803320301552 (2020).
36. Joesaar, A. *et al.* DNA-based communication in populations of synthetic protocells. *Nature Nanotechnology* **14,** 369–378. ISSN: 1748-3387. http://www.nature.com/articles/s41565-019-0399-9 (2019).
37. Yang, S. *et al.* Light-Activated Signaling in DNA-Encoded Sender–Receiver Architectures. *ACS Nano* **14,** 15992–16002. ISSN: 1936-0851. https://pubs.acs.org/doi/10.1021/acsnano.0c07537 (2020).
38. Guo, S. *et al.* Engineered Living Materials Based on Adhesin-Mediated Trapping of Programmable Cells. *ACS Synthetic Biology* **9,** 475–485. ISSN: 2161-5063. https://pubs.acs.org/doi/10.1021/acssynbio.9b00404 (2020).
39. Mitchell, A., Wei, P. & Lim, W. A. Oscillatory stress stimulation uncovers an Achilles heel of the yeast MAPK signaling network. *Science* **350,** 1379–1383. ISSN: 0036-8075. https://www.sciencemag.org/lookup/doi/10.1126/science.aab0892 (2015).
40. Rosener, B. *et al.* Evolved bacterial resistance against fluoropyrimidines can lower chemotherapy impact in the Caenorhabditis elegans host. *eLife* **9.** ISSN: 2050-084X. https://elifesciences.org/articles/59831 (2020).
41. You, L., Cox, R. S., Weiss, R. & Arnold, F. H. Programmed population control by cell–cell communication and regulated killing. *Nature* **428,** 868–871. ISSN: 0028-0836. http://www.nature.com/articles/nature02491 (2004).
42. Ghilardi, S. J., O'Reilly, B. M. & Sgro, A. E. Intracellular signaling dynamics and their role in coordinating tissue repair. *Wiley Interdisciplinary Reviews: Systems Biology and Medicine* **12,** e1479. ISSN: 19395094. http://doi.wiley.com/10.1002/wsbm.1479 (2020).
43. Sgro, A. E. *et al.* From intracellular signaling to population oscillations: bridging size- and time-scales in collective behavior. *Molecular Systems Biology* **11,** 779. ISSN: 1744-4292. https://onlinelibrary.wiley.com/doi/10.15252/msb.20145352 (2015).
44. Tarnita, C. E., Washburne, A., Martinez-Garcia, R., Sgro, A. E. & Levin, S. A. Fitness tradeoffs between spores and nonaggregating cells can explain the coexistence of diverse genotypes in cellular slime molds. *Proceedings of the National Academy of Sciences* **112,** 2776–2781. ISSN: 0027-8424. http://www.pnas.org/lookup/doi/10.1073/pnas.1424242112 (2015).
45. Gurdon, J. B. A community effect in animal development. *Nature* **336,** 772–774. ISSN: 0028-0836. http://www.nature.com/articles/336772a0 (1988).
46. Gurdon, J., Lemaire, P. & Kato, K. Community effects and related phenomena in development. *Cell* **75,** 831–834. ISSN: 00928674. https://linkinghub.elsevier.com/retrieve/pii/009286749390526V (1993).

47. Polonsky, M. *et al.* Induction of CD4 T cell memory by local cellular collectivity. *Science (New York, N.Y.)* **360.** ISSN: 10959203 (2018).
48. Miller, M. B. & Bassler, B. L. Quorum Sensing in Bacteria. *Annual Review of Microbiology* **55,** 165–199. ISSN: 0066-4227. http://www.annualreviews.org/doi/10.1146/annurev.micro.55.1.165 (2001).
49. Waters, C. M. & Bassler, B. L. QUORUM SENSING: Cell-to-Cell Communication in Bacteria. *Annual Review of Cell and Developmental Biology* **21,** 319–346. ISSN: 1081-0706. http://www.annualreviews.org/doi/10.1146/annurev.cellbio.21.012704.131001 (2005).
50. Papenfort, K. & Bassler, B. L. Quorum sensing signal–response systems in Gram-negative bacteria. *Nature Reviews Microbiology* **14,** 576–588. ISSN: 1740-1526. http://www.nature.com/articles/nrmicro.2016.89 (2016).
51. Laman Trip, D. S. & Youk, H. Yeasts collectively extend the limits of habitable temperatures by secreting glutathione. *Nature Microbiology* **5,** 943–954. ISSN: 2058-5276. http://www.nature.com/articles/s41564-020-0704-2 (2020).
52. Dal Co, A., van Vliet, S., Kiviet, D. J., Schlegel, S. & Ackermann, M. Short-range interactions govern the dynamics and functions of microbial communities. *Nature Ecology Evolution* **4.** ISSN: 2397-334X (2020).
53. Van Gestel, J. *et al.* Short-range quorum sensing controls horizontal gene transfer at micron scale in bacterial communities. *Nature Communications* **12,** 2324. ISSN: 2041-1723. http://www.nature.com/articles/s41467-021-22649-4 (2021).
54. Alladin, A. *et al.* Tracking cells in epithelial acini by light sheet microscopy reveals proximity effects in breast cancer initiation. *eLife* **9.** ISSN: 2050-084X. https://elifesciences.org/articles/54066 (2020).
55. Hodgkin, P., Rush, J, Gett, A., Bartell, G & Hasbold, J. The logic of intercellular communication in the immune system. *Immunology and Cell Biology* **76,** 448–453. ISSN: 08189641. http://doi.wiley.com/10.1046/j.1440-1711.1998.00776.x (1998).
56. Frankenstein, Z., Alon, U. & Cohen, I. R. The immune-body cytokine network defines a social architecture of cell interactions. *Biology direct* **1,** 32. ISSN: 1745-6150. http://www.ncbi.nlm.nih.gov/pubmed/17062134http://www.pubmedcentral.nih.gov/articlerender.fcgi?artid=PMC1636025 (2006).
57. Natsuaki, Y. *et al.* Perivascular leukocyte clusters are essential for efficient activation of effector T cells in the skin. *Nature Immunology* **15,** 1064–1069. ISSN: 1529-2908. http://www.nature.com/articles/ni.2992 (2014).
58. Hart, Y. *et al.* Paradoxical signaling by a secreted molecule leads to homeostasis of cell levels. *Cell* **158,** 1022–1032. ISSN: 10974172 (2014).

59. Hart, Y., Antebi, Y. E., Mayo, A. E., Friedman, N. & Alon, U. Design principles of cell circuits with paradoxical components. *Proceedings of the National Academy of Sciences* **109,** 8346–8351. ISSN: 0027-8424. http://www.pnas.org/cgi/doi/10.1073/pnas.1117475109 (2012).
60. Zhou, X. *et al.* Circuit Design Features of a Stable Two-Cell System. *Cell* **172,** 744–757.e17. ISSN: 10974172 (2018).
61. Adler, M. & Alon, U. *Fold-change detection in biological systems* 2018.
62. Thurley, K., Gerecht, D., Friedmann, E. & Höfer, T. Three-Dimensional Gradients of Cytokine Signaling between T Cells. *PLOS Computational Biology* **11** (ed Antia, R.) e1004206. ISSN: 1553-7358. https://dx.plos.org/10.1371/journal.pcbi.1004206 (2015).
63. Perona-Wright, G., Mohrs, K. & Mohrs, M. Sustained signaling by canonical helper T cell cytokines throughout the reactive lymph node. *Nature Immunology* **11,** 520–526. ISSN: 1529-2908. http://www.nature.com/articles/ni.1866 (2010).
64. Oyler-Yaniv, J. *et al.* Catch and Release of Cytokines Mediated by Tumor Phosphatidylserine Converts Transient Exposure into Long-Lived Inflammation. *Molecular Cell* **66,** 635–647.e7. ISSN: 10974164 (2017).
65. Oyler-Yaniv, A. *et al.* A Tunable Diffusion-Consumption Mechanism of Cytokine Propagation Enables Plasticity in Cell-to-Cell Communication in the Immune System. *Immunity* **46,** 609–620. ISSN: 10747613. https://linkinghub.elsevier.com/retrieve/pii/S1074761317300924 (2017).
66. Voisinne, G. *et al.* T Cells Integrate Local and Global Cues to Discriminate between Structurally Similar Antigens. *Cell Reports* **11,** 1208–1219. ISSN: 22111247 (2015).
67. Chen, C.-C. *et al.* Organ-Level Quorum Sensing Directs Regeneration in Hair Stem Cell Populations. *Cell* **161,** 277–290. ISSN: 00928674. https://linkinghub.elsevier.com/retrieve/pii/S0092867415001828 (2015).
68. Tischer, D. K. & Weiner, O. D. Light-based tuning of ligand half-life supports kinetic proofreading model of T cell signaling. *eLife* **8.** ISSN: 2050-084X. https://elifesciences.org/articles/42498 (2019).
69. Feinerman, O. *et al.* Single-cell quantification of IL-2 response by effector and regulatory T cells reveals critical plasticity in immune response. *Molecular Systems Biology* **6,** 437. ISSN: 1744-4292. https://onlinelibrary.wiley.com/doi/10.1038/msb.2010.90 (2010).
70. Ma, Q., Wang, Y., Lo, A. S.-Y., Gomes, E. M. & Junghans, R. P. Cell Density Plays a Critical Role in Ex Vivo Expansion of T Cells for Adoptive Immunotherapy. *Journal of Biomedicine and Biotechnology* **2010,** 1–13. ISSN: 1110-7243. http://www.hindawi.com/journals/bmri/2010/386545/ (2010).

71. Busse, D. *et al.* Competing feedback loops shape IL-2 signaling between helper and regulatory T lymphocytes in cellular microenvironments. *Proceedings of the National Academy of Sciences* **107,** 3058–3063. ISSN: 0027-8424. http://www.pnas.org/cgi/doi/10.1073/pnas.0812851107 (2010).
72. Gett, A. V. & Hodgkin, P. D. A cellular calculus for signal integration by T cells. *Nature Immunology* **1,** 239–244. ISSN: 1529-2908. http://www.nature.com/articles/ni0900_239 (2000).
73. Burroughs, N., Miguel Paz Mendes de Oliveira, B. & Adrego Pinto, A. Regulatory T cell adjustment of quorum growth thresholds and the control of local immune responses. *Journal of Theoretical Biology* **241,** 134–141. ISSN: 00225193. https://linkinghub.elsevier.com/retrieve/pii/S0022519305004959 (2006).
74. Almeida, A. R. M. *et al.* Quorum-Sensing in CD4+ T Cell Homeostasis: A Hypothesis and a Model. *Frontiers in Immunology* **3.** ISSN: 1664-3224. http://journal.frontiersin.org/article/10.3389/fimmu.2012.00125/abstract (2012).
75. Butler, T. C., Kardar, M. & Chakraborty, A. K. Quorum sensing allows T cells to discriminate between self and nonself. *Proceedings of the National Academy of Sciences* **110,** 11833–11838. ISSN: 0027-8424. http://www.pnas.org/cgi/doi/10.1073/pnas.1222467110 (2013).
76. Marchingo, J. M. *et al.* Antigen affinity, costimulation, and cytokine inputs sum linearly to amplify T cell expansion. *Science* **346,** 1123–1127. ISSN: 0036-8075. https://www.sciencemag.org/lookup/doi/10.1126/science.1260044 (2014).
77. Tkach, K. E. *et al.* T cells translate individual, quantal activation into collective, analog cytokine responses via time-integrated feedbacks. *eLife* **3.** ISSN: 2050-084X. https://elifesciences.org/articles/01944 (2014).
78. Hopfield, J. J. Kinetic Proofreading: A New Mechanism for Reducing Errors in Biosynthetic Processes Requiring High Specificity. *Proceedings of the National Academy of Sciences* **71,** 4135–4139. ISSN: 0027-8424. http://www.pnas.org/cgi/doi/10.1073/pnas.71.10.4135 (1974).
79. Ninio, J. Kinetic amplification of enzyme discrimination. *Biochimie* **57,** 587–595. ISSN: 03009084. https://linkinghub.elsevier.com/retrieve/pii/S0300908475801398 (1975).
80. Germain, R. N. & Stefanová, I. THE DYNAMICS OF T CELL RECEPTOR SIGNALING: Complex Orchestration and the Key Roles of Tempo and Cooperation. *Annual Review of Immunology* **17,** 467–522. ISSN: 0732-0582. http://www.annualreviews.org/doi/10.1146/annurev.immunol.17.1.467 (1999).
81. Gascoigne, N. R., Zal, T. & Alam, S. M. T-cell receptor binding kinetics in T-cell development and activation. *Expert Reviews in Molecular Medicine* **3,**

1–17. ISSN: 1462-3994. https://www.cambridge.org/core/product/identifier/S1462399401002502/type/journal_article (2001).

82. Yousefi, O. S. *et al.* Optogenetic control shows that kinetic proofreading regulates the activity of the T cell receptor. *eLife* **8.** ISSN: 2050-084X. https://elifesciences.org/articles/42475 (2019).
83. McKeithan, T. W. Kinetic proofreading in T-cell receptor signal transduction. *Proceedings of the National Academy of Sciences* **92,** 5042–5046. ISSN: 0027-8424. http://www.pnas.org/cgi/doi/10.1073/pnas.92.11.5042 (1995).
84. Le, K. Y. & Otto, M. Quorum-sensing regulation in staphylococci—an overview. *Frontiers in Microbiology* **6.** ISSN: 1664-302X. http://journal.frontiersin.org/Article/10.3389/fmicb.2015.01174/abstract (2015).
85. Abtin, A. *et al.* Perivascular macrophages mediate neutrophil recruitment during bacterial skin infection. *Nature Immunology* **15,** 45–53. ISSN: 1529-2908. http://www.nature.com/articles/ni.2769 (2014).
86. Lee, S. & Margolin, K. Cytokines in Cancer Immunotherapy. *Cancers* **3,** 3856–3893. ISSN: 2072-6694. http://www.mdpi.com/2072-6694/3/4/3856 (2011).
87. Lim, W. A. & June, C. H. The Principles of Engineering Immune Cells to Treat Cancer. *Cell* **168,** 724–740. ISSN: 00928674. https://linkinghub.elsevier.com/retrieve/pii/S0092867417300648 (2017).
88. Labanieh, L., Majzner, R. G. & Mackall, C. L. Programming CAR-T cells to kill cancer. *Nature Biomedical Engineering* **2,** 377–391. ISSN: 2157-846X. http://www.nature.com/articles/s41551-018-0235-9 (2018).
89. Holm, A. & VikstrÃ¶m, E. Quorum sensing communication between bacteria and human cells: signals, targets, and functions. *Frontiers in Plant Science* **5.** ISSN: 1664-462X. http://journal.frontiersin.org/article/10.3389/fpls.2014.00309/abstract (2014).
90. Kolaczkowska, E. & Kubes, P. Neutrophil recruitment and function in health and inflammation. *Nature Reviews Immunology* **13,** 159–175. ISSN: 1474-1733. http://www.nature.com/articles/nri3399 (2013).
91. Lämmermann, T. *et al.* Neutrophil swarms require LTB4 and integrins at sites of cell death in vivo. *Nature* **498,** 371–375. ISSN: 0028-0836. http://www.nature.com/articles/nature12175 (2013).
92. TILL, J. E. & McCULLOCH, E. A. A direct measurement of the radiation sensitivity of normal mouse bone marrow cells. *Radiation research* **14,** 213–22. ISSN: 0033-7587. http://www.ncbi.nlm.nih.gov/pubmed/13776896 (1961).
93. BECKER, A. J., McCULLOCH, E. A. & TILL, J. E. Cytological Demonstration of the Clonal Nature of Spleen Colonies Derived from Transplanted Mouse

Marrow Cells. *Nature* **197,** 452–454. ISSN: 0028-0836. http://www.nature.com/articles/197452a0 (1963).

94. Till, J. E., McCulloch, E. A. & Siminovitch, L. A STOCHASTIC MODEL OF STEM CELL PROLIFERATION, BASED ON THE GROWTH OF SPLEEN COLONY-FORMING CELLS. *Proceedings of the National Academy of Sciences* **51,** 29–36. ISSN: 0027-8424. http://www.pnas.org/cgi/doi/10.1073/pnas.51.1.29 (1964).
95. Barker, N. *et al.* Identification of stem cells in small intestine and colon by marker gene Lgr5. *Nature* **449,** 1003–1007. ISSN: 0028-0836. http://www.nature.com/articles/nature06196 (2007).
96. Bonaguidi, M. A. *et al.* In Vivo Clonal Analysis Reveals Self-Renewing and Multipotent Adult Neural Stem Cell Characteristics. *Cell* **145,** 1142–1155. ISSN: 00928674. https://linkinghub.elsevier.com/retrieve/pii/S009286741100585X (2011).
97. Encinas, J. M. *et al.* Division-Coupled Astrocytic Differentiation and Age-Related Depletion of Neural Stem Cells in the Adult Hippocampus. *Cell Stem Cell* **8,** 566–579. ISSN: 19345909. https://linkinghub.elsevier.com/retrieve/pii/S1934590911001202 (2011).
98. Stevens, L. C. & Little, C. C. Spontaneous Testicular Teratomas in an Inbred Strain of Mice. *Proceedings of the National Academy of Sciences* **40,** 1080–1087. ISSN: 0027-8424. http://www.pnas.org/cgi/doi/10.1073/pnas.40.11.1080 (1954).
99. Martin, G. R. Isolation of a pluripotent cell line from early mouse embryos cultured in medium conditioned by teratocarcinoma stem cells. *Proceedings of the National Academy of Sciences* **78,** 7634–7638. ISSN: 0027-8424. http://www.pnas.org/cgi/doi/10.1073/pnas.78.12.7634 (1981).
100. Evans, M. J. & Kaufman, M. H. Establishment in culture of pluripotential cells from mouse embryos. *Nature* **292,** 154–156. ISSN: 0028-0836. http://www.nature.com/articles/292154a0 (1981).
101. Pauklin, S., Pedersen, R. A. & Vallier, L. Mouse pluripotent stem cells at a glance. *Journal of Cell Science* **124,** 3727–3732. ISSN: 1477-9137. https://journals.biologists.com/jcs/article/124/22/3727/64640/Mouse-pluripotent-stem-cells-at-a-glance (2011).
102. Hayashi, K., de Sousa Lopes, S. M. C. & Surani, M. A. Germ Cell Specification in Mice. *Science* **316,** 394–396. ISSN: 0036-8075. https://www.sciencemag.org/lookup/doi/10.1126/science.1137545 (2007).
103. Bateson, P. & Gluckman, P. Plasticity and robustness in development and evolution. *International Journal of Epidemiology* **41,** 219–223. ISSN: 0300-5771. https://academic.oup.com/ije/article-lookup/doi/10.1093/ije/dyr240 (2012).

104. Cockburn, K. & Rossant, J. Making the blastocyst: lessons from the mouse. *Journal of Clinical Investigation* **120,** 995–1003. ISSN: 0021-9738. http://www.jci.org/articles/view/41229 (2010).
105. Thomson, J. A. Embryonic Stem Cell Lines Derived from Human Blastocysts. *Science* **282,** 1145–1147. https://www.sciencemag.org/lookup/doi/10.1126/science.282.5391.1145 (1998).
106. Shamblott, M. J. *et al.* Derivation of pluripotent stem cells from cultured human primordial germ cells. *Proceedings of the National Academy of Sciences* **95,** 13726–13731. ISSN: 0027-8424. http://www.pnas.org/cgi/doi/10.1073/pnas.95.23.13726 (1998).
107. Ohtsuka, S., Nakai-Futatsugi, Y. & Niwa, H. LIF signal in mouse embryonic stem cells. *JAK-STAT*. ISSN: 2162-3996. arXiv: arXiv:1011.1669v3 (2015).
108. Nichols, J., Chambers, I., Taga, T. & Smith, A. Physiological rationale for responsiveness of mouse embryonic stem cells to gp130 cytokines. *Development* **128,** 2333–2339. ISSN: 1477-9129. https://journals.biologists.com/dev/article/128/12/2333/41276/Physiological-rationale-for-responsiveness-of (2001).
109. Jaenisch, R. & Young, R. Stem Cells, the Molecular Circuitry of Pluripotency and Nuclear Reprogramming. *Cell* **132,** 567–582. ISSN: 00928674. https://linkinghub.elsevier.com/retrieve/pii/S0092867408001153 (2008).
110. Gagliardi, P. A. *et al.* Collective ERK/Akt activity waves orchestrate epithelial homeostasis by driving apoptosis-induced survival. *Developmental Cell*. ISSN: 15345807. https://linkinghub.elsevier.com/retrieve/pii/S1534580721004366 (2021).
111. Gross, V. S., Hess, M. & Cooper, G. M. Mouse embryonic stem cells and preimplantation embryos require signaling through the phosphatidylinositol 3-kinase pathway to suppress apoptosis. *Molecular Reproduction and Development* **70,** 324–332. ISSN: 1040452X (2005).
112. O'Neill, C. The potential roles for embryotrophic ligands in preimplantation embryo development. *Human Reproduction Update* **14,** 275–288. ISSN: 1460-2369. http://academic.oup.com/humupd/article/14/3/275/682900/The-potential-roles-for-embryotrophic-ligands-in (2008).
113. O'Neill, C. Phosphatidylinositol 3-kinase signaling in mammalian preimplantation embryo development. *REPRODUCTION* **136,** 147–156. ISSN: 1470-1626. https://rep.bioscientifica.com/view/journals/rep/136/2/147.xml (2008).
114. Niwa, H., Miyazaki, J.-i. & Smith, A. G. Quantitative expression of Oct-3/4 defines differentiation, dedifferentiation or self-renewal of ES cells. *Nature Genetics* **24,** 372–376. ISSN: 1061-4036. http://www.nature.com/articles/ng0400_372 (2000).

115. Chambers, I. *et al.* Nanog safeguards pluripotency and mediates germline development. *Nature* **450,** 1230–1234. ISSN: 0028-0836. http://www.nature.com/articles/nature06403 (2007).
116. Silva, J. *et al.* Promotion of Reprogramming to Ground State Pluripotency by Signal Inhibition. *PLoS Biology* **6** (ed Goodell, M. A.) e253. ISSN: 1545-7885. https://dx.plos.org/10.1371/journal.pbio.0060253 (2008).
117. Gawlik-Rzemieniewska, N. & Bednarek, I. The role of NANOG transcriptional factor in the development of malignant phenotype of cancer cells. *Cancer Biology Therapy* **17,** 1–10. ISSN: 1538-4047. http://www.tandfonline.com/doi/full/10.1080/15384047.2015.1121348 (2016).
118. Kalmar, T. *et al.* Regulated Fluctuations in Nanog Expression Mediate Cell Fate Decisions in Embryonic Stem Cells. *PLoS Biology* **7** (ed Goodell, M. A.) e1000149. ISSN: 1545-7885. https://dx.plos.org/10.1371/journal.pbio.1000149 (2009).
119. Thomson, M. *et al.* Pluripotency Factors in Embryonic Stem Cells Regulate Differentiation into Germ Layers. *Cell* **145,** 875–889. ISSN: 00928674. https://linkinghub.elsevier.com/retrieve/pii/S0092867411005435 (2011).
120. Wong, C.-W. *et al.* Krüppel-Like Transcription Factor 4 Contributes to Maintenance of Telomerase Activity in Stem Cells. *STEM CELLS* **28,** 1510–1517. ISSN: 10665099. http://doi.wiley.com/10.1002/stem.477 (2010).
121. Cartwright, P. LIF/STAT3 controls ES cell self-renewal and pluripotency by a Myc-dependent mechanism. *Development.* ISSN: 0950-1991 (2005).
122. Scognamiglio, R. *et al.* Myc Depletion Induces a Pluripotent Dormant State Mimicking Diapause. *Cell* **164,** 668–680. ISSN: 10974172 (2016).
123. Díaz-Díaz, C. *et al.* Pluripotency Surveillance by Myc-Driven Competitive Elimination of Differentiating Cells. *Developmental Cell* **42,** 585–599.e4. ISSN: 15345807. https://linkinghub.elsevier.com/retrieve/pii/S1534580717306718 (2017).
124. Takahashi, K. & Yamanaka, S. Induction of Pluripotent Stem Cells from Mouse Embryonic and Adult Fibroblast Cultures by Defined Factors. *Cell* **126,** 663–676. ISSN: 00928674. https://linkinghub.elsevier.com/retrieve/pii/S0092867406009767 (2006).
125. Takahashi, K. *et al.* Induction of Pluripotent Stem Cells from Adult Human Fibroblasts by Defined Factors. *Cell* **131,** 861–872. ISSN: 00928674. https://linkinghub.elsevier.com/retrieve/pii/S0092867407014717 (2007).
126. Ying, Q. L. & Smith, A. G. *Defined Conditions for Neural Commitment and Differentiation* 2003.
127. Chang, H. H., Hemberg, M., Barahona, M., Ingber, D. E. & Huang, S. Transcriptome-wide noise controls lineage choice in mammalian progenitor cells. *Nature* **453,** 544–547. ISSN: 0028-0836. http://www.nature.com/articles/nature06965 (2008).

128. Lu, R. *et al.* Systems-level dynamic analyses of fate change in murine embryonic stem cells. *Nature.* ISSN: 0028-0836. arXiv: NIHMS150003 (2009).
129. Lu, J. *et al.* All-trans retinoic acid promotes neural lineage entry by pluripotent embryonic stem cells via multiple pathways. *BMC Cell Biology* **10,** 57. ISSN: 1471-2121. http://bmccellbiol.biomedcentral.com/articles/10.1186/1471-2121-10-57 (2009).
130. MacArthur, B. D., Ma'ayan, A. & Lemischka, I. R. Systems biology of stem cell fate and cellular reprogramming. *Nature Reviews Molecular Cell Biology.* ISSN: 1471-0072. arXiv: NIHMS150003 (2009).
131. Burdon, T., Smith, A. & Savatier, P. *Signalling, cell cycle and pluripotency in embryonic stem cells* 2002. arXiv: NIHMS150003.
132. Kosaka, N., Sakamoto, H., Terada, M. & Ochiya, T. Pleiotropic function of FGF-4: Its role in development and stem cells. *Developmental Dynamics* **238,** 265–276. ISSN: 10588388. http://doi.wiley.com/10.1002/dvdy.21699 (2009).
133. Kunath, T. *et al.* FGF stimulation of the Erk1/2 signalling cascade triggers transition of pluripotent embryonic stem cells from self-renewal to lineage commitment. *Development.* ISSN: 0950-1991 (2007).
134. Thisse, B. & Thisse, C. Functions and regulations of fibroblast growth factor signaling during embryonic development. *Developmental Biology* **287,** 390–402. ISSN: 00121606. https://linkinghub.elsevier.com/retrieve/pii/S0012160605006184 (2005).
135. Ornitz, D. M. & Itoh, N. The Fibroblast Growth Factor signaling pathway. *Wiley Interdisciplinary Reviews: Developmental Biology* **4,** 215–266. ISSN: 17597684. http://doi.wiley.com/10.1002/wdev.176 (2015).
136. Mossahebi-Mohammadi, M., Quan, M., Zhang, J.-S. & Li, X. FGF Signaling Pathway: A Key Regulator of Stem Cell Pluripotency. *Frontiers in Cell and Developmental Biology* **8.** ISSN: 2296-634X. https://www.frontiersin.org/article/10.3389/fcell.2020.00079/full (2020).
137. Gadue, P., Huber, T. L., Paddison, P. J. & Keller, G. M. Wnt and TGF-beta signaling are required for the induction of an in vitro model of primitive streak formation using embryonic stem cells. *Proceedings of the National Academy of Sciences* **103,** 16806–16811. ISSN: 0027-8424. http://www.pnas.org/cgi/doi/10.1073/pnas.0603916103 (2006).
138. Augustin, I. *et al.* Autocrine Wnt regulates the survival and genomic stability of embryonic stem cells. *Science Signaling.* ISSN: 19379145 (2017).
139. Yamaguchi, T. P., Takada, S., Yoshikawa, Y., Wu, N. & McMahon, A. P. T (Brachyury) is a direct target of Wnt3a during paraxial mesoderm specification. *Genes Development* **13,** 3185–3190. ISSN: 0890-9369. http://www.genesdev.org/cgi/doi/10.1101/gad.13.24.3185 (1999).

140. Habib, S. J. *et al.* A Localized Wnt Signal Orients Asymmetric Stem Cell Division in Vitro. *Science* **339,** 1445–1448. ISSN: 0036-8075. https://www.sciencemag.org/lookup/doi/10.1126/science.1231077 (2013).
141. Bashamboo, A. *et al.* The survival of differentiating embryonic stem cells is dependent on the SCF-KIT pathway. *Journal of Cell Science* **119,** 3039–3046. ISSN: 1477-9137. https://journals.biologists.com/jcs/article/119/15/3039/29092/The-survival-of-differentiating-embryonic-stem (2006).
142. Lim, J. J. *et al.* Stem cell factor/c-Kit signaling in in vitro cultures supports early mouse embryonic development by accelerating proliferation via a mechanism involving Akt-downstream genes. *Journal of Assisted Reproduction and Genetics.* ISSN: 10580468 (2010).
143. Fraser, L., Taylor, A. H. & Forrester, L. M. SCF/KIT Inhibition Has a Cumulative but Reversible Effect on the Self-Renewal of Embryonic Stem Cells and on the Survival of Differentiating Cells. *Cellular Reprogramming* **15,** 259–268. ISSN: 2152-4971. http://www.liebertpub.com/doi/10.1089/cell.2013.0015 (2013).
144. Babaei, M. A., Kamalidehghan, B., Saleem, M., Huri, H. Z. & Ahmadipour, F. *Receptor tyrosine kinase (c-Kit) inhibitors: A potential therapeutic target in cancer cells* 2016.
145. Cai, C., Thorne, J. & Grabel, L. Hedgehog Serves as a Mitogen and Survival Factor During Embryonic Stem Cell Neurogenesis. *Stem Cells* **26,** 1097–1108. ISSN: 10665099 (2008).
146. Ying, Q.-L., Nichols, J., Chambers, I. & Smith, A. BMP Induction of Id Proteins Suppresses Differentiation and Sustains Embryonic Stem Cell Self-Renewal in Collaboration with STAT3. *Cell* **115,** 281–292. ISSN: 00928674. https://linkinghub.elsevier.com/retrieve/pii/S009286740300847X (2003).
147. Chaigne, A. *et al.* Abscission Couples Cell Division to Embryonic Stem Cell Fate. *Developmental Cell* **55,** 195–208.e5. ISSN: 15345807. https://linkinghub.elsevier.com/retrieve/pii/S1534580720306717 (2020).
148. Meier, P., Finch, A. & Evan, G. Apoptosis in development. *Nature* **407,** 796–801. ISSN: 00280836 (2000).
149. O'Neill, C., Li, Y. & Jin, X. L. Survival signalling in the preimplantation embryo. *Advances in Experimental Medicine and Biology* **843,** 129–149. ISSN: 22148019 (2015).
150. Corominas-Murtra, B. *et al.* Stem cell lineage survival as a noisy competition for niche access. *Proceedings of the National Academy of Sciences* **117,** 16969–16975. ISSN: 0027-8424. http://www.pnas.org/lookup/doi/10.1073/pnas.1921205117 (2020).

151. Lin, T. *et al.* p53 induces differentiation of mouse embryonic stem cells by suppressing Nanog expression. *Nature Cell Biology* **7,** 165–171. ISSN: 1465-7392. http://www.nature.com/articles/ncb1211 (2005).
152. Cheung, T. H. & Rando, T. A. Molecular regulation of stem cell quiescence. *Nature Reviews Molecular Cell Biology* **14,** 329–340. ISSN: 14710072. http://dx.doi.org/10.1038/nrm3591 (2013).
153. Bulut-Karslioglu, A. *et al.* Inhibition of mTOR induces a paused pluripotent state. *Nature* **540,** 119–123. ISSN: 14764687. http://dx.doi.org/10.1038/nature20578 (2016).
154. Barry, E. R. & Camargo, F. D. The Hippo superhighway: signaling crossroads converging on the Hippo/Yap pathway in stem cells and development. *Current Opinion in Cell Biology* **25,** 247–253. ISSN: 09550674. https://linkinghub.elsevier.com/retrieve/pii/S095506741200213X (2013).
155. Deglincerti, A. *et al.* Self-organization of the in vitro attached human embryo. *Nature* **533,** 251–254. ISSN: 0028-0836. http://www.nature.com/articles/nature17948 (2016).
156. Ellison, D., Munden, A. & Levchenko, A. Computational model and microfluidic platform for the investigation of paracrine and autocrine signaling in mouse embryonic stem cells. *Molecular BioSystems.* ISSN: 1742206X (2009).
157. Przybyla, L. & Voldman, J. Probing Embryonic Stem Cell Autocrine and Paracrine Signaling Using Microfluidics. *Annual Review of Analytical Chemistry* **5,** 293–315. ISSN: 1936-1327. http://www.annualreviews.org/doi/10.1146/annurev-anchem-062011-143122 (2012).
158. Saiz, N. *et al.* Growth-factor-mediated coupling between lineage size and cell fate choice underlies robustness of mammalian development. *eLife* **9.** ISSN: 2050-084X (2020).
159. Bauwens, C. L. *et al.* Control of Human Embryonic Stem Cell Colony and Aggregate Size Heterogeneity Influences Differentiation Trajectories. *Stem Cells* **26,** 2300–2310. ISSN: 10665099. http://doi.wiley.com/10.1634/stemcells.2008-0183 (2008).
160. Keller, G. Embryonic stem cell differentiation: emergence of a new era in biology and medicine. *Genes Development* **19,** 1129–1155. ISSN: 0890-9369. http://www.genesdev.org/cgi/doi/10.1101/gad.1303605 (2005).
161. Daneshmandi, L. *et al.* Emergence of the Stem Cell Secretome in Regenerative Engineering. *Trends in Biotechnology* **38,** 1373–1384. ISSN: 01677799. https://linkinghub.elsevier.com/retrieve/pii/S0167779920301189 (2020).
162. Kim, R.-J. & Nam, J.-S. OCT4 Expression Enhances Features of Cancer Stem Cells in a Mouse Model of Breast Cancer. *Laboratory Animal Research* **27,**

147. ISSN: 1738-6055. https://synapse.koreamed.org/DOIx.php?id=10.5625/lar.2011.27.2.147 (2011).

163. Ngangan, A. V., Waring, J. C., Cooke, M. T., Mandrycky, C. J. & McDevitt, T. C. Soluble factors secreted by differentiating embryonic stem cells stimulate exogenous cell proliferation and migration. *Stem Cell Research and Therapy* **5.** ISSN: 17576512 (2014).

164. Maire, T. & Youk, H. Molecular-Level Tuning of Cellular Autonomy Controls the Collective Behaviors of Cell Populations. *Cell Systems* **1.** ISSN: 24054712 (2015).

165. Wilder, P. J. *et al.* Inactivation of the FGF-4 gene in embryonic stem cells alters the growth and/or the survival of their early differentiated progeny. *Developmental Biology.* ISSN: 00121606 (1997).

166. Kook, S.-H. *et al.* Fibroblast Growth Factor-4 Enhances Proliferation of Mouse Embryonic Stem Cells via Activation of c-Jun Signaling. *PLoS ONE.* ISSN: 1932-6203 (2013).

167. Raina, D. *et al.* Cell-cell communication through FGF4 generates and maintains robust proportions of differentiated cell fates in embryonic stem cells. *BioRxiv* (2020).

168. Mistri, T. K. *et al.* Dynamic changes in Sox2 spatio-temporal expression promote the second cell fate decision through Fgf4/Fgfr2 signaling in preimplantation mouse embryos. *Biochemical Journal* **475.** ISSN: 0264-6021 (2018).

169. Liu, G., David, B. T., Trawczynski, M. & Fessler, R. G. Advances in Pluripotent Stem Cells: History, Mechanisms, Technologies, and Applications. *Stem Cell Reviews and Reports* **16.** ISSN: 2629-3269 (2020).

170. Phadnis, S. M. *et al.* Dynamic and social behaviors of human pluripotent stem cells. *Scientific Reports.* ISSN: 20452322 (2015).

171. Mulas, C. *et al.* Defined conditions for propagation and manipulation of mouse embryonic stem cells. *Development* **146.** ISSN: 1477-9129. https://journals.biologists.com/dev/article/146/6/dev173146/49077/Defined-conditions-for-propagation-and (2019).

172. Fehling, H. J. *et al.* Tracking mesoderm induction and its specification to the hemangioblast during embryonic stem cell differentiation. *Development* **130,** 4217–4227. ISSN: 1477-9129. https://journals.biologists.com/dev/article/130/17/4217/52278/Tracking-mesoderm-induction-and-its-specification (2003).

173. Pearson, S., Cuvertino, S., Fleury, M., Lacaud, G. & Kouskoff, V. In Vivo Repopulating Activity Emerges at the Onset of Hematopoietic Specification during Embryonic Stem Cell Differentiation. *Stem Cell Reports* **4,** 431–444. ISSN: 22136711. https://linkinghub.elsevier.com/retrieve/pii/S2213671115000247 (2015).

174. Nichols, J. *et al.* Formation of Pluripotent Stem Cells in the Mammalian Embryo Depends on the POU Transcription Factor Oct4. *Cell* **95,** 379–391. ISSN: 00928674. https://linkinghub.elsevier.com/retrieve/pii/S0092867400817699 (1998).
175. Dieterich, P., Klages, R., Preuss, R. & Schwab, A. Anomalous dynamics of cell migration. *Proceedings of the National Academy of Sciences* **105,** 459–463. ISSN: 0027-8424. http://www.pnas.org/cgi/doi/10.1073/pnas.0707603105 (2008).
176. Luzhansky, I. D. *et al.* Anomalously diffusing and persistently migrating cells in 2D and 3D culture environments. *APL Bioengineering* **2,** 026112. ISSN: 2473-2877. http://aip.scitation.org/doi/10.1063/1.5019196 (2018).
177. LeBlanc, L. *et al.* Yap1 safeguards mouse embryonic stem cells from excessive apoptosis during differentiation. *eLife* **7.** ISSN: 2050-084X. https://elifesciences.org/articles/40167 (2018).
178. Mugahid, D. *et al.* YAP regulates cell size and growth dynamics via non-cell autonomous mediators. *eLife* **9.** ISSN: 2050-084X. https://elifesciences.org/articles/53404 (2020).
179. Vigneron, A. M. & Vousden, K. H. An indirect role for ASPP1 in limiting p53-dependent p21 expression and cellular senescence. *The EMBO Journal* **31,** 471–480. ISSN: 02614189. http://emboj.embopress.org/cgi/doi/10.1038/emboj.2011.402 (2012).
180. Kim, M., Kim, T., Johnson, R. L. & Lim, D.-S. Transcriptional Co-repressor Function of the Hippo Pathway Transducers YAP and TAZ. *Cell Reports* **11,** 270–282. ISSN: 22111247. https://linkinghub.elsevier.com/retrieve/pii/S2211124715002685 (2015).
181. Zhou, Y. *et al.* The TEAD Family and Its Oncogenic Role in Promoting Tumorigenesis. *International Journal of Molecular Sciences* **17,** 138. ISSN: 1422-0067. http://www.mdpi.com/1422-0067/17/1/138 (2016).
182. Yu, O. M. *et al.* YAP and MRTF-A, transcriptional co-activators of RhoA-mediated gene expression, are critical for glioblastoma tumorigenicity. *Oncogene* **37,** 5492–5507. ISSN: 0950-9232. http://www.nature.com/articles/s41388-018-0301-5 (2018).
183. Zhu, Q. *et al.* The transcription factor Pou3f1 promotes neural fate commitment via activation of neural lineage genes and inhibition of external signaling pathways. *eLife* **3.** ISSN: 2050-084X. https://elifesciences.org/articles/02224 (2014).
184. Huh, H., Kim, D., Jeong, H.-S. & Park, H. Regulation of TEAD Transcription Factors in Cancer Biology. *Cells* **8,** 600. ISSN: 2073-4409. https://www.mdpi.com/2073-4409/8/6/600 (2019).
185. Varelas, X. The Hippo pathway effectors TAZ and YAP in development, homeostasis and disease. *Development* **141,** 1614–1626. ISSN: 1477-9129. https:

//journals.biologists.com/dev/article/141/8/1614/46642/The-Hippo-pathway-effectors-TAZ-and-YAP-in (2014).

186. Chung, H. *et al.* Yap1 is dispensable for self-renewal but required for proper differentiation of mouse embryonic stem (<scp>ES</scp>) cells. *EMBO reports* **17,** 519–529. ISSN: 1469-221X. https://onlinelibrary.wiley.com/doi/10.15252/embr.201540933 (2016).
187. Walko, G. *et al.* A genome-wide screen identifies YAP/WBP2 interplay conferring growth advantage on human epidermal stem cells. *Nature Communications* **8,** 14744. ISSN: 2041-1723. http://www.nature.com/articles/ncomms14744 (2017).
188. Hartman, A. A. *et al.* YAP Non-cell-autonomously Promotes Pluripotency Induction in Mouse Cells. *Stem Cell Reports* **14,** 730–743. ISSN: 22136711. https://linkinghub.elsevier.com/retrieve/pii/S2213671120300965 (2020).
189. Brodowska, K. *et al.* The clinically used photosensitizer Verteporfin (VP) inhibits YAP-TEAD and human retinoblastoma cell growth in vitro without light activation. *Experimental Eye Research* **124,** 67–73. ISSN: 00144835. https://linkinghub.elsevier.com/retrieve/pii/S0014483514001079 (2014).
190. Moon, S. *et al.* Phosphorylation by <scp>NLK</scp> inhibits <scp>YAP</scp> -14-3-3-interactions and induces its nuclear localization. *EMBO reports* **18,** 61–71. ISSN: 1469-221X. https://onlinelibrary.wiley.com/doi/10.15252/embr.201642683 (2017).
191. Mittal, N. & Voldman, J. Nonmitogenic survival-enhancing autocrine factors including cyclophilin A contribute to density-dependent mouse embryonic stem cell growth. *Stem Cell Research.* ISSN: 18735061. arXiv: NIHMS150003 (2011).
192. Mohammadi, M. Crystal structure of an angiogenesis inhibitor bound to the FGF receptor tyrosine kinase domain. *The EMBO Journal* **17,** 5896–5904. ISSN: 14602075. http://emboj.embopress.org/cgi/doi/10.1093/emboj/17.20.5896 (1998).
193. Bateman, A. *et al.* UniProt: the universal protein knowledgebase in 2021. *Nucleic Acids Research* **49,** D480–D489. ISSN: 0305-1048. https://academic.oup.com/nar/article/49/D1/D480/6006196 (2021).
194. Artimo, P. *et al.* ExPASy: SIB bioinformatics resource portal. *Nucleic Acids Research* **40,** W597–W603. ISSN: 0305-1048. https://academic.oup.com/nar/article-lookup/doi/10.1093/nar/gks400 (2012).
195. Milo, R., Jorgensen, P., Moran, U., Weber, G. & Springer, M. BioNumbers—the database of key numbers in molecular and cell biology. *Nucleic Acids Research* **38,** D750–D753. ISSN: 0305-1048. https://academic.oup.com/nar/article-lookup/doi/10.1093/nar/gkp889 (2010).

196. Tosolini, M. & Jouneau, A. in, 41–48 (2015). http://link.springer.com/10.1007/7651_2015_207.
197. Ying, Q.-L. & Smith, A. The Art of Capturing Pluripotency: Creating the Right Culture. *Stem Cell Reports* **8,** 1457–1464. ISSN: 22136711. https://linkinghub.elsevier.com/retrieve/pii/S2213671117302278 (2017).
198. Brewer, G. J., Torricelli, J. R., Evege, E. K. & Price, P. J. Optimized survival of hippocampal neurons in B27-supplemented neurobasal?, a new serum-free medium combination. *Journal of Neuroscience Research* **35,** 567–576. ISSN: 0360-4012. http://doi.wiley.com/10.1002/jnr.490350513 (1993).
199. Trapnell, C. *et al.* Differential gene and transcript expression analysis of RNA-seq experiments with TopHat and Cufflinks. *Nature Protocols* **7,** 562–578. ISSN: 1754-2189. http://www.nature.com/articles/nprot.2012.016 (2012).
200. Thomas, P. D. PANTHER: A Library of Protein Families and Subfamilies Indexed by Function. *Genome Research* **13,** 2129–2141. ISSN: 1088-9051. http://www.genome.org/cgi/doi/10.1101/gr.772403 (2003).
201. Thomas, P. D. *et al.* Applications for protein sequence-function evolution data: mRNA/protein expression analysis and coding SNP scoring tools. *Nucleic Acids Research* **34,** W645–W650. ISSN: 0305-1048. https://academic.oup.com/nar/article-lookup/doi/10.1093/nar/gkl229 (2006).
202. Mi, H. *et al.* PANTHER version 7: improved phylogenetic trees, orthologs and collaboration with the Gene Ontology Consortium. *Nucleic Acids Research* **38,** D204–D210. ISSN: 0305-1048. https://academic.oup.com/nar/article-lookup/doi/10.1093/nar/gkp1019 (2010).
203. GURDON, J. B. Factors responsible for the abnormal development of embryos obtained by nuclear transplantation in Xenopus laevis. *Journal of embryology and experimental morphology* **8,** 327–40. ISSN: 0022-0752. http://www.ncbi.nlm.nih.gov/pubmed/13709841 (1960).
204. GURDON, J. B. The Effects of Ultraviolet Irradiation on Uncleaved Eggs of Xenopus Laevis. *Journal of Cell Science* **s3-101,** 299–311. ISSN: 1477-9137. https://journals.biologists.com/jcs/article/s3-101/55/299/63607/The-Effects-of-Ultraviolet-Irradiation-on (1960).
205. GURDON, J. B. The developmental capacity of nuclei taken from intestinal epithelium cells of feeding tadpoles. *Journal of embryology and experimental morphology* **10,** 622–40. ISSN: 0022-0752. http://www.ncbi.nlm.nih.gov/pubmed/13951335 (1962).
206. Standley, H., Zorn, A. & Gurdon, J. eFGF and its mode of action in the community effect during Xenopus myogenesis. *Development* **128,** 1347–1357. ISSN: 1477-9129. https://journals.biologists.com/dev/article/128/8/1347/41655/eFGF-and-its-mode-of-action-in-the-community (2001).

207. Paria, B. C. & Dey, S. K. Preimplantation embryo development in vitro: cooperative interactions among embryos and role of growth factors. *Proceedings of the National Academy of Sciences* **87,** 4756–4760. ISSN: 0027-8424. http://www.pnas.org/cgi/doi/10.1073/pnas.87.12.4756 (1990).
208. Lane, M. & Gardner, D. K. Effect of incubation volume and embryo density on the development and viability of mouse embryos in vitro. *Human Reproduction* **7,** 558–562. ISSN: 1460-2350. https://academic.oup.com/humrep/article-lookup/doi/10.1093/oxfordjournals.humrep.a137690 (1992).
209. Salahuddin, S., Ookutsu, S., Goto, K., Nakanishi, Y. & Nagata, Y. Fertilization and early embryology: Effects of embryo density and co-culture of unfertilized oocytes on embryonic development of in-vitro fertilized mouse embryos. *Human Reproduction* **10,** 2382–2385. ISSN: 0268-1161. https://academic.oup.com/humrep/article-lookup/doi/10.1093/oxfordjournals.humrep.a136303 (1995).
210. Stojanov, T. In-vitro fertilization and culture of mouse embryos in vitro significantly retards the onset of insulin-like growth factor-II expression from the zygotic genome. *Molecular Human Reproduction* **5,** 116–124. ISSN: 14602407. https://academic.oup.com/molehr/article-lookup/doi/10.1093/molehr/5.2.116 (1999).
211. Holm, P., Booth, P., Schmidt, M., Greve, T. & Callesen, H. High bovine blastocyst development in a static in vitro production system using sofaa medium supplemented with sodium citrate and myo-inositol with or without serum-proteins. *Theriogenology* **52,** 683–700. ISSN: 0093691X. https://linkinghub.elsevier.com/retrieve/pii/S0093691X99001624 (1999).
212. Spindler, R. E. & Wildt, D. E. Quality and Age of Companion Felid Embryos Modulate Enhanced Development by Group Culture1. *Biology of Reproduction* **66,** 167–173. ISSN: 0006-3363. https://academic.oup.com/biolreprod/article-lookup/doi/10.1095/biolreprod66.1.167 (2002).
213. Vajta, G. *et al.* Handmade Somatic Cell Cloning in Cattle: Analysis of Factors Contributing to High Efficiency In Vitro1. *Biology of Reproduction* **68,** 571–578. ISSN: 0006-3363. https://academic.oup.com/biolreprod/article-lookup/doi/10.1095/biolreprod.102.008771 (2003).
214. Reed, M. *Embryo Culture* (eds Smith, G. D., Swain, J. E. & Pool, T. B.) 273–312. ISBN: 978-1-61779-970-9. http://link.springer.com/10.1007/978-1-61779-971-6 (Humana Press, Totowa, NJ, 2012).
215. Tao, T., Robichaud, A., Mercier, J. & Ouellette, R. Influence of group embryo culture strategies on the blastocyst development and pregnancy outcome. *Journal of Assisted Reproduction and Genetics* **30,** 63–68. ISSN: 1058-0468. http://link.springer.com/10.1007/s10815-012-9892-x (2013).
216. O'Neill, C. Autocrine Mediators are Required to act on the Embryo by the 2-Cell Stage to Promote Normal Development and Survival of Mouse Preim-

plantation Embryos in Vitro1. *Biology of Reproduction* **58,** 1303–1309. ISSN: 0006-3363. https://academic.oup.com/biolreprod/article-lookup/doi/10.1095/biolreprod58.5.1303 (1998).

217. Stokes, P. J., Abeydeera, L. R. & Leese, H. J. Development of porcine embryos in vivo and in vitro; evidence for embryo 'cross talk' in vitro. *Developmental Biology* **284,** 62–71. ISSN: 00121606. https://linkinghub.elsevier.com/retrieve/pii/S0012160605002721 (2005).
218. Gopichandran, N. & Leese, H. J. The effect of paracrine/autocrine interactions on the in vitro culture of bovine preimplantation embryos. *Reproduction* **131,** 269–277. ISSN: 1470-1626. https://rep.bioscientifica.com/view/journals/rep/131/2/1310269.xml (2006).
219. Swain, J. E. & Smith, G. D. Advances in embryo culture platforms: novel approaches to improve preimplantation embryo development through modifications of the microenvironment. *Human Reproduction Update* **17,** 541–557. ISSN: 1355-4786. https://academic.oup.com/humupd/article-lookup/doi/10.1093/humupd/dmr006 (2011).
220. Kelley, R. L. & Gardner, D. K. In vitro culture of individual mouse preimplantation embryos: the role of embryo density, microwells, oxygen, timing and conditioned media. *Reproductive BioMedicine Online* **34,** 441–454. ISSN: 14726483. https://linkinghub.elsevier.com/retrieve/pii/S1472648317300469 (2017).
221. Lowell, S. You should always keep in touch with your friends: Community effects in biology. *Nature Reviews Molecular Cell Biology* **21,** 568–569. ISSN: 1471-0072. http://www.nature.com/articles/s41580-020-00290-1 (2020).
222. DeWitt, A., Dong, J. & Lauffenburger, D. Quantitative analysis of the EGF receptor autocrine system reveals cryptic regulation of cell response by ligand capture. *J Cell Sci* **114,** 2301–2313 (2001).
223. Harrison, S. E., Sozen, B., Christodoulou, N., Kyprianou, C. & Zernicka-Goetz, M. Assembly of embryonic and extraembryonic stem cells to mimic embryogenesis in vitro. *Science* **356,** eaal1810. ISSN: 0036-8075. https://www.sciencemag.org/lookup/doi/10.1126/science.aal1810 (2017).
224. Rivron, N. C. *et al.* Blastocyst-like structures generated solely from stem cells. *Nature* **557,** 106–111. ISSN: 0028-0836. http://www.nature.com/articles/s41586-018-0051-0 (2018).
225. Sozen, B. *et al.* Self-Organization of Mouse Stem Cells into an Extended Potential Blastoid. *Developmental Cell* **51,** 698–712.e8. ISSN: 15345807. https://linkinghub.elsevier.com/retrieve/pii/S1534580719309451 (2019).
226. Moris, N. *et al.* An in vitro model of early anteroposterior organization during human development. *Nature* **582,** 410–415. ISSN: 0028-0836. http://www.nature.com/articles/s41586-020-2383-9 (2020).

227. O'Neill, C., Li, Y. & Jin, X. Survival signaling in the preimplantation embryo. *Theriogenology* **77,** 773–784. ISSN: 0093691X. https://linkinghub.elsevier.com/retrieve/pii/S0093691X11006662 (2012).
228. Wong, A. P. *et al.* Conversion of human and mouse fibroblasts into lung-like epithelial cells. *Scientific Reports* **9,** 9027. ISSN: 2045-2322. http://www.nature.com/articles/s41598-019-45195-y (2019).
229. Gunne-Braden, A. *et al.* GATA3 Mediates a Fast, Irreversible Commitment to BMP4-Driven Differentiation in Human Embryonic Stem Cells. *Cell Stem Cell* **26,** 693–706.e9. ISSN: 19345909. https://linkinghub.elsevier.com/retrieve/pii/S1934590920300977 (2020).
230. Malaguti, M., Migueles, R. P., Blin, G., Lin, C.-Y. & Lowell, S. Id1 Stabilizes Epiblast Identity by Sensing Delays in Nodal Activation and Adjusting the Timing of Differentiation. *Developmental Cell* **50,** 462–477.e5. ISSN: 15345807. https://linkinghub.elsevier.com/retrieve/pii/S1534580719304459 (2019).
231. Segel, M. *et al.* Niche stiffness underlies the ageing of central nervous system progenitor cells. *Nature* **573,** 130–134. ISSN: 0028-0836. http://www.nature.com/articles/s41586-019-1484-9 (2019).
232. Nandagopal, N. *et al.* Dynamic Ligand Discrimination in the Notch Signaling Pathway. *Cell* **172,** 869–880.e19. ISSN: 00928674. https://linkinghub.elsevier.com/retrieve/pii/S0092867418300023 (2018).
233. Elowitz, M. & Lim, W. A. Build life to understand it. *Nature* **468,** 889–890. ISSN: 0028-0836. http://www.nature.com/articles/468889a (2010).
234. Liu, J. *et al.* Coupling between distant biofilms and emergence of nutrient time-sharing. *Science* **356,** 638–642. ISSN: 0036-8075. https://www.sciencemag.org/lookup/doi/10.1126/science.aah4204 (2017).
235. Wrenn, E. D. *et al.* Regulation of Collective Metastasis by Nanolumenal Signaling. *Cell* **183,** 395–410.e19. ISSN: 00928674. https://linkinghub.elsevier.com/retrieve/pii/S0092867420310874 (2020).
236. Grosse-Wilde, A. *et al.* Loss of inter-cellular cooperation by complete epithelial-mesenchymal transition supports favorable outcomes in basal breast cancer patients. *Oncotarget* **9,** 20018–20033. ISSN: 1949-2553. https://www.oncotarget.com/lookup/doi/10.18632/oncotarget.25034 (2018).
237. Petridou, N. I., Corominas-Murtra, B., Heisenberg, C.-P. & Hannezo, E. Rigidity percolation uncovers a structural basis for embryonic tissue phase transitions. *Cell* **184,** 1914–1928.e19. ISSN: 00928674. https://linkinghub.elsevier.com/retrieve/pii/S0092867421001677 (2021).
238. Gunawardena, J. Models in biology: 'accurate descriptions of our pathetic thinking'. *BMC Biology* **12,** 29. ISSN: 1741-7007. https://bmcbiol.biomedcentral.com/articles/10.1186/1741-7007-12-29 (2014).

239. Mojtahedi, M. *et al.* Cell Fate Decision as High-Dimensional Critical State Transition. *PLOS Biology* **14,** e2000640. ISSN: 1545-7885. https://dx.plos.org/10.1371/journal.pbio.2000640 (2016).
240. WADDINGTON, C. H. Canalization of Development and Genetic Assimilation of Acquired Characters. *Nature* **183,** 1654–1655. ISSN: 0028-0836. http://www.nature.com/articles/1831654a0 (1959).
241. WADDINGTON, C. H. Evolutionary Systems–Animal and Human. *Nature* **183,** 1634–1638. ISSN: 0028-0836. http://www.nature.com/articles/1831634a0 (1959).
242. Jacobson, M. D., Weil, M. & Raff, M. C. Programmed Cell Death in Animal Development. *Cell* **88,** 347–354. ISSN: 00928674. https://linkinghub.elsevier.com/retrieve/pii/S0092867400818735 (1997).
243. Roulston, A., Marcellus, R. C. & Branton, P. E. Viruses and Apoptosis. *Annual Review of Microbiology* **53,** 577–628. ISSN: 0066-4227. http://www.annualreviews.org/doi/10.1146/annurev.micro.53.1.577 (1999).
244. Coucouvanis, E. & Martin, G. R. Signals for death and survival: A two-step mechanism for cavitation in the vertebrate embryo. *Cell* **83,** 279–287. ISSN: 00928674 (1995).
245. Siegal, M. L. & Bergman, A. Waddington's canalization revisited: Developmental stability and evolution. *Proceedings of the National Academy of Sciences* **99,** 10528–10532. ISSN: 0027-8424. http://www.pnas.org/cgi/doi/10.1073/pnas.102303999 (2002).
246. Sherr, C. J. & Weber, J. D. The ARF/p53 pathway. *Current Opinion in Genetics Development* **10,** 94–99. ISSN: 0959437X. https://linkinghub.elsevier.com/retrieve/pii/S0959437X99000386 (2000).
247. Guo, Y., Graham-Evans, B. & Broxmeyer, H. E. Murine Embryonic Stem Cells Secrete Cytokines/Growth Modulators That Enhance Cell Survival/Anti-Apoptosis and Stimulate Colony Formation of Murine Hematopoietic Progenitor Cells. *STEM CELLS*. ISSN: 10665099 (2006).
248. Bell, R. A. & Megeney, L. A. Evolution of caspase-mediated cell death and differentiation: Twins separated at birth. *Cell Death and Differentiation* **24,** 1359–1368. ISSN: 14765403. http://dx.doi.org/10.1038/cdd.2017.37 (2017).
249. Thornberry, N. A. Caspases: Enemies Within. *Science* **281,** 1312–1316. https://www.sciencemag.org/lookup/doi/10.1126/science.281.5381.1312 (1998).
250. Fernando, P. & Megeney, L. A. Is caspase-dependent apoptosis only cell differentiation taken to the extreme? *The FASEB Journal* **21,** 8–17. ISSN: 0892-6638. https://onlinelibrary.wiley.com/doi/abs/10.1096/fj.06-5912hyp (2007).

251. Akbari-Birgani, S., Hosseinkhani, S., Mollamohamadi, S. & Baharvand, H. Delay in apoptosome formation attenuates apoptosis in mouse embryonic stem cell differentiation. *Journal of Biological Chemistry* **289,** 16905–16913. ISSN: 1083351X (2014).
252. Fujita, J. *et al.* Caspase Activity Mediates the Differentiation of Embryonic Stem Cells. *Cell Stem Cell.* ISSN: 19345909. arXiv: NIHMS150003 (2008).
253. Jeon, K. *et al.* Bax inhibitor-1 enhances survival and neuronal differentiation of embryonic stem cells via differential regulation of mitogen-activated protein kinases activities. *Biochimica et Biophysica Acta - Molecular Cell Research* **1823,** 2190–2200. ISSN: 01674889. http://dx.doi.org/10.1016/j.bbamcr.2012.08.005 (2012).
254. Karimzadeh, S., Hosseinkhani, S., Fathi, A., Ataei, F. & Baharvand, H. Insufficient Apaf-1 expression in early stages of neural differentiation of human embryonic stem cells might protect them from apoptosis. *European Journal of Cell Biology* **97,** 126–135. ISSN: 16181298. https://doi.org/10.1016/j.ejcb.2018.01.005 (2018).
255. Duval, D., Reinhardt, B., Kedinger, C. & Boeuf, H. Role of suppressors of cytokine signaling (Socs) in leukemia inhibitory factor (LIF) -dependent embryonic stem cell survival. *The FASEB Journal* **14,** 1577–1584. ISSN: 0892-6638 (2000).
256. Duval, D., Malaisé, M., Reinhardt, B., Kedinger, C. & Boeuf, H. A p38 inhibitor allows to dissociate differentiation and apoptotic processes triggered upon LIF withdrawal in mouse embryonic stem cells. *Cell Death and Differentiation.* ISSN: 13509047 (2004).
257. Duval, D *et al.* Apoptosis and differentiation commitment: novel insights revealed by gene profiling studies in mouse embryonic stem cells. *Cell Death Differentiation* **13,** 564–575. ISSN: 1350-9047. http://www.nature.com/articles/4401789 (2006).
258. Trouillas, M. *et al.* Bcl2, a transcriptional target of p38α, is critical for neuronal commitment of mouse embryonic stem cells. *Cell Death and Differentiation* **15,** 1450–1459. ISSN: 14765403 (2008).
259. Wang, E. S. *et al.* Fas-activated mitochondrial apoptosis culls stalled embryonic stem cells to promote differentiation. *Current Biology.* ISSN: 09609822 (2015).
260. Lander, A. D. Pattern, Growth, and Control. *Cell* **144,** 955–969. ISSN: 00928674. https://linkinghub.elsevier.com/retrieve/pii/S0092867411002467 (2011).
261. Stubbendieck, R. M. & Straight, P. D. Multifaceted Interfaces of Bacterial Competition. *Journal of Bacteriology* **198** (ed Margolin, W.) 2145–2155. ISSN: 0021-9193. https://jb.asm.org/content/198/16/2145 (2016).

262. Stubbendieck, R. M., Vargas-Bautista, C. & Straight, P. D. Bacterial Communities: Interactions to Scale. *Frontiers in Microbiology* **7.** ISSN: 1664-302X. http://journal.frontiersin.org/Article/10.3389/fmicb.2016.01234/abstract (2016).
263. Verma, S. C. & Miyashiro, T. Quorum sensing in the squid-Vibrio symbiosis. *International journal of molecular sciences* **14,** 16386–401. ISSN: 1422-0067. http://www.ncbi.nlm.nih.gov/pubmed/23965960http://www.pubmedcentral.nih.gov/articlerender.fcgi?artid=PMC3759917 (2013).
264. Ratzke, C., Denk, J. & Gore, J. Ecological suicide in microbes. *Nature Ecology Evolution* **2,** 867–872. ISSN: 2397-334X. http://www.nature.com/articles/s41559-018-0535-1 (2018).
265. Scheffer, M. *et al.* Early-warning signals for critical transitions. *Nature* **461,** 53–59. ISSN: 00280836. http://dx.doi.org/10.1038/nature08227 (2009).
266. Scheffer, M. *et al.* Anticipating critical transitions. *Science* **338,** 344–348. ISSN: 10959203 (2012).
267. May, R. M., Levin, S. A. & Sugihara, G. Ecology for bankers. *Nature* **451,** 893–894. ISSN: 0028-0836. http://www.nature.com/articles/451893a (2008).
268. Crowley, T. J. & Hyde, W. T. Transient nature of late Pleistocene climate variability. *Nature* **456,** 226–230. ISSN: 0028-0836. http://www.nature.com/articles/nature07365 (2008).
269. Bellwood, D. R., Hughes, T. P., Folke, C. & Nyström, M. Confronting the coral reef crisis. *Nature* **429,** 827–833. ISSN: 0028-0836. http://www.nature.com/articles/nature02691 (2004).
270. Dai, L., Vorselen, D., Korolev, K. S. & Gore, J. Generic Indicators for Loss of Resilience Before a Tipping Point Leading to Population Collapse. *Science* **336,** 1175–1177. ISSN: 0036-8075. https://www.sciencemag.org/lookup/doi/10.1126/science.1219805 (2012).
271. Bargaje, R. *et al.* Cell population structure prior to bifurcation predicts efficiency of directed differentiation in human induced pluripotent cells. *Proceedings of the National Academy of Sciences* **114,** 2271–2276. ISSN: 0027-8424. http://www.pnas.org/lookup/doi/10.1073/pnas.1621412114 (2017).
272. Kerkar, S. P. *et al.* Timing and intensity of exposure to interferon-γ critically determines the function of monocyte-derived dendritic cells. *Immunology* **143,** 96–108. ISSN: 00192805. http://doi.wiley.com/10.1111/imm.12292 (2014).
273. Matejka, N. & Reindl, J. Perspectives of cellular communication through tunneling nanotubes in cancer cells and the connection to radiation effects. *Radiation Oncology* **14,** 218. ISSN: 1748-717X. https://ro-journal.biomedcentral.com/articles/10.1186/s13014-019-1416-8 (2019).
274. Punovuori, K. *et al.* N-cadherin stabilises neural identity by dampening anti-neural signals. *Development*. ISSN: 1477-9129. https://journals.biologists.

com/dev/article/doi/10.1242/dev.183269/266709/N-cadherin-stabilises-neural-identity-by-dampening (2019).

275. Punovuori, K., Malaguti, M. & Lowell, S. Cadherins in early neural development. *Cellular and Molecular Life Sciences*. ISSN: 1420-682X. http://link.springer.com/10.1007/s00018-021-03815-9 (2021).
276. Kalkan, T. & Smith, A. Mapping the route from naive pluripotency to lineage specification. *Philosophical Transactions of the Royal Society B: Biological Sciences* **369,** 20130540. ISSN: 0962-8436. https://royalsocietypublishing.org/doi/10.1098/rstb.2013.0540 (2014).
277. Kalkan, T. *et al.* Tracking the embryonic stem cell transition from ground state pluripotency. *Development*. ISSN: 1477-9129. https://journals.biologists.com/dev/article/doi/10.1242/dev.142711/264306/Tracking-the-embryonic-stem-cell-transition-from (2017).
278. Ritchie, M. E. Reaction and diffusion thermodynamics explain optimal temperatures of biochemical reactions. *Scientific Reports* **8,** 11105. ISSN: 2045-2322. http://www.nature.com/articles/s41598-018-28833-9 (2018).
279. Charlebois, D. A., Hauser, K., Marshall, S. & Balázsi, G. Multiscale effects of heating and cooling on genes and gene networks. *Proceedings of the National Academy of Sciences* **115,** E10797–E10806. ISSN: 0027-8424. http://www.pnas.org/lookup/doi/10.1073/pnas.1810858115 (2018).
280. He, X. Thermostability of Biological Systems: Fundamentals, Challenges, and Quantification. *The Open Biomedical Engineering Journal* **5,** 47–73. ISSN: 18741207. http://benthamopen.com/ABSTRACT/TOBEJ-5-47 (2011).
281. Byerly, L., Cassada, R. & Russell, R. The life cycle of the nematode Caenorhabditis elegans. *Developmental Biology* **51,** 23–33. ISSN: 00121606. https://linkinghub.elsevier.com/retrieve/pii/0012160676901196 (1976).
282. Kimmel, C. B., Ballard, W. W., Kimmel, S. R., Ullmann, B. & Schilling, T. F. Stages of embryonic development of the zebrafish. *Developmental Dynamics* **203,** 253–310. ISSN: 10588388. http://doi.wiley.com/10.1002/aja.1002030302 (1995).
283. Kuntz, S. G. & Eisen, M. B. Drosophila Embryogenesis Scales Uniformly across Temperature in Developmentally Diverse Species. *PLoS Genetics* **10** (ed Desplan, C.) e1004293. ISSN: 1553-7404. https://dx.plos.org/10.1371/journal.pgen.1004293 (2014).
284. Grodzinsky, E. & Sund Levander, M. in *Understanding Fever and Body Temperature* 49–65 (Springer International Publishing, Cham, 2020). http://link.springer.com/10.1007/978-3-030-21886-7_5.
285. Depken, M. & Schiessel, H. Nucleosome Shape Dictates Chromatin Fiber Structure. *Biophysical Journal* **96,** 777–784. ISSN: 00063495. https://linkinghub.elsevier.com/retrieve/pii/S0006349508000891 (2009).

286. Meshorer, E. & Misteli, T. Chromatin in pluripotent embryonic stem cells and differentiation. *Nature Reviews Molecular Cell Biology* **7,** 540–546. ISSN: 1471-0072. http://www.nature.com/articles/nrm1938 (2006).
287. Meshorer. Imaging chromatin in embryonic stem cells. *StemBook*. ISSN: 19403429. http://www.stembook.org/node/481 (2008).
288. Efroni, S. *et al.* Global Transcription in Pluripotent Embryonic Stem Cells. *Cell Stem Cell* **2,** 437–447. ISSN: 19345909. https://linkinghub.elsevier.com/retrieve/pii/S1934590908001616 (2008).
289. Cantone, I. *et al.* Ordered chromatin changes and human X chromosome reactivation by cell fusion-mediated pluripotent reprogramming. *Nature Communications* **7,** 12354. ISSN: 2041-1723. http://www.nature.com/articles/ncomms12354 (2016).
290. Margueron, R. & Reinberg, D. The Polycomb complex PRC2 and its mark in life. *Nature* **469,** 343–349. ISSN: 0028-0836. http://www.nature.com/articles/nature09784 (2011).

Curriculum Vitæ

Hirad DANESHPOUR ARYADI

2016–2021	**Doctor of Philosophy (PhD)** Department of Bionanoscience, Kavli Institute of Nanoscience Delft University of Technology, Delft, the Netherlands Promotor and daily supervisor: prof.dr. H.O. Youk Promotor: prof.dr. Y.M. Blanter Copromotor: prof.dr. G.E. Bokinsky
2015	Research Intern - Cancer Institute / HollandPTC Erasmus University Medical Center, Rotterdam, the Netherlands
2014–2016	**Master of Science (MSc)** Applied Physics, with minor in Life Sciences and Biochemistry Delft University of Technology, Delft, the Netherlands Leiden University, Leiden, the Netherlands
2011–2014	**Bachelor of Science (BSc)**, *cum laude* Applied Physics Delft University of Technology, Delft, the Netherlands
2005–2011	Secondary School (VWO Atheneum), *with distinction* Lentiz Reviuslyceum, Maassluis, the Netherlands
21-04-1993	Born in Vlaardingen, the Netherlands

List of Publications

2. **Daneshpour, H.**, van den Bersselaar, P., Youk, H. Global community effect: Large-scale cooperation yields collective survival of differentiating embryonic stem cells, *bioRxiv* (2020) (*Cell Systems*, manuscript in revision).

1. **Daneshpour, H.**, Youk, H. Modeling cell–cell communication for immune systems across space and time, *Current Opinion in Systems Biology* **18**, 44-52 (2019).